

UNIVERSITY OF MINES AND TECHNOLOGY  
TARKWA

FACULTY OF GEOSCIENCES AND ENVIRONMENTAL STUDIES  
DEPARTMENT OF ENVIRONMENTAL AND SAFETY ENGINEERING

A THESIS REPORT ENTITLED

SILVER NANOPARTICLES SYNTHESISED IN NATURAL RUBBER LATEX  
NANOFIBRE FOR HEAVY METALS REMOVAL IN WATER



LINDA BENTUMA OSEI

SUBMITTED IN FULFILLMENT OF THE REQUIREMENT FOR THE AWARD OF THE  
DEGREE OF DOCTOR OF PHILOSOPHY IN ENVIRONMENTAL ENGINEERING

THESIS SUPERVISORS

A handwritten signature in blue ink, appearing to be 'S. Ndur', written over a dotted line.

ASSOC PROF SAMUEL A. NDUR

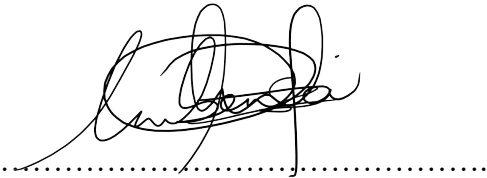
A handwritten signature in blue ink, appearing to be 'S. Fosú', written over a dotted line.

DR SHADRACK FOSU

TARKWA, GHANA  
OCTOBER 2023

## DECLARATION

I declare that this thesis is my own work. It is being submitted for the degree of Doctor of Philosophy in Environmental Engineering at the University of Mines and Technology (UMaT), Tarkwa. It has not been submitted for any degree or examination in any other University.



(Signature of candidate)

.....18th.....day of.....October.....2023



## ABSTRACT

Water treatment methods, including adsorption by nanoparticles, is an efficient method for contaminant removal in wastewater. Nanoparticles used for water treatment incorporate nanoparticles in micro-matrices, which are non-biodegradable. However, removing remnant nanoparticles from treated water, which forms part of the contamination problem, is expensive. This research aims to synthesise silver nanoparticles (AgNP) in green nanofibre matrix using natural rubber latex (NRL) and polyvinyl alcohol (PVA). The efficiency of the nanofibre composites (AgNP-PVA/NRL) to remove  $\text{Cd}^{2+}$  and Hg from wastewater was determined. The NRL mixed with PVA at ratios of 40%, 50%, 60% and 70% PVA/NRL (w/v) were electrospun, using water as solvent. Optimum ratio at which the PVA/NRL nanofibre could be applied in aqueous processes without excess dissolution of the nanofibre was determined. Scanning electron microscopy (SEM) analyses revealed that decreasing PVA content produced relatively rougher but thinner fibres with smaller average pore diameters and matings, and vice versa. Fourier-transform infrared spectroscopy (FT-IR) analysis and weight loss test by dissolution showed that decreasing PVA content decreased the fibre's solubility. Silver nitrate ( $\text{AgNO}_3$ ) was added to PVA/NRL solution and electrospun to form 0.01 M AgNP and 0.015 M AgNP. SEM and energy dispersive x-ray spectroscopy (EDS) analyses revealed that most AgNP in 0.01 M AgNP were formed near or on the fibre surfaces, whilst that of 0.015 M were mainly within the fibre walls. Transmission electron microscopy (TEM) analysis revealed AgNP sizes were relatively smaller in 0.015 M AgNP ( $2.82 \pm 0.04$  nm) than in 0.01 M AgNP ( $8.15 \pm 0.09$  nm). X-ray diffractometry (XRD) analysis confirmed the presence of AgNP, and FT-IR analysis showed that amine group in NRL and hydroxyl group in PVA reduced  $\text{Ag}^+$  to  $\text{Ag}^0$ , whilst *cis*-isoprene (in NRL) stabilised AgNP in the solid matrix. Maximum uptake of Hg occurred at pH 7 and around 60 min for both 0.01 M (40.92 mg/g) and 0.015 M AgNP (19.48 mg/g). Maximum uptake of  $\text{Cd}^{2+}$  occurred at pH 7 but at different reaction times of 20 min for 0.01 M AgNP (14.97 mg/g) and 40 min for 0.015 M AgNP (30.11 mg/g). It was also revealed that Hg adsorption was relatively better when the AgNPs were larger and near or on the surface (0.01 M AgNP), forming a monolayer (Langmuir isotherm). Mercury adsorption in 0.015 M AgNP followed the Dubinin-Radushkevich (D-R) isotherm and the Elovich kinetic model, indicating chemisorption, with 0.01 M AgNP having a larger boundary layer ( $C = 9.9354$  mg/g) and smaller desorption constant ( $\beta = 0.1217$  g/mg). It was revealed that  $\text{Cd}^{2+}$  adsorption was relatively better when the AgNPs were relatively more (0.015 M AgNP),

and the adsorption behaviour of both nanofibre composites followed Freundlich isotherm. Generally, the nanofibre composites adsorbed Hg better than Cd. In the binary system, the nanofibre composites adsorbed Hg better than Cd, except in 0.015 M AgNP. Measured Ag concentrations (after adsorption experiments) were 0.04 mg/L (0.01 M AgNP) to 0.21 mg/L (Mix 2), all below US EPA SMCL and WHO drinking water guidelines of 0.10 mg/L except for Mix 2. This shows that green synthesised AgNP-PVA/NRL nanofibre composites are good enough for wastewater treatment.



This thesis is dedicated to my parents,

Mr Lawrence Osei Kwame and Mrs Janet Afrakomah Osei, and

my siblings,

Frank Agyapong (Esq.), Doris Osei Akoto, Joseph Osei Akoto, Augusta Marfowaa Osei, Betty Akosua Boakyewaa Teye, Dr Akosua Dwamena Appiah and Gideon Owusu-Ansah Osei.



## ACKNOWLEDGEMENTS

My appreciation first goes to God, whose kindness and mercies have sustained me in this research's highs and lows. I am most grateful to my Supervisors, Assoc Prof Samuel A. Ndur, who has shown unwavering support and encouragement in my studies and life since my bachelor's degree and Dr Shadrack Fosu, who has always motivated me during this research. I appreciate your expertise, time and advice in bringing this project to life.

Secondly, I am grateful to David Gyapong (Esq.), Mr Kofi Takyi, Okyeame Lartey of Awudua and Mr George Wofemenu for providing fresh natural rubber latex. Special thanks to Mr Marconi Azadah and Mr Nikao Lasidzi Adziman for supporting field latex collection. I am also grateful to Mr Eric Appah and Mr Emmanuel K. Mensah for providing an ignition coil and simulation of an electrospinner, respectively. I appreciate Mr Emmanuel K. Mensah for sacrificing his time during the simulations. I also thank Dr Eric Stern for providing his camera for this project.

Prof William K. Buah, Prof E. K. Assiam, Dr Thomas Wi-Afedzi, Dr Clement Owusu and Dr Eric Argorhom are among the lecturers who provided inputs to this research, and I appreciate their contributions. To Prof George Agyei, Dr Yao Ziggah, Dr Ishmael Quaioco, Dr Francis Krampah and Miss Vivian I. Seshie, I appreciate their support and encouragement during this research.

I am also thankful to all former and present Laboratory Technicians of the Environmental and Safety Engineering Department and Petroleum Engineering Department, especially Messrs Isaac Agyarko, Emmanuel Shanks Quainoo, Derrick Obri, Daniel Amoah, Prince Oppong Amoh, Meshack Tei, David Yankson, Celestine Amankwah-Poku, Roger Arhin and Cyril Opare for their support in the laboratory. I also appreciate all Demonstrators and Postgraduate Assistants for their moral support.

I wish to express my gratitude to Theophilus Joe-Asare, my dear husband and friend, for his words of encouragement and moral support at all times.

Lastly, I wish to express my gratitude to the University of Mines and Technology for funding this project and especially to Assoc Prof Victor Temeng, the Ghana National Petroleum Corporation (GNPC) Professorial Chair in Mining Engineering (University of

Mines and Technology, Tarkwa, Ghana) for providing funds to purchase the electrospinner for this project.



# TABLE OF CONTENTS

<b>Contents</b>	<b>Page</b>
<b>DECLARATION</b>	<b>i</b>
<b>ABSTRACT</b>	<b>ii</b>
<b>ACKNOWLEDGEMENTS</b>	<b>v</b>
<b>TABLE OF CONTENTS</b>	<b>vii</b>
<b>LIST OF FIGURES</b>	<b>xiv</b>
<b>LIST OF TABLES</b>	<b>xvii</b>
<b>CHAPTER 1 INTRODUCTION</b>	<b>1</b>
1.1 Background	1
1.2 Research Problem	2
1.3 Objectives of the Research	4
1.4 Methods Used	4
1.5 Organisation of Thesis	5
<b>CHAPTER 2 LITERATURE REVIEW</b>	<b>8</b>
2.1 Heavy Metals Contamination in Water	8
2.1.1 Mercury (Hg) in Water	8
2.1.2 Cadmium (Cd) in Water	10
2.2 Nanoparticles	11
2.2.1 Nanoparticles for Hg and Cd <sup>2+</sup> Contaminants Removal from Wastewater	11
2.2.2 Silver Nanoparticle (AgNP) Synthesis	16
	vii





2.2.3	Negative Impact of Using Nanoparticles in Water Treatment	17
2.2.4	Potential Method(s) of Minimising the Toxicological Effects of Nanoparticles in Water Treatment	18
2.3	Nanofibres	19
2.3.1	Nanofibre Fabrication	19
2.3.2	Electrospinning	19
2.4	Natural Rubber Latex (NRL)	22
2.4.1	Overview, Sources and Uses	22
2.4.2	Nanoparticles Synthesised Using NRL	24
2.5	Polyvinyl Alcohol (PVA)	24
2.5.1	Overview, Source and Uses	24
2.5.2	Nanoparticles Synthesised Using PVA	25
2.6	Characterisation of Nanoparticles and Nanofibres	25
2.6.1	Morphological Studies	26
2.6.2	Elemental Studies using Energy Dispersive X-Ray Spectroscopy (EDS)	28
2.6.3	Surface Functionalisation using Fourier Transform – Infrared Spectroscopy (FT-IR)	28
2.6.4	Crystallographic Studies using X-Ray Diffractometry (XRD)	29
2.7	Adsorption	30
2.7.1	Factors Affection Adsorption	31
2.7.2	Adsorption Isotherm	32
2.7.3	Adsorption Kinetics	32
2.8	Atomic Absorption Spectrophotometry (AAS)	33

**CHAPTER 3 MATERIALS AND METHODS 35**

3.1	Materials	35
-----	-----------	----

3.2	Sampling of Natural Rubber Latex (NRL)	36
3.3	Characterisation of Natural Rubber Latex	37
	3.3.1 Determination of Total Solid Content (TSC)	37
	3.3.2 Determination of Dry Rubber Content (DRC)	38
	3.3.3 Protein Analysis	39
	3.3.4 Metal Content Determination	40
3.4	Preparation of Polyvinyl Alcohol/Natural Rubber Latex (PVA/NRL) Solutions for Electrospinning	40
3.5	Electrospinning NRL, PVA and PVA/NRL Solutions	40
	3.5.1 Electrospinning NRL	40
	3.5.2 Electrospinning PVA, PVA/NRL and AgNO <sub>3</sub> -PVA/NRL Solutions	41
3.6	Weight Loss Test by Dissolution on PVA/NRL Nanofibres	42
3.7	Synthesis of Silver Nanoparticles (AgNP)	43
3.8	Characterisation of the Electrospun Nanofibre Composites	44
	3.8.1 Morphology, Size Distribution and Elemental Composition of Electrospun Fibres and AgNP	44
	3.8.2 Crystallography of AgNP-PVA/NRL Nanofibre Composites	44
	3.8.3 Functional Group Characterisation of Electrospun Nanofibres	45
3.9	Point of Zero Charge Analyses of AgNP-PVA/NRL Nanofibre Composites	45
3.10	Adsorption Studies of AgNP-PVA/NRL Nanofibre Composite for Hg and Cd <sup>2+</sup> Contaminants	45
	3.10.1 Adsorption Experiment	45
	3.10.2 Adsorption Isotherm	47
	3.10.3 Adsorption Kinetics	49
3.11	Elemental Analysis of Adsorbates in Solution	50
	3.11.1 Mercury Concentration in Solution	50
	3.11.2 Cadmium Concentration in Solution	50

**CHAPTER 4 GREEN SYNTHESIS AND CHARACTERISATION OF ELECTROSPUN PVA/NRL NANOFIBRE FOR NANOPARTICLE LOADING AND APPLICATION IN AQUEOUS SOLUTIONS 51**

4.1	Background	51
4.2	Characteristics of NRL Used	52
4.3	Viscosities of NRL and PVA/NRL Solutions	54
4.4	Morphology of Fibre Films	55
	4.4.1 Morphology of NRL Films	55
	4.4.2 Morphology of PVA/NRL Films	59
4.5	Characterisation of PVA/NRL Films by Fourier Transform - Infrared (FT-IR) Spectroscopy	63
4.6	Weight Loss Analysis by Dissolution	65
4.7	Summary	67

**CHAPTER 5 GREEN SYNTHESIS AND CHARACTERISATION OF SILVER NANOPARTICLES IN PVA/NRL NANOFIBRE COMPOSITE (AgNP-PVA/NRL) FOR ADSORPTION STUDIES 69**

5.1	Background	69
5.2	Morphology and Elemental Composition of AgNP-PVA/NRL Nanofibre Composites	70
	5.2.1 Characterisation by Scanning Electron Microscopy (SEM) and Energy Dispersive X-Ray Spectrometer (EDS)	71
	5.2.2 Characterisation by Transmission Electron Microscopy (TEM)	73
5.3	Characterisation of AgNP-PVA/NRL Nanofibre Composite by X-Ray Diffractometry (XRD)	76

5.4	Characterisation of AgNP-PVA/NRL Nanofibre Composite by Fourier Transform Infrared Spectroscopy (FT-IR)	77
5.5	Point of Zero Charge (PZC) and Surface Charge AgNP-PVA/NRL Nanofibre Composite	79
5.6	Summary	80

**CHAPTER 6 ASORPTION OF MERCURY AND CADMIUM FROM AQUEOUS SOLUTIONS USING SYNTHESISED AgNP-PVA/NRL NANOFIBRE COMPOSITES** **81**

6.1	Background	81
6.2	Sorption of Hg by AgNP-PVA/NRL Nanofibre Composites	82
	6.2.1 Effect of pH on Hg Adsorption	82
	6.2.2 Effect of Contact Time on Hg Adsorption	86
	6.2.3 Effect of Initial Concentration on Hg Adsorption	88
	6.2.4 Adsorption Isotherm Study for Hg	89
	6.2.5 Adsorption Kinetic Study for Hg	94
	6.2.6 Morphology and Elemental Composition of AgNP-PVA/NRL Nanofibre Composites after Hg Adsorption	98
6.3	Sorption of Cd <sup>2+</sup> by AgNP-PVA/NRL Nanofibre Composites	99
	6.3.1 Effect of pH on Cd <sup>2+</sup> Adsorption	99
	6.3.2 Effect of Contact Time on Cd <sup>2+</sup> Adsorption	102
	6.3.3 Effect of Initial Concentration on Cd <sup>2+</sup> Adsorption	103
	6.3.4 Adsorption Isotherm Study for Cd	104
	6.3.5 Adsorption Kinetic Study for Cd <sup>2+</sup>	108
	6.3.6 Morphology and Elemental Composition of AgNP-PVA/NRL Nanofibre Composites after Cd <sup>2+</sup> Adsorption	112

6.4	Comparison of Hg Adsorption to Cd Adsorption by AgNP-PVA/NRL Nanofibre Composites	113
6.5	Summary	114

**CHAPTER 7 COMPETITIVE ADSORPTION OF MERCURY AND CADMIUM FROM AQUEOUS SOLUTION USING AgNP-PVA/NRL NANOFIBRE COMPOSITES** **116**

7.1	Background	116
7.2	Efficiency of Various AgNP-PVA/NRL Nanofibre Composites to Adsorb Hg and Cd <sup>2+</sup> Simultaneously from A Binary System (Cd-Hg Solution)	117
7.3	Silver Released into Solution After Adsorption Experiment	122
7.4	Summary	124

**CHAPTER 8 CONCLUSIONS AND RECOMMENDATIONS** **126**

8.1	Conclusions	126
	8.1.1 Green Electrospinning of PVA/NRL Nanofibre	126
	8.1.2 Green Synthesis of AgNP Incorporated in PVA/NRL Nanofibre Composite (Ag-PVA/NRL)	127
	8.1.3 Adsorption of Hg and Cd from Water by the Synthesised AgNP-PVA/NRL Nanofibre Composites	128
8.2	Significance and Contributions	130
8.3	Recommendations and Future Works	130

**REFERENCES** **132**

APPENDIX A: POINT OF ZERO CHARGE (PZC) ANALYSIS OF THE Ag-NP-PVA/NRL NANOFIBRE COMPOSITES 156

APPENDIX B: MERCURY ADSORPTION FROM AQUEOUS SOLUTION BY AgNP-PVA/NRL NANOFIBRE COMPOSITES IN A SINGLE-COMPONENT ADSORPTION STUDY 157

APPENDIX C: CADMIUM ADSORPTION FROM AQUEOUS SOLUTION BY AgNP-PVA/NRL NANOFIBRE COMPOSITES IN A SINGLE-COMPONENT ADSORPTION STUDY 161

APPENDIX D: MERCURY AND CADMIUM ADSORPTION FROM AQUEOUS SOLUTION BY AgNP-PVA/NRL NANOFIBRE COMPOSITES IN A BINARY ADSORPTION STUDY 165



## LIST OF FIGURES

Figure	Title	Page
2.1	Schematic Diagram of a Basic Electrospinning Unit	20
2.2	Structural Formula of Natural Rubber ( <i>cis</i> -1,4-polyisoprene)	24
2.3	Structural Formula of Polyvinyl Alcohol	24
2.4	Scanning Electron Microscope (SEM) Equipped With An Energy Dispersive X-Ray Spectrometer (EDS)	26
2.5	Basic Terms Used in Adsorption Processes	30
2.6	Atomic Absorption Spectrophotometer (AAS)	34
3.1	Fresh NRL from <i>Hevea brasiliensis</i> Tree at Bepo, Western Region of Ghana	37
3.2	TSC Analysis (Before Drying)	38
3.3	Rolled Coagulated Latex Sheets Before Drying in DRC Analysis	39
3.4	Electrospinning Unit TL-01	41
3.5	PVA/NRL Nanofibre After Filtration	43
3.6	AgNP-PVA/NRL Nanofibre Composites in Hg Solution Agitated on an Orbital Shaker	46
4.1	TSC Analysis (After Drying)	53
4.2	DRC Analysis (After Drying)	53
4.3	Canon EOS 60D Camera Image of NRL Being Electrospayed at 24 kV	55
4.4	(a) SEM and (b) Canon EOS 60D Camera Image of Electrospayed NRL at 24 kV	59
4.5	Electrospinning 50% PVA/NRL Solution	59
4.6	SEM Image of Electrospun (a) 100% PVA, (c) 40% PVA/NRL, (e) 50% PVA/NRL, (g) 60% PVA/NRL and Their Corresponding Fibre Diameter Distributions (b, d, f and h, respectively)	60
4.7	Electrospun 70% PVA/NRL (a) SEM Image (b) Fibre Diameter Distribution	61
4.8	FT-IR Spectra of 100% PVA, % PVA/NRL and NRL Fibre Films	64
4.9	Aqueous Solution with % PVA/NRL Fibre Film After Shaking in Distilled Water	66
4.10	SEM Images of 50% PVA/NRL After Weight Loss Analysis	67

5.1	Electrospun 0.01 M AgNP and 0.015 M AgNP Nanofibre Composite (a) Before and (b) After Drying	71
5.2	(a) BSD-SEM Image of 0.01 M AgNP with (b)EDS Map and (c) EDS Spectral Analysis	72
5.3	(a) BSD-SEM Image of 0.015 M AgNP with (b) EDS Map and (c) EDS Spectral Analysis	73
5.4	TEM Images of AgNP in 0.01 M AgNP (a and b) and 0.015 M AgNP (c and d) with their Corresponding Size Distribution (e and f, respectively)	74
5.5	XRD Patterns for PVA/NRL and AgNP-PVA/NRL Nanofibre Composites	77
5.6	FT-IR Spectra of PVA/NRL Nanofibre and AgNP-PVA/NRL Nanofibre Composites	78
5.7	Illustration of AgNP Formation in the PVA/NRL Nanofibre Matrix	79
5.8	Point of Zero Charge for 0.01 M and 0.015 M AgNP Nanofibre Composites	80
6.1	Effect of pH on the Adsorption of Hg by AgNP-PVA/NRL Nanofibre Composites	83
6.2	Eh-pH Diagram of Hg-O-H System (Geochemist's Workbench). $\Sigma\text{Hg} = 10^{-10}$ , 298.15 K, $10^5$ Pa	85
6.3	Effect of Contact Time on the Adsorption of Hg by PVA/NRL Nanofibre, 0.01 M AgNP and 0.015 M AgNP	87
6.4	Effect of Initial Concentration on the Adsorption of Hg by AgNP-PVA/NRL Nanofibre Composites	89
6.5	(a) Langmuir (b) Freundlich and (c) Dubinin-Radushkevich Isotherm for Hg Adsorption by AgNP-PVA/NRL Nanofibre Composites	92
6.6	(a) Pseudo-First Order (b) Pseudo-Second Order (c) Elovich and (d) Intra-Particle Diffusion Kinetic Models for Hg Adsorption by AgNP-PVA/NRL Nanofibre Composites	95
6.7	(a) BSD-SEM Image with (b) EDX Analysis After Hg Adsorption by AgNP-PVA/NRL Nanofibre Composite	98
6.8	Effect of pH on the Adsorption of $\text{Cd}^{2+}$ by AgNP-PVA/NRL Nanofibre Composites	100
6.9	Eh-pH Diagram of Cd-O-H System (Geochemist's Workbench). $\Sigma\text{Cd} = 10^{-10}$ , 298.15 K, $10^5$ Pa	101



6.10	Effect of Contact Time on the Adsorption of $Cd^{2+}$ by PVA/NRL Nanofibre, 0.01 M AgNP and 0.015 M AgNP	103
6.11	Effect of Initial Concentration on the Adsorption of $Cd^{2+}$ by AgNP-PVA/NRL Nanofibre Composites	104
6.12	(a) Langmuir (b) Freundlich and (c) Dubinin-Radushkevich Isotherm for $Cd^{2+}$ Adsorption by AgNP-PVA/NRL Nanofibre Composites	106
6.13	(a) Pseudo-First Order (b) Pseudo-Second Order (c) Elovich and (d) Intra-Particle Diffusion Kinetic Models for $Cd^{2+}$ Adsorption by AgNP-PVA/NRL Nanofibre Composites	110
6.14	(a) BSD-SEM Image with (b) EDX Analysis After $Cd^{2+}$ Adsorption by AgNP-PVA/NRL Nanofibre Composite	112
7.1	Removal Efficiency of Hg and $Cd^{2+}$ from Cd-Hg Solution by AgNP-Nanofibre Composites	118



## LIST OF TABLES

Table	Title	Page
2.1	Some Nanoparticles and Nanocomposites Used for Removing Hg and Cd Contaminants from Wastewater	13
4.1	Characteristics of NRL Used	53
4.2	Viscosities of NRL and PVA/NRL Solutions	54
4.3	Characteristics of Electrosprayed NRL at 15 kV-26 kV	56
4.4	Pore Diameters of PVA/NRL Fibre Films	62
4.5	Weight Loss Analysis of PVA/NRL Nanofibres	66
6.1	Parameters of Adsorption Isotherms for Hg Adsorption onto AgNP-PVA/NRL Nanofibre Composites	93
6.2	Parameters of Adsorption Kinetics for Hg Adsorption onto AgNP-PVA/NRL Nanofibre Composites	96
6.3	Parameters of Adsorption Isotherms for Cd <sup>2+</sup> Adsorption onto AgNP-PVA/NRL Nanofibre Composites	107
6.4	Parameters of Adsorption Kinetics for Cd <sup>2+</sup> Adsorption onto AgNP-PVA/NRL Nanofibre Composites	111
7.1	Adsorption Capacity of Hg and Cd <sup>2+</sup> from Cd-Hg Solution by AgNP-PVA/NRL Nanofibre Composites	118
7.2	Silver (Ag) Concentration in Aqueous Solutions After Hg and Cd Adsorption	123
7.3	Guidelines for Ag Concentration in Drinking Water	123

# CHAPTER 1

## INTRODUCTION

### 1.1 Background

Water is an indispensable resource to humans. No matter the source, water for human consumption and domestic purposes must always be of good quality and affordable (Chinn, 2009).

However, heavy metals and factors such as environmental changes due to industrialisation and population growth have led to the continuous deterioration of water quality (Ali, 2012). In addition, the neurotoxic, carcinogenic and mutagenic effects of some water pollutants have awakened the need for strict health-based water and wastewater regulations (Tiwari *et al.*, 2008; Verma and Dwivedi, 2013). This has made producing clean water and the treatment of wastewater for domestic use challenging.

Existing water and wastewater treatment methods include adsorption, coagulation, ion exchange, precipitation and reverse osmosis (Ali, 2012; Gunatilake, 2015; Azimi *et al.*, 2017). Considering the ease of operation, cost and material availability, adsorption has become one of the suitable methods for removing heavy metals and other contaminants from polluted or contaminated water (Ali, 2012; Ariffin *et al.*, 2017). Unfortunately, due to the unavailability of suitable adsorbents with high adsorption capacity and the incapability of a single adsorbent to remove all kinds of pollutants, adsorption at a large scale has not achieved good commercial status (Ali, 2012). Earlier, activated carbon was used in the adsorption process to remove pollutants. However, activated carbon regeneration is expensive (Ali, 2012; Ariffin *et al.*, 2017).

Currently, nano-sized adsorbents are under study in water treatment because of their superior efficiency over conventional adsorbents (Padil *et al.*, 2016). In recent times, nano-sized adsorbents such as carbon nanotubes, metal oxide nanoparticles, zero-valent metal nanoparticles and chitosan nanocomposites have been used to effectively remove pollutants such as heavy metals, inorganic anions, dyes, pesticides, halogenated organics, tetracycline antibiotics and dorzolamide (Lu *et al.*, 2016; Basheer, 2018; Singh *et al.*, 2018).

## 1.2 Research Problem

Over the past years, nanotechnology has played an outstanding and superior role in numerous environmental applications (Thavasi *et al.*, 2008; Ali, 2012; Padil *et al.*, 2016). Nanomaterials have small sizes and large surface areas, which are beneficial for adsorption in water and wastewater treatment (Qu *et al.*, 2013; Lu *et al.*, 2016; Khan *et al.*, 2017). According to Roksana (2016), nanomaterials can be used at any stage in the water treatment process for removing heavy metals. However, though efficient, nanomaterials such as carbon nanotubes and silver nanoparticles (AgNP) are expensive and may require further separation or filtration to remove the nanomaterials from the treated water. This is currently difficult to achieve (Camilli *et al.*, 2014; Roksana, 2016). Also, the small sizes of nanoparticles have made humans more susceptible to their toxicological effects (Ali, 2012; Khan *et al.*, 2017; Sahu and Hayes, 2017; Pietroiusti *et al.*, 2018). Therefore, if these materials are to form part of the contamination problem after the water treatment process, it will threaten nanomaterials' commercialisation for the purpose. Nevertheless, these issues can be addressed if the nanomaterials are incorporated into a matrix, which could be easily separated from treated water.

In nanoparticle production, synthetic capping and reducing agents are used, which are usually detrimental to animal and plant life and the environment (Duan *et al.*, 2015; Saif *et al.*, 2016). This has necessitated the need to use green approaches in synthesising nanomaterials. Green nanotechnological approaches employ methods in which materials used are: from natural sources which are readily available, non-hazardous, biodegradable and energy-efficient (Iravani, 2011; Duan *et al.*, 2015; Padil *et al.*, 2016). Various authors have suggested biopolymers such as natural rubber (NR) (Cabrera *et al.*, 2013; Danna *et al.*, 2016), leaf extracts (Saif *et al.*, 2016; Mohammadi *et al.*, 2019) and fruit extracts (Moldovan *et al.*, 2016) as good reducing and stabilisation agents for nanoparticle synthesis.

Natural rubber latex (NRL) is an inexpensive and environmentally friendly colloidal suspension extracted from *Hevea brasiliensis* and is widely cultivated in West Africa (including Ghana) (Venkatachalam *et al.*, 2013). Nanoparticles such as AgNP and iron (II, III) oxide nanoparticles ( $\text{Fe}_3\text{O}_4$ ) have been synthesised using NRL (Guidelli *et al.*, 2011; Arsalani *et al.*, 2018). Silver nanoparticles, in particular, have been used to remove heavy metals such as mercury (Hg) and cadmium (Cd) from aqueous solutions (Al-Qahtani, 2017; Ganzagh *et al.*, 2016). These heavy metals are bioaccumulative, non-biodegradable, highly

toxic, and unnecessary for any normal body function and, therefore, must be removed from contaminated waters before discharge (Park and Zheng, 2012; Mahmood *et al.*, 2019).

Though AgNP are beneficial in removing Hg and Cd<sup>2+</sup> from wastewater, excess silver (Ag) in drinking water may lead to argyria (Anon., 2011a). Nanomaterials such as AgNP forming part of the contamination problem after water treatment could be reduced if the nanoparticles are encapsulated in a matrix. Encapsulating nanoparticles in a film may reduce the surface area-to-volume ratio of the nanoparticle. However, due to the porous nature of fibres, when nanoparticles are incorporated in the fibre matrix, a relatively higher number of nanoparticles are exposed, resulting in a higher surface area-to-volume ratio when compared to nanoparticles incorporated into a non-porous film. A higher surface area-to-volume ratio is a desired characteristic in contaminant removal in water treatment by adsorption.

Nanoparticles can be directly incorporated into fibres by methods such as electrospinning (Zhang and Yu, 2014). However, electrospinning rubber requires using solvents such as chloroform, dimethylformamide (DMF), tetrahydrofuran (THF) and toluene which are all harmful (Costa *et al.*, 2013; Hasanuddin *et al.*, 2017). In the latex form, other polymers such as chitosan, polycaprolactone and polylactic acid could be added to natural rubber to increase its electrospinnability. However, these polymers also require hazardous solvents such as formic acid, acetone and acetic acid to dissolve (Costa *et al.*, 2013; Riyajan and Sukhlaaied, 2015; Cosme *et al.*, 2016). Alternatively, polyvinyl alcohol (PVA), a biopolymer, could be mixed with NRL and electrospun, using water as its solvent. Nevertheless, 2-[4-(2,4,4-trimethylpentan-2-yl)phenoxy]ethanol (Triton-X 100), which is also hazardous, is added to PVA/NRL mixtures to improve fibre morphology (Anon., 2018; Panichpakdee *et al.*, 2019; Luo *et al.*, 2020).

Notwithstanding these findings, synthesising AgNP and incorporating the nanoparticles into an electrospun NRL fibre without using harmful solvents and reagents, and using this biopolymer to provide a synergistic effect in removing mixed heavy metals from wastewater has not been investigated. Therefore, this research seeks to produce AgNP incorporated into a fibre matrix through a green approach and determine its efficiency in removing contaminants (Hg and Cd) from wastewater without releasing excess Ag.

### 1.3 Objectives of the Research

The aim of this research was to produce green AgNP in PVA/NRL (AgNP-PVA/NRL) nanofiber composite to remove heavy metals from wastewater.

The objectives of the research were to:

- a) Establish the optimum ratio of NRL to PVA for nanofibre fabrication, nanoparticle synthesis and aqueous application (water treatment) without using harmful solvents
- b) Investigate the possibility of synthesising AgNP in PVA/NRL nanofibre composite matrix via electrospinning
- c) Investigate the possibility of synthesised AgNP-PVA/NRL nanofibre composite to remove  $\text{Cd}^{2+}$  and Hg from water; and
- d) Establish the optimum conditions such as pH and contact time at which AgNP-PVA/NRL nanofibre composite can remove  $\text{Cd}^{2+}$  and Hg from an aqueous solution.

In order to achieve the outlined aim and objectives, the following questions were answered:

- Can NRL and PVA mixture be electrospun with only water as its solvent?
- What is the best ratio of PVA/NRL to be electrospun for aqueous process application to prevent excess dissolution of the fibre composite?
- Can AgNP be successfully synthesised in PVA/NRL composite using electrospinning without adding other reducing and capping agents?
- How does the concentration of AgNP precursor affect AgNP distribution in the nanofibre composite?
- Can AgNP incorporated in PVA/NRL nanofibre composite efficiently remove  $\text{Cd}^{2+}$  and Hg from wastewater?
- At what optimum pH and contact time can AgNP-PVA/NRL nanofibre composite remove  $\text{Cd}^{2+}$  and Hg from wastewater?
- Can the synthesised AgNP-PVA/NRL nanofibre composite remove  $\text{Cd}^{2+}$  and Hg simultaneously from wastewater in competitive adsorption?

### 1.4 Methods Used

Firstly, fresh NRL was collected, characterised and electrospayed, and the best conditions used to produce the NRL film were adopted to electrospin PVA/NRL nanofibres of varying

ratios. Next, the electrospun PVA/NRL nanofibre composites were characterised (morphology, surface functionalisation and weight loss test) to determine the best ratio of PVA to NRL that can be used in aqueous applications. After this, varying concentrations of a precursor for AgNP synthesis were added to the solution whose PVA/NRL nanofibre composite was selected as a matrix or substrate, and these were electrospun. The synthesised AgNP-PVA/NRL nanofibre composites were characterised (morphology, elemental composition, crystallography, surface functionalisation and point of zero charge) prior to single-component adsorption studies.

For contaminant removal, the AgNP-PVA/NRL nanofibre composites were investigated for their efficiency in removing  $\text{Cd}^{2+}$  and Hg from separate aqueous solutions. This was done by determining the optimum conditions (pH, contact time and initial concentration) at which AgNP-PVA/NRL nanofibre composites could remove maximum concentration of  $\text{Cd}^{2+}$  and Hg from the aqueous solution. Based on the optimum conditions determined in the single-component adsorption studies, the efficiencies of AgNP-PVA/NRL nanofibre composites to remove  $\text{Cd}^{2+}$  and Hg concurrently from a single aqueous solution were then investigated.

## 1.5 Organisation of Thesis

### Chapter 1: Introduction

This chapter outlines the background of the research, problem statement, research objectives, questions asked in addressing the objectives, and methods used to achieve the objectives.

### Chapter 2: Literature Review

This chapter reviews the basic knowledge of NRL and previous research on nanoparticle application in water treatment. The chapter also discusses the theory behind the formulation of nanoparticles, why electrospinning is an appropriate technique to consider in water treatment and why nanoparticle-nanofibre composite is a good alternative in water treatment.

### Chapter 3: Materials and Method

This chapter highlights the materials and methods used in sampling and characterising the NRL; electrospinning NRL, PVA and PVA/NRL solutions; characterising PVA/NRL

nanofibres; and synthesising and characterising AgNP-PVA/NRL nanofibre composites. The chapter also discusses methods used in the adsorption studies of AgNP-PVA/NRL nanofibre composites for Hg and Cd<sup>2+</sup> contaminant removal.

#### Chapter 4: Green Synthesis and Characterisation of Electrospun PVA/NRL Nanofibre for Nanoparticle Loading and Application in Aqueous Solutions

This chapter highlights the characteristics of NRL used in the study. The chapter also discusses the characteristics of electrospun NRL and the optimum parameters for electrospinning PVA/NRL solutions without using harmful solvents. Finally, the chapter captures the characteristics of electrospun PVA/NRL nanofibres in order to determine the matrix for AgNP synthesis.

#### Chapter 5: Green Synthesis and Characterisation of Silver Nanoparticles in PVA/NRL Nanofibre Composite (AgNP-PVA/NRL) for Adsorption Studies

This chapter presents characteristics of the synthesised AgNP-PVA/NRL nanofibre composites. The characterisation includes morphological studies, elemental composition, crystallography, surface functionalisation and point of zero charge. Chapter 5 also explains the possible reasons for the differences in characteristics of the two synthesised AgNP-PVA/NRL nanofibre composites.

#### Chapter 6: Sorption of Mercury and Cadmium from Aqueous Solutions Using Synthesised AgNP-PVA/NRL Nanofibre Composites

This chapter highlights the findings of the single-component adsorption studies, where the synthesised AgNP-PVA/NRL nanofibre composites were used to adsorb Hg and Cd<sup>2+</sup> in separate aqueous solutions. The chapter outlines the optimum conditions (pH, contact time and initial concentration) at which the AgNP-PVA/NRL nanofibre composites could efficiently remove Hg and Cd<sup>2+</sup> from separate aqueous solutions. Possible reasons for the differences in adsorption mechanisms and kinetics for Hg and Cd<sup>2+</sup> adsorption by the nanofibre composites are also captured in this chapter.

#### Chapter 7: Competitive Adsorption of Mercury and Cadmium from Aqueous Solution Using AgNP-PVA/NRL Nanofibre Composites



In this chapter, the synthesised AgNP-PVA/NRL nanofibre composites and other mixtures of AgNP-PVA/NRL nanofibre composites were used to remove Hg and Cd<sup>2+</sup> from an aqueous solution concurrently. The chapter discusses the removal efficiency of the nanofibre composites in the binary system and the possible reasons for the detected deficiencies. Chapter 7 also discusses the amount of Ag released into the solution after adsorption.

#### Chapter 8: Conclusions and Recommendations

This chapter summarises the findings of this research and its contribution to literature on nanoparticles and nanofibres' use in water treatment. The chapter also suggests recommendations to enhance and understand biosynthesised AgNPs in an electrospun matrix for water treatment.



## CHAPTER 2

### LITERATURE REVIEW

#### 2.1 Heavy Metals Contamination in Water

Access to potable water is a basic need for all humans. However, there is limited access to potable water due to over-exploitation by industries, rapid population growth and climate change, leading to long-term droughts. Also, contaminants like heavy metals have made potable water expensive due to different methods or materials required to remove different contaminants (Azimi *et al.*, 2017). Some heavy metals such as cobalt (Co), copper (Cu), iron (Fe), manganese (Mn), molybdenum (Mo) and zinc (Zn) are vital for normal body functioning at the right concentration (Zoroddu *et al.*, 2019). Contrarily, other heavy metals found in water, like Hg and Cd, have no known biological function for the human body but can cause adverse health effects even at low concentrations (Park and Zheng, 2012; Mahmood *et al.*, 2019). Mercury and Cd in water can therefore pose a threat to humans.

##### 2.1.1 Mercury (Hg) in Water

###### *Sources of Hg*

Mercury is a pervasive heavy metal that is highly toxic, non-biodegradable and bioaccumulative. The metal is liquid at room temperature and exists as elemental or metallic Hg (Hg<sup>0</sup>), inorganic Hg (mercuric (Hg<sup>+</sup>) and mercurous (Hg<sup>2+</sup>) salts) and organic Hg (methylmercury (CH<sub>3</sub>Hg<sup>+</sup>), ethyl mercury (C<sub>2</sub>H<sub>5</sub>Hg<sup>+</sup>) and similar groups) in the environment (Bernhoft, 2012; Park and Zheng, 2012; Balali-Mood *et al.*, 2021).

Mercury is released as vapour (elemental Hg) into the atmosphere through re-evaporation of previously deposited Hg vapour, volcanic processes, and degassing of mineral deposits in aquatic systems and terrestrial systems (Anon., 2000a; Gworek *et al.*, 2016). This heavy metal is frequently employed in scientific instruments, electrical equipment and industries because of its reflective surface, high density, high electrical conductivity and low viscosity (Scoullos *et al.*, 2001; Park and Zheng, 2012). Also, since artisanal and small-scale gold mining is largely unregulated (Esdaile and Chalker, 2018), Hg is extensively used in this sector and has significantly contributed to anthropogenically released Hg in the environment. In artisanal and small-scale gold mining, Hg is added to gold in sediments, bonds with the gold, and forms an amalgam. The gold is separated by heating this amalgam

either on the field or at mine shops. Heating causes Hg to evaporate into the atmosphere. About 60% of Hg utilised in artisanal and small-scale gold mining is directly released into the environment, which in the long run accumulates in rivers, lakes, sediments and soils, and later may seep into groundwaters (Diringer *et al.*, 2015; Esdaile and Chalker, 2018).

### *Hg in the Food Chain*

Mercury is methylated to  $\text{CH}_3\text{Hg}^+$  by algae and bacteria when released into water bodies (Tchounwou *et al.*, 2012). Bacteria in the gut of fish can also methylate Hg (Anon., 2000a). The metal bioaccumulates in fishes and aquatic mammals, with predatory aquatic species at the highest trophic level having the highest concentration. Through this, humans are mostly exposed to organomercurials by consuming fish contaminated with Hg (Nielsen, 1992; Anon., 2000a). It is important to note that, since fish is an essential source of nutrition, primary exposure of humans to Hg can be limited by restricting Hg release or treating Hg-laden effluents, which in turn will limit methylation of Hg and its biomagnification in food web.

### *Negative Effects of Hg Contamination*

Due to the bioaccumulative nature of Hg, exposure to low concentrations is also deemed dangerous as humans later experience its chronic effects. Methylmercury is readily adsorbed into the gastrointestinal tract, distributed throughout the human body and can easily cross the placental and blood-brain barriers. The  $\text{CH}_3\text{Hg}^+$  can also accumulate in the liver, kidney and neurological tissues (Tchounwou *et al.*, 2012; Diringer *et al.*, 2015; Balali-Mood *et al.*, 2021). These may impair neurodevelopment, cognitive function, kidney function and motor skills (Diringer *et al.*, 2015). Severe Hg poisoning can also lead to the infamous Minamata disease, which affects the neurological system of humans (Bernhoft, 2012; Balali-Mood *et al.*, 2021).

According to the Ghana Standard Authority (GSA) and Environmental Protection Agency of the United States of America (US EPA), the concentration of Hg in drinking water should not exceed 0.001 mg/L and 0.002 mg/L, respectively (Anon., 2017; Anon., 2023a; Anon., 2023b). The guideline for inorganic Hg by World Health Organisation (WHO) is 0.006 mg/L (Anon., 2011a).

### 2.1.2 Cadmium (Cd) in Water

#### *Sources of Cd*

Cadmium is a silver-white metal which is toxic, non-biodegradable and bioaccumulative. This rare metal is naturally associated with sulphide ores of Zn, lead (Pb) and Cu (Anon., 2000b). Anthropogenically, Cd is released into the environment when used in industrial processes such as battery production, alloy production, inorganic pigments and electroplating (Tchounwou *et al.*, 2012; Colantonio and Kim, 2016). Other sources of groundwater, surface water and drinking water contamination by Cd are from the corrosion of galvanised water supply pipes and steel roofs, desorption from some plastic water supply pipes, municipal landfill leachates, runoff from the application of organic fertilisers and pesticides, and mining and smelting sites (Aoshima, 2016; Elkhatib *et al.*, 2016; Salehi *et al.*, 2017; Balali-Mood *et al.*, 2021). The main form of Cd in contaminated waters is Cd<sup>2+</sup> (Elkhatib *et al.*, 2016)

#### *Cd in the Food Chain*

The primary exposure of Cd<sup>2+</sup> to humans is through food consumption (Anon., 2011a). In humans, Cd<sup>2+</sup> has a biological half-life of about 10 to 33 years (Idrees *et al.*, 2018). Cadmium in water bodies may settle in sediments, whilst Cd-laden runoff and that used in irrigation may settle in soils (Balali-Mood *et al.*, 2021). The metal in soil and sediment is assimilated by plants such as grains, seeds, tubers and leafy vegetables (Aoshima, 2012; Tchounwou *et al.*, 2012; Aoshima, 2016). Rice, for instance, is a staple food for most African and Asian countries; therefore, it is inevitable for humans to consume Cd-laden foodstuff. Hence, Cd<sup>2+</sup> in the food chain can be controlled if Cd<sup>2+</sup> release in water is also controlled.

#### *Negative Effects of Cd Contamination*

Ingesting acute levels of Cd<sup>2+</sup> can lead to gastrointestinal tract erosion and hepatic and renal injuries (Tchounwou *et al.*, 2012). Chronic exposure to low concentrations of Cd<sup>2+</sup> is considered dangerous due to its bioaccumulative nature. After long-term exposure, Cd accumulated in the liver and kidney may result in renal tubular dysfunction. Consistent human exposure can also lead to the notorious *Itai-Itai* disease, which has characteristics of osteoporosis and osteomalacia accompanied by severe bone pain (Aoshima, 2016).

According to the GSA and US EPA, the concentration of Cd in drinking water should not exceed 0.003 mg/L and 0.005 mg/L, respectively (Anon., 2017; Anon., 2023b). The guideline for Cd in drinking water by World Health Organisation (WHO) is also 0.003 mg/L (Anon., 2011a).

## 2.2 Nanoparticles

Nanoparticles are particulates with at least one of its dimensions less than 100 nm (Khan *et al.*, 2017; Jeevanandam *et al.*, 2018), and nanotechnology refers to the engineering or manipulation of structures at the nanoscale (Ramsden, 2005; Ramsden, 2011). The fast-growing field of nanotechnology has paved the way for nanoparticle usage in several fields, including drug delivery, food processing and removal of water pollutants, among others (Al-Qahtani, 2017; Ealias and Saravankumar, 2017; Khan *et al.*, 2017). For example, in water treatment, nanoparticles have proven superior and efficient in removing heavy metals such as Hg and Cd from water via adsorption (Ganzagh *et al.*, 2016; Gargiulo *et al.*, 2017). However, though nanoparticles are beneficial in these fields, conventional methods and materials used for their synthesis have potential toxicity when released into the environment (Ariffin *et al.*, 2017; Pietroiusti *et al.*, 2018). This harmful effect has retarded the incorporation of nanoparticles into commercial-scale processes. As a result, developing efficient green methods for synthesising metal nanoparticles and their application has become a great concern to researchers.

### 2.2.1 Nanoparticles for Hg and Cd<sup>2+</sup> Contaminants Removal from Wastewater

Nanomaterials such as nanowastewater residue, silver nanoparticles (AgNP), silver-doped nanocomposites, and magnetite nanoparticles are used to remove Hg and Cd<sup>2+</sup> from wastewater. Table 2.1 shows some nanoparticles and nanocomposites used in removing Hg and Cd<sup>2+</sup> from wastewater.

From Table 2.1, it can be seen that AgNP or AgNP-based nanocomposites are used more often in removing Cd<sup>2+</sup> and Hg from aqueous solution due to its high efficiency in removing the contaminants and the few reagents required for its synthesis. However, similar to the other nanoparticles and nanocomposites, AgNP is plagued with the challenges of using toxic reagents and high temperatures needed for synthesis and, also, the extra effort required for AgNP separation after its use in water treatment. These challenges have piqued researchers' interest in seeking green methods for producing AgNP and a simple or easier method to

remove these nanoparticles from the treated water. It is also worth noting that though AgNP are sometimes incorporated in a silica matrix (Table 2.1), micro or ultrafiltration may still be needed to separate the nanocomposite from the treated water.



**Table 2.1 Some Nanoparticles and Nanocomposites Used for Removing Hg and Cd Contaminants from Wastewater**

Nanoparticle/ Nanocomposite	Metal Adsorbed	Advantage(s) of the Nanomaterial	Disadvantage(s) of the Nanomaterial	Reference
<i>Nanowastewater residue (residue from treating aluminium and iron salts)</i>	Cd <sup>2+</sup>	<ul style="list-style-type: none"> <li>Removal efficiency = 98.35%</li> </ul>	<ul style="list-style-type: none"> <li>Milling was the synthesis method, and this required high levels of energy for nanoparticle production</li> <li>Ultrafiltration which uses high pressure may be required to remove the nanoparticles after wastewater treatment</li> </ul>	(Elkhatib <i>et al.</i> , 2016)
<i>AgNP-nanomesoporous silica</i>	Hg	<ul style="list-style-type: none"> <li>Removal efficiency ~ 95%</li> </ul>	<ul style="list-style-type: none"> <li>A high temperature (up to 530 °C) is required for nanoparticle synthesis</li> <li>Microfiltration may be needed to separate the nanocomposite (particle size &gt; 5 µm) from the treated water</li> </ul>	(Ganzagh <i>et al.</i> , 2016)
<i>Silver/quartz nanoparticle</i>	Hg	<ul style="list-style-type: none"> <li>Removal efficiency = 96%</li> </ul>	<ul style="list-style-type: none"> <li>A high temperature (up to 350 °C) is required for nanoparticle synthesis</li> <li>Ultrafiltration may be required to remove the nanoparticles after wastewater treatment</li> </ul>	(El-Tawil <i>et al.</i> , 2019)

<i>Silver-doped synthetic ash-derived zeolites</i>	Hg	<ul style="list-style-type: none"> <li>Removal efficiency = 99%</li> </ul>	<ul style="list-style-type: none"> <li>Sodium borohydride (NaBH<sub>4</sub>), which is toxic, was used in AgNP synthesis</li> <li>A high temperature (up to 500 °C) is required for nanoparticle synthesis</li> <li>Microfiltration may be needed to separate the nanocomposite (particle size &gt; 5 µm) from the treated water</li> </ul>	(Tauanov <i>et al.</i> , 2018)
<i>Silver-doped synthetic sodalite nanocomposite</i>	Hg	<ul style="list-style-type: none"> <li>Removal efficiency = 98.65%</li> </ul>	<ul style="list-style-type: none"> <li>Sodium borohydride (NaBH<sub>4</sub>), which is toxic, was used in AgNP synthesis</li> <li>A high temperature (up to 500 °C) is required for nanoparticle synthesis</li> <li>Microfiltration may be needed to separate the nanocomposite (particle size &gt; 5 µm) from the treated water</li> </ul>	(Tauanov <i>et al.</i> , 2019)
<i>AgNP synthesised using Ficus benjamina</i>	Cd <sup>2+</sup>	<ul style="list-style-type: none"> <li>Removal efficiency = 85%</li> <li>AgNP were synthesised at 25 °C</li> </ul>	<ul style="list-style-type: none"> <li>Ultrafiltration will be required to remove the nanoparticles after wastewater treatment</li> </ul>	(Al-Qahtani, 2017)

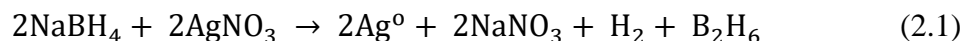


<i>Colloidal carbon-based nanoparticle</i>	Cd <sup>2+</sup>	<ul style="list-style-type: none"> <li>• Silica-supported hydrophilic nanoparticles have a wide pH range for adsorption</li> </ul>	<ul style="list-style-type: none"> <li>• Good colloidal stability of hydrophilic nanoparticles inhibits the nanoparticles' filterability at pH &gt; 2.5</li> <li>• Silica-supported hydrophilic nanoparticles may require separation via micro or ultrafiltration from the treated water</li> </ul>	(Gargiulo <i>et al.</i> , 2017)
<i>Magnetite nanoparticle</i>	Hg	<ul style="list-style-type: none"> <li>• Removal efficiency = 74 - 85%</li> </ul>	<ul style="list-style-type: none"> <li>• 3-aminopropyltriethoxysilane used in magnetite nanoparticle synthesis and functionalisation is toxic</li> <li>• Multiple reagents are required for nanoparticle synthesis and functionalisation compared to AgNP synthesis</li> </ul>	(Marimón-Bolívar <i>et al.</i> , 2018)
<i>Magnetite-sulfonated nanoparticle</i>	Cd <sup>2+</sup>	<ul style="list-style-type: none"> <li>• Adsorption occurs at pH 7 – 10</li> <li>• The nanoparticle is reusable</li> </ul>	<ul style="list-style-type: none"> <li>• Ethylenediamine, mercaptopropyl trimethoxysilane and toluene used in nanoparticle synthesis are toxic to the environment.</li> </ul>	(Chen <i>et al.</i> , 2017a)

## 2.2.2 Silver Nanoparticle (AgNP) Synthesis

### *Non-Green Synthesis of AgNP*

In nanoparticle synthesis, a reducing and capping agent (stabilising agent) is required to convert the Ag precursor to AgNP. The precursor used is usually an Ag salt, such as silver nitrate (AgNO<sub>3</sub>) and silver perchlorate (AgClO<sub>4</sub>) (Henglein, 1998; Desai *et al.*, 2012). Non-green synthesised AgNP utilises NaBH<sub>4</sub>, which is highly toxic, as the principal reducing agent for Ag (Desai *et al.*, 2012; Li *et al.*, 2012; Mavani and Shah, 2013; Tauanov *et al.*, 2018; Tauanov *et al.*, 2019). The reaction is as presented in Equation (2.1) (Mavani and Shah, 2013).



Another highly toxic reducing agent in AgNP synthesis is the hydrazine hydrates (N<sub>2</sub>H<sub>4</sub>·xH<sub>2</sub>O) (Cinar *et al.*, 2011; Nakamura *et al.*, 2011; Gurusamy *et al.*, 2016). In other instances, the AgNP is green synthesised but incorporated into a non-renewable matrix such as silica (Ganzagh *et al.*, 2016; El-Tawil *et al.*, 2019). Other reactions may require high temperatures (up to 530 °C), rendering the synthesis process non-green (Ganzagh *et al.*, 2016; Tauanov *et al.*, 2018; El-Tawil *et al.*, 2019; Tauanov *et al.*, 2019). All the aforementioned methods are not entirely environmentally friendly, hence the need to search for green methods, which involve green reducing agents, green capping agents, low temperatures for AgNP synthesis and incorporating these green nanoparticles into green matrices.

### *Green Synthesis of AgNP*

Microorganisms, plants and plant extracts have shown great potential in forming nanoparticles (Iravani, 2011; Makarov *et al.*, 2014). In addition, plant extracts such as proteins, polysaccharides, and organic acids play vital roles in reducing metal ions and serving as stabilising agents (Henglein and Giersig, 1999; Guidelli *et al.*, 2011; Desai *et al.*, 2012; Chowdhury *et al.*, 2014; Mohapatra *et al.*, 2015; Siddiqi *et al.*, 2018).

Abu Bakar *et al.* (2007), for instance, used the cream fraction of centrifuged natural rubber latex (NRL) to synthesise AgNP. The authors added AgNO<sub>3</sub> to the diluted cream fraction of NRL, which was cast into a film at 50 °C. The final film was later exposed to ultraviolet

(UV) light. The authors reported that proteins in the NRL resulted in AgNP growth and stabilisation, whilst UV exposure caused the reduction of silver ions ( $\text{Ag}^+$ ). Danna *et al.* (2016) also synthesised AgNP using natural rubber. However, the NRL used was annealed, and the resulting film (natural rubber) was placed in an  $\text{AgNO}_3$  solution at 80 °C. The authors reported that proteins in the natural rubber must have reduced  $\text{Ag}^+$  to  $\text{Ag}^0$  (Danna *et al.*, 2016). Guidelli *et al.* (2011) also used NRL to synthesise AgNP. These authors diluted the centrifuged NRL, added  $\text{AgNO}_3$  solution and the resultant solution was heated in a water bath at 100 °C, yielding a yellow solution, which shows AgNP had formed. The authors then proposed that amine groups must have reduced the  $\text{Ag}^+$  and *cis*-isoprene of NRL must have stabilised the nanoparticles (Guidelli *et al.*, 2011).

Other researchers such as Al-Qahtani (2017), Moldovan *et al.* (2016) and Kyrychenko *et al.* (2017) used *Ficus benjamina* leaves extract, *Sambucus nigra* L. fruits extract and polyvinyl alcohol (PVA) to synthesise AgNP. Al-Qahtani (2017) suggested that flavonoids, polyphenols and proteins present in *Ficus benjamina* leaves extract reduced the  $\text{Ag}^+$  to  $\text{Ag}^0$  and Moldovan *et al.* (2016) also proposed that the hydroxyl and carbonyl groups of flavonoids in *Sambucus nigra* L. fruits extract reduced  $\text{Ag}^+$  to  $\text{Ag}^0$ . Using computational studies and simulations, Kyrychenko *et al.* (2017) found that PVA forms a water protecting coating around AgNP, which is further stabilised by hydrogen bonds. All the aforementioned works shows that AgNP can be produced using green methods or green nanotechnology.

### 2.2.3 Negative Impact of Using Nanoparticles in Water Treatment

Using green nanotechnological methods to generate nanoparticles is an eco-friendly alternative. However, its application may lead to nanotoxicological effects, which have raised concerns from stakeholders. The advantages of nanoparticles include their small size (< 100 nm), larger surface area, high reactivity and aggregation. However, these could become harmful factors as these characteristics can induce undesirable cellular toxic and detrimental consequences, unusual in their bulk counterparts (Khan *et al.*, 2017). Skin absorption, inhalation and ingestion are the three common pathways through which nanoparticles enter the human body. Upon entering the bloodstream, nanoparticles can travel to other organs of the body easily (Ali, 2012; Sahu and Hayes, 2017; Pietroiusti *et al.*, 2018). Though literature on the cytotoxicity, hepatotoxicity and nephrotoxicity of

nanomaterials is limited, studies have shown that nanoparticles are potential cytotoxins, hepatotoxins and nephrotoxins (Sahu and Hayes, 2017).

Silver nanoparticles, for instance, are extensively used in water treatment. However, separating these AgNP after water purification may require huge investments in processes such as nanofiltration (Roksana, 2016). In addition, when consumed, excess Ag in treated water can cause generalised or localised argyria, a discolouration of the dermis and other organs to a blue-grey or slate-grey hue (Kim *et al.*, 2009; Chung *et al.*, 2010; Han *et al.*, 2011). Though argyria is benign, it causes social discomfort because the victims or patients are cognisant of the change in skin colour, causing them to withdraw from society.

#### 2.2.4 Potential Method(s) of Minimising the Toxicological Effects of Nanoparticles in Water Treatment

Spending great investments to treat water (separate AgNP from treated water) after wastewater treatment using AgNP is a potential risk hindering this nanoparticle's commercialisation (Roksana, 2016). Incorporating the nanoparticles in a matrix can minimise the risk of having AgNP in the treated water. Matrices such as silica/quartz, sodalite and fly ash, among others, have been studied by researchers who seek to reduce AgNP concentration in treated water (Ganzagh *et al.*, 2016; Tauanov *et al.*, 2018; El-Tawil *et al.*, 2019; Tauanov *et al.*, 2019). However, the disadvantage of the aforementioned matrices is that these matrices are either micro or nanoparticles, which may require micro or ultrafiltration for separation. This also requires huge investments. In addition, although these matrices are benign, these materials are not biodegradable. Hence, these matrices are not entirely green to be used in water treatment.

Danna *et al.* (2016) synthesised AgNP onto a biodegradable matrix, natural rubber; however, the synthesis was done on the surface of a flat film. Since the natural rubber film is non-porous, there was relatively limited surface area for AgNP growth compared to its porous counterpart. Again, if this flat film is to be used in water treatment, there is the likelihood that most of the AgNP will be washed into the treated water, rendering the purpose of incorporating the AgNP into that matrix illogical. In view of that, it would be rather beneficial to incorporate the AgNP in a porous matrix, such as nanofibres, near the surface or far within the matrix. According to Kipling (1965), the specific surface area of an adsorbent can be increased by increasing its porosity, which will subsequently magnify

selective adsorption. The porous matrix will also have a relatively higher surface area for AgNP growth which will subsequently be beneficial in water treatment processes such as contaminant removal via adsorption.

## 2.3 Nanofibres

### 2.3.1 Nanofibre Fabrication

Nanofibres are thread-like materials with fibre width of less than 500 nm (Xue *et al.*, 2019; Yamini and Begum, 2020). These fibres are flexible, stable, have high porosity and a small fibre-to-fibre distance, making them essential in water treatment, tissue engineering, and wound dressing (Ramakrishna *et al.*, 2005; Padil *et al.*, 2016). Polymeric nanofibres can be produced through phase separation, template synthesis, drawing or electrospinning. Electrospinning is the most preferred method for nanofibre fabrication because it is scalable, repeatable, cost-efficient, and convenient. Also, fibre diameter can be controlled, and long fibres can be produced during electrospinning (Ramakrishna *et al.*, 2005).

### 2.3.2 Electrospinning

Electrospinning is an electrohydrodynamic process where a liquid is charged at a high voltage such that the ejected liquid stretches and dries during flight, forming ultrafine fibres (Xue *et al.*, 2019). A typical electrospinning device features a syringe pump, spinneret, collector and high-voltage power supply, as shown in Figure 2.1. The liquid's stretching is possible due to the fluid being electrically charged. This charged liquid features a common charge which repels each other, breaking the surface tension of the liquid droplet and deforming it into a Taylor cone. As a result, a straight jet of the electrified liquid stretches out from the apex of the Taylor cone. The viscoelastic force and surface tension impair the jet's acceleration, causing the jet to move in a whipping motion with a gradual reduction in the jet's diameter. This motion is referred to as bending instability, and the thin jet finally solidifies into a nanofibre (Reneker and Yarin, 2008; Xue *et al.*, 2019). However, electrospinning will occur if the liquid droplet deforms into an ellipsoidal shape instead of a Taylor cone with two jets, known as Rayleigh's jet.

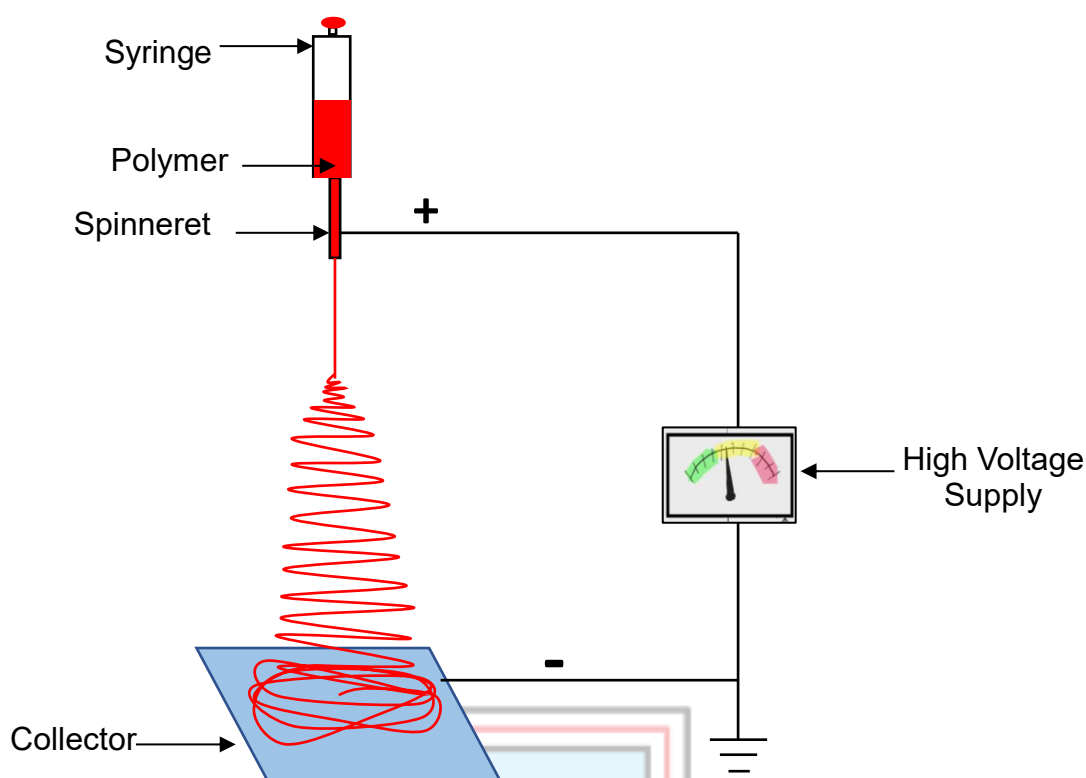


**Figure 2.1 Schematic Diagram of a Basic Electrospinning Unit**

Electrospraying is another electrohydrodynamic process that follows a similar principle as electrospinning, but in electrospraying, the jet breaks up into droplets instead of fibres (Azarian and Boochathum, 2018; Xue *et al.*, 2019). A higher voltage is required to overcome surface tension in order for electrospinning to occur.

### *Electrospinning Parameters*

Several parameters come into play in achieving electrospun fibres' desired morphology and diameter. These parameters are grouped into polymer solution parameters (viscosity, conductivity and surface tension), ambient parameters (temperature, air velocity in the chamber and humidity) and processing parameters (flow rate, applied voltage and distance between the tip and collector) (Doshi and Reneker, 1995; Huang *et al.*, 2003; Ramakrishna *et al.*, 2005).

*Viscosity:* Viscosity is a significant solution parameter that regulates a solution's or melt's spinnability and the morphology of the resulting fibre. Viscosity also determines whether a solution will be electrosprayed or electrospun (Xue *et al.*, 2019). Low viscosity causes the electrified jet to break into beads (electrospraying) or form beaded fibres. Beads form due to the lower polymer chain entanglement at lower viscosities. On the other hand, higher

viscosity is associated with higher polymer chain entanglement; therefore, the electrified jet can be maintained, resulting in smoother and continuous fibres (Ramakrishna *et al.*, 2005; Husain *et al.*, 2016). From Simons (1966) patent, it was also discovered that spinnable solutions with relatively lower viscosity produced fine but shorter fibres, whilst relatively higher viscosity solutions produced coarse but continuous fibres.

Furthermore, the viscosity of a solution is proportional to its polymer concentration. A review by Shi *et al.* (2015) stated that a decrease in polymer concentration would reduce the fibre's diameter. Therefore, determining the optimum concentration for one's desired fibre diameter is necessary. It is also worth noting that when the viscosity is too high, it will be difficult ejecting the solution from the spinneret due to the cohesive forces of the solution (Huang *et al.*, 2003; Xue *et al.*, 2019).

*Conductivity:* Electrical conductivity also influences fibre morphology. It is impossible to electrospin zero conducting solutions for their inability to conduct charges from within the fluid to the surface. Moreover, stretching the solution is possible because of the repulsion of charges at the surface (Ramakrishna *et al.*, 2005; Angamma and Jayaram, 2011). An increase in conductivity increases the fluid's net charge density, which has been reported to reduce the number of bead formations in electrospun fibres and reduce fibre diameter (Kim *et al.*, 2005).

*Surface Tension:* Electrospinning can occur if the voltage is high enough to generate enough electrostatic repulsion to overpower the fluid's surface tension. As the jet stretches, surface tension may cause the jet to break into droplets resulting in electrospraying (Ramakrishna *et al.*, 2005; Xue *et al.*, 2019). However, when temperature increases, the fluid's molecules gain more energy to move, reducing the magnitude of the cohesive forces at the surface. This, in turn, reduces surface tension, making the fluid more electrospinnable. Nevertheless, methane/nonane mixtures contradict this principle; their surface tension increases with increasing temperature (Ramakrishna *et al.*, 2005).

*Applied Voltage:* The high voltage applied is one of the main elements that initiate electrospinning. During jet initiation, the high voltage causes the drop of solution at the tip of the spinneret to deform into a Taylor Cone (Ramakrishna *et al.*, 2005). In most cases, increasing the applied voltage results in greater stretching of the solution, favouring the production of a relatively smaller fibre diameter (Ramakrishna *et al.*, 2005; Shi *et al.*, 2015;

Xue *et al.*, 2019). On the contrary, it has been reported that higher voltages may cause bead formation and even changes in bead shape. Higher voltages cause the Taylor Cone to shrink back into the spinneret, causing jet instability and increasing fibre diameter and bead density (Deitzel *et al.*, 2001; Zong *et al.*, 2002). Krishnappa *et al.* (2003) even reported that increasing the applied voltage increases bead density, and the beads eventually combine to form thicker fibres.

*Polymer Flow Rate and Distance Between Spinneret Tip and Collector:* The flow rate of a polymer solution affects the morphology and diameter of the electrospun fibres. A high flow rate may result in larger fibre diameters and bead formation since there is not enough time for the solvent to completely evaporate (Shi *et al.*, 2015; Xue *et al.*, 2019). This is because a greater volume of the polymer solution is mostly drawn from the spinneret tip at a particular time (Ramakrishna *et al.*, 2005). Efficient solvent evaporation requires a minimum distance between the spinneret tip and the collector. Thinner fibres are produced when wider distances are used. However, relatively shorter or longer distances may yield beads (Shi *et al.*, 2015; Xue *et al.*, 2019).

Generally, the interplay and optimisation of all electrospinning parameters will yield the researcher's desired fibre diameter (Xue *et al.*, 2019). This optimisation also helps in controlling bead formation. Polymers such as NRL and PVA can be electrospun into nanofibres.

## 2.4 Natural Rubber Latex (NRL)

### 2.4.1 Overview, Sources and Uses

Natural rubber latex is a colloidal suspension extracted from *Hevea brasiliensis* (para rubber) (Rippel and Galembeck, 2009; Sakdapipanich and Rojruthai, 2012; Arsalani *et al.*, 2018; Rooshenass *et al.*, 2018). The biopolymer is renewable, inexpensive and environmentally friendly. Natural rubber is an elastomer that is essential in most industries worldwide. The rubber is utilised in products such as toys, gardening tools, medical gloves, medical devices, and car and aeroplane tyres, among others. Although rubber can be synthesised in the laboratory, natural rubber cannot be replaced by its synthetic counterpart in some applications. This is due to its unique properties such as exceptional elasticity, resistance to abrasion, pliability at low temperatures and insulating properties (Rippel and Galembeck, 2009; Arias and van Dijk, 2019).



Natural rubber can be obtained from the latices of over 2 500 plant species, but the latex from *H. brasiliensis* is the sole source of commercially relevant latex because of its high rubber yield. The *Hevea* tree is extensively grown in southeast Asia and part of Africa. In Africa, Ghana (Western Region) is one of the major cultivators of *H. brasiliensis* (Haque *et al.*, 1995; Mooibroek and Cornish, 2000; Ho, 2013; Venkatachalam *et al.*, 2013). Rubber tapping is done once every 2-3 days after 6-7 years of *Hevea* tree growth, and this is done for nine months each year for about 25 tapping years (Omo-Ikerodah *et al.*, 2009; Sakdapipanich and Rojruthai, 2012). Again NRL from *H. brasiliensis* is preferred because, unlike para rubber, rubber from *Parthenium argentatum* Gray (guayule) is produced only during winter when the shrubs experience cold temperatures (Stonebloom and Scheller, 2019). Rubber from *Taraxacum kok-saghyz* (Russian dandelion) contains more allergenic proteins, making it inappropriate in applications where several human contacts may be possible (van Beilen and Poirier, 2007; Arias and van Dijk, 2019; Nowicki *et al.*, 2019).

The latex from *H. brasiliensis* contains 30-45% rubber component (*cis*-1,4-poly isoprene), often referred to as Dry Rubber Content (DRC) and about 5% non-rubber component (Borges *et al.*, 2014; Arsalani *et al.*, 2018). The structural formula of *cis*-1,4-poly isoprene is presented in Figure 2.2. The non-rubber components include carbohydrates, lipids, proteins and inorganics. Total solid content (TSC), which is always higher than DRC, is the total of rubber and non-rubber components (Rippel and Galembeck, 2009; Ho, 2013; Hwee, 2014). For producing foams, dipped goods and adhesives, NRL is concentrated, and before concentration, it is desirable to determine the latex's characteristics.

Metals such as Cu and Mn are crucial elements in the growth of the *Hevea* tree. However, in latex, Cu may catalyse aerial oxidation, causing discolouration of rubber products. The presence of Mn may also catalyse the degradation of the rubber (Duangthong *et al.*, 2017; Forrest, 2018). Therefore, these two metals are of great importance in determining the quality of NRL.

About 1-2% of NRL is of proteins. Proteins are responsible for the biosynthesis of rubber, colloidal stability and increased moisture absorption (Hwee, 2014). Though beneficial, some proteins in rubber have also been reported as allergenic. The severity of this allergy may range from mild to severe (Hwee, 2014; von der Gathen *et al.*, 2017; Cornish *et al.*, 2019; Orbecido *et al.*, 2019).

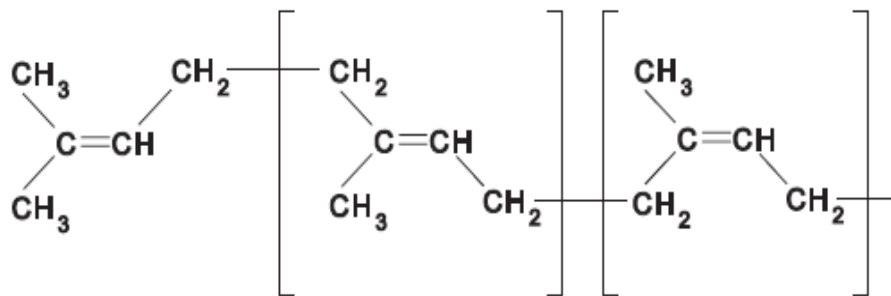


**Figure 2.2 Structural Formula of Natural Rubber (*cis*-1,4-polyisoprene) (Mooibroek and Cornish, 2000)**

#### 2.4.2 Nanoparticles Synthesised Using NRL

Over the past few years, several authors have used natural rubber in dry and latex forms to synthesise different nanoparticles. Existing literature shows that proteins, *cis*-isoprene and hydroxyl groups of NRL aid in the synthesis of nanoparticles such as AgNP, gold nanoparticles and magnetite nanoparticles (Abu Bakar *et al.*, 2007; Guidelli *et al.*, 2011; Cabrera *et al.*, 2013; Danna *et al.*, 2016; Arsalani *et al.*, 2018). However, these authors have not synthesised nanoparticles such as AgNP within an NRL nanofibre matrix.

### 2.5 Polyvinyl Alcohol (PVA)

#### 2.5.1 Overview, Source and Uses

Polyvinyl alcohol ( $[-\text{CH}_2\text{CHOH}-]_n$ ) is a non-toxic, synthetic biopolymer yielded from the hydrolysis of polyvinyl acetate ( $[\text{CH}_2\text{CH}(\text{O}_2\text{CCH}_3)]_n$ ). The structural formula of PVA is presented in Figure 2.3, and the major producers are Europe, the USA, Japan and China (Muppalaneni, 2013). This thermostable polymer has excellent mechanical, electrical and optical properties, making it ideal in several applications (Aslam *et al.*, 2018).

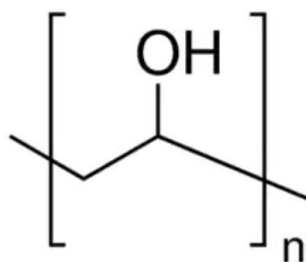


**Figure 2.3 Structural Formula of Polyvinyl Alcohol (Anon., 2023c)**

PVA is typically considered biocompatible and safe due to its stability and inertness. Orally administered PVA is considered relatively safe since the polymer is rapidly excreted and poorly adsorbed by the gastrointestinal system (Muppalaneni, 2013). Owing to the unique properties of PVA, such as safety, biocompatibility, film forming, non-carcinogenicity, adhesiveness and as an emulsifying agent, the polymer is used extensively in the biomedical, textiles, food, paper and pharmaceutical industries (Mansur *et al.*, 2008; Muppalaneni, 2013).

Different from its polymer counterparts, such as polylactic acid, chitosan and polycaprolactone, which require harmful solvents like acetic acid, acetone, formic acid and chloroform for their dissolution, PVA is water soluble. This makes PVA desirable in green electrospinning and also for increasing the electrospinnability of other polymers (Osei *et al.*, 2022).

#### 2.5.2 Nanoparticles Synthesised Using PVA

PVA effectively protects nanoparticles from agglomeration (Ghanipour and Dorrnian, 2013; Kyrychenko *et al.*, 2017). Nanoparticles such as Ag and gold (Au) have been successfully synthesised using PVA (Ghanipour and Dorrnian, 2013; Sagitha *et al.*, 2016; Chen *et al.*, 2017b; Kyrychenko *et al.*, 2017; Das and Das, 2019). Sagitha *et al.* (2016) also reported that the hydroxyl group of PVA aids the reduction of  $\text{Ag}^+$  to  $\text{Ag}^0$ . However, due to PVA's ability to completely dissolve in water, using this biopolymer as a matrix for nanoparticle synthesis and subsequently in water treatment seems irrational since all the nanoparticles will be released into the treated water. This, in turn, will defeat the purpose of creating an environmentally friendly alternative for nanoparticle use in water treatment.

### 2.6 Characterisation of Nanoparticles and Nanofibres

In nanotechnology, the characteristics of a biopolymer play a crucial role in nanoparticle synthesis. In addition, the physical nature (size, surface morphology and crystallography) and chemical composition (elemental composition, surface functionalisation) of nanomaterials (nanofibre and nanoparticles) play a vital role in its application.

### 2.6.1 Morphological Studies

#### *Scanning Electron Microscopy (SEM)*

The scanning electron microscope (SEM) is an equipment used to visualise the topography of structures, mostly at the microscopic and nanoscopic levels (Stokes, 2008; Bhatia, 2016). Figure 2.4 shows an SEM with an energy dispersive x-ray spectrometer (EDS). However, additional information can be obtained depending on the type of detector used.

The Everhart-Thornley (ET) detector, also known as the secondary electron (SE) detector, is commonly used to analyse a sample's topography and surface structure. A backscattered electron detector (BSD) which is also commonly used, aids in visualising the topography and compositional contrast of the sample. The SEM works based on a principle of the bombardment of a specimen with electrons (primary electrons) at a high electron voltage (~ 1 - 30 kV) and analysis of the resulting interaction between the emissions and the specimen (Vida-Simiti *et al.*, 2004; Anon., 2023d).



**Figure 2.4 Scanning Electron Microscope (SEM) Equipped With An Energy Dispersive X-Ray Spectrometer (EDS)**

The BSD detector detects backscattered primary electrons which have deflected from the sample after collision with the specimen's surface or a little beyond the specimen's surface (Stokes, 2008). On the other hand, the SE detector detects loosely bound electrons emitted from the conduction band for metals or loosely bound valence electrons in the valence band, which have been promoted to the conduction band after bombardment with primary electrons. These valence electrons become excited and experience inelastic collision and energy loss (Stokes, 2008).

A typical requirement for SEM imaging is high vacuum conditions, usually  $10^{-3} - 10^{-5}$  Pa or better. Another requirement is for the specimen to be conductive (Stokes, 2008). A less conductive specimen is coated with Au, palladium (Pd) or platinum (Pt), among others. This provides a conductive layer for efficient imaging. These requirements are to achieve a focused beam and prevent the build-up of negative charges, resulting in poor image quality (Stokes, 2008). The depth of information an SEM provides can be as high as 2 to 3 nm and has a magnification capability of about 5 – 1 000 000 times as that of Zeiss EVO MA 15 SEM (Anon., 2015; Mohammed and Abdullah, 2018).

With the aid of the SEM, most physical characteristics of nanofibres and nanoparticles can be visualised and may be measured. The size of nanoparticles and nanofibre diameters, the shape of nanoparticles and nanofibre strands, such as determining whether there are beads along the fibre strands and fibre-to-fibre or pore diameter can also be measured. Also, with the BSD detector giving a compositional contrast image, nanoparticles on nanofibres can be imaged if the elemental composition of the nanoparticles is different from the nanofibres.

#### *Transmission Electron Microscopy (TEM)*

The transmission electron microscope (TEM) works by a principle similar to the SEM. However, in TEM analysis, a higher electron voltage is required (~ 60 kV to 300 kV) (Anon., 2023d). Another requirement is for the specimen to be extremely thin (< 150 nm) to transmit electrons through the sample for detection, unlike in SEM. The extremely high voltage and extremely thin nature of samples enable the microscope to visualise inner structures of the specimen with a resolution as high as < 0.05 nm (Anon., 2023d). In summary, whilst an SEM is used to image the surface of samples, such as the morphology of nanofibres and nanoparticles on nanofibre surfaces, TEM would instead visualise the

internal structures, such as nanoparticles within nanofibres which would be obscured in SEM imaging.

### 2.6.2 Elemental Studies using Energy Dispersive X-Ray Spectroscopy (EDS)

SEM and TEM are usually equipped with an EDS for elemental analysis (Sarecka-Hujar *et al.*, 2017) (Figure 2.4). This technique is employed chiefly in detecting environmental pollution and in the biomedical fields (Scimeca *et al.*, 2018).

The EDS is a microanalytical technique based on generating characteristic x-rays that reveal the chemical elements of a sample. With the aid of a BSD detector which provides compositional contrast based on the elemental composition of the specimen, the EDS can be easily applied to areas of interest during analysis. The EDS detector shows mild-energy (1-20 kV) x-rays collected during analysis, displaying these energies as a spectrum (a histogram plot of a number of counts against x-ray energy). The energy of the resulting x-rays depends on the element's atomic number, and they are characteristic of the element from which the energies originate (Scimeca *et al.*, 2018). An element is identified by the position of a peak in the spectrum. The area beneath the peak represents the number of atoms of that element in the irradiated area. The spectrum provides both semi-qualitative and semi-quantitative information (Sarecka-Hujar *et al.*, 2017; Scimeca *et al.*, 2018). For example, in nanofibre-nanoparticle composites, the EDS aids in identifying the type of particles (elemental composition) present on or within the fibres. This helps analysts avoid mistakes such as attributing particles with different contrast (in BSD mode) as nanoparticles but may not have the elemental composition of the nanoparticles.

### 2.6.3 Surface Functionalisation using Fourier Transform – Infrared Spectroscopy (FT-IR)

Fourier Transform – Infrared spectroscopy (FT-IR) is one of the most suitable and time-saving methods for surface characterisation. Its spectra give information on molecular structure, molecular environment and the nature of bond between the surface and adsorbed molecules (Baraton *et al.*, 1996; Gerwert and Kötting, 2010).

To analyse a material, the surface is first heated under a dynamic vacuum for one or two hours. This process frees the surface from physisorbed and weakly chemisorbed species. (Baraton *et al.*, 1996). Molecular vibrational frequencies lie in the infrared spectrum (Berthomieu and Hienerwadel, 2009). Hence, when infrared radiations are subjected to a

specimen, characteristic infrared adsorption bands are produced, corresponding to fundamental vibrations of specific functional groups (Berthomieu and Hienerwadel, 2009; Nandiyanto *et al.*, 2019). These vibrational bands in FT-IR spectroscopy aid in determining the functional groups of a polymer which assist in reducing and stabilising nanoparticles.

#### 2.6.4 Crystallographic Studies using X-Ray Diffractometry (XRD)

X-ray diffractometry (XRD) is a technique used to determine the crystallographic size and orientation of a thin film or pulverised specimen (Sharma *et al.*, 2012). X-ray interacting with a crystalline substance produces a diffraction pattern. These diffraction patterns are compared to a database such as the International Centre Diffraction Data (ICDD) (Sharma *et al.*, 2012). This analysis is based on Bragg's law, which enables accurate crystal structure determination. The angle between the x-ray projection and detector is  $2\theta$ , where  $\theta$  is Bragg's angle. The intensity of the diffraction is usually plotted against  $2\theta$ , and the common wavelength used is  $1.54 \times 10^{-10}$  m (Cu  $K\alpha$  radiation). The average particle size can be calculated using the Debye-Scherrer formula (Equation 2.2) (Awwad and Salem, 2012; Sharma *et al.*, 2012; Yew *et al.*, 2016):

$$D = K \lambda / \beta \cos \theta \quad (2.2)$$

where, D = mean diameter of nanoparticles

K = Scherrer constant with a value from 0.9 to 1

$\lambda$  = wavelength of the x-ray radiation source

$\beta$  = full width of half-maximum value of XRD diffraction lines

$\theta$  = Bragg's angle

Though the Debye-Scherrer formula can be used to determine the particle size, this tends to be difficult when diffraction peaks of different crystal structures overlap. SEM, TEM, EDS, and FT-IR analysis may indicate the presence of a nanoparticle; however, it may be another compound with the same elemental composition and shape. Therefore, XRD analysis is conducted to confirm the existence of the nanoparticle of interest by investigating the nanoparticle's crystallographic structure.

## 2.7 Adsorption

Adsorption is the movement of ions or molecules of interest from one phase to another by condensing and concentrating on the surface of a second phase, which is usually a solid (Sawyer *et al.*, 2003). The material adsorbed from the first phase is called the adsorbate, and the second phase unto which the adsorbate concentrates is the adsorbent. Figure 2.5 presents some basic terms used in adsorption processes. Adsorption processes are utilised in numerous fields, such as in contaminant removal in wastewater treatment, drug adsorption in pharmacology and gold extraction in metallurgical studies.

There are three main types of adsorption processes, namely, physical adsorption (physisorption), chemical adsorption (chemisorption) and exchange or electrostatic adsorption (preferably referred to as electrostatic interaction or adsorption) (Sawyer *et al.*, 2003; Tran *et al.*, 2017).

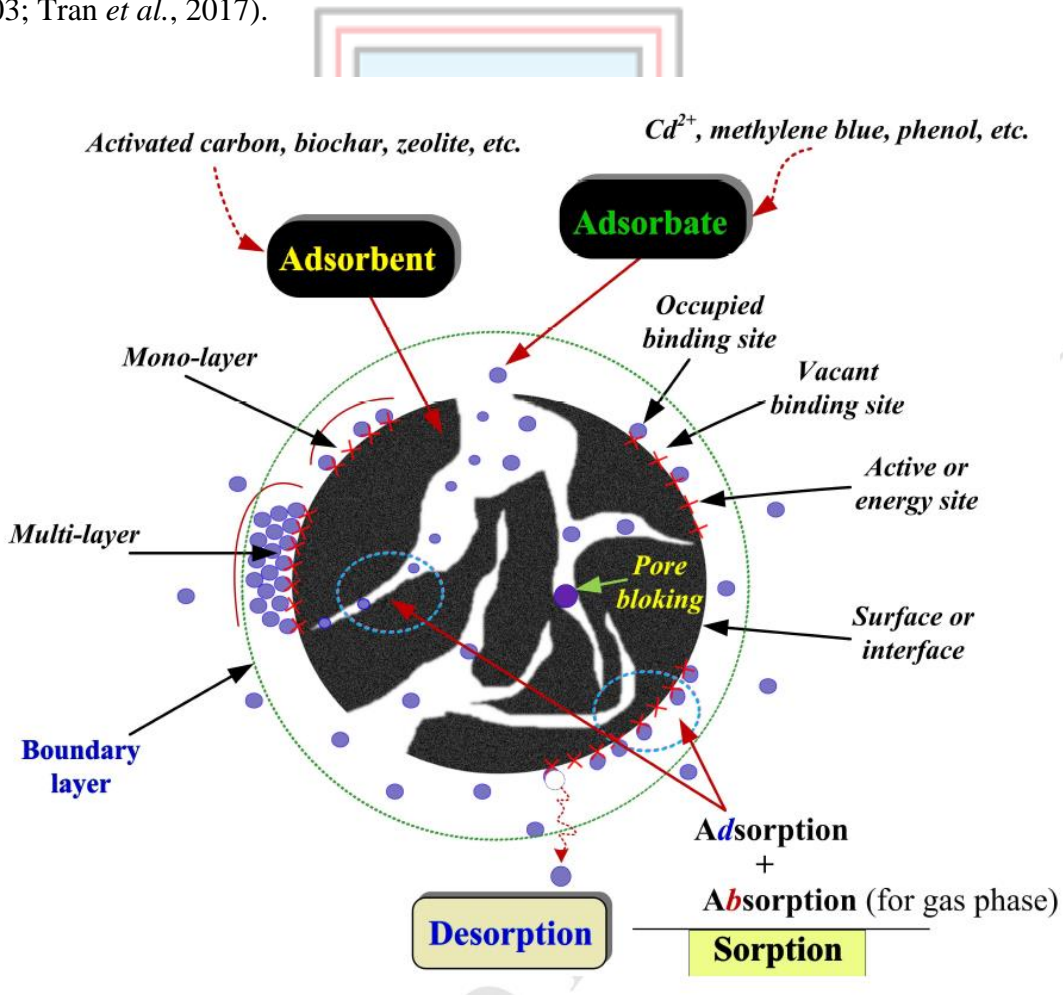


Figure 2.5 Basic Terms Used in Adsorption Processes (Tran *et al.*, 2017)

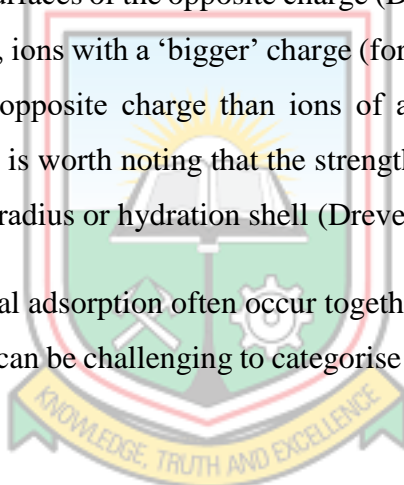


Physical adsorption occurs due to weak intermolecular forces, such as van der Waals forces between the surfaces of the adsorbate and adsorbent (Patterson, 2009; Hu and Xu, 2020). Due to weak intermolecular forces, the adsorbate can easily be separated from the adsorbent. In physisorption, the molecular structure of the adsorbate barely changes, and the adsorption energy is relatively small (Hu and Xu, 2020).

The action of chemical bonding between the surfaces of the adsorbent and adsorbate causes chemical adsorption to occur. Since relatively stronger forces are involved, chemical compounds are found. This encompasses the formation and destruction of chemical bonds (Sawyer *et al.*, 2003; Hu and Xu, 2020). In chemisorption, the activation energy required is relatively larger.

Exchange or electrostatic adsorption is distinguished by electrostatic attraction between the adsorbate and adsorbent surfaces of the opposite charge (Drever, 1997; Sawyer *et al.*, 2003). In electrostatic adsorption, ions with a ‘bigger’ charge (for example, bivalent ions) are more strongly attracted to the opposite charge than ions of a ‘smaller’ charge (for example, monovalent ions). Also, it is worth noting that the strength of the attraction depends on the size of the ion’s hydrated radius or hydration shell (Drever, 1997; Sawyer *et al.*, 2003).

Both physical and chemical adsorption often occur together (Hu and Xu, 2020). According to Sawyer *et al.* (2003), it can be challenging to categorise the adsorption process as a single type in some instances.



### 2.7.1 Factors Affecting Adsorption

An efficient adsorption process depends on several parameters, such as the nature of the adsorbate and adsorbent, which includes the surface area of the adsorbent, the presence of other compounds other than the adsorbate and experimental conditions. Experimental adsorption conditions include the adsorbate concentration, adsorbent concentration, pH of the adsorbate solution, temperature of the adsorbate solution, and contact time for the adsorption experiment (Ali, 2012). Changes in the aforementioned parameters can significantly influence the adsorption process. It is worth noting that every adsorbent has specific conditions at which a particular adsorbate can be efficiently adsorbed.

### 2.7.2 Adsorption Isotherm

Due to structural diversity, adsorbates may bind to different nanomaterials differently. Therefore, adsorption isotherms are mathematical equations used to understand the relationship between the adsorbate in solution and adsorbent (Sawyer *et al.*, 2003; Singh, 2016). Several adsorption isotherms have been used in literature. However, the most commonly applied are the Langmuir, Freundlich and Dubinin-Radushkevich (D-R) isotherms due to their simplicity, usefulness of model parameters and ease of interpretation (Tran *et al.*, 2017).

Langmuir isotherm assumes that all active sites of the adsorbent have the same affinity for the adsorbate, and therefore the adsorbate binds to a single site on the adsorbent. This causes the adsorbate to form a monolayer on the surface of the adsorbent (see Figure 2.5) (Sawyer *et al.*, 2003; Tran *et al.*, 2017). Freundlich isotherm, which is derived from the Langmuir isotherm, on the other hand, assumes that the active sites of the adsorbent have different affinities for different adsorbates. Hence, the adsorbate may form a multi-layer on the surface of the adsorbent (see Figure 2.5) (Tran *et al.*, 2017). The D-R isotherm is mostly used in adsorption processes where the adsorbent is a porous structure (Tran *et al.*, 2017). The aforementioned adsorption isotherms are further discussed in Chapter 3.

### 2.7.3 Adsorption Kinetics

Adsorption kinetics describes the rate of reaction as well as the adsorption mechanisms (Tran *et al.*, 2017; Krstic, 2021). The commonly used adsorption kinetic models in literature are the pseudo-first order (PFO), pseudo-second order (PSO), Elovich and intra-particle diffusion kinetic models. Though the PFO and PSO kinetic models provide insights into adsorption kinetics, the Elovich and intra-particle diffusion models provide additional knowledge on the adsorption mechanisms (Tran *et al.*, 2017; Krstic, 2021). The adsorption mechanism has different phases, including bulk transfer, film diffusion, intra-particle diffusion and adsorptive attachment (Tran *et al.*, 2017; Krstic, 2021). For instance, a linear intra-particle diffusion plot which passes through the origin indicates that the adsorption is completely governed by intra-particle diffusion. However, the adsorption may be a multi-step mechanism if the intra-particle diffusion plot contains multiple linear regions (Tran *et al.*, 2017). It is also worth noting that the mathematical equations of the adsorption kinetic models provide additional information about the initial rate constant, desorption constant

and the size of a boundary layer of an adsorbent. The aforementioned adsorption kinetic models are further discussed in Chapter 3.

## 2.8 Atomic Absorption Spectrophotometry (AAS)

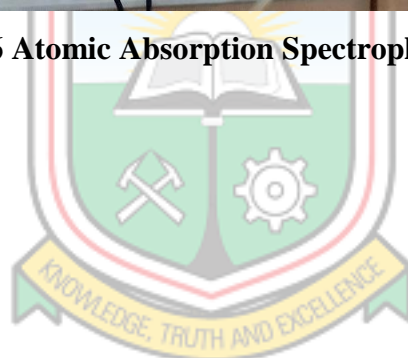
Atomic absorption spectrophotometer (AAS) is used to determine a trace metal's concentrations in solution. Figure 2.6 shows an AAS. The AAS is used to analyse the efficiency of a metal adsorption process by determining the final absorbate concentration or adsorbate concentration on the adsorbent. Cadmium concentration is determined via flame atomic absorption spectrophotometry (FAAS), whilst Hg concentration is determined using the cold vapour technique of hydride vapour generation (HVG-AAS).

The main principle in FAAS is that the analyte in the solution is atomised in a flame (González and de la Guardia, 2013; Mariella, 2019). The sample is first aspirated through a nebulizer and converted into aerosols. Then, the aerosol is transported to the flame by a carrier gas, and the analyte is atomised (Mariella, 2019). A lamp with the wavelength of the analyte throws light onto the atomised metal, and by absorption and Beer-Lambert's principle, detectors and processors in the AAS detect and calculate, respectively, the analyte concentration in the solution.

The HVG-AAS technique uses a similar technique; however, with the aid of  $\text{NaBH}_4$  (reducing agent) and hydrochloric acid to aid reactions (Anon., 1996; de Diego *et al.*, 1999; Anon., 2016). The reaction produces a gaseous hydride of the metal and hydrogen gas which is transported by argon gas into a quartz cell for atomisation and absorption. Mercury, in particular, requires no flame therefore determined in a cold vapour technique of HVG-AAS due to Hg's volatility at high temperatures (Anon., 1996; de Diego *et al.*, 1999; Anon., 2016).



**Figure 2.6 Atomic Absorption Spectrophotometer (AAS)**



## CHAPTER 3

### MATERIALS AND METHODS

This Chapter outlines materials used in the study, sampling of natural rubber latex (NRL) and methods for characterising the NRL before use. Experimental works summarised in this Chapter include procedures for electrospinning NRL, polyvinyl alcohol/natural rubber latex (PVA/NRL) and silver nanoparticles (AgNP) embedded in PVA/NRL nanofibre. The experimental works also include characterising the electrospun nanofibres and adsorption studies.

#### 3.1 Materials

Materials used in this study are listed in Table 3.1. Material purity or concentration, purpose, and source are also listed in Table 3.1.

**Table 3.1 Materials Used**

Material (Chemical Formula, Purity/Concentration)	Source	Purpose
<i>Ammonium hydroxide</i> ( $NH_4OH$ , 26.5%)	Daejung Chemical and Metals Co. Ltd.	Used as an ammonia ( $NH_3$ ) source to stabilise NRL.
<i>Acetic acid</i> ( $CH_3COOH$ , >99.7%)	Daejung Chemical and Metals Co. Ltd	Utilised as a coagulant in NRL's dry rubber content (DRC) determination
<i>Polyvinyl alcohol</i> (PVA) powder	Tong Li Tech Co. Ltd. (molecular weight = 80 kDa and degree of saponification = 80%) and Eastchem (molecular weight = 105.6 kDa and alcoholysis degree = 88%).	PVA powder was added to the NRL to increase its spinnability.
<i>Nitric acid</i> ( $HNO_3$ , 68.0%)	Brenntag Ghana Ltd.	Used to adjust the pH of the solutions used in this study
<i>Sodium hydroxide</i> ( $NaOH$ , > 97.0%)	Paskem Fine Chem Pvt. Ltd.	Used to adjust the pH of the solutions used in this study.

<i>Hydrochloric acid (HCl, 25.0%)</i>	Merck	Used to adjust the pH of solutions for point of zero charge (PZC) analysis.
<i>Silver nitrate (AgNO<sub>3</sub>)</i>	Merck	Utilised as a precursor for AgNP synthesis.
<i>Sodium chloride (NaCl, 99.5%)</i>	Paskem Fine Chem Pvt. Ltd.	Utilised as a salt for PZC analysis.
<i>Mercury (Hg, 1000 mg/L)</i>	Sigma-Aldrich	Primary standard from which standard solutions for adsorption experiments were prepared.
<i>Cadmium (Cd, 1000 mg/L)</i>	pg Instruments	Primary standard from which standard solutions for adsorption experiments were prepared.
<i>n-dodecane (C<sub>12</sub>H<sub>26</sub>, 99%)</i>	Thermoscientific	Used as an antifoaming agent in atomic absorption spectrophotometry (AAS) analysis.

### 3.2 Sampling of Natural Rubber Latex (NRL)

Fresh NRL composite sample was collected from the stem *Hevea brasiliensis* in a farm (N 05° 37.637' W 002° 02.469') located at Bepo, Western Region of Ghana. Figure 3.1 shows the collection of Afresh NRL from the *H. brasiliensis* tree at Bepo. All latex samples were collected from ten (10) trees for this work. The NRL was preserved with 0.7% w/w ammonia (NH<sub>3</sub>) to prevent spontaneous coagulation (Sirisomboon and Lim, 2019). This was further preserved at 4 °C in a refrigerator at the laboratory.



**Figure 3.1 Fresh NRL from *Hevea brasiliensis* Tree at Bepo, Western Region of Ghana**

### **3.3 Characterisation of Natural Rubber Latex**

To characterise natural rubber, parameters such as total solid content (TSC), dry rubber content (DRC), protein content and concentrations of Cu and Mn were analysed to determine the integrity of the freshly taken NRL. The presence of Cu ( $> 8$  mg/kg) and Mn ( $> 8$  mg/kg) can cause photo- and biodegradation of the NRL, which affects its storage and ageing processes (Anon., 2010; Duangthong *et al.*, 2017; Forrest, 2018). Therefore, these metals are not desirable at high concentrations in NRL. Silver and  $\text{Cd}^{2+}$  concentrations in NRL were also investigated since AgNP would be synthesised into an NRL nanofibre matrix, and the nanofibre composite would be used to remove  $\text{Cd}^{2+}$  in wastewater (adsorption process). However, Hg, one of the contaminants to be investigated during adsorption studies, was not analysed due to the high temperature ( $550$  °C) required in NRL's metal analysis. Mercury has a boiling point of  $357$  °C; hence, at  $550$  °C, Hg in NRL would vaporise.

#### **3.3.1 Determination of Total Solid Content (TSC)**

The TSC of NRL is the mass concentration (expressed as a percentage) of solids present in the latex after evaporation to dryness under specified drying conditions (Hamza *et al.*, 2008). First, 2 g of NRL was collected in a 60 mm flat-bottom dish. Then, one (1) mL of distilled water was added and swirled for the NRL to cover the base of the dish. Figure 3.2 shows NRL in flat-bottom dishes for TSC analysis.

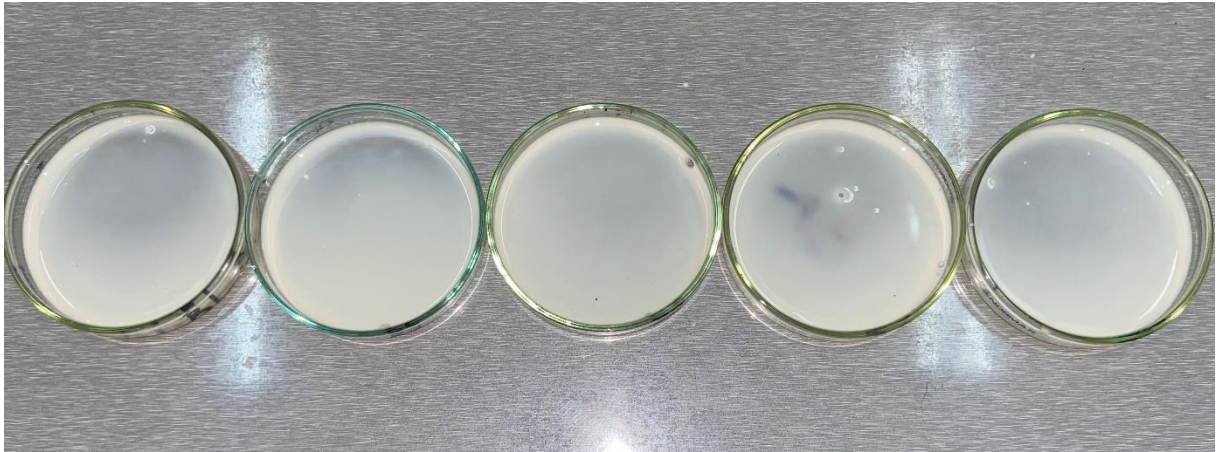


**Figure 3.2 TSC Analysis (Before Drying)**

This was dried in an oven at 70 °C for 16 h, cooled in a desiccator for 30 min, and weighed. The sample was then reheated for 30 min, cooled in a desiccator for 30 min and reweighed. This step was repeated until a weight difference of  $\leq 0.50$  mg was achieved. The analysis was conducted per ISO 124:2011 on five replicates for quality assurance (Anon., 2011b), and the TSC was calculated using Equation (3.1).

$$\text{TSC} = \frac{m_1}{m_0} \times 100 \quad (3.1)$$

where,  $m_1$  = mass of dried NRL

$m_0$  = mass of NRL before drying

### 3.3.2 Determination of Dry Rubber Content (DRC)

The DRC of NRL refers to the mass per cent of acid-coagulated latex dried under specified conditions (Duangthong *et al.*, 2017). Ten grams (10 g) of NRL was poured into an Erlenmeyer flask. Sufficient distilled water was added to the NRL to reduce its TSC to  $20 \pm 1\%$ . Next,  $35 \pm 5$  mL  $\text{CH}_3\text{COOH}$  (20 g/L) was added to aid coagulation, and the solution was placed over a steam bath. After steam bath heating for 30 min, a transparent serum was obtained. The coagulate was removed and soaked in several washes of distilled water until the water was no longer acidic. Finally, coagulates were pressed into thin sheets ( $\leq 2$  mm thickness) and rinsed again with distilled water. Figure 3.3 shows rolled coagulated latex sheets for DRC analysis.



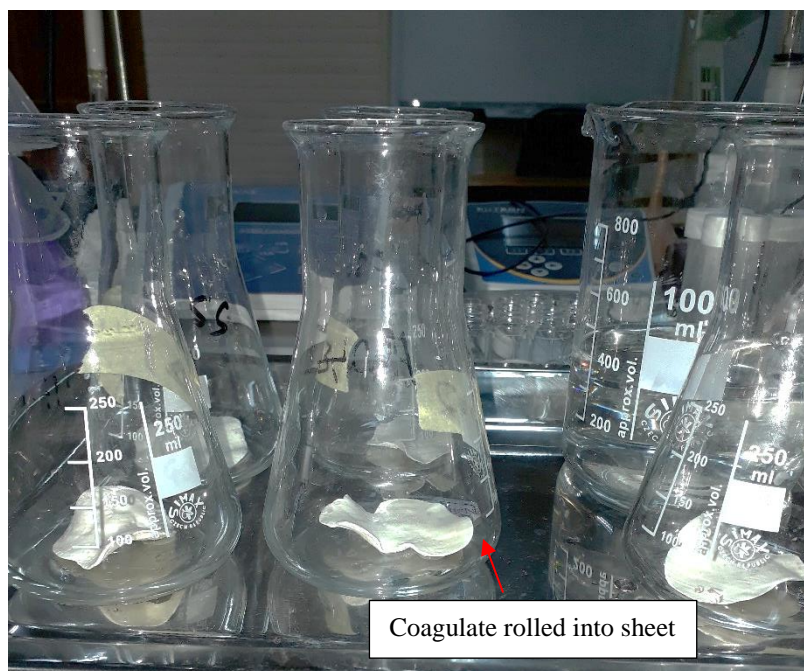


**Figure 3.3 Rolled Coagulated Latex Sheets Before Drying in DRC Analysis**

At 70 °C, the pressed sheet was dried until no white patch was visible. The dried sheet was cooled in a desiccator for 30 min, weighed, and re-dried for 30 min. This step was repeated until a weight difference of  $\leq 1.00$  mg was achieved. The analysis was conducted per ISO 126:2005 (E) on five replicates for quality assurance (Anon., 2005), and the DRC of NRL was calculated using Equation (3.2):

$$\text{DRC} = \frac{m_3}{m_2} \times 100 \quad (3.2)$$

where,  $m_3$  = mass of final dried NRL sheet

$m_2$  = mass of test portion

### 3.3.3 Protein Analysis

Nitrogen content was determined using the Kjeldahl method. The total protein concentration was estimated using Equation (3.3). Protein analysis was conducted at the Food Science Laboratory of Kwame Nkrumah University of Science and Technology (KNUST), Kumasi, Ghana.

$$\text{Protein content (\%)} = \text{nitrogen content} \times 6.25 \quad (3.3)$$

where 6.25 = the protein factor for natural rubber latex (Aik-Hwee *et al.*, 1993; Hwee, 2014).

### 3.3.4 Metal Content Determination

Twenty grams (20 g) of NRL sample wrapped in an ashless filter paper (chm SHIFT\_filtration–F2042 grade) was ashed at 550 °C in borosilicate Petri dishes (15×80 mm). A 20 mL aqua regia mixture was added to the cooled ash and heated in a water bath at 90 °C for about 30 min. The mixture was allowed to cool and topped up with distilled water to 100 mL. The final solution was filtered to remove insoluble matter, after which Cu, Mn, Ag and Cd concentrations were determined using an atomic absorption spectrophotometer (AAS; Shimadzu AA-7000). This was done in duplicates.

### 3.4 Preparation of Polyvinyl Alcohol/Natural Rubber Latex (PVA/NRL) Solutions for Electrospinning

Fifteen per cent (15%) (w/v) PVA solution was prepared by dissolving powdered PVA in distilled water at 60 °C. The NRL was mixed with the prepared PVA solution at room temperature to form 40% PVA/NRL (w/v), 50% PVA/NRL (w/v), 60% PVA/NRL (w/v) and 70% PVA/NRL (w/v) to increase its spinnability. Viscosities of the prepared solutions, including pure NRL, were measured using an atmospheric viscometer (AMETECK® CHANDLER ENGINEERING®). These solutions were electrospun to determine the best matrix or wall material for nanoparticle synthesis and adsorption studies.

### 3.5 Electrospinning NRL, PVA and PVA/NRL Solutions

#### 3.5.1 Electrospinning NRL

Electrospinner TL-01 (Tong Li Tech Co. Ltd), shown in Figure 3.4, was employed to electrospin NRL. This was done to determine the optimal values at which PVA/NRL solution would be electrospun. The voltage applied to the NRL was varied between 15 kV to 26 kV, and spinneret sizes used were also varied between 20 G to 23 G. The internal diameters of 20, 21, 22 and 23 G needles are 0.603, 0.514, 0.413 and 0.337 mm, respectively. Electrospinning was conducted at a flow rate of 2 mL/h, sliding unit speed of 5 mm/s, rotating collector (diameter = 76 mm) speed of 1000 rpm and the distance between the spinneret tip and collector at 20 cm.



**Figure 3.4 Electrospinning Unit TL-01**

The ambient condition of the electrospinning chamber was kept at 30 °C and relative humidity (RH) at 40%. At relatively high temperatures, NRL dries up quickly; therefore, low temperature prevents frequent clogging of the spinneret by dried NRL. Also, a high RH may affect the morphology of the fibres by creating pores, whilst a low RH enhances solvent evaporation and creates thinner fibres. Hence, a low RH (40%) was used in this study (Xue *et al.*, 2019). The nanofibres were collected on aluminium foil wrapped around the collector. The collected fibres were dried overnight in an oven at 50 °C.

### 3.5.2 Electrospinning PVA, PVA/NRL and AgNO<sub>3</sub>-PVA/NRL Solutions

The operating condition at which the smoothest NRL films were produced was selected as the optimum condition for electrospinning PVA/NRL and AgNO<sub>3</sub>-PVA/NRL solutions. AgNO<sub>3</sub>-PVA/NRL solutions electrospun were 0.01 M AgNO<sub>3</sub>-PVA/NRL and 0.015 M AgNO<sub>3</sub>-PVA/NRL. Higher concentrations were not electrospun since, for instance, at 0.02 M AgNO<sub>3</sub>-PVA/NRL, the solution became extremely watery and thus required modification

of electrospinning parameters due to the gross change in viscosity. This would not be beneficial in a comparative study since 0.01 M AgNO<sub>3</sub>-PVA/NRL, 0.015 M AgNO<sub>3</sub>-PVA/NRL and 0.02 M AgNO<sub>3</sub>-PVA/NRL would not have been subjected to the same experimental conditions. The solutions were electrospun using 20 G spinneret, an applied voltage of 24 kV and a flow rate of 1.0 mL/h. Due to the PVA/NRL solution continuously dripping onto the collector at 2.0 mL/h (flow rate for electrospinning NRL), the flow rate was reduced to 1.0 mL/h. Only 100% PVA was electrospun at 20 kV since PVA dried relatively faster. The fibres collected were dried in an oven at 50 °C overnight.

Other nanofibres were electrospun, namely Mix 1 and 2. Mix 1 refers to AgNP-PVA/NRL nanofibre composite synthesised by electrospinning 0.01 M and 0.015 M AgNO<sub>3</sub>-PVA/NRL solutions simultaneously onto a single aluminium foil in 8 h. The method involved using two spinnerets (about 3.5 cm apart), one ejecting 0.01 M AgNO<sub>3</sub>-PVA/NRL solution and the other 0.015 M AgNO<sub>3</sub>-PVA/NRL solution. A side-by-side spinneret was not used since that would increase the electrospun fibres' diameter. Contrary to Mix 1's synthesis, Mix 2 was prepared in a sequence. This was done by electrospinning 0.01 M AgNO<sub>3</sub>-PVA/NRL solution in the first 8 h, after which 0.015 M AgNO<sub>3</sub>-PVA/NRL solution was electrospun in the next 8 h (total electrospinning time = 16 h). Between the first 8 and second 8 h, the electrospun 0.01 M AgNO<sub>3</sub>-PVA/NRL solution was allowed to air-dry for 12 h before 0.015 M AgNO<sub>3</sub>-PVA/NRL solution was electrospun.

### 3.6 Weight Loss Test by Dissolution on PVA/NRL Nanofibres

After electrospinning PVA/NRL solutions, there was a need to determine the nanofibre most suitable as a wall material or substrate for AgNP synthesis. A weight loss test was selected as the final analysis to determine the amount or fraction of the fibre that would dissolve if placed in an aqueous solution. This process was necessary since the study's aim was to use the AgNP-coated nanofibre to remove heavy metals contaminants from water without a significant amount of nanoparticles being released into the treated water to cause pollution.

The PVA/NRL nanofibres (40% to 70% PVA/NRL) were peeled from the aluminium foil, placed into 50 mL of distilled water and agitated on an orbital shaker for 60 min at 300 rpm. The fibres were filtered from the solution, dried (50 °C) and weighed. Figure 3.5 shows the PVA/NRL nanofibre after filtration in a weight loss test.

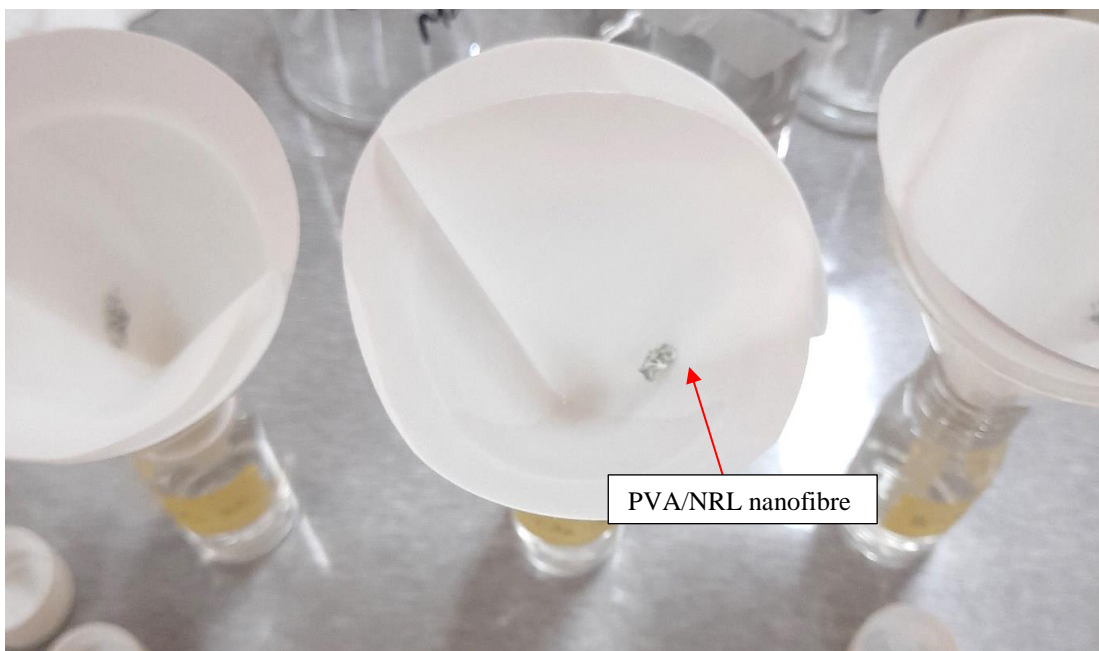


**Figure 3.5 PVA/NRL Nanofibre After Filtration**

The fibres were then dried again and reweighed until a difference of < 0.50 mg was obtained. Weight loss was determined using Equation (3.4).

$$\text{Weight loss (\%)} = \frac{W_1 - W_2}{W_1} \times 100 \quad (3.4)$$

where  $W_1$  = weight of fibre before shaking in distilled water for 60 min at 300 rpm

$W_2$  = weight of fibre after drying

### 3.7 Synthesis of Silver Nanoparticles (AgNP)

Using  $\text{AgNO}_3$  as a Ag source, 0.10 M  $\text{AgNO}_3$  solution was added to 50% PVA/NRL solution to form 0.01 M and 0.015 M  $\text{AgNO}_3$ -PVA/NRL solutions. These solutions were electrospun at conditions and parameters outlined in section 3.5 and a travel distance of 23 cm. For each nanofibre, 8 mL of the prepared solution was dispensed. A relatively small amount of the  $\text{AgNO}_3$ -PVA/NRL solution was lost to the chamber walls due to  $\text{AgNO}_3$  salt, which increased the conductivity of the solution. In line with this, the distance between the spinneret tip and the collector was reduced to 15 cm. This increased the electric field strength for most of the fibre to be directed towards the collector for capturing. The electrospun fibres were dried at 50 °C in an oven overnight.

### 3.8 Characterisation of the Electrospun Nanofibre Composites

#### 3.8.1 Morphology, Size Distribution and Elemental Composition of Electrospun Fibres and AgNP

A Canon EOS 60D camera was first used to capture images of electrospun NRL. Surface morphology of electrospun NRL, PVA and AgNP-NRL/PVA nanofibre composites were investigated using a scanning electron microscope (SEM; Zeiss EVO MA 15). The SEM micrographs were first taken with a secondary electron (SE) detector, viewed at magnifications between 3 500 to 11 000 $\times$  and a working distance between 8.5 to 11.0 mm. Due to the carbonaceous nature of the samples, the nanofibres were sputter-coated with gold/palladium alloy, serving as a conductive layer for good imaging at 3 kV. The accelerating voltage was later increased to 20 kV, and with a backscatter detector (BSD), micrographs of the sample showing different phases (by contrast) were captured. An energy dispersive x-ray spectrometer (EDS; Bruker) equipped with an XFlash Detector 610M was used to quantify the elemental composition of the AgNP-PVA/NRL nanofibre composites.

To investigate the ‘naked’ AgNP without a polymer covering, a transmission electron microscope (TEM; FEI Tecnai T20) working at an accelerating voltage of 200 keV was used to capture the micrographs. TEM analysis was conducted at the Electron Microscope Unit of the University of Cape Town (UCT), South Africa. Based on 1 206 AgNPs, ImageJ software was used to measure the sizes of the nanoparticles on and within the nanofibre composite. The software was similarly employed in determining the fibre diameter distribution of PVA and PVA/NRL nanofibres. Also, the average pore diameters of electrospun PVA and PVA/NRL nanofibres were determined by measuring the fibre-to-fibre distance of the various pores. Since the study aimed to determine each generated fibre’s diameter, the analysis did not include matted areas.

#### 3.8.2 Crystallography of AgNP-PVA/NRL Nanofibre Composites

To confirm the formation of AgNP, the crystallography of the nanofibre composites was determined using an X-ray diffractometer (XRD; Malvern Panalytical Empyrean). This analysis was conducted at the University of Ghana’s (UG) Physics Department, Accra, Ghana. The fibres were retained on the aluminium foil and pulverised. This was because the nanofibre composite’s elastomeric and thin nature made the sample small for pulverisation

and also caused low detection of crystal phases in the nanofibre composite. The diffraction patterns obtained were compared to International Centre Diffraction Data (ICDD).

### 3.8.3 Functional Group Characterisation of Electrospun Nanofibres

A Fourier transform-infrared spectrometer (FT-IR; Bruker ALPHA Platinum-ATR) was used to determine the functional groups in NRL and PVA at the Central Laboratory of KNUST. The spectrometer was also used to determine the interaction between NRL and PVA in electrospun PVA/NRL nanofibres, as well as the interaction between AgNP and PVA/NRL in AgNP-PVA/NRL nanofibre composites.

### 3.9 Point of Zero Charge Analyses of AgNP-PVA/NRL Nanofibre Composites

Point of zero charge (PZC) for both 0.01 M and 0.015 M AgNP-PVA/NRL were determined to identify the point at which the surface charge density of the nanofibre composites in solution was zero (Tran *et al.*, 2017). This test was necessary as the PZC, in conjunction with the pH at which maximum adsorption occurs, aids in determining the surface charge of the adsorbent. Identifying the surface charge helps in determining the adsorption mechanism that takes place during the study. The determination of PZC was carried out as described by Nasiruddin Khan and Sarwar (2012) with minor modifications. First, 0.50 M HCl and 0.05 M NaOH were used to adjust the pH of 0.05 M NaCl to between 3 and 10. Then, to 20 mL of the pH-adjusted NaCl solution,  $3 \times 3 \text{ cm}^2$  of the AgNP was added, and the resulting solution was agitated on an orbital shaker at 200 rpm for 60 min, after which the final pH was determined. Then, using SigmaPlot software (version 10.0), the difference between the initial and final pH ( $\text{pH}_{\text{initial}} - \text{pH}_{\text{final}}$ ) was plotted against the initial pH ( $\text{pH}_{\text{initial}}$ ), and the point at which  $\text{pH}_{\text{initial}} - \text{pH}_{\text{final}}$  was zero (0) was identified as the PZC.

### 3.10 Adsorption Studies of AgNP-PVA/NRL Nanofibre Composite for Hg and Cd<sup>2+</sup> Contaminants

#### 3.10.1 Adsorption Experiment

A  $5 \times 5 \text{ cm}^2$  AgNP-PVA/NRL nanofibre composite was placed in 50 mL Hg solution, and at a temperature of 27°C, the solution was shaken on an orbital shaker at 200 rpm. After agitation, the solutions were analysed for Hg concentration. Figure 3.6 shows AgNP-PVA/NRL nanofibre composites in an adsorbate solution and agitated on an orbital shaker.

The adsorption study was carried out to determine how contact time (0-120 min), initial concentration (0.01-1.00 mg/L) and pH (4-7) affected the amount of Hg adsorbed by the nanofibre composites. Adsorption studies on  $\text{Cd}^{2+}$  were carried out using the same conditions mentioned earlier for Hg. Higher initial concentrations, such as 5 mg/L and 10 mg/L were investigated for both Hg and  $\text{Cd}^{2+}$ . However, the removal efficiencies at these initial concentrations were extremely low; hence, these were not further investigated. The removal efficiency (RE) and adsorption capacity of the AgNP-PVA/NRL nanofibre composites were calculated using Equations (3.5) and (3.6), respectively, after the final concentrations of Hg and Cd in the solutions were obtained using an AAS (Shimadzu AA-7000).

$$\text{RE (\%)} = \frac{C_0 - C_e}{C_0} \times 100 \quad (3.5)$$

$$q_e = \frac{(C_0 - C_e) \cdot V_1}{m_4} \quad (3.6)$$

where  $C_0$  (mg/L) and  $C_e$  (mg/L) are the initial and equilibrium concentrations of the adsorbate in solution, respectively;  $q_e$  (mg/g) is the adsorption capacity of the adsorbent at equilibrium;  $V_1$  (L) is the volume of the adsorbate solution; and  $m_4$  (g) is the mass of the adsorbent.



**Figure 3.6 AgNP-PVA/NRL Nanofibre Composites in Hg Solution Agitated on an Orbital Shaker**



The mass of Ag in each  $5 \times 5 \text{ cm}^2$  nanofibre composite was estimated by first determining the mass of  $\text{AgNO}_3$  in 0.01 M and 0.015 M  $\text{AgNO}_3$ , respectively, per 8 mL  $\text{AgNO}_3$ -PVA/NRL solution electrospun (Equation (3.7)).

$$C = \frac{m_5}{M_1 \cdot V_2} \quad (3.7)$$

where C (mol/L) is the concentration of  $\text{AgNO}_3$ ;  $m_5$  (g) and  $M_1$  (g/mol) are the mass and molar mass of  $\text{AgNO}_3$ , respectively; and  $V_2$  (L) is the volume of the solution to be electrospun. By rearranging, Equation (3.7) becomes:

$$m_5 = C \cdot M_1 \cdot V_2 \quad (3.8)$$

Using Equation (3.8), the mass of  $\text{AgNO}_3$  in 0.01 M and 0.015 M  $\text{AgNO}_3$  were found to be 13.5898 and 20.3848 mg, respectively. Next, the mass of Ag in the 8 mL solution was obtained by determining its equivalent weight in  $\text{AgNO}_3$  (Equations (3.9)).

$$\text{Equivalent weight per cent of Ag} = \frac{M_2}{M_1} \times 100\% \quad (3.9)$$

where  $M_2$  is the molar mass of Ag. This implies that the equivalent weight per cent of Ag in  $\text{AgNO}_3$  is 63.4992%. Therefore, the mass of Ag in 0.01 M and 0.015 M  $\text{AgNO}_3$  is 8.6294 and 12.944 mg, respectively. Finally, since the total area electrospun was  $549.1504 \text{ cm}^2$ ,  $5 \times 5 \text{ cm}^2$  of 0.01 M and 0.015 M AgNP nanofibre composite contained  $\sim 0.3929 \text{ mg}$  and  $\sim 0.5893 \text{ mg}$  of Ag, respectively.

### 3.10.2 Adsorption Isotherm

Adsorption data obtained from the experiments were fitted to the Langmuir, Freundlich and Dubinin-Radushkevich (D-R) isotherms using Microsoft Office Excel (2019 version) and SigmaPlot 10.0. The isotherms were used to examine the relationship between the adsorbent and the adsorbates in the solution (Sawyer *et al.*, 2003; Tran *et al.*, 2017). Langmuir model, which assumes that all the adsorbent's active sites have the same affinity for the adsorbent and its separation factor ( $R_L$ ), are presented in Equations (3.10) and (3.11), respectively (Langmuir, 1918; Hall *et al.*, 1966; Tran *et al.*, 2017).

$$q_e = \frac{q_{\max} \cdot (K_L \cdot C_e)}{1 + (K_L \cdot C_e)} \quad (3.10)$$

$$R_L = \frac{1}{1+(K_L \cdot C_o)} \quad (3.11)$$

where  $q_{\max}$  (mg/g) represents maximum adsorption capacity of the adsorbent and  $K_L$  (L/mg) represents the Langmuir constant. The  $R_L$  values provide information on whether the adsorption was favourable ( $0 < R_L < 1$ ), unfavourable ( $R_L > 1$ ), linear ( $R_L = 1$ ) or irreversible ( $R_L = 0$ ).

Freundlich isotherm, which assumes that the adsorbent's active sites have different affinities for different adsorbates, is presented in Equation (3.12) (Freundlich, 1906; Sawyer *et al.*, 2003).

$$q_e = K_F \cdot C_e^{\frac{1}{n}} \quad (3.12)$$

where  $K_F$  (mg/g)/(mg/L)<sup>1/n</sup> is the Freundlich constant and  $n$  is a measure of the change in affinity for the adsorbate with changes in adsorption density. The adsorption may be favourable ( $1/n < 1$ ) or unfavourable ( $1/n > 1$ ) depending on the value of  $1/n$ .

Due to the porous nature of the nanofibre composites, the adsorption data were also fitted to the D-R isotherm to provide additional information on the adsorption mechanism. The isotherm is expressed in Equation (3.13), and its mean adsorption energy,  $E$  (kJ/mol), is also presented in Equation (3.14) (Dubinin and Radushkevich, 1947).

$$q_e = q_{DR} \cdot e^{(-K_{DR} \cdot \epsilon^2)} \quad (3.13)$$

$$E = \frac{1}{\sqrt{2 \cdot K_{DR}}} \quad (3.14)$$

where  $q_{DR}$  (mg/g) represents the adsorption capacity of the adsorbent,  $K_{DR}$  (mol<sup>2</sup>/kJ<sup>2</sup>) represents a constant related to sorption energy, and  $\epsilon$  (kJ/mol) is the Polanyi potential. The value of  $\epsilon$  is calculated per Equation (3.15).

$$\epsilon = RT \cdot \ln\left(1 + \frac{C^o}{C_e}\right) \quad (3.15)$$

where  $R$  ( $8.314 \times 10^{-3}$  kJ/mol·K) is the universal gas constant,  $T$  (K) is the temperature at which adsorption occurs, and  $C^o$  (mg/g) is the concentration of the adsorbate in the standard state (1 mol/dm<sup>3</sup>) (Zhou, 2020). That is, 1 mol/dm<sup>3</sup> equals 200 590 mg/L and 112 411 mg/L for Hg and Cd, respectively.

### 3.10.3 Adsorption Kinetics

The effect of contact time on the adsorption process and the equilibrium time were studied by fitting the adsorption data to the pseudo-first order (PFO), pseudo-second order (PSO), Elovich and intra-particle diffusion kinetic models using Microsoft Office Excel (2019 version) and SigmaPlot 10.0. According to Ho and McKay (1998), the PFO kinetic model proposed by Lagergren (1898) is mostly applicable for only the first 20 to 30 min of contact time. The PFO equation is expressed as follows (Equation (3.16)):

$$q_t = q_e \cdot (1 - e^{-k_1 \cdot t}) \quad (3.16)$$

where  $q_t$  (mg/g) is the amount of adsorbate adsorbed at time  $t$  (min) and  $k_1$  (1/min) is the rate constant of the PFO equation.

As proposed by Blanchard *et al.* (1984), the PSO model is expressed as shown in Equation (3.17).


$$q_t = \frac{k_2(q_e)^2 t}{1 + (k_2 q_e t)} \quad (3.17)$$

where  $k_2$  (g/(mg × min)) is the rate constant of the PSO equation.

The Elovich model provides insight into an adsorption process's initial rate constant and desorption constant. As proposed by Roginsky and Zeldovich (1934), the Elovich model (Equation (3.18)) is expressed as follows:

$$q_t = \frac{1}{\beta} \ln(1 + \alpha \beta t) \quad (3.18)$$

where  $\beta$  (g/mg) is the desorption constant of the adsorption experiment, and  $\alpha$  (mg/(g × min)) is the initial rate constant.

Weber and Morris (1963) proposed the intra-particle diffusion model, which can predict the rate-controlling step. The model can also identify the reaction pathway and adsorption mechanisms (Tran *et al.*, 2017). The intra-particle diffusion model is expressed as follows (Equation (3.19)):

$$q_t = k_p \sqrt{t} + C \quad (3.19)$$

where  $k_p$  ( $\text{mg}/(\text{g} \times \text{min}^{1/2})$ ) represents the diffusion rate constant, and  $C$  ( $\text{mg}/\text{g}$ ) represents the constant associated with the thickness of the boundary layer.

### 3.11 Elemental Analysis of Adsorbates in Solution

#### 3.11.1 Mercury Concentration in Solution

Before and after agitation of solutions with the nanofibre composites immersed, Hg concentrations were determined using an AAS in conjunction with a hydride vapour generator (AAS-HVG; Shimadzu AA 7000-HVG-1). This technique does not require heating during the atomic adsorption measurement (Anon., 2016). Before analysis, 2.5 mL of concentrated  $\text{HNO}_3$  (7.54 M) was added to 50 mL of the sample solution per American Public Health Association (APHA) 3111B. A few drops of  $\text{C}_{12}\text{H}_{26}$  were added to the solution, swirled, and allowed to stand until no visible reaction was seen. The solution was then heated on a hot plate at  $90^\circ\text{C}$ . After this, the sample was allowed to cool and then topped with distilled water to 50 mL before AAS analysis. Digestion was required because of the addition of  $\text{C}_{12}\text{H}_{26}$ , which served as an antifoaming agent for the hydride technique.

#### 3.11.2 Cadmium Concentration in Solution

Cadmium concentration of the solutions before and after agitation with the nanofibre immersed were determined using Flame AAS (FAAS; Shimadzu AA 7000). Before analysis, the solutions were acidified with 5% concentrated  $\text{HNO}_3$  (7.54 M). This analysis was done per the APHA 3111B standard method.

## CHAPTER 4

### GREEN SYNTHESIS AND CHARACTERISATION OF ELECTROSPUN PVA/NRL NANOFIBRE FOR NANOPARTICLE LOADING AND APPLICATION IN AQUEOUS SOLUTIONS

Various fabricated PVA/NRL nanofibre films, with water as the solvent, are discussed in this Chapter. The morphology of electrospayed NRL and electrospun PVA/NRL fibre films based on scanning electron microscopy (SEM) analysis and visual inspection, the interaction between PVA and NRL in the electrospun film based on Fourier transform infrared (FT-IR) analysis and a weight loss or dissolution test (since the nanofibre will be used in an aqueous media for adsorption of contaminants) are all discussed in this Chapter.

#### 4.1 Background

In order to curb issues of nanoparticles forming part of the contamination problem after water treatment, there is the need to incorporate nanoparticles into a matrix, which can be removed easily after water treatment. Also, even if this matrix is partially soluble in water, it should not excessively dissolve and release nanoparticles at detrimental levels into the treated water.

Electrospun nanofibres, a plausible option for nanoparticle loading, are fibrous, highly porous, have a high surface area-to-volume ratio and have a small fibre-to-fibre distance. These characteristics make nanofibres desirable for filtration, adsorption and water treatment (Ramakrishna *et al.*, 2005; Padil *et al.*, 2016; Xue *et al.*, 2019). However, the utilisation of several non-renewable and hazardous organic solvents (such as dimethylformamide (DMF), methylene chloride and acetone) has made producing green electrospun nanofibres a daunting task (Padil *et al.*, 2016). This challenge has warranted the need for researchers to seek out environmentally sustainable alternatives which do not require toxic solvents for electrospinning.

Natural rubber, a renewable resource which is readily available (in Ghana), usually requires solvents such as DMF, tetrahydrofuran (THF), chloroform and toluene for its dissolution, and these are all toxic (Costa *et al.*, 2013; Hasanuddin *et al.*, 2017; Taweepreda, 2017). In its latex form, other polymers such as polycaprolactone, polylactic acid and chitosan may be added to increase the natural rubber latex's (NRL) electrospinnability; however, these

polymers also require non-environmentally friendly solvents (such as acetic acid, chloroform and formic acid) (Costa *et al.*, 2013; Riyajan and Sukhlaaied, 2015; Cosme *et al.*, 2016). Nevertheless, a potential alternative for converting NRL into green electrospun nanofibres is by adding polyvinyl alcohol (PVA), a non-toxic biopolymer, which uses water as its solvent, before electrospinning. Unfortunately, PVA is soluble in water, making the biopolymer undesirable as a matrix for nanoparticle loading in water treatment processes. Therefore, there is a need to identify the optimum ratio of NRL to PVA for electrospun nanofibre fabrication, which would be suitable for nanoparticle loading and for aqueous applications without using harmful solvents.

## 4.2 Characteristics of NRL Used

The nature of NRL after drying for total solid content (TSC) and dry rubber content (DRC) analyses are presented in Figures 4.1 and 4.2, respectively, and the results of TSC, DRC, protein and metal content of the NRL are also presented in Table 4.1. The latex used in this study contained a high DRC of  $43.52 \pm 0.03\%$ , which was within the existing range of 30-45%, and its protein content ( $3.42 \pm 0.10\%$ ) was above the existing 1-2% range for fresh latex. However, metal concentrations of Cu (1.42 mg/kg) and Mn (0.11 mg/kg) were below the ISO 2004:2010 (E) upper limit (8 mg/kg). There was no significant error in duplicates analysed for Cu and Mn concentration. Since Ag and Cd would be used in the adsorption studies, their concentrations in the NRL were also analysed. The results showed that both metals had concentrations below the detection limit of  $< 0.01$  mg/kg.

High DRC measured in the NRL indicates the abundance of *cis*-1,4-polyisoprene, which serves as a capping agent for some nanoparticles, such as magnetite, in its synthesis (Arsalani *et al.*, 2018). The NRL's protein content exceeded the 1-2% range mainly because the latex was stabilised using NH<sub>3</sub>. This may have accounted for the extra nitrogen measured in the Khedjal analysis. However, this does not deem the latex as low quality. In literature, the amine group of ammonia and proteins of NRL are responsible for metal ions reduction, especially Ag ions, in solution (Abu Bakar *et al.*, 2007; Guidelli *et al.*, 2011; Cabrera *et al.*, 2013; Danna *et al.*, 2016).

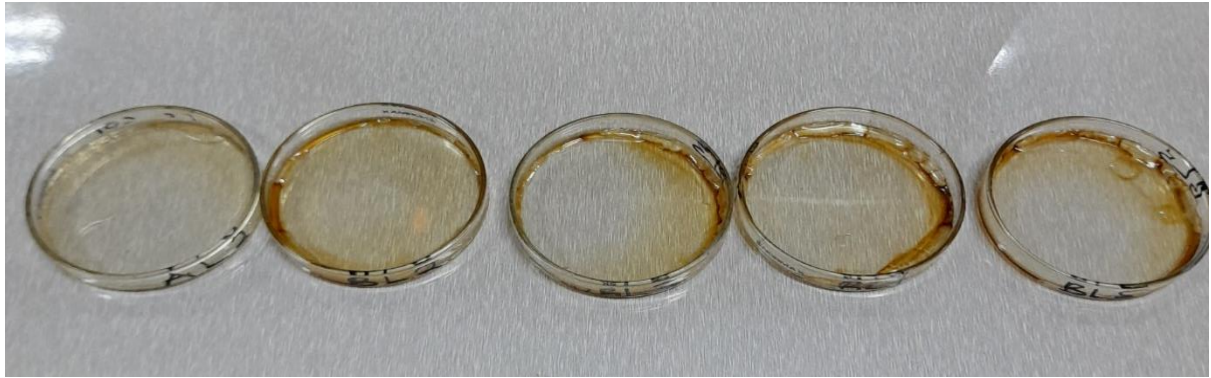


**Figure 4.1 TSC Analysis (After Drying)**

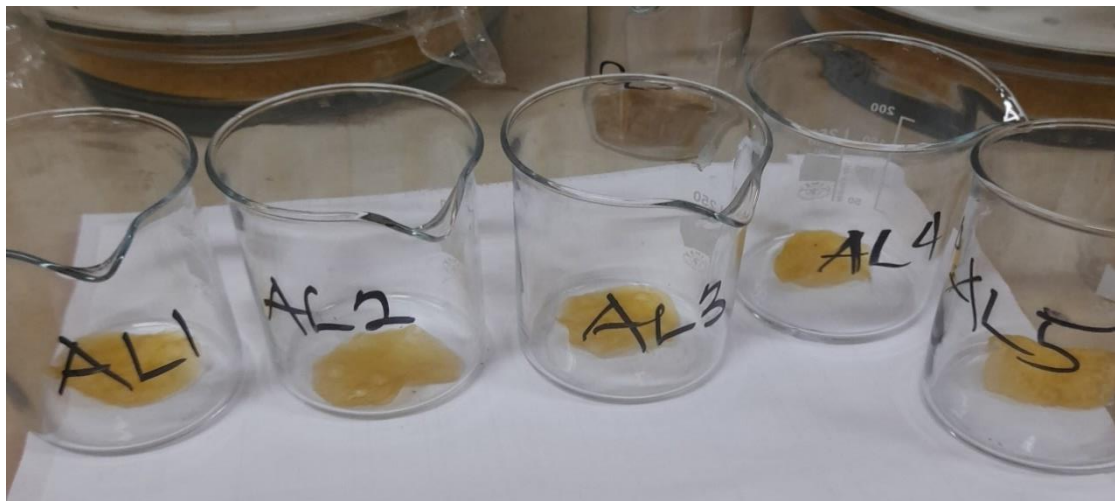


**Figure 4.2 DRC Analysis (After Drying)**

**Table 4.1 Characteristics of NRL Used**

Parameter	Concentration $\pm$ SEM <sup>a</sup>	Existing Range/Standard	Reference
TSC (%)	47.68 $\pm$ 0.12	30-50%	(Rippel and Galembeck, 2009)
DRC (%)	43.52 $\pm$ 0.03	30-45%	(Borges <i>et al.</i> , 2014)
Protein (%)	3.42 $\pm$ 0.10	1-2%	(Hwee, 2014)
Cu (mg/kg)	1.44 $\pm$ 0.00	8	(Anon., 2010)
Mn (mg/kg)	0.11 $\pm$ 0.00	8	(Anon., 2010)
Ag (mg/kg)	<0.01	-	-
Cd (mg/kg)	<0.01	-	-

<sup>a</sup>SEM=Standard error of the mean

Since the concentrations of metals responsible for photodegradation (that is, Cu) and accelerated ageing (that is, Mn) of NRL were below the ISO 2004:2010 (E) upper limit (8

mg/kg), it indicated that the NRL is good enough to be processed into rubber goods and also for nanoparticle synthesis. Also, since the concentrations of Ag and Cd were below the detection limit of < 0.01 mg/kg, it shows that the NRL when used, would pose no known interference in the adsorption studies of the selected metals.

### 4.3 Viscosities of NRL and PVA/NRL Solutions

Viscosities of NRL and PVA/NRL solutions are presented in Table 4.2. The PVA solution's viscosity was above the detection limit of the viscometer used in this study. From Table 4.2, it can be seen that as the PVA concentration increases, the viscosity of the solution also increases in the order: NRL < 40% PVA/NRL < 50% PVA/NRL < 60% PVA/NRL < 70% PVA/NRL. This trend shows that adding a highly viscous polymer, such as a PVA solution, would increase the polymer chain entanglement of NRL in the solution, a characteristic required in electrospinning. Increasing polymer chain entanglement would aid in producing thinner and smoother fibres with less beading during electrospinning (Ramakrishna *et al.*, 2005). Since NRL had the least viscosity, the latex was expected to form many beads during electrospinning, or it may be electrospayed instead.

**Table 4.2 Viscosities of NRL and PVA/NRL Solutions**

Shear Stress	Viscosity (Centipoise (cP))				
	NRL	40% PVA/NRL	50% PVA/NRL	60% PVA/NRL	70% PVA/NRL
600	105.6	1 440+	1 440+	1 440+	1 440+
300	57.6	1 440+	1 440+	1 440+	1 440+
200	43.2	1 440+	1 440+	1 440+	1 440+
100	28.8	1 440+	1 440+	1 440+	1 440+
60	19.2	1 440+	1 440+	1 440+	1 440+
30	19.2	1 430.4	1 440+	1 440+	1 440+
20	19.2	1 046.4	1 420.8	1 440+	1 440+
10	19.2	595.2	844.8	1 022.4	1 440+
6	19.2	393.6	580.8	667.2	1 113.6
3	19.2	220.8	336	364.8	633.6
2	19.2	158.4	240	259.2	446.4
1	19.2	96	139.2	144	235.2



## 4.4 Morphology of Fibre Films

### 4.4.1 Morphology of NRL Films

The study revealed that NRL could not be electrospun at the voltages used (15 kV– 26 kV) but could only be electrospayed. Figure 4.3 shows NRL being electrospayed at 24 kV. During this process, the electrified fluid produced two jets in opposite directions with distinct NRL droplets (Figure 4.3-red arrows) falling on the collector without stretching and whipping, as expected in electrospinning. The jet, which is characteristic of electrospaying, known as Rayleigh’s jet (Xue *et al.*, 2019), was observed at all voltages and spinneret sizes used in this study.

Characteristics of the electrospayed NRL at 15 kV – 26 kV, using 20 G – 23 G spinneret sizes, are shown in Table 4.3. It can be observed that as the applied voltage increased, the film’s roughness and thickness reduced. Another observation was that as the spinneret sizes decreased, the film became thinner in most cases. The decrease in roughness and thickness occurred because applied voltage has an inverse relationship with the size of polymer droplets and their tendency to aggregate (Jadhav *et al.*, 2012; Jadhav *et al.*, 2013). At a voltage of 26 kV, it was expected that NRL films produced would be thinner and less rough compared to films produced at 24 kV, but that was not the case. Instead, the NRL films electrospayed at a voltage of 24 kV were rather thinner and less rough, with films electrospayed at 26 kV being the second least in thickness and roughness.

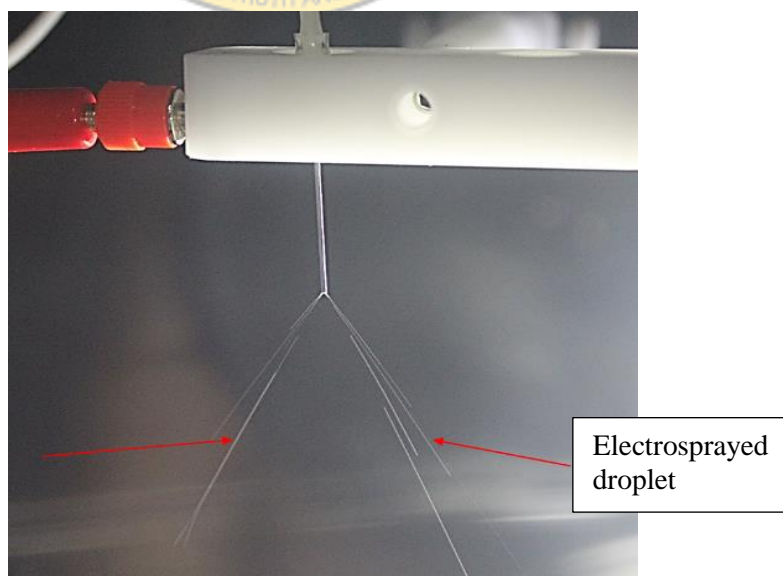


**Figure 4.3 Canon EOS 60D Camera Image of NRL Being Electrospayed at 24 kV**

**Table 4.3 Characteristics of Electrospayed NRL at 15 kV-26 kV**

Parameter	Syringe Gauge			
	20 G	21 G	22 G	23 G
<b>15 kV</b>				
<i>Taylor Cone (T)/ Rayleigh's Jet (R)</i>	R	R	R	R
<i>Texture (Surface)</i>	Rough	Rough	Rough	Rough
<i>Thickness</i>	Thin	Thin (< 15-22 kV, 20 G)	Thin ( $\leq$ 15 kV, 20 G)	Thin ( $\approx$ 24-26 kV, 22 G)
<b>18 kV</b>				
<i>Taylor Cone (T)/ Rayleigh's Jet (R)</i>	R	R	R	R
<i>Texture (Surface)</i>	Rough	Rough	Rough	Rough
<i>Thickness</i>	Thin (< 15 kV, 20 G)	Thin (breaks up during removal)	Thin (breaks up during removal)	Thin (breaks up during removal)
<b>20 kV</b>				
<i>Taylor Cone (T)/ Rayleigh's Jet (R)</i>	R	R	R	R
<i>Texture (Surface)</i>	Rough	Rough	Rough	Rough
<i>Thickness</i>	Thin (< 18 kV, 20 G)	Thin ( $\approx$ 18 kV, 21 G and breaks up during removal)	Thin ( $\approx$ 18 kV, 22 G and breaks up during removal)	Thin (< 18 kV, 23 G breaks up during removal)
<b>22 kV</b>				
<i>Taylor Cone (T)/ Rayleigh's Jet (R)</i>	R	R	R	R
<i>Texture (Surface)</i>	Rough	Rough	Rough	Rough
<i>Thickness</i>	Thin (< 20 kV, 20 G)	Thin (< 20-22 kV, 20 G)	Thicker (> 15 kV, 22 G)	Thicker (> 18- 20 kV, 23 G)

<b>24 kV</b>				
<i>Taylor Cone (T)/ Rayleigh's Jet (R)</i>	R	R	R	R
<i>Texture (Surface)</i>	Rough; smoother than all kV	Rough; smoother than all kV	Rough; smoother than all kV	Rough
<i>Thickness</i>	Thinner than all kV	Thinner than all kV except 15 kV, 20 G and 24 kV, 20 G)	Thinner than all kV except 24 kV, 20 G	Thin (< 22 kV, 23 G; > 18-20 kV, 23 G)
<b>26 kV</b>				
<i>Taylor Cone (T)/ Rayleigh's Jet (R)</i>	R	R	R	R
<i>Texture (Surface)</i>	Rougher than 24 kV but less rough than 22 kV	Rougher than 24 kV and similar to 20 G	Rough; smoother than all kV	Rough
<i>Thickness</i>	Thicker than 24 kV, 20 G but thinner than 22 kV, 20 G	Thicker than 24 kV, 21 G but similar to 26 kV, 20 G	Similar to 24 kV, 22 G but thicker than 26 kV, 20 G	Thin (< 22-24 kV, 23 G); thicker than 20 kV, 23 G

As indicated in Xue *et al.* (2019) review on the electrospinning of nanofibres, increasing the applied voltage results in thinner fibres; however, this increase will also result in a relatively larger volume of fluid being ejected per minute and forming fibres with larger diameters (Deitzel *et al.*, 2001; Demir *et al.*, 2002; Zong *et al.*, 2002; Hu *et al.*, 2011). Hence, the thicker film of NRL electrospayed at a voltage of 26 kV in this work. These findings suggest that the thinnest fibres would be produced by electrospinning PVA/NRL solution at a voltage of 24 kV. Also, at 26 kV, an electrostatic field was felt sporadically, by touch, outside the electrospinning chamber. Therefore, to produce thinner fibres and for safety reasons, 24 kV was selected as the optimum voltage to electrospin PVA/NRL nanofibres.

In studies where poly(L-lactide-co- $\epsilon$ -caprolactone) [P(LLA-CL)] (Mo *et al.*, 2004) and bismuth (III) oxide ( $\text{Bi}_2\text{O}_3$ )/epoxy-PVA (Abunahel *et al.*, 2018) were electrospun, the researchers reported that smaller internal diameter of spinneret resulted in smaller amounts of beads; hence, thinner films were produced. Mo *et al.* (2004) and Ramakrishna *et al.* (2005) also reported that a smaller internal diameter reduces clogging of the spinneret; however, this work observed the opposite. Electrospaying with 23 G spinneret caused frequent clogging; therefore, the process was stopped several times to clean the clogged spinneret. Ramakrishna *et al.* (2005) explained that a smaller internal diameter would result in relatively higher surface tension of the droplet from the spinneret, consequently requiring a higher columbic force at the same voltage for the same voltage jet initiation. This will cause a decrease in jet acceleration, therefore, allowing the jet to stretch and elongate. However, in the case of electrospaying NRL, as the rate of jet acceleration decreases, relatively more NRL is retained in the spinneret per second during electrospaying at a relatively smaller internal diameter. It is worth noting that NRL naturally dries up quickly. Thus, this causes the NRL to dry quickly since more solution is retained in the spinneret tip at a particular time. Therefore, to avoid excessive clogging, 20 G was selected as the spinneret size for further studies in electrospaying PVA/NRL.

The morphology of the electrospayed NRL film (Canon camera and SEM images) is presented in Figure 4.4. SEM image (Figure 4.4a) showed the NRL film had no fibre formation and by visual inspection (Figure 4.4b), had a rough texture. This observation confirmed that the NRL was electrospayed at the voltages (15 kV – 26 kV) and spinneret sizes used (20 G – 23 G) in this work. It can also be inferred that the minimum concentration or viscosity needed for polymer chain entanglement had not been reached, causing the jet to break into polymer beads or droplets with no fibres forming. This means the NRL could only be electrospun at a higher viscosity, hence, the subsequent addition of PVA.

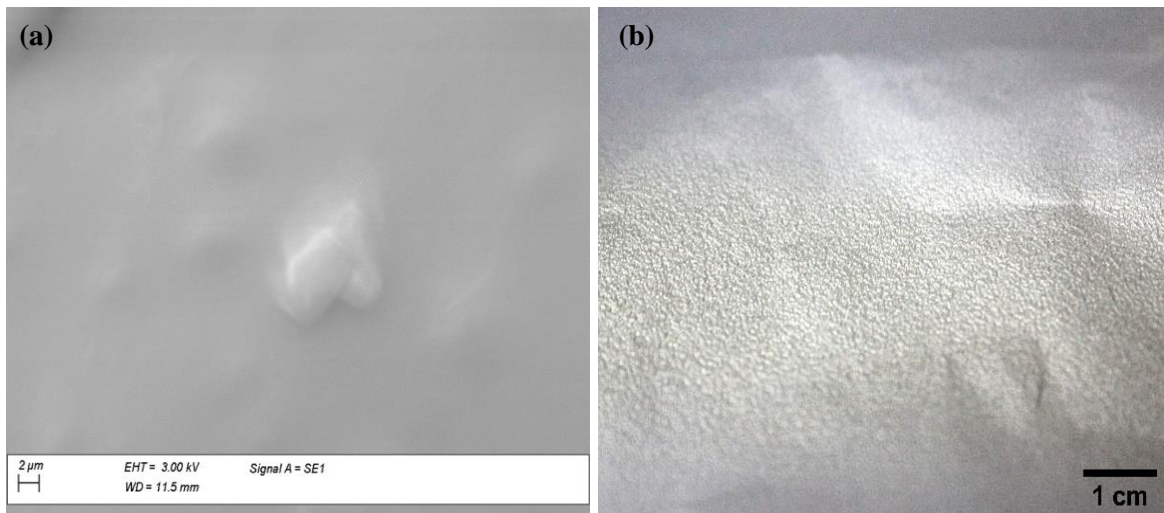


**Figure 4.4 (a) SEM and (b) Canon EOS 60D Camera Image of Electrospun NRL at 24 kV (Osei *et al.*, 2022)**

#### 4.4.2 Morphology of PVA/NRL Films

Figure 4.5 shows electrospinning of 50% PVA/NRL solution, and Figure 4.6 shows SEM images and fibre diameter distribution of 100% PVA, 40% PVA/NRL, 50% PVA/NRL and 60% PVA/NRL. SEM images and fibre diameter distribution of 70% PVA/NRL are presented in Figure 4.7. After image analysis, the average fibre diameters were in the order: 40% PVA/NRL < 50% PVA/NRL < 100% PVA < 70% PVA/NRL < 60% PVA/NRL. With a mean fibre diameter of  $591.57 \pm 13.07$  nm, electrospun 100% PVA had smooth fibres with no beadings (Figure 4.6a, b).

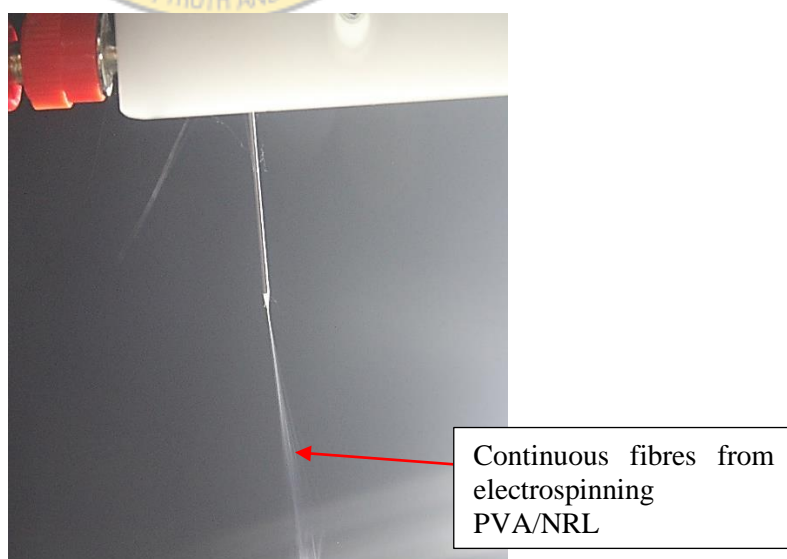


**Figure 4.5 Electrospinning 50% PVA/NRL Solution**

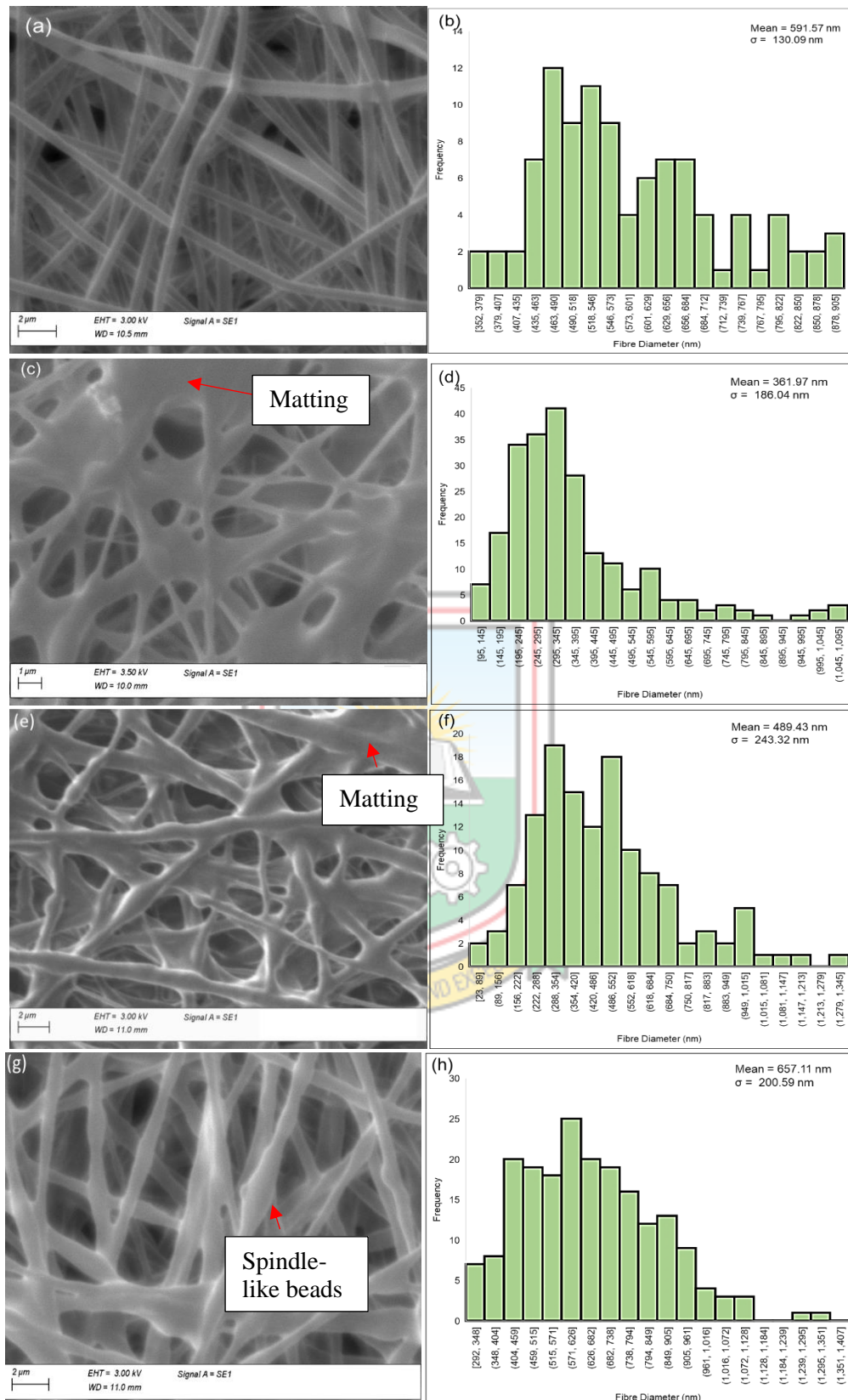


**Figure 4.6 SEM Image of Electrospun (a) 100% PVA, (c) 40% PVA/NRL, (e) 50% PVA/NRL, (g) 60% PVA/NRL and Their Corresponding Fibre Diameter Distributions (b, d, f and h, respectively) (Osei *et al.*, 2022)**

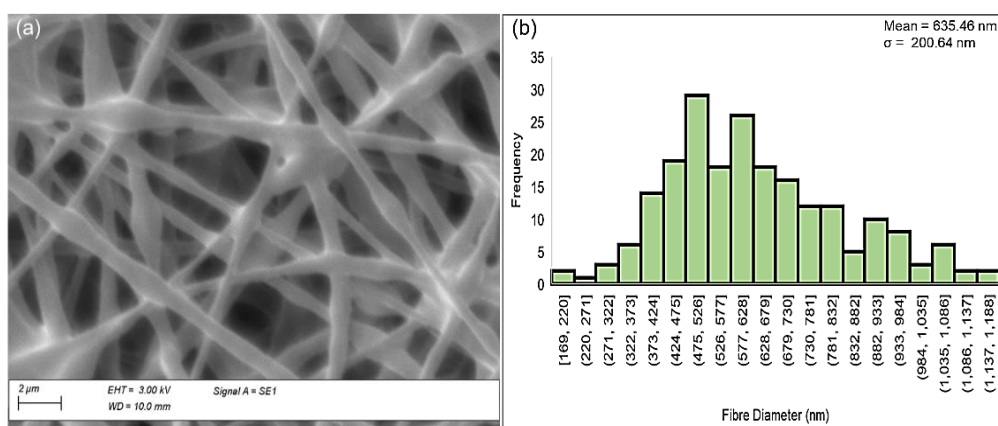


**Figure 4.7 Electrospun 70% PVA/NRL (a) SEM Image (b) Fibre Diameter Distribution (Osei *et al.*, 2022)**

Though 100% PVA had the most PVA content, the highest average diameter of  $657.11 \pm 14.22$  nm was recorded for 60% PVA/NRL (Figure 4.6h). The spindle-like beads observed in 60% PVA/NRL made the fibres appear larger at several locations (Figure 4.6g). This is similar to observations by Krishnappa *et al.* (2003). On the other hand, fibres of 70% PVA/NRL were slightly smoother with a lower average diameter of  $635.46 \pm 11.60$  nm (Figure 4.7a, b) compared to 60% PVA/NRL. This was because as the PVA content increased, smoother fibres were produced with less beading. Since the average fibre diameter of 70% PVA/NRL was smaller than 60% PVA/NRL but larger than 100% PVA, it is worth noting that if the study had continued for 80% and 90% PVA/NRL, their average fibre diameters would have been lower than 70% PVA/NRL, approaching 100% PVA's diameter. From this, it can be inferred that an increase in viscosity of the PVA/NRL solution due to increased PVA content resulted in smoother and continuous fibres with its average diameter also increasing. Increased viscosity produced relatively fewer, smaller beadings and matting because of enhanced polymer chain entanglement. Enhanced polymer chain entanglement enables an electrified jet to stretch fully, forming continuous and smooth fibres (Ramakrishna *et al.*, 2005; Xue *et al.*, 2019).

Smaller average fibre diameters of  $361.97 \pm 12.40$  nm and  $489.43 \pm 21.34$  nm were observed in 40% and 50% PVA/NRL, respectively (Figure 4.6d, f). Since the study aimed at producing nanofibres as a matrix for nanoparticle synthesis, nanoparticle loading and adsorption studies, smaller fibre diameters were preferred. Smaller diameters infer an increased surface area-to-volume ratio, an essential factor for enhancing adsorption in aqueous processes. A smaller average fibre diameter also means a relatively larger area

would be available for nanoparticles to be attached in its synthesis. However, the challenge encountered was the presence of mattings in the 40% and 50% PVA/NRL, and the fibres were relatively less smooth (Figure 4.6c, e). Matting occurs when the fibre's solvent does not evaporate completely before the fibre reaches the collector, causing the fibre to collapse and form a non-porous structure (50% PVA/NRL) (Sun *et al.*, 2012). Matting can also occur if the extended jet intermittently breaks and, therefore, is not continuous, resulting in the charged droplet landing on the collector (40% PVA/NRL). Matting lowers the surface area-to-volume ratio, which is a drawback in producing nanofibers and for adsorption studies.

The pore diameters of the PVA/NRL fibre films are presented in Table 4.4. Mean pore diameters were in the order; 40% PVA/NRL < 50% PVA/NRL < 70% PVA/NRL < 60% PVA/NRL. All fibre films had pore sizes in the macroporous range (> 50 nm). As the PVA concentration increased, the pore diameter also increased, similar to the PVA/NRL fibre diameter distribution trend. Smaller pore diameters observed in 40% (890.90 ± 36.24 nm) and 50% PVA/NRL (896.30 ± 41.02 nm) meant relatively more fibres per area since their fibre diameters were also relatively smaller. This also meant that although mattings in 40% and 50% PVA/NRL may reduce the surface area-to-volume ratio, its smaller average fibre size and pore diameter may compensate for it by increasing the surface area-to-volume ratio. A relatively smaller fibre size and pore diameter also infer a larger area for nanoparticle attachment and adsorption. In general, the observation was that as PVA concentration increased, the electrospun fibres became smoother, fibre diameter increased, pore diameter increased, and matting and beading decreased.

**Table 4.4 Pore Diameters of PVA/NRL Fibre Films**

PVA/NRL Ratio (%)	Pore Diameter (nm)			
	<i>Min</i>	<i>Max</i>	<i>Mean ± SEM<sup>a</sup></i>	<i>Standard Deviation</i>
<b>40%</b>	152.80	3044.52	890.90 ± 36.24	511.28
<b>50%</b>	216.06	2537.01	896.30 ± 41.02	449.35
<b>60%</b>	186.36	5718.67	1416.14 ± 77.75	939.42
<b>70%</b>	210.82	3594.58	1135.20 ± 51.06	623.22

(Osei *et al.*, 2022)



#### 4.5 Characterisation of PVA/NRL Films by Fourier Transform - Infrared (FT-IR) Spectroscopy

Intermolecular interactions of the electrospun fibres were investigated via FT-IR analysis. Figure 4.8 shows the FT-IR spectra of NRL, PVA and PVA/NRL fibre films. One of the prominent vibrational bands observed in NRL spectra was the C-H stretching at  $2961\text{ cm}^{-1}$ . Also, the symmetric and asymmetric bending of  $\text{CH}_2$  at  $1448$  and  $1374\text{ cm}^{-1}$ , and the tri-substituted olefinic of polyisoprene at  $842\text{ cm}^{-1}$  observed were characteristic of NRL (Abu Bakar *et al.*, 2007; Saengdee *et al.*, 2020). On the other hand, as observed by Bhat *et al.* (2005) and Mansur *et al.* (2008), the prominent vibrational bands of PVA were the O-H stretching, C-H stretching at  $2939\text{ cm}^{-1}$ , C=O stretching of the remaining acetate groups of PVA at  $1738\text{ cm}^{-1}$ ,  $\text{CH}_2$  bending at  $1430\text{ cm}^{-1}$ , C-O stretching of the crystalline portion at  $1142\text{ cm}^{-1}$  and C-O stretching of the amorphous portion at  $1089\text{ cm}^{-1}$ .

From Figure 4.8, both NRL and PVA vibration bands were observed in the spectra of all the PVA/NRL fibre films. This shows that NRL and PVA had been merged in these fibres. A general observation was that as the PVA content increased, vibration bands at  $2961$  and  $842\text{ cm}^{-1}$  as observed by Abu Bakar *et al.* (2007), which are characteristic of NRL decreased. On the other hand, the vibration bands at  $1738$  and  $1089\text{ cm}^{-1}$  as observed by Bhat *et al.* (2005) and Mansur *et al.* (2008), which are characteristic of PVA, increased. In addition, the spectra around  $1430\text{ cm}^{-1}$ , which is part of the acetate group, also diminished with increased PVA content. Another observation was that the 40% and 50% PVA/NRL spectra had relatively more intense peaks of NRL, whilst 60% and 70% PVA/NRL spectra had relatively more intense peaks of PVA. Nonetheless, the 40% and 50% PVA/NRL spectra were similar, whilst PVA peaks were relatively more prominent in 70% PVA/NRL than in 60% PVA/NRL.

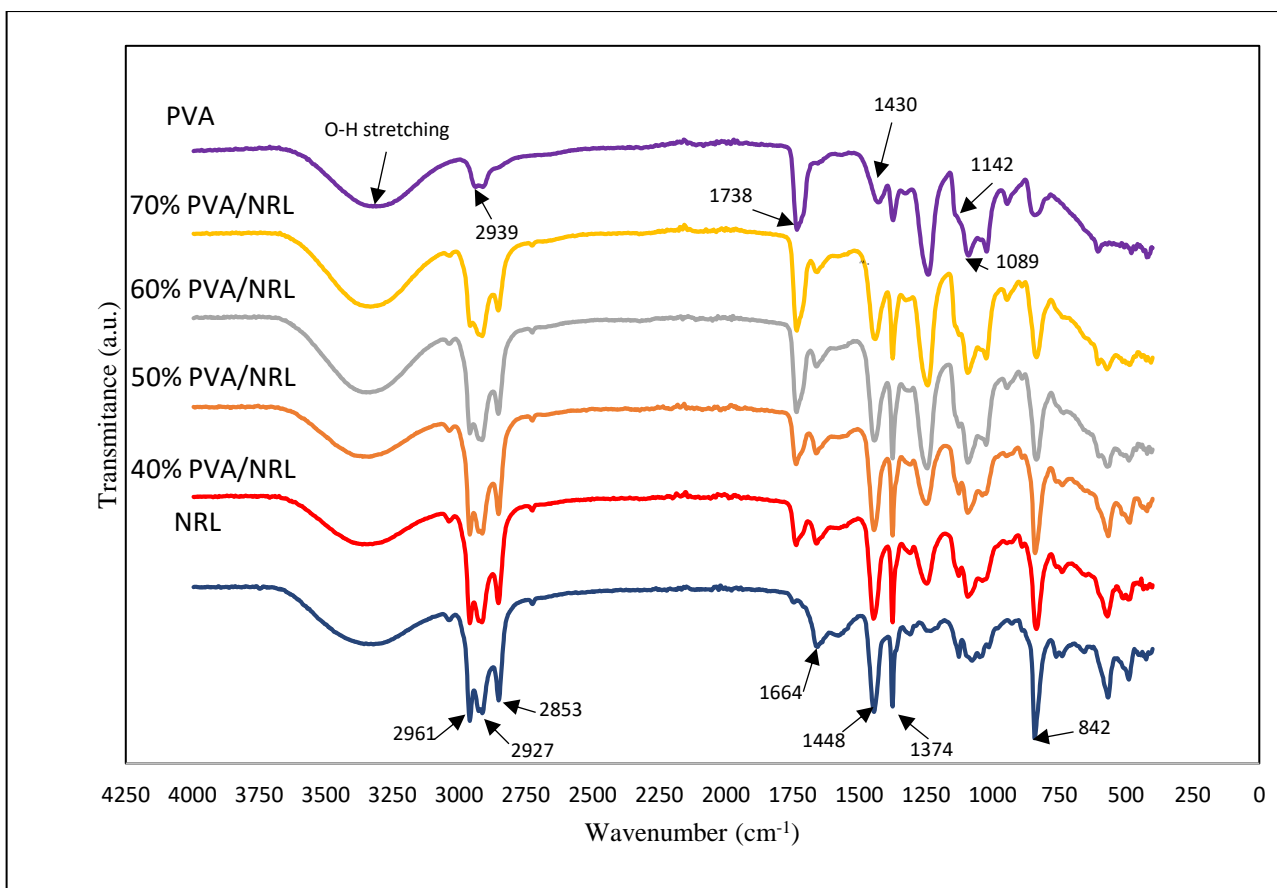


**Figure 4.8 FT-IR Spectra of 100% PVA, % PVA/NRL and NRL Fibre Films (Osei *et al.*, 2022)**

Since PVA has several -OH groups that interact with water molecules through hydrogen bonding, it is soluble in water (Harpaz *et al.*, 2019). Hence, the degree of hydrolysis (DH) of the NRL/PVA fibre films was studied from the FT-IR spectra. Mansur *et al.* (2008) explained in a study on PVA hydrogel of different DH that DH of PVA correlates with its remaining acetate groups. Mansur *et al.* (2008) further explained that the DH of PVA could be calculated as a ratio of the spectra at  $1738\text{ cm}^{-1}$  (C=O stretching) to that at  $1430\text{ cm}^{-1}$  ( $\text{CH}_2$  bending). In Figure 4.8, it can be seen that the ratio of the absorption band intensities at  $1738\text{ cm}^{-1}$  to  $1430\text{ cm}^{-1}$  decreases with an increase in PVA content. From this, it can be inferred that 60% and 70% PVA/NRL had lower DH than 40% and 50% PVA/NRL. It is also worth noting that a lower DH means relatively lower water resistance or higher solubility (Mansur *et al.*, 2008; Harpaz *et al.*, 2019). Therefore, it was anticipated that a relatively greater fraction of 60% and 70% PVA/NRL will dissolve when applied in an aqueous process than that of 40% and 50% PVA/NRL.

#### 4.6 Weight Loss Analysis by Dissolution

The weight loss test was done to determine which PVA/NRL fibre was most suitable for AgNP synthesis and, subsequently, for the adsorption of Hg and Cd<sup>2+</sup>. If the fibre films are used as a matrix for nanoparticle synthesis, nanoparticle loading and adsorption, it would not be ideal for a large portion of the fibre to dissolve into the solution. In addition, if a significant portion dissolves, the fibre may release the adsorbates back into the solution. This will defeat the possibility of using the electrospun PVA/NRL fibre as an efficient adsorbent for contaminant removal in aqueous environmental waste.

Figure 4.9 shows aqueous solutions after PVA/NRL fibre films had been shaken in distilled water. Weight loss percentages of nanofibres in this experiment are presented in Table 4.5. From Figure 4.9, it can be seen that the aqueous solution increased in cloudiness with an increase in PVA content. The relatively cloudier solutions obtained for 60% and 70% PVA/NRL were likely from a greater fraction of the fibre dissolving in the distilled water than for 40% and 50% PVA/NRL. As predicted from FT-IR analysis, 70% PVA/NRL had the highest weight loss of  $48.84 \pm 5.03\%$ . The weight loss was in the order: 50% PVA/NRL < 40% PVA/NRL < 60% PVA/NRL < 70% PVA/NRL. Due to its comparatively low DH, as previously mentioned, 60% and 70% PVA/NRL lost the most weight. This was also observed by Harpaz *et al.* (2019), where the PVA with the lowest DH dissolved fastest amongst three PVAs of different DHs. In PVAs with lower DH, the inter- and intra-molecular hydrogen bonds are reduced because of steric hindrance from hydrophobic acetate groups occurring in abundance. This steric hindrance boosted the interactions between the fibre molecules and water molecules, causing a higher dissolution, hence, higher weight loss.

On the other hand, since a higher DH means a greater reaction between the fibre molecules than with water molecules, it was expected that 40% PVA/NRL would have the least weight loss. On the contrary, 50% PVA/NRL had the least weight loss. The nanofibre 40% PVA/NRL having a higher weight loss may mainly be attributed to severe matting experienced after electrospinning. Excessive matting amongst relatively thin fibres may have caused the fibres in 40% PVA/NRL to snap upon removal from the aluminium foil.

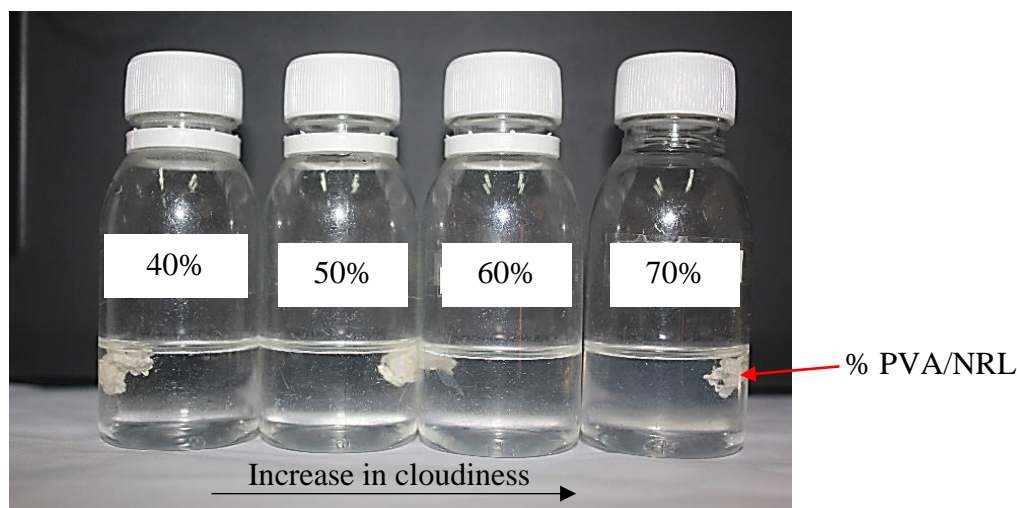


**Figure 4.9 Aqueous Solution with % PVA/NRL Fibre Film After Shaking in Distilled Water (Osei *et al.*, 2022)**

**Table 4.5 Weight Loss Analysis of PVA/NRL Nanofibres**

PVA/NRL Ratio (%)	Weight Loss (%) $\pm$ SEM <sup>a</sup>
40	23.46 $\pm$ 5.37
50	14.09 $\pm$ 1.86
60	44.12 $\pm$ 2.82
70	48.84 $\pm$ 5.03

(Osei *et al.*, 2022)

In addition, some severely matted areas stuck to the aluminium foil, making the fibre difficult to remove. As a result, the fibre fragments may have been lost during shaking and filtering, which is why the solution was relatively less cloudy (Figure 4.9).

After the weight loss test, SEM analysis was conducted to understand the fibres' morphology after contact with an aqueous solution. Figure 4.10 shows SEM images of 50% PVA/NRL after the weight loss test. The individual fibres clamped together, becoming large fibres with macro pores on the individual fibres. It is worth noting that the fibres adsorbed water, causing the fibres to swell and collapse after drying. Again, during the fibre's removal from the aluminium foil, the fibre tends to stick to itself, probably causing some individual fibres to merge and form larger ones.

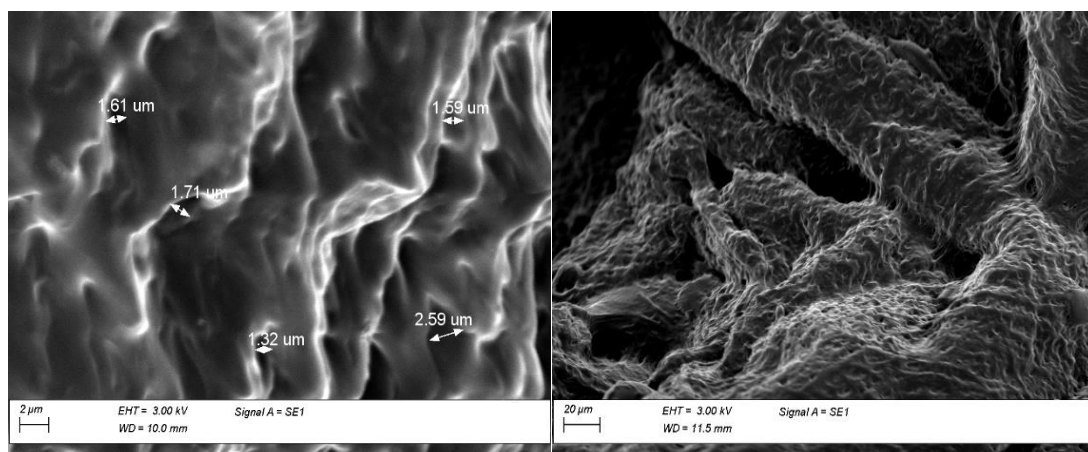


**Figure 4.10 SEM Images of 50% PVA/NRL After Weight Loss Analysis (Osei *et al.*, 2022)**

It is important to note that researchers including Costa *et al.* (2013) mixed polycaprolactone (PCL) and natural rubber, Cosme *et al.* (2016) mixed polylactic acid (PLA) and natural rubber, whilst Taweepreda (2017) also mixed polyvinyl chloride (PVC) and epoxidized rubber in their work. These researchers all obtained smoother fibres after electrospinning. However, these smooth fibres could only be obtained by adding hazardous solvents such as toluene, chloroform, DMF and THF. Synthetic rubbers such as polybutadiene rubber also require DMF and THF for its dissolution and electrospinning (Hu *et al.*, 2012). Again, in the work of Panichpakdee *et al.* (2019), where a similar mixture such as that used in this study (NRL mixed with PVA) was electrospun, the surfactant 2-[4-(2,4,4-trimethylpentan-2-yl)phenoxy]ethanol (Triton-X 100) was used to improve the morphology of the fibres; however, Triton-X 100 is also hazardous (Luo *et al.*, 2020). It is also important to note that in this study, 50% PVA/NRL fibre film, which recorded the least weight loss, dissolved about 14% of the fibre in distilled water. Therefore, adding such harmful solvents and surfactants may leave traces of these substances in aqueous media after water treatment, defeating the purpose of creating an environmentally friendly pollutant remover.

#### 4.7 Summary

In summary, NRL was successfully electrospun without a harmful solvent, but by adding PVA and with water serving as the solvent. Decreasing PVA content produced relatively rougher but thinner electrospun fibres with smaller average pore diameters, whilst increasing PVA content produced smoother fibres with decreased mattings and increased fibre and pore diameters (SEM analysis and visual inspection). Again, decreasing PVA

content decreased the fibre's solubility in water (FT-IR analysis and weight loss analysis by dissolution). However, 40% PVA/NRL lost a relatively higher mass in water, making 50% PVA/NRL the best option for aqueous process application.

The nanofibre's ability to synthesise AgNP can now be tested and analysed upon obtaining the optimum ratio of NRL to PVA for electrospinning. This is discussed in Chapter 5.



## CHAPTER 5

### GREEN SYNTHESIS AND CHARACTERISATION OF SILVER NANOPARTICLES IN PVA/NRL NANOFIBRE COMPOSITE (AgNP-PVA/NRL) FOR ADSORPTION STUDIES

This chapter discusses AgNP synthesised in PVA/NRL nanofibre composite (AgNP-PVA/NRL) by adding AgNP precursor to the solution before electrospinning. The discussion on the synthesised nanofibre composites includes that of its morphology and elemental composition based on scanning electron microscopy (SEM), energy dispersive x-ray spectroscopy (EDS) and transmission electron microscopy (TEM); the crystallographic composition (to confirm the presence of AgNP) based on x-ray diffractometry (XRD); the interaction of the AgNP with NRL and PVA in the fibre matrix based on Fourier transform - infrared spectroscopy (FT-IR) and finally the point of zero charge (PZC) of the nanofibre composite. The Chapter also discusses the possible reasons for the observed sizes of AgNP in the nanofibre composites.

#### 5.1 Background

Over the years, silver nanoparticles (AgNP) have proven efficient in removing heavy metals and as an antimicrobial agent in water treatment processes (Hu, 2010; Tauanov *et al.*, 2018; Mohammadi *et al.*, 2019; Tauanov *et al.*, 2019). Several methods have been explored for producing AgNP, including synthetic reducing and stabilising agents, which are toxic to the environment, such as sodium borohydride ( $\text{NaBH}_4$ ) (Li *et al.*, 2012; Badi'ah *et al.*, 2019). As a result, in searching for green methods to synthesise AgNP, other researchers have resorted to plant extracts as a green alternative for producing AgNP (Ajitha *et al.*, 2015; Moldovan *et al.*, 2016; Kumar *et al.*, 2018). For instance, some researchers have successfully used natural rubber latex (NRL) to synthesise AgNP (Abu Bakar *et al.*, 2007; Guidelli *et al.*, 2011).

As stated in Chapters 1 and 4, it would not be desirable to have nanoparticles remain in treated water, as it would form part of the contamination problem. In line with that, AgNP-NRL solutions are usually dried to form flat non-porous films (Abu Bakar *et al.*, 2007; Abu Bakar *et al.*, 2010). However, it is well established that a porous film has a higher surface area-to-volume ratio than its non-porous counterpart, which is desirable in adsorption processes. Therefore, synthesising the AgNP and casting the nanoparticles on the surface of

electrospun NRL is a plausible option. However, since the nanoparticles are on the surface, the AgNP may be easily released into the solution during water treatment. Alternatively, the precursor for AgNP synthesis could be added to NRL before electrospinning. This means most of the AgNP would be near or within the fibre's surface and would not be easily released into the treated water. Nevertheless, the persisting question is, 'Will AgNP form, though the electrospun NRL fibres would be almost dry before reduction and stabilisation of Ag<sup>+</sup> occur?' This is because the environmental condition (temperature) necessary for AgNP growth would be provided only after electrospinning.

## **5.2 Morphology and Elemental Composition of AgNP-PVA/NRL Nanofibre Composites**

The procedure for synthesising AgNP in PVA/NRL nanofibre composites using AgNO<sub>3</sub> concentrations of 0.01 M and 0.015 M is described in Chapter 3. Electrospun AgNP-PVA/NRL nanofibre composites (0.01 M AgNP and 0.015 M AgNP) before and after drying are presented in Figure 5.1. As shown in Fig 5.1a, the nanofibre composites were off-white in colour after electrospinning. However, after drying overnight, the nanofibre composites turned pale yellowish-brown (Figure 5.1b). The colour change indicates the possible formation of AgNP in the nanofibre composites. This was also observed in other research works involving AgNP synthesis, where there was a change in colour from white or colourless to a yellow, yellowish-brown or brownish-yellow solution, indicating AgNP formation (Guidelli *et al.*, 2011; Ajitha *et al.*, 2015; Sagitha *et al.*, 2016; Mohammadi *et al.*, 2019).



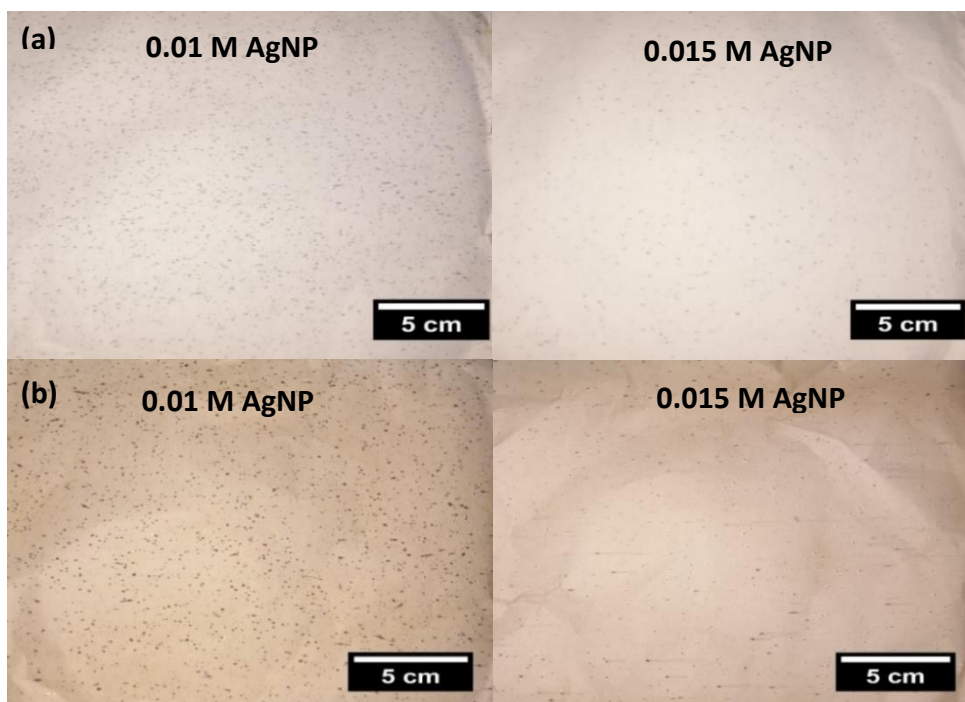


**Figure 5.1 Electrospun 0.01 M AgNP and 0.015 M AgNP Nanofibre Composite (a) Before and (b) After Drying**

### 5.2.1 Characterisation by Scanning Electron Microscopy and Energy Dispersive X-Ray Spectrometer

Scanning electron microscopy and EDS analyses were conducted to confirm the formation of AgNP in the nanofibre composites. Figure 5.2 shows some BSD-SEM images of 0.01 M AgNP with its EDS analysis. BSD-SEM images of 0.015 M AgNP with EDS analysis are also presented in Figure 5.3. From both Figure 5.2a and 5.3a, a few distinctive white dots (red arrow) were observed on the fibre's surface, which was confirmed by the EDS spectral analysis to be AgNP (Figure 5.2c and 5.3c). By comparison, there were relatively more AgNPs on the surface of 0.01 M AgNP (Figure 5.2a) than on 0.015 M AgNP (Figure 5.3a). Although a few AgNPs were observed in the SEM-EDS images, EDS analysis showed relatively more AgNPs on or in the fibres (Figure 5.2b and 5.3b).

According to existing literature, increasing  $\text{AgNO}_3$  concentration will produce relatively more AgNP due to the higher Ag/polymer ratio (Abu Bakar *et al.*, 2007; Guidelli *et al.*, 2011); however, more AgNP were observed on 0.01 M AgNP than 0.015 M AgNP. This could result from Ag particles on 0.01 M AgNP forming relatively larger nanoparticles or aggregates on the fibre's surface or having a relatively thinner polymer covering (compared to the size of the AgNP). This might have resulted in an easier detection of the nanoparticles

by only SEM. Another possibility is that AgNP on 0.015 M AgNP were relatively smaller and well dispersed to the extent that even the thin polymer coverage seemed thick (compared to the size of the AgNP). This may have inhibited the accurate detection of the nanoparticles by SEM only.

Hence, EDS analysis, which provides information on elemental composition on the surface and a few microns beneath the surface, showed that AgNP were well dispersed on both fibres. This means that increasing AgNO<sub>3</sub> concentration probably caused AgNP produced to be relatively smaller and with a relatively thicker polymer coverage; hence, most nanoparticles stayed within the fibre walls.

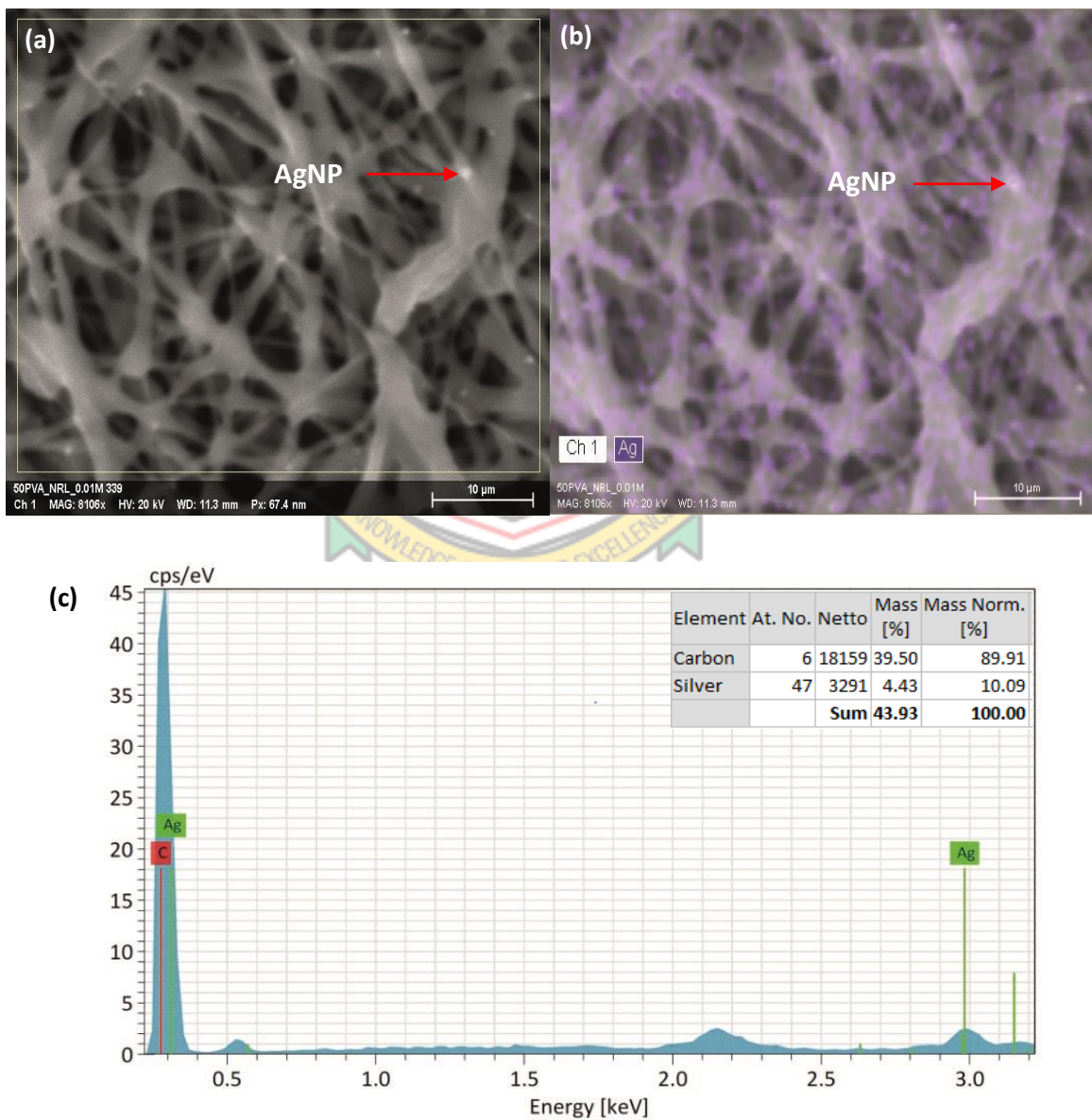


**Figure 5.2 (a) BSD-SEM Image of 0.01 M AgNP with (b)EDS Map and (c) EDS Spectral Analysis**

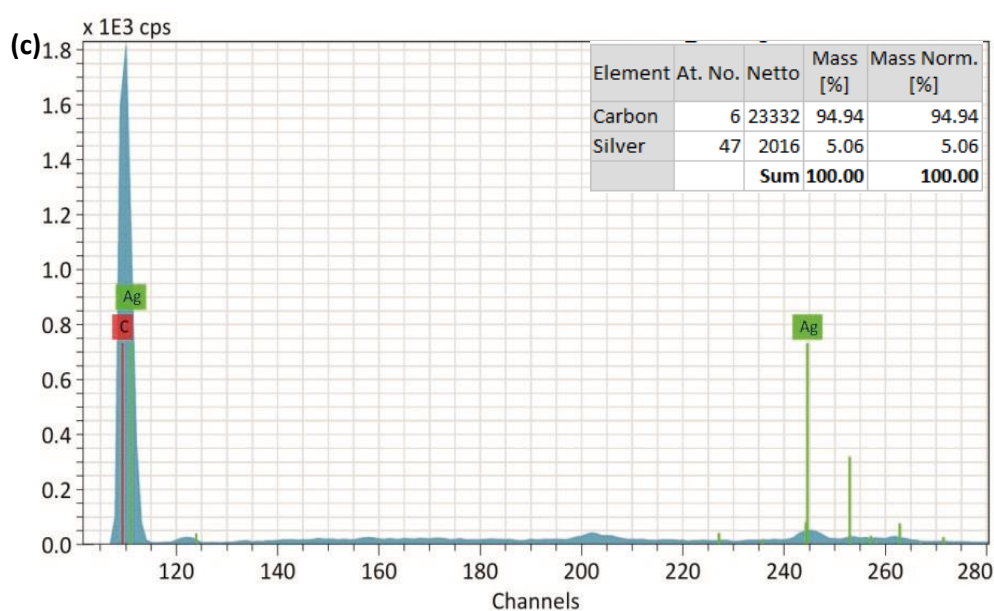
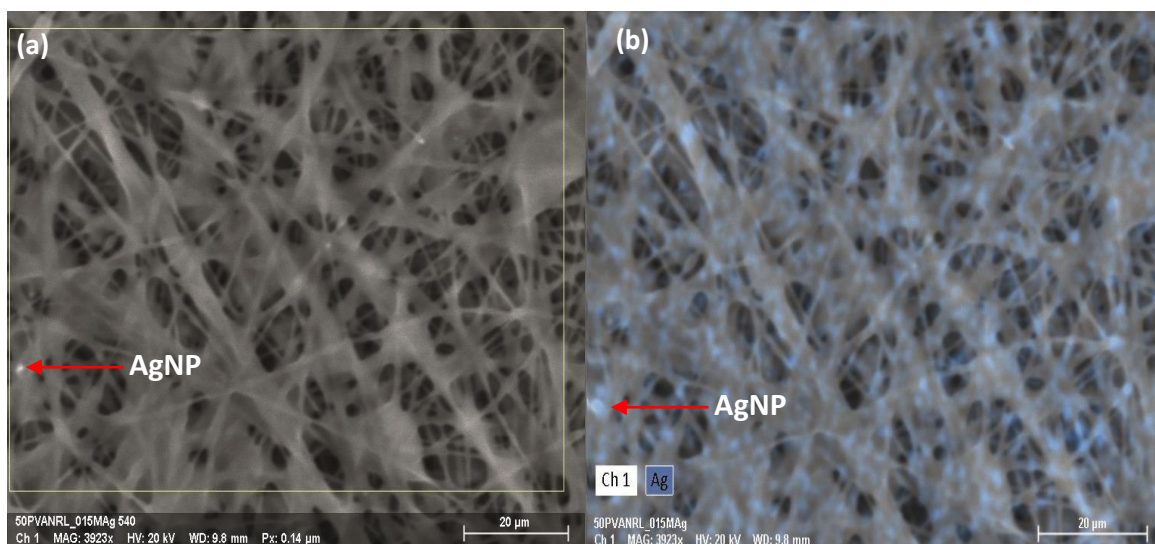


**Figure 5.3 (a) BSD-SEM Image of 0.015 M AgNP with (b) EDS Map and (c) EDS Spectral Analysis**

Also, due to the relatively smaller size of the AgNP in 0.015 M AgNP compared to the thickness of the polymer coverage, most AgNP could not be detected by the BSD-SEM but were visible in its corresponding EDS analysis. Again, it may be possible that this study's method for synthesising AgNP might have caused most AgNP to be produced within the fibre walls when AgNO<sub>3</sub> concentration was increased.

### 5.2.2 Characterisation by Transmission Electron Microscopy (TEM)

In order to verify the distribution of AgNP in 0.01 M and 0.015 M AgNP and if the nanoparticles were relatively smaller in 0.015 M AgNP, the nanofibre composites were

subjected to TEM analysis to view the ‘naked’ AgNP without a polymer coverage. Figure 5.4 presents TEM images and size distribution of AgNP for 0.01 M and 0.015 M AgNP.

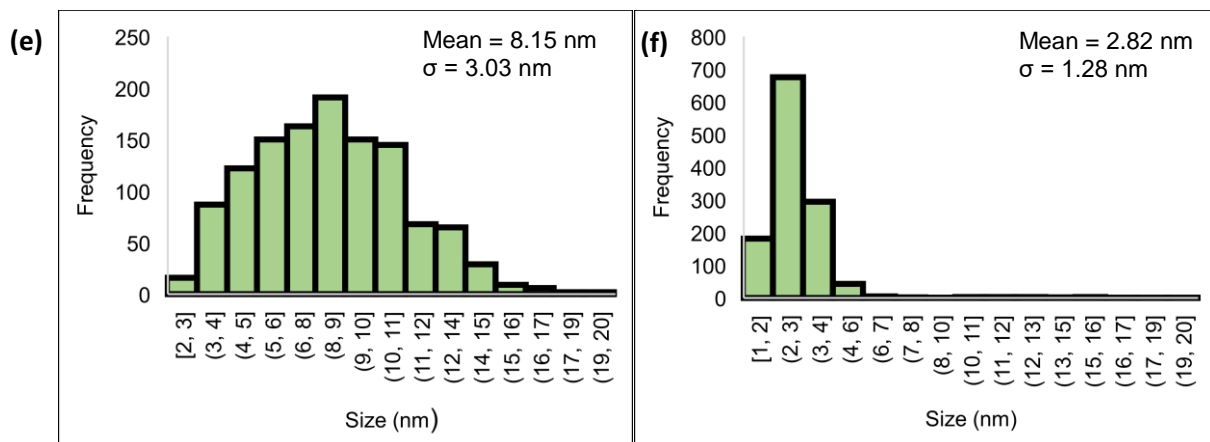
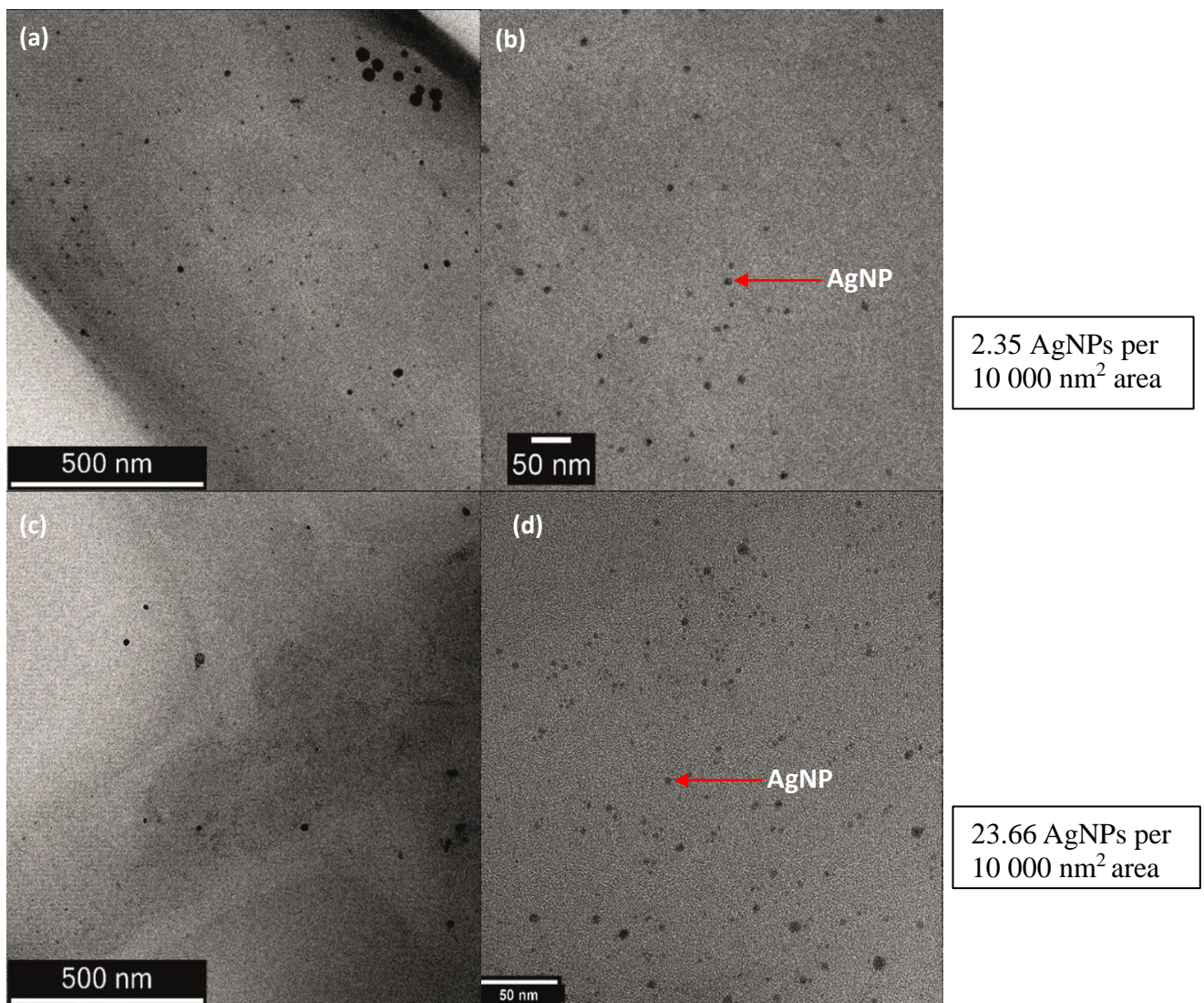


**Figure 5.4** TEM Images of AgNP in 0.01 M AgNP (a and b) and 0.015 M AgNP (c and d) with their Corresponding Size Distribution (e and f, respectively)

Produced nanoparticles were virtually spherical in both 0.01 M and 0.015 M AgNP. Figures 5.4a and 5.4b show 0.01 M AgNP at different magnifications with the nanoparticles well distributed throughout the fibre. The AgNP had a larger polydispersity with diameters ranging from 1.57-19.76 nm and an average size of  $8.15 \pm 0.09$  nm (Figure 5.4e). Figures 5.4c and 5.4d show 0.015 M AgNP at different magnifications. The nanoparticles in 0.015 M AgNP were also well dispersed but had a smaller polydispersity with diameters ranging from 0.61-19.90 nm. The average nanoparticle size in 0.015 M AgNP was  $2.82 \pm 0.04$  nm. Additionally, it was found that there were 2.35 AgNP per  $10\,000\text{ nm}^2$  area in 0.01 M AgNP whilst there were 23.66 AgNP per  $10\,000\text{ nm}^2$  area in 0.015 M AgNP. This indicates that the TEM was able to go beyond the magnification of SEM to visualise within the 0.015 M AgNP fibre composite for all the hidden particles. The relatively more AgNP observed in 0.015 M AgNP was anticipated, given the higher Ag/polymer in 0.015 M AgNP.

Similar to observations made by Guidelli *et al.* (2011), it was found in this study that  $\text{AgNO}_3$  concentration affected the size distribution of AgNP; that is, higher  $\text{AgNO}_3$  concentration produced nanoparticles with a smaller dispersity (Figure 5.4e, f). Guidelli *et al.* (2011) and Abu Bakar *et al.* (2007) recorded a smaller average size for AgNP synthesised as  $\text{AgNO}_3$  concentration increased; however, this study observed the opposite (0.01 M AgNP = 8.15 nm; 0.015 M AgNP = 2.82 nm). It is worth noting that, Henglein and Giersig (1999) found out that a lower stabilising agent/ $\text{Ag}^+$  ratio resulted in the coalescence of Ag cluster, hence, forming larger AgNP. Coalescence of AgNP occurs because the stabilising agent in NRL, which prevents uncontrolled growth and agglomeration, has not been adequately built around the Ag clusters. The difference between Henglein and Giersig (1999), Abu Bakar *et al.* (2007) and Guidelli *et al.* (2011) research and this study is that in their research, AgNP growth occurred in a liquid medium. In this study, the NRL/PVA had already solidified before nanoparticle growth fully occurred. Therefore, in the liquid medium, the clusters could easily diffuse and combine with other Ag clusters to form larger AgNP even when a lower stabilising agent/ $\text{Ag}^+$  ratio existed (that is, when  $\text{AgNO}_3$  concentration was increased). However, in this study, the matrix is solid. Assuming homogenous nucleation of AgNP in the nanofibre matrix, since there is a relatively lower reducing agent/ $\text{Ag}^+$  and stabilising agent/ $\text{Ag}^+$  ratios in 0.015 M AgNP, Ag clusters formed would ideally diffuse and coalesce to form larger nanoparticles, however since the matrix is solid, effective diffusion is impossible. Hence the smaller average-sized AgNP observed in 0.015 M AgNP.

On the other hand, as stated by Henglein and Giersig (1999), for 0.01 M AgNP where there is a relatively higher reducing agent/ $\text{Ag}^+$  and stabilising agent/ $\text{Ag}^+$  ratios, further reduction of  $\text{Ag}^+$  on the surface of the Ag clusters may have resulted in the larger average size particles. It is worth noting that though further reduction of  $\text{Ag}^+$  on the surface of Ag clusters may have resulted in the larger nanoparticles, the average particle size in 0.01 M AgNP was less than 10 nm, meaning the stabilising agent was enough to prevent further agglomeration.

### **5.3 Characterisation of AgNP-PVA/NRL Nanofibre Composite by X-Ray Diffractometry (XRD)**

The crystallographic structures in the nanofibre composites were analysed using the XRD to verify whether AgNP had indeed formed. Figure 5.5 illustrates the XRD patterns of PVA/NRL, 0.01 M AgNP and 0.015 M AgNP nanofibre composites. Similar to XRD peaks of Ag in NRL composites observed by Abu Bakar *et al.* (2007) and Abu Bakar *et al.* (2010), for 0.01 M and 0.015 M AgNP, the prominent peaks were seen at  $38.3^\circ$ ,  $44.6^\circ$ ,  $65.0^\circ$  and  $78.2^\circ$ , relative to (111), (200), (220) and (311) planes, respectively. These peaks correlate to face-centred cubic Ag (ICDD 01-071-4612), meaning the particles observed in both SEM and TEM analysis were truly AgNP.

It must be pointed out that aluminium foil was analysed as part of the sample, and its prominent peaks were also observed, at  $44.7^\circ$ ,  $65.1^\circ$  and  $78.3^\circ$  (ICDD 03-065-2869), as seen in PVA/NRL (Figure 5.5). The aluminium affected the intensities of Ag by dwarfing its peaks in 0.01 M and 0.015 M AgNP. Despite this, the growing intensity at  $38.3^\circ$ , which is a prominent peak in both 0.01 M and 0.015 M AgNP, showed that AgNP were indeed present in the nanofibre composites. The hump observed in Figure 5.5 may be attributed to an amorphous halo of NRL. This is similar to the observation made by Abu Bakar *et al.* (2007) at  $2\theta = 20.0^\circ$ , but at a slightly lower  $2\theta$  ( $17.0^\circ$ ) in this study.

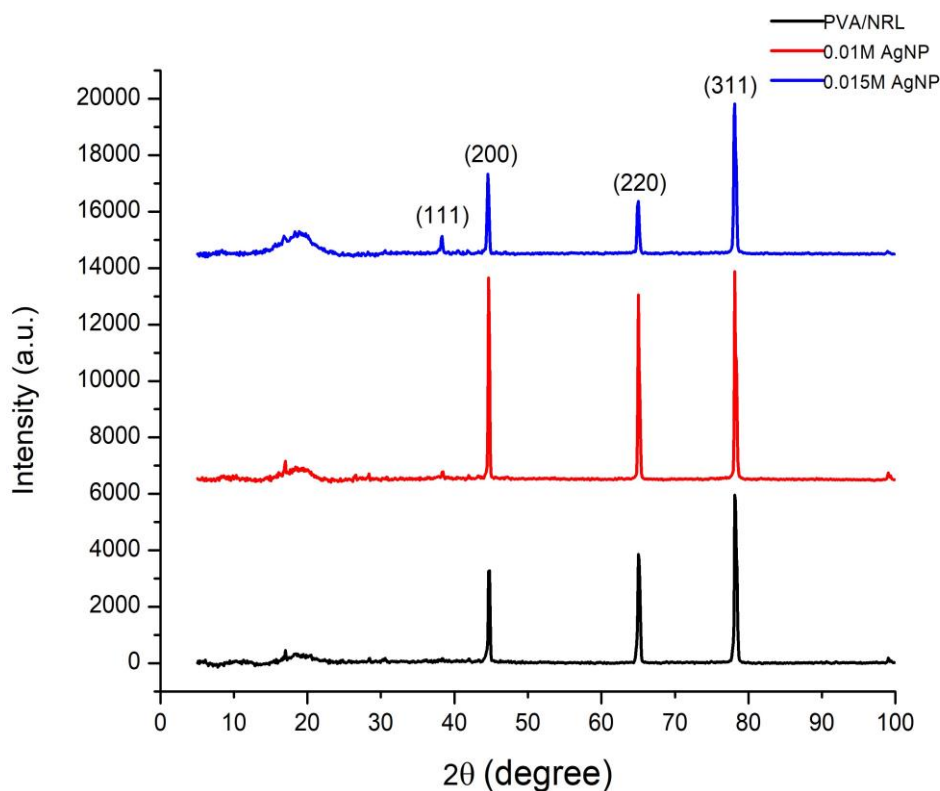


**Figure 5.5 XRD Patterns for PVA/NRL and AgNP-PVA/NRL Nanofibre Composites**

#### **5.4 Characterisation of AgNP-PVA/NRL Nanofibre Composite by Fourier Transform Infrared Spectroscopy (FT-IR)**

The FT-IR spectra of PVA/NRL and AgNP nanofibre composites are presented in Figure 5.6. In the spectrum of PVA/NRL nanofibre, eight distinct peaks of NRL were observed at 2 961, 2 927, 2 853, 1 660, 1 444, 1 375, 1 125 and 840  $\text{cm}^{-1}$ . These observations were also made by Abu Bakar *et al.* (2007). Four other peaks, characteristic of PVA, were also observed in the PVA/NRL nanofibre at 1 735, 1 248, 1 093 and 1 038  $\text{cm}^{-1}$  as observed by Bhat *et al.* (2005) and Mansur *et al.* (2008). All the peaks mentioned earlier were also observed in the spectra of 0.01 M and 0.015 M AgNP. However, a new peak emerged at 1 717  $\text{cm}^{-1}$ , and the intensities of peaks at 1 735, 1 248, 1 125, and 1 038  $\text{cm}^{-1}$  reduced significantly relative to the others. The relatively less noticeable changes are the slight broadening of the O-H stretch and the reduction in peaks at 759  $\text{cm}^{-1}$  and 738  $\text{cm}^{-1}$  corresponding to the skeleton of isoprene (Danna *et al.*, 2016).

The diminished peak at 1 735  $\text{cm}^{-1}$  could be attributed to the carbonyl group of PVA. However, in a similar study by Abu Bakar *et al.* (2007), where only NRL was used, the

authors observed new peaks at 1 717  $\text{cm}^{-1}$  and 1 723  $\text{cm}^{-1}$ , which were from a possible mixture of ketones and aldehydes. Similar reaction observed in this study may suggest possible oxidation of the nanofibre composites (Abu Bakar *et al.*, 2007). Also, the diminished peak at 1 125  $\text{cm}^{-1}$  (which may be assigned to the  $\text{CH}_2$  wagging) and the one at 1 038  $\text{cm}^{-1}$  (which may be attributed to C-N and C-O stretching) indicates the presence of amine group in the NRL might have reduced  $\text{Ag}^+$  ions as proposed in literature (Guidelli *et al.*, 2011; Danna *et al.*, 2016). Similar to the observation made by Guidelli *et al.* (2011) on natural rubber, the alterations at 759  $\text{cm}^{-1}$  and 738  $\text{cm}^{-1}$  in this study imply that *cis*-isoprene may have served as a stabilising agent in the reaction. It is also worth noting that though the nanofibre composites were almost dry before significant AgNP growth could be observed, the -OH group might have aided in reducing  $\text{Ag}^+$  ions to  $\text{Ag}^0$  (Sagitha *et al.*, 2016). In all, it can be seen that both NRL and PVA played vital roles in reducing  $\text{Ag}^+$  ions and preventing AgNP agglomeration, but NRL played a major role. The possible mechanisms through which AgNP are formed are illustrated as a schematic diagram in Figure 5.7. Equations (5.1), (5.2) and (5.3) propose the reduction reactions of  $\text{Ag}^+$  to  $\text{Ag}^0$  by amines ( $\text{RNH}_2$ ) and -OH groups (Sagitha *et al.*, 2016) in the nanofibre composites.

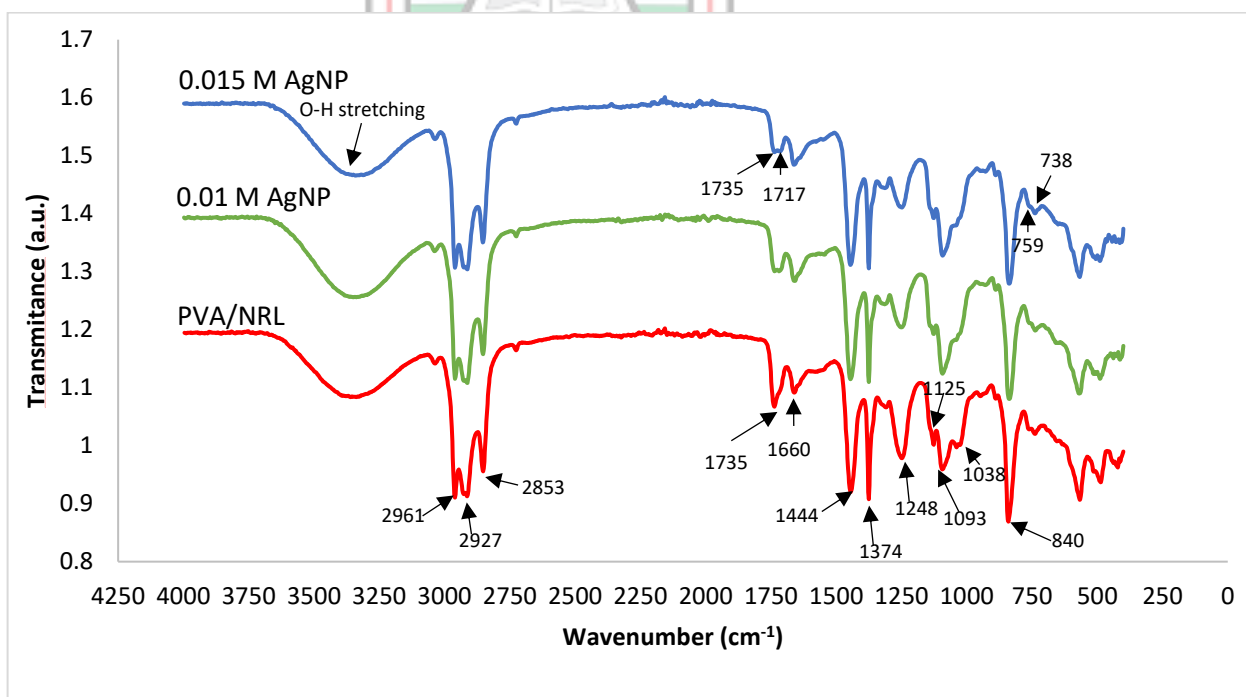
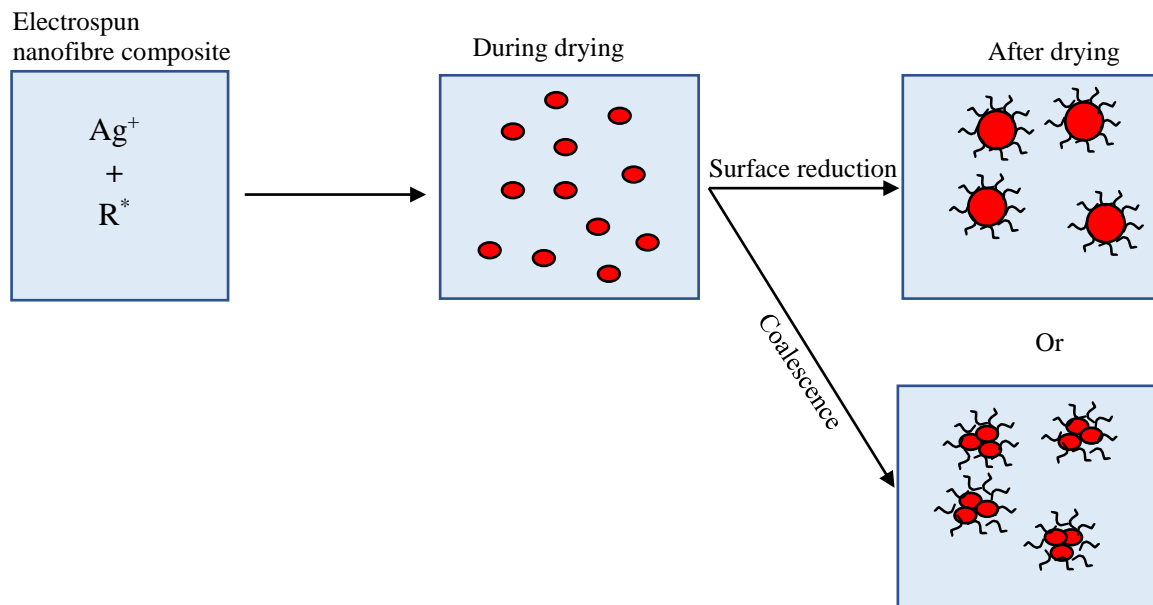


**Figure 5.6 FT-IR Spectra of PVA/NRL Nanofibre and AgNP-PVA/NRL Nanofibre Composites**



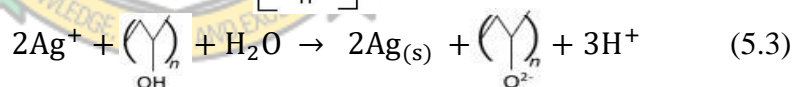
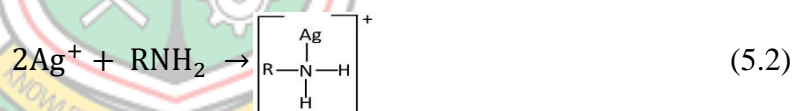


$R^*$  = reducing agent (amine/hydroxyl group)

● = Ag clusters

~ = stabilising agent (*cis*-isoprene)

**Figure 5.7 Illustration of AgNP Formation in the PVA/NRL Nanofibre Matrix**



### 5.5 Point of Zero Charge (PZC) and Surface Charge of AgNP-PVA/NRL Nanofibre Composite

Point of zero charge determination was carried out to predict the surface charge of AgNP-PVA/NRL nanofibre composites when used in different aqueous pH environments. Results of the experiment are presented in Figure 5.8. The PZC of 0.01 M and 0.015 M AgNP were found to be 5.07 and 4.31, respectively. This shows that the nanofibre composites are electrically neutral at the aforementioned pHs. These values aid in determining whether the nanocomposites are positively or negatively charged during adsorption of Hg and  $Cd^{2+}$  from aqueous solutions at a particular pH.

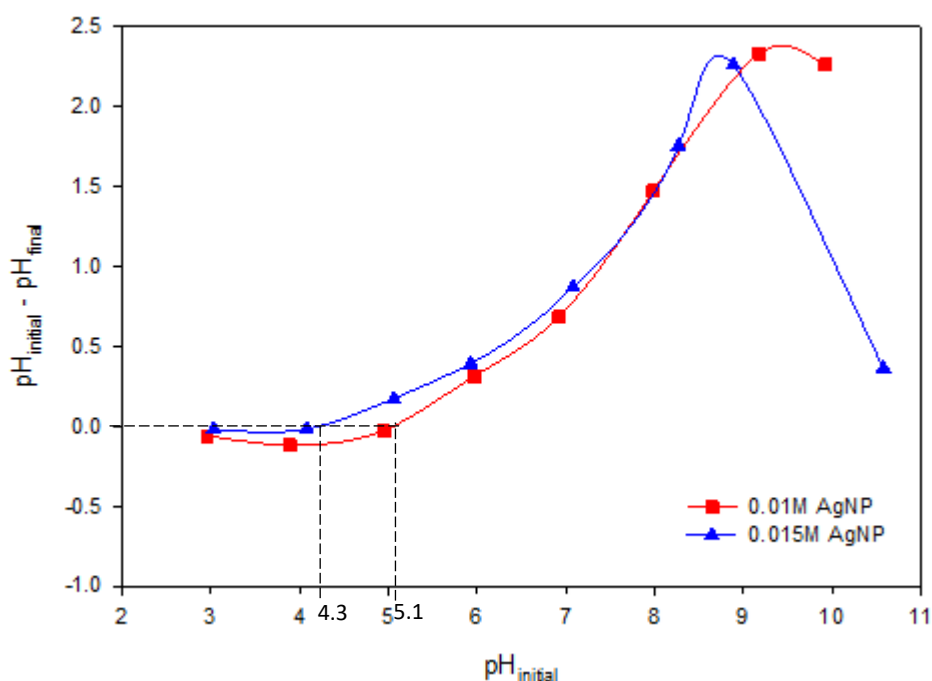


**Figure 5.8 Point of Zero Charge for 0.01 M and 0.015 M AgNP Nanofibre Composites**

## 5.6 Summary

In summary, AgNP were successfully synthesised within the PVA/NRL fibre matrix via electrospinning (confirmed by SEM, EDS, TEM, XRD and FT-IR analysis). The AgNP formed were spherical, with an average diameter < 10 nm, and dispersed on and within the fibre matrix. Increasing the AgNO<sub>3</sub> concentration resulted in relatively smaller-sized AgNP due to the relatively lower reducing agent/Ag<sup>+</sup> ratio, relatively lower stabilising agent/Ag<sup>+</sup> ratio and particle growth occurring in a solid matrix, hence limiting diffusion to form larger particles as shown by TEM analysis. Increasing AgNO<sub>3</sub> concentration also lead to AgNP mostly forming within the fibre walls, whilst decreasing AgNO<sub>3</sub> concentration lead to a significant portion of AgNP forming on or near the surface of the fibre walls (as shown by SEM and EDS analysis). Both PVA (hydroxyl group) and NRL (amine) aided in reducing Ag<sup>+</sup> to Ag<sup>0</sup>, but NRL (*cis*-isoprene) might have been solely responsible for stabilising the AgNP.

Since the AgNP-PVA/NRL nanofibre composites have been successfully synthesised, their ability to adsorb environmental pollutants such as Hg and Cd<sup>2+</sup> from aqueous media can be tested. This is discussed in Chapters 6 and 7.

## CHAPTER 6

### ASORPTION OF MERCURY AND CADMIUM FROM AQUEOUS SOLUTIONS USING SYNTHESISED AgNP-PVA/NRL NANOFIBRE COMPOSITES

This Chapter discusses the sorption of Hg and Cd<sup>2+</sup> from separate aqueous solutions by the synthesised AgNP-PVA/NRL nanofibre composites. The discussion involves the nanofibre composites' removal efficiency, adsorption isotherms (Langmuir, Freundlich and Dubinin-Radushkevich (D-R)), adsorption kinetics (pseudo-first order (PFO), pseudo-second order (PSO), Elovich and intra-particle diffusion) and finally, the surface charge of the nanofibre composites in aqueous solution. The Chapter also discusses the possible reasons for the observed efficiencies of the nanofibre composites.

#### 6.1 Background

Mercury and Cd<sup>2+</sup> poisoning have detrimental health effects with worldwide recognition. Chronic exposure to low concentrations of Hg and Cd<sup>2+</sup> leads to their bioaccumulation in humans. This long-term exposure may result in neurological and renal diseases such as the Minamata (Hg poisoning) and *Itai-Itai* (Cd poisoning) diseases (Aoshima, 2016; Balali-Mood *et al.*, 2021). These heavy metals have no known biological role in the human body (Park and Zheng, 2012; Mahmood *et al.*, 2019). Hence, they must be removed from water before animals ingest and plants assimilate them, which in the long run, will move up the food chain for humans to consume. Removing Hg and Cd<sup>2+</sup> at low concentrations from wastewater has become challenging. Conventional methods such as filtration and ion exchange used are expensive, time-consuming and inefficient (Colantonio and Kim, 2016; Ganzagh *et al.*, 2016).

Silver nanoparticles (AgNP) have proven promising in removing Hg and Cd<sup>2+</sup> from wastewater (Ganzagh *et al.*, 2016; Al-Qahtani, 2017). To reduce the possibility of AgNP forming part of the contamination problem after water treatment, the nanoparticles are incorporated into a matrix.

## 6.2 Sorption of Hg by AgNP-PVA/NRL Nanofibre Composites

Factors such as the pH of the adsorbate solution, contact duration for the adsorption process and initial concentration of the adsorbate, among others, affect adsorption processes. Some of these factors that can affect Hg adsorption are discussed in sections 6.2.1 – 6.2.3.

### 6.2.1 Effect of pH on Hg Adsorption

Figure 6.1 shows the effect of pH on Hg adsorption by AgNP-PVA/NRL nanofibre composites. A solution's pH plays a significant role in the surface chemistry of an adsorbate and the corresponding adsorbent during sorption processes. Therefore, the sorption experiment was conducted at a pH of 4 - 9 whilst maintaining contact time and initial concentration at 60 min and 0.75 mg/L, respectively. This was done to determine the pH at which maximum adsorption will occur. Maximum uptake of Hg by 0.01 M AgNP, which occurred at pH 7 was 45.77 mg/g, representing 47.74%. On the other hand, the uptake of Hg at pH 7 for 0.015 M AgNP was 21.38 mg/g, representing 33.45%, with a relatively slightly higher uptake of 23.53 mg/g, representing 36.80%, at pH 9. Similar to the finding of Ganzagh *et al.* (2016), where Hg was adsorbed by Ag-supported nanomesoporous silica, there was a gradual increase in the removal efficiency from pH 4 to 7 by both AgNP-PVA/NRL nanofibre composites (Figure 6.1). However, after pH 7, a decrease in the percentage of Hg removed was observed in both AgNP-PVA/NRL nanofibre composites. As a result, pH 7 was used for all other experiments. By comparison, 0.01 M AgNP was a better adsorbent for Hg than 0.015 M AgNP.

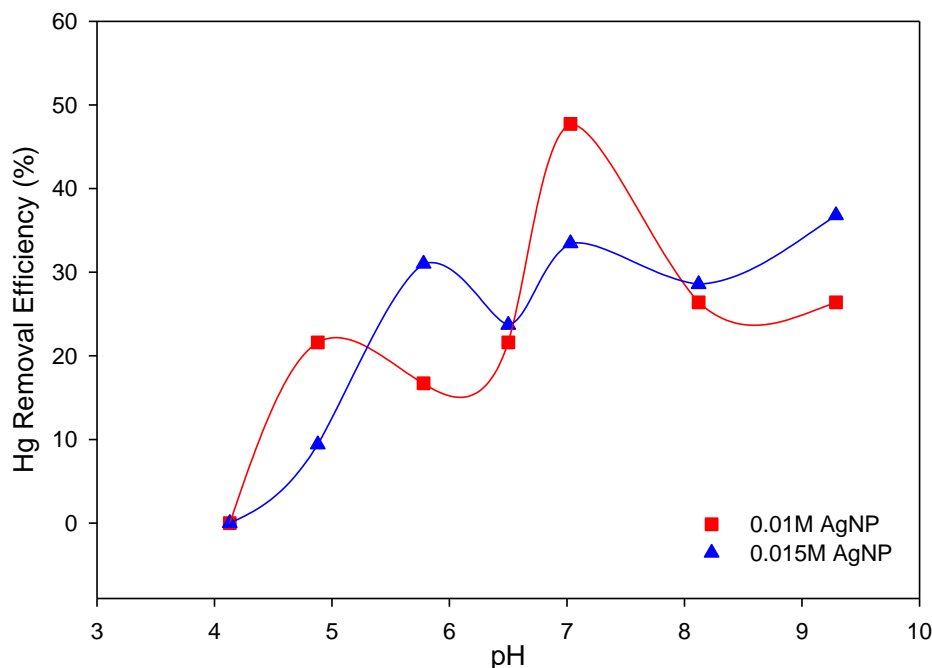


**Figure 6.1 Effect of pH on the Adsorption of Hg by AgNP-PVA/NRL Nanofibre Composites**

The adsorption of ions to an adsorbent's surface depends on the surface charge (Eby, 2004). Therefore, considering the PZC of 0.01 M AgNP (pH 5.07) and 0.015 M AgNP (pH 4.31), as discussed in Chapter 5, and maximum Hg uptake occurring at pH 7, it can be deduced that the surfaces of both nanofibre composites were negatively charged at pH 7. This can be confirmed using Equation 6.1, as proposed in Stanley L. Hem's personal communication (Lindblad and Duroux, 2017):

$$\text{Surface Charge} = 59 \text{ mV (PZC} - \text{pH)} \quad (6.1)$$

From Equation 6.1, the surface charge for 0.01 M AgNP would be -113.87 mV, whilst that of 0.015 M AgNP would be -158.71 mV, thus confirming that the surfaces of the nanofibre composites were negatively charged at pH 7. For negatively charged particles, cations are expected to be adsorbed easily. However, cation adsorption can be considered a competition between hydrogen ions ( $\text{H}^+$ ) and cations for surface sites (Drever, 1997). At a lower pH, cation adsorption may be minimum, and  $\text{H}^+$  would be more strongly and directly adsorbed to the surface groups of the adsorbent in an inner sphere complex than other cations due to their high potential abundance in solution, therefore, limiting cation adsorption (Drever, 1997). Generally, the bond at an inner sphere is stronger and does not depend on electrostatic attraction; thus, a cation can be adsorbed to a positively charged surface (Stumm, 1992;

Drever, 1997). As a rule of thumb, the adsorption of various metal cations may depend on the initial concentration or the adsorption principle and phenomena which depend on charge density of the surface cation (that is, the *ionic potential* which is the ratio of charge of cation divided by its radius) (Eby, 2004; Goher *et al.*, 2015). The lower the ionic potential of a metal cation, the more readily it will lose the attached water molecule (that is, the hydration environment) in the outer sphere complex and then form an inner sphere complex leading to maximum adsorption and faster equilibrium for the metal (Eby, 2004; Erdem *et al.*, 2004; Goher *et al.*, 2015). This is because the ion is hydrated at the outer sphere complex and does not bind directly to the surface (Stumm, 1992; Drever, 1997; Eby, 2004).

From Figure 6.1, the aforementioned phenomena may contribute to an increase in Hg removal at lower pH since the adsorbent surface may be positively charged. The adsorption of Hg was low at PZC for both adsorbents but increased at higher pH above the PZC since the surface becomes negatively charged. Fluctuations beyond pH 7, where maximum uptake of Hg occurs, could be as a result of the changes in pH leading to either adsorption of Hg from the solution or desorption of Hg from the adsorbent surface. In order to understand the AgNP-PVA/NRL nanofibre composites' mechanism for Hg removal, the corresponding Eh of 0.22 V (SHE) for pH 7, where maximum removal occurs, was determined. At this pH and Eh, Hg may exist as quicksilver (metallic Hg), as presented in Figure 6.2 (Takeno, 2005). This suggests that the removal of Hg can also occur between metallic Hg and the AgNP-PVA/NRL nanofibre composites and not only between Hg cation ( $\text{Hg}^{2+}$ ) and AgNP-PVA/NRL nanofibre composites. Again, at pH 7, there is a balance between  $\text{H}^+$  and hydroxide ions ( $\text{OH}^-$ ), which would result in minimal interference, enabling metallic Hg to bond with AgNP on the nanofibre composite readily. Thus, it is likely that the metallic Hg might have engulfed the AgNP on the nanofibre composite and formed an amalgam, an observation made by Katok *et al.* (2012), rather than  $\text{Hg}^{2+}$  partaking in the reaction. Similar observations were made by Henglein and Brancewicz (1997), Henglein (1998), Sumesh *et al.* (2011), Tauanov *et al.* (2018) and Tauanov *et al.* (2019), who proposed that the mechanism of Hg removal could be as a result of redox reaction between  $\text{Ag}^+/\text{Ag}^0$  (+0.80 V) and  $\text{Hg}^{2+}/\text{Hg}^0$  (+0.85 V).

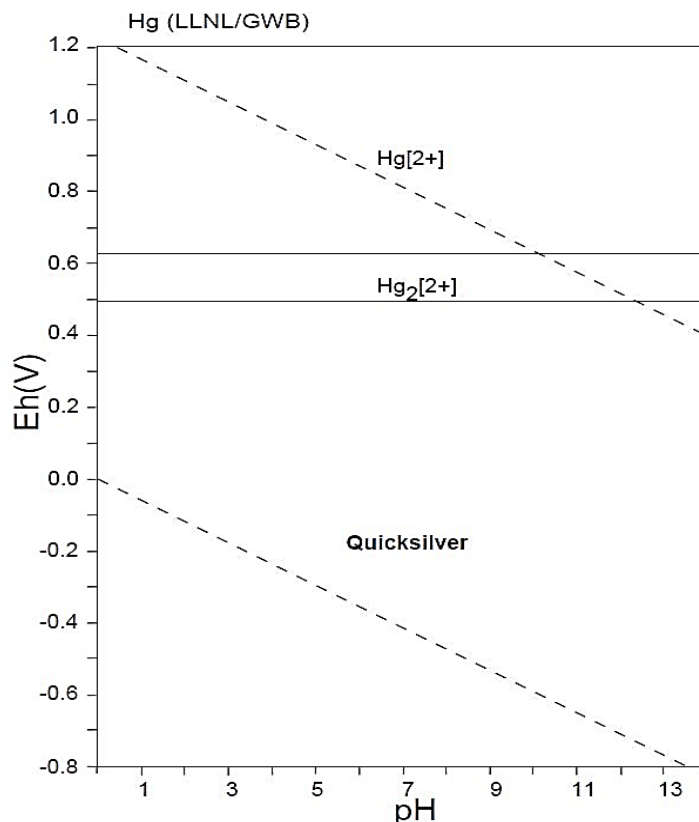
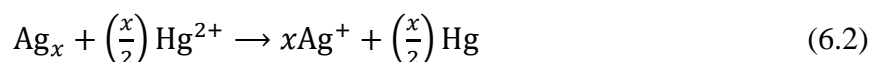


**Figure 6.2 Eh-pH Diagram of Hg-O-H System (Geochemist's Workbench).  $\Sigma\text{Hg} = 10^{-10}$ , 298.15 K,  $10^5$  Pa (Takeno, 2005)**

The works of Tauanov *et al.* (2018) and Tauanov *et al.* (2019) support the hypothesis that  $\text{Hg}^{2+}$  is reduced to form  $\text{Hg}^0$ . This later precipitates on the nanocomposite's surface and reacts with AgNP on the nanocomposite to form an amalgam ( $\text{Ag}_y\text{Hg}_z$ ). The  $\text{Hg}^{2+}$  reduction and formation of amalgam were also realised by Henglein and Brancewicz (1997) and Henglein (1998). These authors proposed Equation 6.2 (redox) and Equation 6.3 (amalgamation) as the reaction mechanism between  $\text{Hg}^{2+}$  and AgNP, where  $x$  represents the number of Ag clusters:



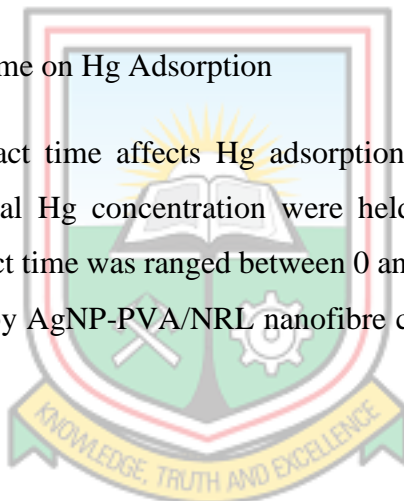
From Equation (6.2) and according to Henglein (1998), small Ag clusters,  $\text{Ag}_x$  ( $x < 10$ ), are electronegative; hence  $\text{Hg}^{2+}$  is reduced to Hg, whilst  $\text{Ag}_x$  is oxidised to  $x\text{Ag}^+$ . Also, considering Equation (6.3), lower values of  $x$  may result in amalgams not forming. This

explains the relatively lower adsorption of Hg in 0.015 M AgNP, where relatively smaller AgNP were formed (Figure 6.1).

From the PZC results of 0.01 M AgNP (pH 5.07) and 0.015 M AgNP (pH 4.31), as discussed in Chapter 5, the surfaces of both AgNP nanofibre composites would be positive at pH lower than the PZC, where minimum removal of Hg (Figure 6.1) occurs. This could be attributed to amalgamation. Also, at pH greater than the PZC for both AgNP nanofibre composites, the surfaces are negatively charged and maximum removal of  $\text{Hg}^{2+}$  occurs. This could be attributed to electrostatic adsorption. Therefore, the removal mechanism of  $\text{Hg}^{2+}$  by AgNP-PVA/NRL nanofibre composites may have many facets that mainly involve adsorption, redox reaction leading to precipitation and Hg-Ag amalgamation similar to observations made by Tauanov *et al.* (2018) and Tauanov *et al.* (2019). It can be proposed that Hg-Ag amalgamation may predominate since, at pH 7, Hg may exist as quicksilver.

#### 6.2.2 Effect of Contact Time on Hg Adsorption

To investigate how contact time affects Hg adsorption by AgNP-PVA/NRL nanofibre composites, pH and initial Hg concentration were held constant at 7 and 0.50 mg/L, respectively, whilst contact time was ranged between 0 and 120 min. Effect of contact time on the adsorption of Hg by AgNP-PVA/NRL nanofibre composites is presented in Figure 6.3.





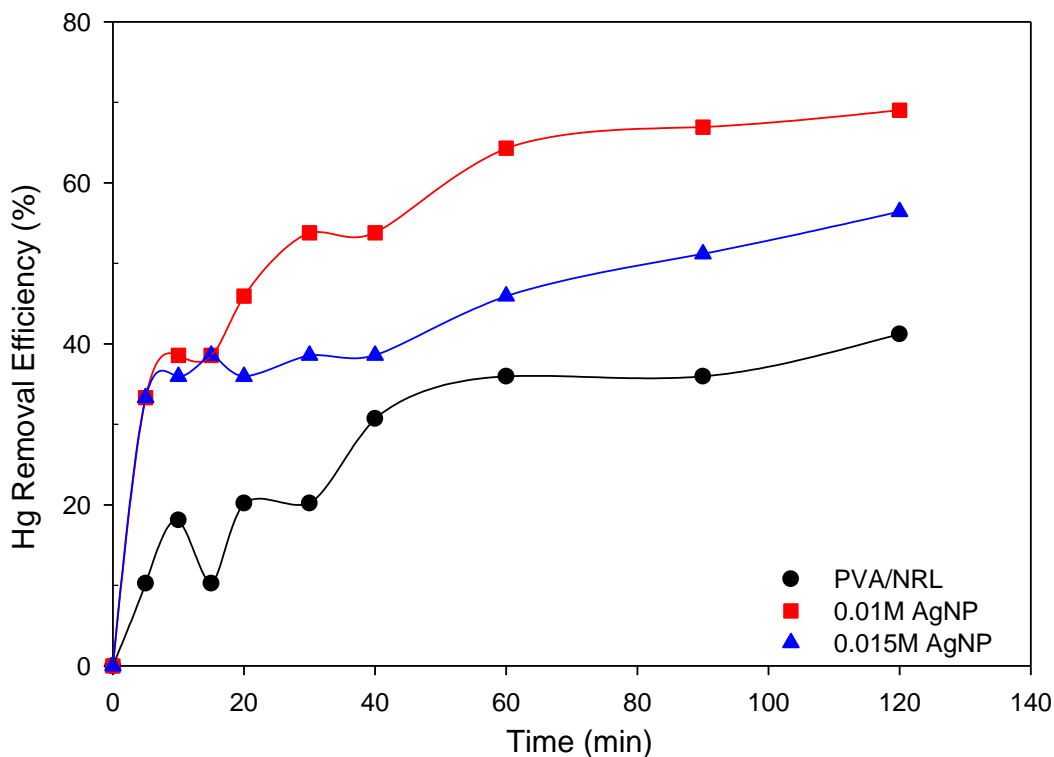


**Figure 6.3 Effect of Contact Time on the Adsorption of Hg by PVA/NRL Nanofibre, 0.01 M AgNP and 0.015 M AgNP**

The nanofibre, PVA/NRL (nanofibre without AgNP), adsorbed 35.90% of 0.50 mg/L Hg, as shown in Figure 6.3; however, both 0.01 M and 0.015 M AgNP adsorbed, 40.92 mg/g (representing 64.30%) and 19.48 mg/g (representing 45.92%), respectively. The relatively higher adsorption in AgNP-PVA/NRL nanofiber composites compared to the PVA/NRL indicated that the AgNP in the fibre had a significant effect in removing Hg from the solution. As the contact time increased, the amount of Hg adsorbed increased gradually up to 60 min, similar to that observed by El-Tawil *et al.* (2019), where Ag/quartz nanocomposite was used to adsorb Hg. A relatively small increase in Hg adsorption was recorded after 60 min; however, it had little impact on the amount of Hg adsorbed except in 0.015 M AgNP.

Comparing the adsorption of Hg by 0.01 M AgNP to that of 0.015 M AgNP, metallic Hg may have easily engulfed nanoparticles near or on the surface of the nanofibre composite, as observed in 0.01 M AgNP. The 0.015 M AgNP, on the other hand, may have experienced a lower adsorption rate due to the fact that most of its AgNP were located within the fibre walls, as discussed in Chapter 5, hence, limiting the nanoparticles' availability for adsorption. The fibre walls reduced the infiltration rate of the metallic Hg into the fibre walls

to engulf the AgNP, hence, its lower removal efficiency. This may also be the reason why some per cent removal of metallic Hg was recorded after 60 min in 0.015 M AgNP. Another possible reason is that adsorption sites near the surface of 0.015 M AgNP were used up, and Hg had to infiltrate the fibre to be adsorbed. It is well established that the diffusion rate within a liquid is faster than with a solid; hence, the slower and lower rate of adsorption in 0.015 M AgNP. Due to this, 0.01 M AgNP adsorbed Hg more efficiently, and 0.015 M AgNP continued to adsorb even after 60 min.

### 6.2.3 Effect of Initial Concentration on Hg Adsorption

Effect of initial concentration on Hg removal from an aqueous solution was studied. Results are shown in Figure 6.4. At pH 7 and contact time of 60 min, the initial concentration was varied between 0.01 – 1.00 mg/L. For 0.01 M AgNP, the maximum amount of Hg removed was at 0.05 mg/L (89.00%), and that by 0.015 M AgNP occurred at 0.02 mg/L (94.50%). The percentage of Hg removed decreased as its initial concentration increased. Also, from Figure 6.4, it can be seen that 0.015 M AgNP removed a higher percentage of Hg from the solution at lower concentrations than 0.01 M AgNP, and this was contrary to the observation made at higher concentrations for both nanofibre composites.

At a lower adsorbate concentration, the ratio of active sites to the number of adsorbates in a solution is relatively higher. Hence, the higher per cent removal of Hg observed at lower concentrations for both nanofibre composites. On the other hand, at higher adsorbate concentrations, the ratio of active sites to the number of adsorbates in a solution is relatively lower. This explains the lower percentage of Hg removed at higher adsorbate concentrations for both nanofibre composites.

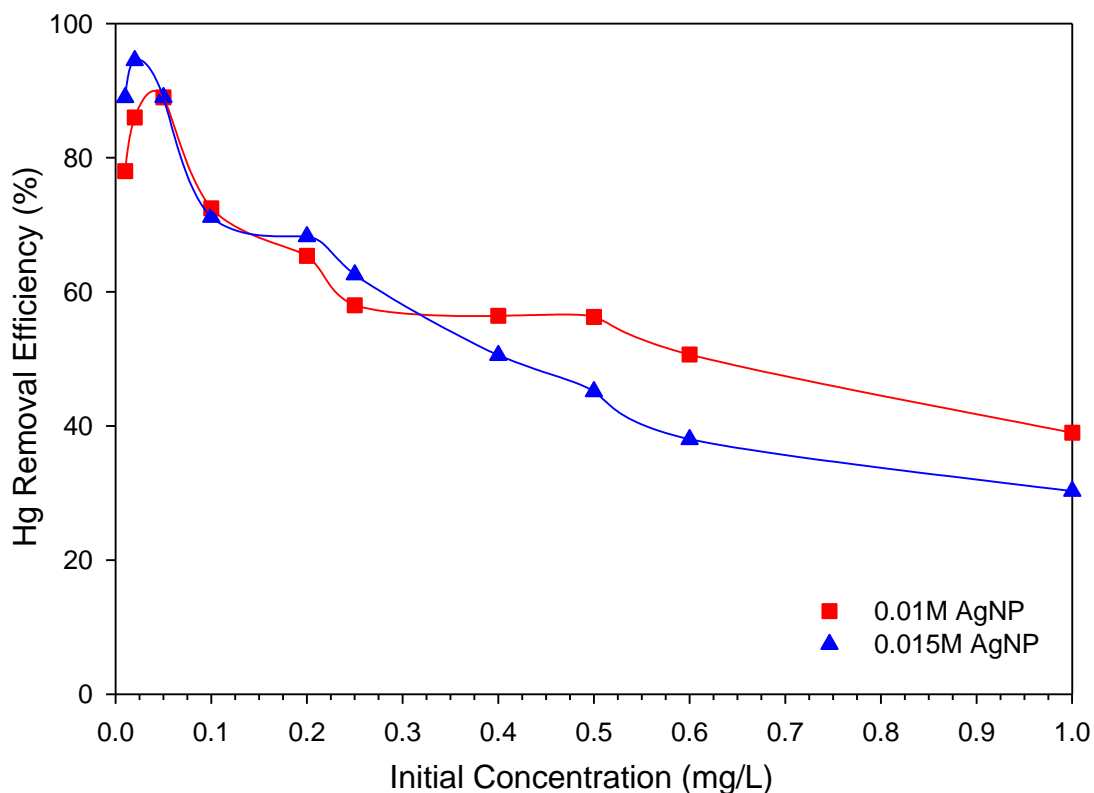


**Figure 6.4 Effect of Initial Concentration on the Adsorption of Hg by AgNP-PVA/NRL Nanofibre Composites**

To understand why 0.015 M AgNP removed a relatively higher percentage of Hg at lower concentrations than 0.01 M AgNP and vice versa at higher concentrations, it is worth noting that there are more AgNP in 0.015 M AgNP, hence more sites for adsorption. This may be the reason why a higher percentage of Hg was removed at lower concentrations. On the other hand, since there are more AgNP available near the surface of 0.01 M AgNP, it was easier for the Hg to diffuse from the solution and be adsorbed readily on the surface rather than infiltrating the fibre to be adsorbed within the same time frame of 60 min.

#### 6.2.4 Adsorption Isotherm Study for Hg

In order to understand the adsorption behaviour of Hg in solution onto the AgNP-PVA/NRL nanofibre composites, the experimental data were fitted to the Langmuir, Freundlich and D-R isotherms. Figure 6.5 shows the adsorption isotherms of Hg on the nanofibre composites. Table 6.1 shows the parameters of each model, their accompanying coefficient of determination ( $R^2$ ), and their respective mean square errors (MSE). The experimental data on Hg removal by both nanofibre composites fitted well to the Langmuir, Freundlich and

D-R isotherms. Figure 6.5 and Table 6.1 show that the nanofibre composite 0.01 M AgNP fitted best to the Langmuir isotherm with  $R^2 = 0.9851$  and  $MSE = 3.8067 \text{ (mg/g)}^2$ . Fitting best to the Langmuir isotherm indicates that Hg adsorption occurred in a monolayer fashion. All separation factor ( $R_L$ ) values of Hg adsorption by 0.01 M AgNP were greater than 0 but less than 1, indicating the adsorption was favourable. The 0.015 M AgNP fitted best to the D-R isotherm, which takes into account the porous structure of the adsorbent, with  $R^2 = 0.9880$  and  $MSE = 0.7903 \text{ (mg/g)}^2$  (Dubinin and Radushkevich, 1947; Tran *et al.*, 2017; Palomba and Frazzica, 2021). Therefore, it can be assumed that most metallic Hg diffused from the solution into the pores of the fibre walls and bonded with the AgNP in 0.015 M AgNP. Though Hg adsorption onto 0.015 M AgNP did not fit best to the Langmuir and Freundlich isotherms, its  $R_L$  and  $1/n$  values ( $n$  is a measure of the change in affinity for the adsorbate with changes in adsorption density) were all between 0 and 1, indicating that the adsorption was favourable.

By comparison, the adsorption of Hg by 0.01 M AgNP was more efficient than that of 0.015 M AgNP. With a maximum adsorption capacity ( $q_{\max}$ ) value of 68.3223 mg/g for 0.01 M AgNP and 26.6855 mg/g for 0.015 M AgNP, it can be deduced that 0.01 M AgNP has a higher adsorption capacity to adsorb more Hg from solution than 0.015 M AgNP. From Table 6.1, it can also be seen that both Freundlich constant ( $K_F$ ) and D-R adsorption capacity ( $q_{DR}$ ) values of 0.01 M AgNP ( $K_F = 67.4295 \text{ (mg/g)/(mg/L)}^{1/n}$ ,  $q_{DR} = 962.7408 \text{ mg/g}$ ) were higher than that of 0.015 M AgNP ( $K_F = 30.0932 \text{ (mg/g)/(mg/L)}^{1/n}$ ,  $q_{DR} = 213.1266 \text{ mg/g}$ ). Furthermore, the smaller  $n$  value of 0.01 M AgNP (1.9716) than 0.015 M AgNP (2.6022) signifies better adsorption and a relatively stronger bond between the adsorbent and adsorbate for the 0.01 M AgNP in removing Hg from solution effectively (Ganzagh *et al.*, 2016).

The constant  $K_{DR}$ , related to the sorption energy, was also higher in 0.01 M AgNP ( $0.0029 \text{ mol}^2/\text{kJ}^2$ ) than in 0.015 M AgNP ( $0.0022 \text{ mol}^2/\text{kJ}^2$ ), confirming that 0.01 M AgNP would perform better in removing Hg from solution than 0.015 M AgNP. On the other hand, the  $E$  value, which denotes the mean adsorption energy, was lower in 0.01 M AgNP (13.0690 kJ/mol) than in 0.015 M AgNP (15.2002 kJ/mol). It is worth noting that  $E$  values for both nanofibre composites were between 8 - 16 kJ/mol, signifying essential features of chemisorption (Das *et al.*, 2013; Maneechakr and Mongkollertlop, 2020).

The relatively better efficiency of 0.01 M AgNP may be due to the availability of more AgNP near or on the surface of 0.01 M AgNP than within the fibre, consequently performing better than 0.015 M AgNP in the experiment's time frame. As earlier mentioned, the slower rate of diffusion of Hg from the solution into the fibre walls to be adsorbed by AgNP may have resulted in the lower adsorption capacity experienced in 0.015 M AgNP.



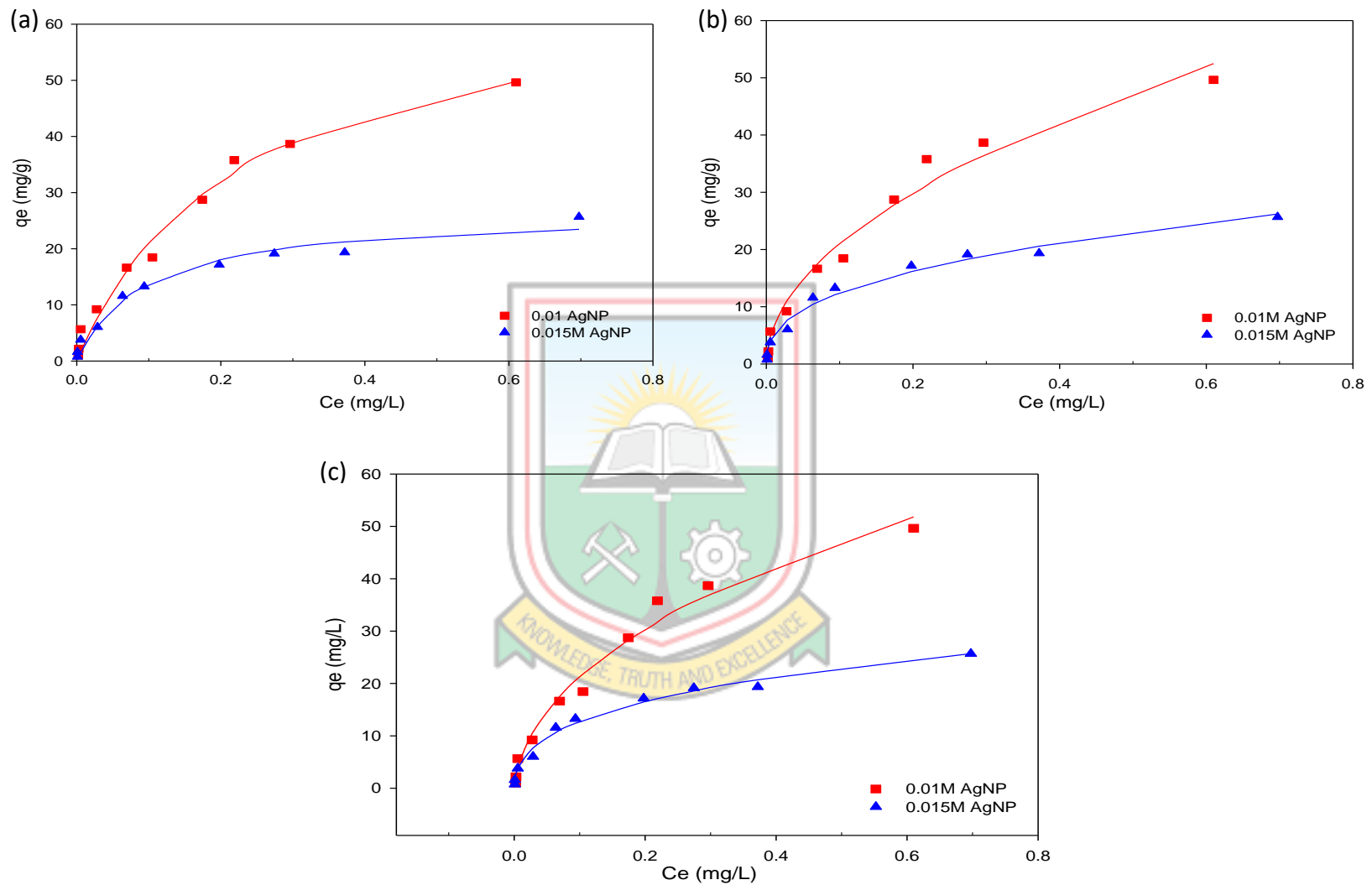
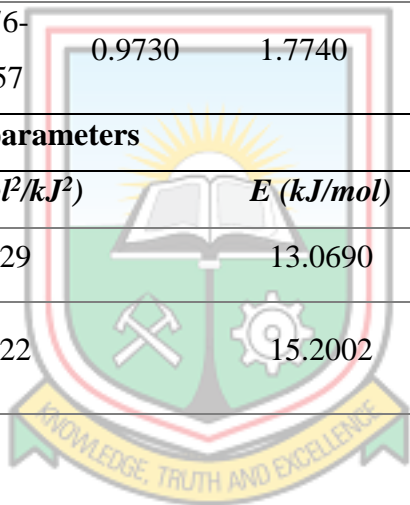


**Figure 6.5 (a) Langmuir (b) Freundlich and (c) Dubinin-Radushkevich Isotherm for Hg Adsorption by AgNP-PVA/NRL Nanofibre Composites**

**Table 6.1 Parameters of Adsorption Isotherms for Hg Adsorption onto AgNP-PVA/NRL Nanofibre Composites**

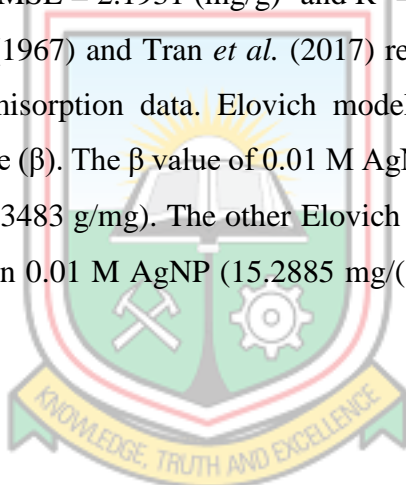
Adsorbent	Langmuir parameters				MSE [(mg/g) <sup>2</sup> ]	Freundlich parameters		R <sup>2</sup>	MSE [(mg/g) <sup>2</sup> ]
	q <sub>max</sub> (mg/g)	K <sub>L</sub> (L/mg)	R <sub>L</sub>	R <sup>2</sup>		1/n	K <sub>F</sub> [(mg/g)/(mg/L) <sup>1/n</sup> ]		
<b>0.01 M AgNP</b>	68.3223	4.4103	0.1848- 0.9578	0.9851	3.8067	0.5072	67.4295	0.9788	5.4414
<b>0.015 M AgNP</b>	26.6855	10.4177	0.0876- 0.9057	0.9730	1.7740	0.3843	30.0932	0.9826	1.1477
Adsorbent	D-R parameters				R <sup>2</sup>	MSE [(mg/g) <sup>2</sup> ]			
	q <sub>DR</sub> (mg/g)	K <sub>DR</sub> (mol <sup>2</sup> /kJ <sup>2</sup> )	E (kJ/mol)						
<b>0.01 M AgNP</b>	962.7408	0.0029	13.0690		0.9832	4.2966			
<b>0.015 M AgNP</b>	213.1266	0.0022	15.2002		0.9880	0.7903			



### 6.2.5 Adsorption Kinetic Study for Hg

In order to understand the reaction rate and sorption mechanism, the experimental data were examined using four adsorption kinetic models: PFO, PSO, Elovich and intra-particle diffusion kinetic models. Plots of the PFO, PSO, Elovich and intra-particle kinetic models and their corresponding parameters are presented in Figure 6.6 and Table 6.2, respectively. Although Ho and McKay (1998) indicated that the PFO equation is mostly suitable for an initial contact time of 20 to 30 min, the PFO equation was also applied to this study. This was done to obtain further information about the reaction, though maximum adsorption occurred at 60 min.

The experimental data fit all four kinetic models; however, the data fit best to the Elovich kinetic model. The  $R^2$  and MSE values from the Elovich model for 0.01 M and 0.015 M AgNP were  $R^2 = 0.9858$ ;  $MSE = 2.1931 \text{ (mg/g)}^2$  and  $R^2 = 0.9533$ ;  $MSE = 1.7198 \text{ (mg/g)}^2$ , respectively. McLintock (1967) and Tran *et al.* (2017) reported that the Elovich model is frequently used for chemisorption data. Elovich model also provides insight into the desorption of the adsorbate ( $\beta$ ). The  $\beta$  value of 0.01 M AgNP (0.1217 g/mg) was lower than that of 0.015 M AgNP (0.3483 g/mg). The other Elovich parameter,  $\alpha$ , which is the initial rate constant, was lower in 0.01 M AgNP (15.2885 mg/(g  $\times$  min)) than in 0.015 M AgNP (47.2445 mg/(g  $\times$  min)).





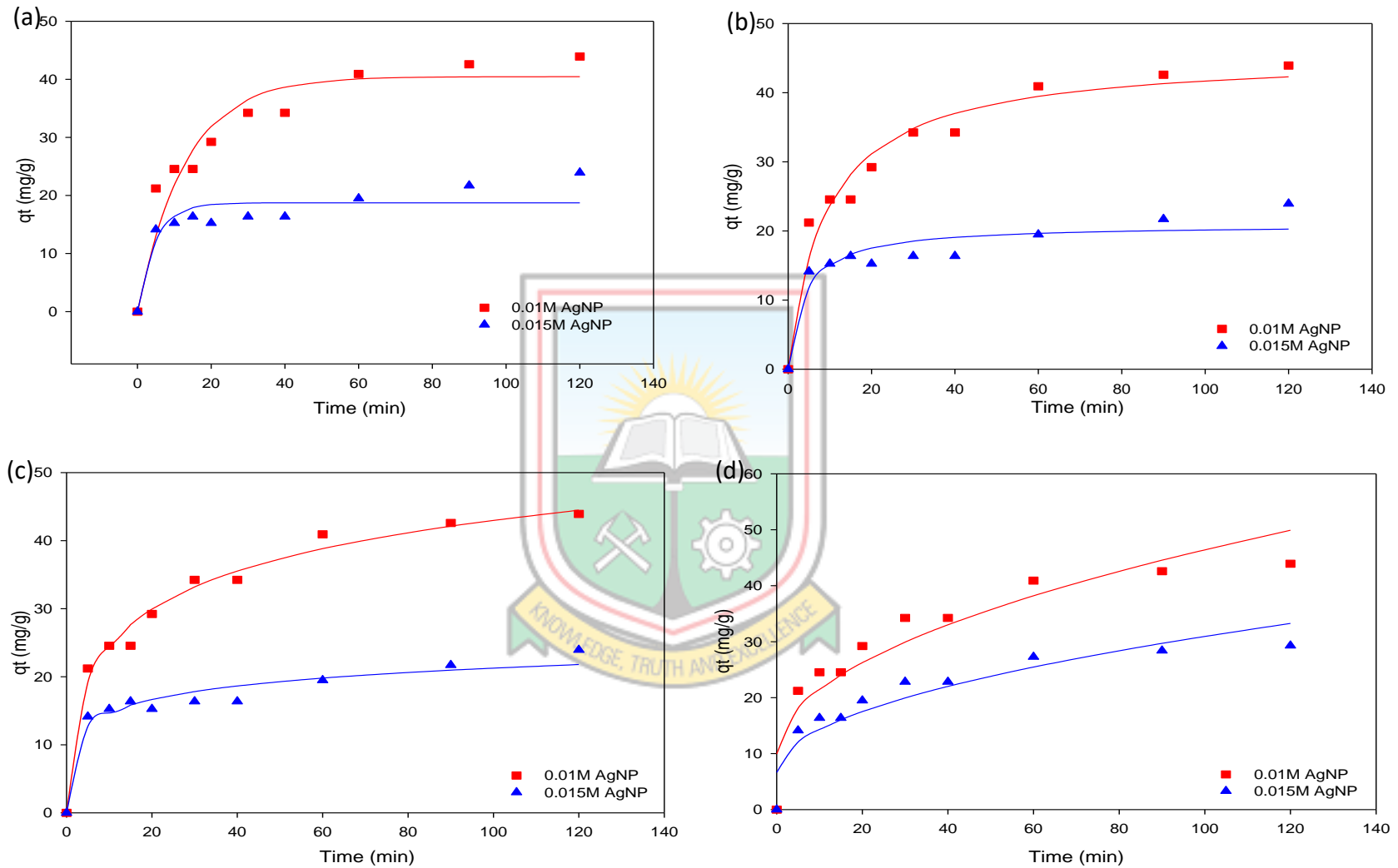


**Figure 6.6 (a) Pseudo-First Order (b) Pseudo-Second Order (c) Elovich and (d) Intra-Particle Diffusion Kinetic Models for Hg Adsorption by AgNP-PVA/NRL Nanofibre Composites**

**Table 6.2 Parameters of Adsorption Kinetics for Hg Adsorption onto AgNP-PVA/NRL Nanofibre Composites**

Model	Parameters	Adsorbent	
		0.01 M AgNP	0.015 M AgNP
PFO	$q_e$ (mg/g)	40.4601	18.7254
	$k_1$ (1/ min)	0.0775	0.2081
	$R^2$	0.9129	0.8223
	$MSE [(mg/g)^2]$	13.4420	6.5492
PSO	$q_e$ (mg/g)	45.5458	20.9128
	$k_2$ [g/(mg × min)]	0.0024	0.0123
	$R^2$	0.9616	0.8941
	$MSE [(mg/g)^2]$	5.9301	3.9049
Elovich	$\alpha$ [mg/(g × min)]	15.2885	47.2445
	$\beta$ (g/mg)	0.1217	0.3483
	$R^2$	0.9858	0.9533
	$MSE [(mg/g)^2]$	2.1931	1.7198
Intra-particle diffusion	$k_p$ [mg/(g × min <sup>1/2</sup> )]	3.6492	2.4328
	C (mg/g)	9.9354	6.6235
	$R^2$	0.8742	0.8742
	$MSE [(mg/g)^2]$	19.4054	8.6245

From the intra-particle diffusion model, a significant observation was that the constant related to the thickness of the boundary layer,  $C$ , was larger in 0.01 M AgNP (9.9354 mg/g) than in 0.015 M AgNP (6.6235 mg/g). Again, by comparing the adsorption capacity of the nanofibre composites at equilibrium ( $q_e$ ), the  $q_e$  values of 0.01 M AgNP (PFO;  $q_e = 40.4601$  mg/g, PSO;  $q_e = 45.5458$  mg/g) were higher than that of 0.015 M AgNP (PFO;  $q_e = 18.7254$  mg/g, PSO;  $q_e = 20.9128$  mg/g). All these show that 0.01 M AgNP outperformed 0.015 M AgNP in adsorbing Hg from the aqueous solution.

It was also evident that since 0.01 M AgNP had a lower  $\beta$  value, it would desorb relatively less Hg in any one experiment, meaning 0.01 M AgNP has a comparatively higher efficiency than 0.015 M AgNP. Meanwhile, since Korobeinyk and Inglezakis (2018) reported in their study that a decrease in AgNP size elevates Hg adsorption, it was expected that 0.015 M AgNP would adsorb more Hg and have a lower  $\beta$  value. However, this was not so. Thus, this supports the notion that despite relatively more AgNP located within the fibre walls of 0.015 M AgNP, the metallic Hg could not diffuse and infiltrate the nanofibre composite quickly enough to bond with AgNP within the experiment's time frame. Also, though the average size of AgNP in 0.01 M AgNP was larger than that of 0.015 M AgNP, the bigger boundary layer,  $C$ , of 0.01 M AgNP, signifies there may have been relatively more nanoparticles available for adsorption near or on the surface of this nanofibre composite than that of 0.015 M AgNP.

On the other hand, since 0.01 M AgNP performed better in adsorbing Hg than 0.015 M AgNP, it was expected that 0.01 M AgNP would have a faster initial rate constant; however, this was not so. This was not surprising since a study by Katok *et al.* (2012) stated that the fastest adsorption kinetics was for the smallest AgNP in a hyperstoichiometric interaction between Hg and Ag at the nanoscale. This finding probably means the smaller-sized AgNP on 0.015 M AgNP's surface may have resulted in the faster initial rate of Hg adsorption. Also, it can be inferred that as contact time increased, a relatively lesser amount of active sites were available on the fibre's surface than that of 0.01 M AgNP, therefore, slowing down the reaction at the later part. Another deduction is that per the total amount of Hg adsorbed in the experiment's time frame, 0.015 M AgNP adsorbed a higher fraction of Hg in a shorter period than the amount adsorbed by 0.01 M AgNP. The higher  $\alpha$  value in 0.015 M AgNP supports the proposed ideas that; a) there are relatively more AgNP in the 0.015 M AgNP's fibre than on its surface, and b) after AgNP near or on the surface has adsorbed

Hg, the metallic Hg could not diffuse from the solution into the fibre fast enough, to bond with AgNP within the fibre. The slow infiltration of AgNP into the 0.015 M AgNP's fibre may have also resulted in the higher desorption constant of 0.015 M AgNP.

### 6.2.6 Morphology and Elemental Composition of AgNP-PVA/NRL Nanofibre Composites after Hg Adsorption

The morphology and elemental composition of the AgNP-PVA/NRL nanofibre composites after Hg adsorption are presented in Figure 6.7. The whitish spots (green arrows) in Figure 6.7a represent clusters of AgNP.

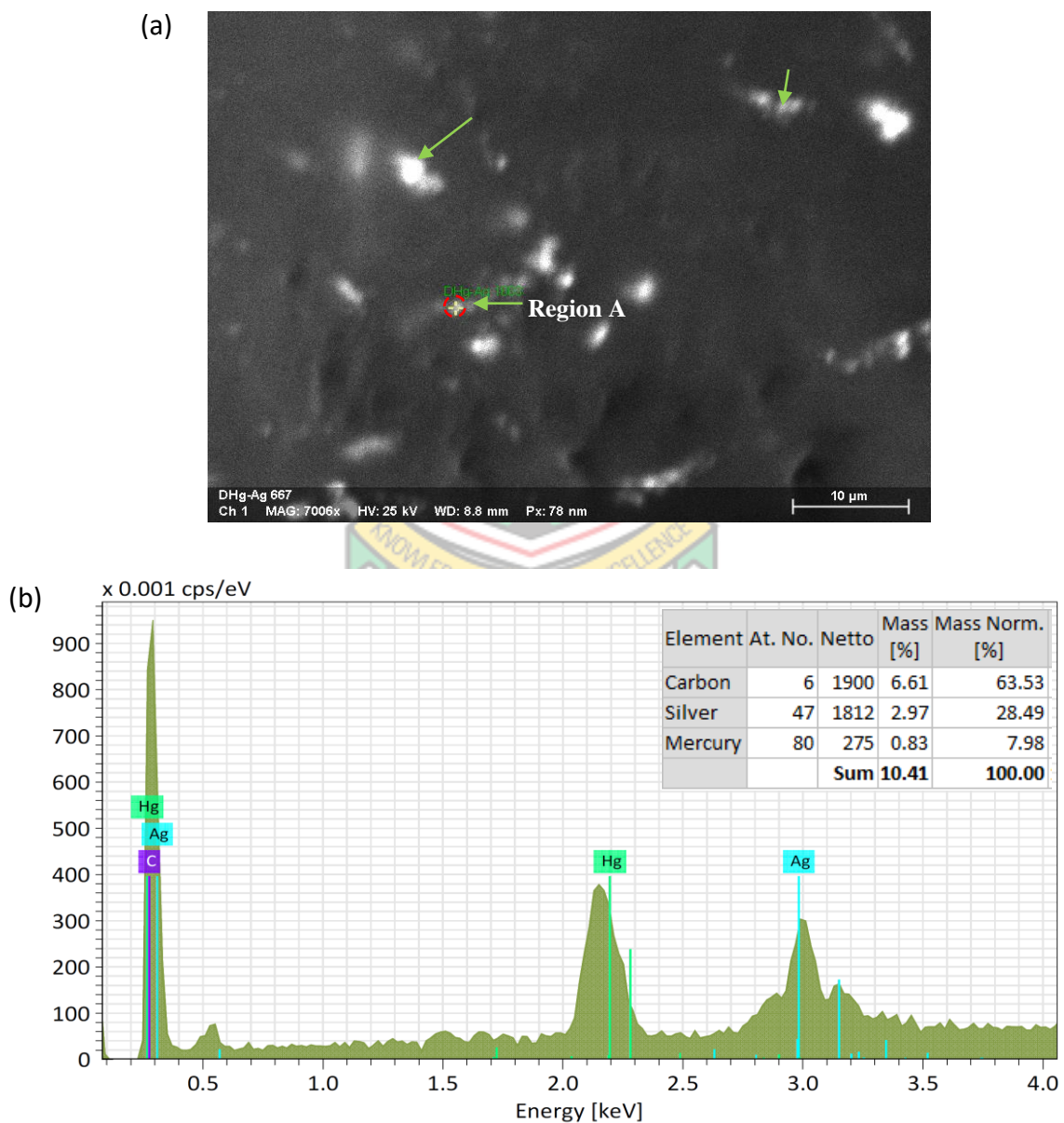


**Figure 6.7 (a) BSD-SEM Image with (b) EDX Analysis After Hg Adsorption by AgNP-PVA/NRL Nanofibre Composite**

Figure 6.7b corresponds to the energy dispersive x-ray spectroscopy (EDS) analysis of Region A shown in Figure 6.7a, which is also a whitish spot. This was done to determine if the AgNP had truly adsorbed Hg from the solution. Figure 6.7b shows that Ag was detected as part of the EDS spectrum (Figure 6.7b), meaning the whitish spots (green arrows) were AgNP clusters. The EDS spectrum of Region A also shows that the AgNP-PVA/NRL nanofibre composite had adsorbed Hg. It can also be seen that since the nanofibre composite was in contact with an aqueous solution and dried before a scanning electron microscope (SEM) micrograph was taken, the fibre had lost its larger pores leaving behind dimple-like pores all over the fibre, similar to the one observed after the weight loss test in Chapter 4.

### 6.3 Sorption of Cd<sup>2+</sup> by AgNP-PVA/NRL Nanofibre Composites

Some factors that may affect Cd<sup>2+</sup> adsorption are discussed in sections 6.3.1 – 6.3.3. These include the pH of the adsorbate solution, contact duration for the adsorption process and initial concentration of the adsorbate, among others.

#### 6.3.1 Effect of pH on Cd<sup>2+</sup> Adsorption

Similar to effect of pH on Hg adsorption discussed in section 6.1.1, the influence of pH on Cd<sup>2+</sup> adsorption by AgNP-PVA/NRL nanofibre composites was also studied. Whilst pH was varied between 4 and 9, contact time was maintained at 20 min for 0.01 M AgNP and 40 min for 0.015 M AgNP. The differences in contact time between the nanofibre composites have been discussed in subsection 6.3.2. The initial concentration was also held constant at 1.00 mg/L. Results of this sorption experiment are presented in Figure 6.8. It was observed that the per cent removal of Cd<sup>2+</sup> from solution increased from 3.33%, representing 4.41 mg/g at pH 4, to 30.04%, representing 39.82 mg/g at pH 7 for 0.01 M AgNP, after which it gradually reduced to below detection limit at pH 9. As shown in Figure 6.8, a similar trend was also observed for 0.015 M AgNP, with a gradual rise in percentage removal of Cd<sup>2+</sup> from 3.33 - 33.67% at a pH range of 4 - 7, representing 2.94 – 29.49 mg/g and a decrease in Cd<sup>2+</sup> removal from 33.67 - 4.32% at a pH range of 7 – 9, representing 29.49 – 3.83 mg/g, respectively.

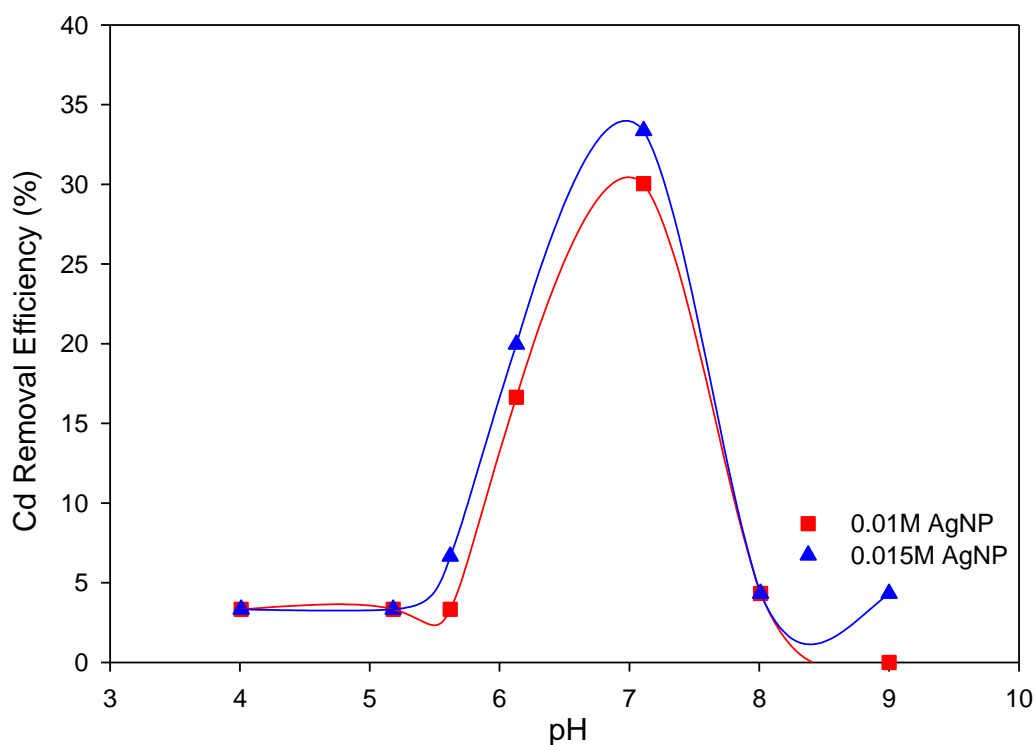


**Figure 6.8 Effect of pH on the Adsorption of  $\text{Cd}^{2+}$  by AgNP-PVA/NRL Nanofibre Composites (Osei *et al.*, 2023)**

Similar to the finding of Jiang *et al.* (2006), where  $\text{Cd}^{2+}$  was removed from an aqueous solution by tourmaline, the pH at which maximum  $\text{Cd}^{2+}$  was removed for both nanofibre composites was at pH 7. However, in a study by Al-Qahtani (2017), where AgNP synthesised by *Benjamina* leaf extracts was used to remove  $\text{Cd}^{2+}$  from an aqueous solution, the maximum amount of  $\text{Cd}^{2+}$  was removed at pH 6, with a sharp decrease in uptake at pH 7. This study observed the opposite since the sharpest uptake was observed at pH 7, with a sharp decrease at pH 8 (Figure 6.8). The low percentage removal of  $\text{Cd}^{2+}$  at pH below the PZCs of the AgNP-PVA/NRL nanofibre composites could be attributed to the positive surface charges, which can electrostatically repel  $\text{Cd}^{2+}$ . Also, as explained by Drever (1997), at a lower pH, cation adsorption may be minimum, and  $\text{H}^+$  would be more strongly and directly adsorbed to the surface groups of the adsorbent than other cations, therefore, limiting cation adsorption. There was an increase in the percentage removal of  $\text{Cd}^{2+}$  beyond the pH of PZCs all the way to pH 7, after which there was a decline as the pH increased beyond 7. The increase in percentage removal of  $\text{Cd}^{2+}$  at pH beyond the PZC could be attributed to the negative surface charges of AgNP nanofibre composites, which could electrostatically attract and adsorb the  $\text{Cd}^{2+}$  from the solution. It is worth noting that  $\text{Cd}^{2+}$

adsorption could also be attributed to the cathodic charging of the AgNP, followed by a reduction of  $\text{Cd}^{2+}$  directly on the surface to form an alloy as proposed by Henglein (1998) in Equation (6.4), where  $x$  represents the number of Ag clusters and  $m$  represents the moles of  $\text{Ag}^+$  (that is,  $m\text{Ag}^+$ ), taking place in the reaction. This is possible because the standard electrode potential of  $\text{Ag}^+/\text{Ag}^0$  (0.80 V) is greater than  $\text{Cd}^{2+}/\text{Cd}^0$  (-0.40 V); hence the AgNP serves as a cathode for deposition.

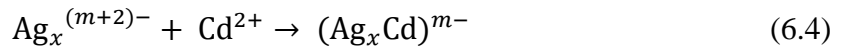
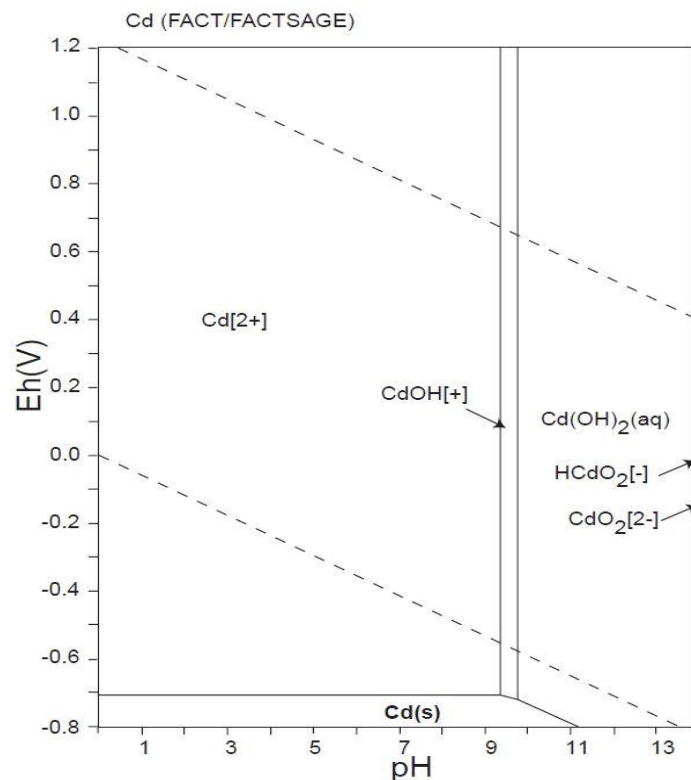
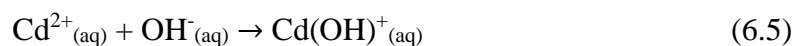


Figure 6.9 shows the Eh-pH diagram of Cd. Between pH 4 - 9 and Eh 0.00 - 1.20, it can be seen that Cd exists as  $\text{Cd}^{2+}$ , meaning  $\text{Cd}^{2+}$  existed at all pH used in this study (Takeno, 2005). It is also worth noting that at pH 7 both nanofibre composites were negatively charged (see subsection 6.1.1). This will result in more  $\text{H}^+$  ions being adsorbed at lower pH than other cations, such as  $\text{Cd}^{2+}$ ; thus, the lower amount of Cd removed at pH < 7 in this study. Conversely, at pH 7,  $\text{H}^+$  and  $\text{OH}^-$  ions are balanced in the aqueous system, hence giving room for  $\text{Cd}^{2+}$  to be adsorbed readily.



**Figure 6.9 Eh-pH Diagram of Cd-O-H System (Geochemist's Workbench).  $\Sigma\text{Cd} = 10^{-10}$ , 298.15 K,  $10^5$  Pa (Takeno, 2005)**

On the other hand, as pH increases into the alkali region, there are excess OH<sup>-</sup> ions in the solution, which may readily bond with Cd<sup>2+</sup> to form Cd(OH)<sup>+</sup><sub>(aq)</sub> and Cd(OH)<sub>2(aq)</sub>, as presented in Equations 6.5 and 6.6, therefore, hindering Cd<sup>2+</sup> adsorption by the nanofibre composite (Figure 6.9). This also explains the reason why there was a drastic decrease in per cent removal of Cd<sup>2+</sup> at pH > 7.



### 6.3.2 Effect of Contact Time on Cd<sup>2+</sup> Adsorption

How contact time affects Cd<sup>2+</sup> adsorption by AgNP-PVA/NRL nanofibre composites was also studied. With pH and initial concentration held constant at 7 and 1.04 mg/L, respectively, the contact time for the experiment was varied between 0 – 120 min. The experiment's results are presented in Figure 6.10. It can be seen that PVA/NRL (nanofibre without AgNP) adsorbed a relatively smaller amount of Cd<sup>2+</sup> than 0.01 M and 0.015 M AgNP, meaning the AgNP present in the nanofibre composites contributed to Cd<sup>2+</sup> adsorption. The sharpest uptake of Cd<sup>2+</sup> by 0.01 M AgNP occurred at 20 min (14.97 mg/g, representing 11.90%), whilst that of 0.015 M AgNP occurred at 40 min (30.11 mg/g, representing 35.92%). For 0.01 M AgNP, a sharp drop in uptake was realised after 20 min until 120 min. There was a slight drop in the uptake of Cd<sup>2+</sup> at 60 min for 0.015 M AgNP. Al-Qahtani (2017) also recorded the sharpest uptake of Cd<sup>2+</sup> by AgNP at 40 min, whilst Jiang *et al.* (2006) recorded the sharpest uptake at 60 min for Cd<sup>2+</sup> uptake by tourmaline.

Comparing the percentage of Cd<sup>2+</sup> removed from the aqueous solution, it can be seen that 0.015 M AgNP is more efficient than 0.01 M AgNP (Figure 6.10). Moreover, it is important to note that there were relatively more AgNP in 0.015 M AgNP than in 0.01 M AgNP. As seen in Equation (6.4), higher  $m\text{Ag}^{+}$  (that is, a higher number of moles of Ag<sup>+</sup>) would result in a relatively higher charged reduced complex (Ag<sub>x</sub>Cd)<sup>y-</sup>; and the higher the magnitude of a charge, the greater its attraction is. Therefore, this explains why 0.015 M AgNP, which contains relatively higher moles of Ag<sup>+</sup>, could adsorb Cd<sup>2+</sup> better. It is also possible that there were relatively more active sites in 0.015 M AgNP for Cd<sup>2+</sup> to be adsorbed.



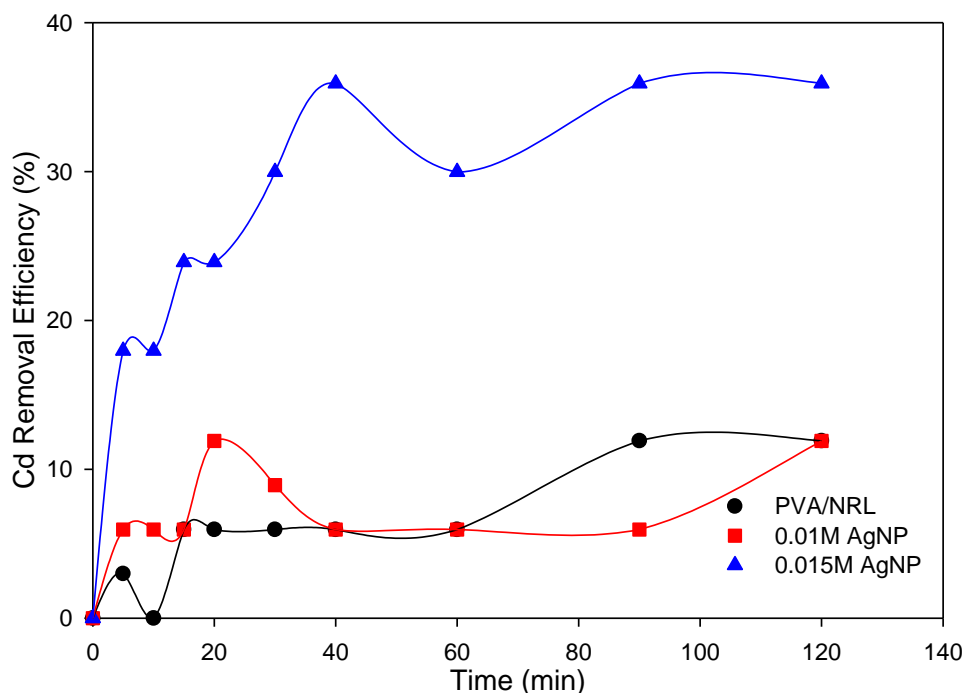


**Figure 6.10 Effect of Contact Time on the Adsorption of Cd<sup>2+</sup> by PVA/NRL Nanofibre, 0.01 M AgNP and 0.015 M AgNP (Osei *et al.*, 2023)**

It is possible that, contrary to Hg adsorption, the relatively smaller atomic radius (calculated) (<sup>48</sup>Cd = 161 pm; <sup>80</sup>Hg = 171 pm) and lower density (Cd = 8.65 g/cm<sup>3</sup>; Hg = 13.53 g/cm<sup>3</sup>) of Cd than Hg may have contributed to its better absorption in 0.015 M AgNP than 0.01 M AgNP (Kipling, 1965; Anon., 2023e). That is, Cd<sup>2+</sup> may have found it relatively easier to diffuse or infiltrate the fibre walls of 0.015 M AgNP, thereby binding to the active sites within this nanofibre composite. The smaller percentage removal of Cd<sup>2+</sup> experienced in 0.01 M AgNP may likely result from relatively less active sites in the nanofibre composite resulting in desorption after 20 min and re-adsorption at 120 min. All other experiments were conducted at 40 min for 0.015 M AgNP and 20 min for 0.01 M AgNP.

### 6.3.3 Effect of Initial Concentration on Cd<sup>2+</sup> Adsorption

The effect of initial concentration on Cd<sup>2+</sup> removal from an aqueous solution was also studied. Results of this study are presented in Figure 6.11. While maintaining the pH at 7 for both AgNP-PVA/NRL nanofibre composites and contact time at 20 min for 0.01 M AgNP and 40 min for 0.015 M AgNP, the initial concentration was ranged between 0.00 – 1.00 mg/L. Similar to the trend in Hg adsorption, the percentage of Cd<sup>2+</sup> removed decreased with an increase in Cd<sup>2+</sup> concentration.

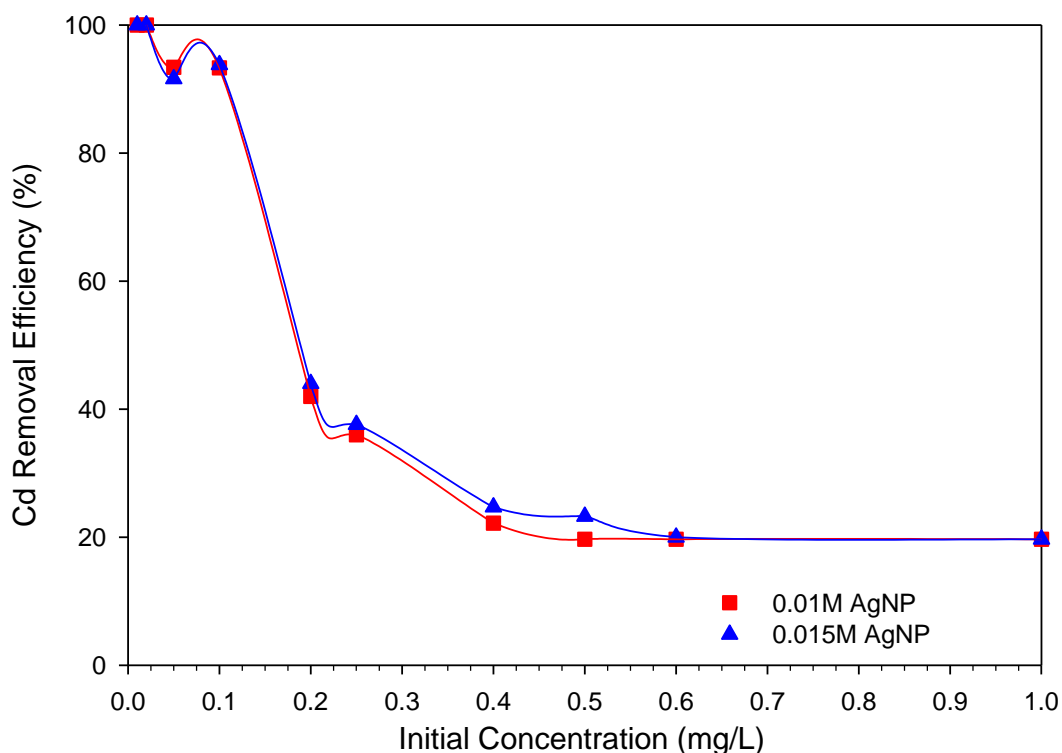


**Figure 6.11 Effect of Initial Concentration on the Adsorption of  $\text{Cd}^{2+}$  by AgNP-PVA/NRL Nanofibre Composites (Osei *et al.*, 2023)**

The highest percentage of  $\text{Cd}^{2+}$  removed by 0.01 M AgNP was at 0.05 mg/L (93.40%), with a slight decrease at 0.10 mg/L (93.30%). Similar to  $\text{Cd}^{2+}$  adsorption by 0.01 M AgNP, one of the highest percentages of  $\text{Cd}^{2+}$  removed by 0.015 M AgNP was at 0.05 mg/L, with the highest percentage at 0.10 mg/L (93.80%). For both AgNP-PVA/NRL nanofibre composites, there was a sharp decrease in the percentage of  $\text{Cd}^{2+}$  removed at 0.20 mg/L (0.01 M AgNP = 27.00%; 0.015 M AgNP = 28.50%) (Figure 6.11). This shows that more active sites were available when  $\text{Cd}^{2+}$  concentration was lower, resulting in a higher removal percentage.

#### 6.3.4 Adsorption Isotherm Study for Cd

Experimental data for  $\text{Cd}^{2+}$  adsorption was also fitted to the Langmuir, Freundlich and D-R isotherms to describe the adsorption behaviour. Figure 6.12 and Table 6.3 show the adsorption isotherms of  $\text{Cd}^{2+}$  by the AgNP-PVA/NRL nanofibre composites and the models' parameters, respectively. The  $R^2$  and MSE of the isotherms are also presented in Table 6.3. Adsorption data for both 0.01 M and 0.015 M AgNP were a weak fit to the

Langmuir isotherm and a fairly good fit to the D-R isotherm. Experimental data for both 0.01 M and 0.015 M AgNP fitted best to the Freundlich isotherm meaning adsorption by both AgNP occurred in a multilayered fashion. The  $R^2$  and MSE of 0.01 M AgNP were 0.7413 and  $10.5678 \text{ (mg/g)}^2$ , respectively, whilst that of 0.015 M AgNP were 0.8066 and  $3.6705 \text{ (mg/g)}^2$ , respectively. As presented in Equation (6.4), the Cd-Ag alloy  $((\text{Ag}_x\text{Cd})^{y-})$  formed is negatively charged, causing the alloy to attract  $\text{Cd}^{2+}$  in the solution. This probably resulted in the multilayered adsorption of  $\text{Cd}^{2+}$ . The  $1/n$  values ( $n$  is a measure of the change in affinity for the adsorbate with changes in adsorption density), which determines whether the adsorption was favourable or not, for both 0.01 M AgNP (0.2245) and 0.015 M AgNP (0.2315) were less than 1 but greater than 0. Since  $1/n$  values were  $< 1$  but  $> 0$ , the reaction was favourable, and the adsorbent sites had different affinities for the adsorbate (Sawyer *et al.*, 2003). The  $K_F$  values for the reaction were also  $19.2994 \text{ (mg/g)/(mg/L)}^{1/n}$  for 0.01 M AgNP and  $13.6678 \text{ (mg/g)/(mg/L)}^{1/n}$  for 0.015 M AgNP.

The Freundlich isotherm assumes that the active sites of the adsorbent have different affinities for the adsorbate (Sawyer *et al.*, 2003). Thus, it can be deduced that AgNP present within the fibre walls must have contributed to the different affinities all over the nanofibre composites, resulting in  $\text{Cd}^{2+}$  adsorption in a heterogenous fashion. Comparing  $\text{Cd}^{2+}$  adsorption of the two nanofibre composites (Table 6.3), 0.01 M AgNP (47.7059 mg/g) had a higher  $q_{DR}$  value than that of 0.015 M AgNP (35.4335 mg/g), which refers to the maximum adsorption capacity per D-R isotherm. This signifies that 0.01 M AgNP has better capability in adsorbing more  $\text{Cd}^{2+}$  than 0.015 M AgNP. The higher  $q_{DR}$ ,  $K_F$  and  $n$  values for 0.01 M AgNP in this isotherm indicates that if the experiment's time frame had been extended beyond 120 min for this nanofibre composite, more  $\text{Cd}^{2+}$  might have been adsorbed. However, since the time frame for 0.01 M AgNP was limited to 20 min, its kinetics showed otherwise (Section 6.2.5). Another important parameter,  $E$ , of the D-R isotherm, was 20.8791 kJ/mol and 20.3996 kJ/mol for 0.01 M AgNP and 0.015 M AgNP, respectively. These  $E$  values were beyond the 8 - 16 kJ/mol range for chemisorption in literature (Das *et al.*, 2013; Maneechakr and Mongkollertlop, 2020). Therefore, further analysis would be required, including extending the experiment's time frame to understand the adsorption mechanism better.

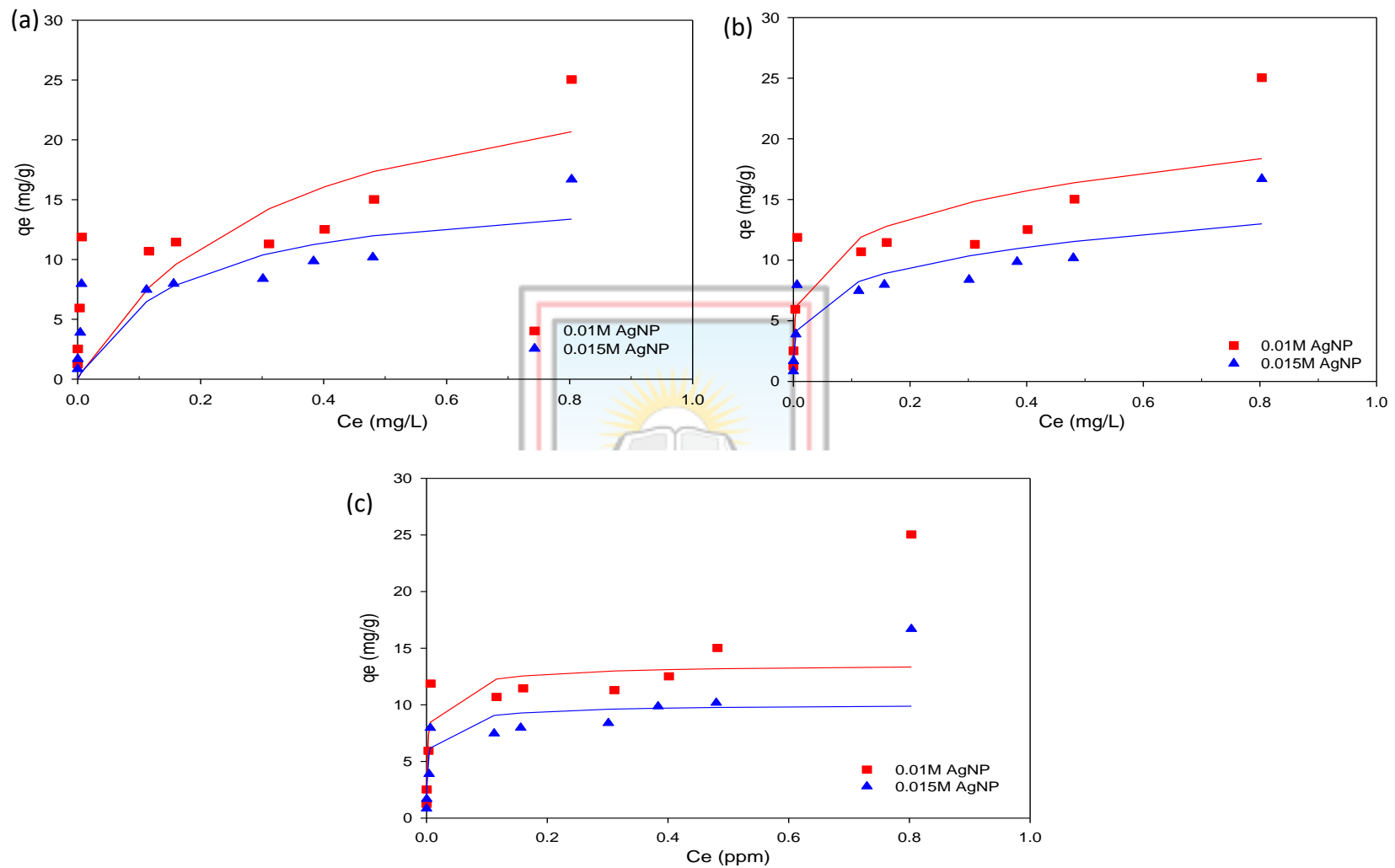
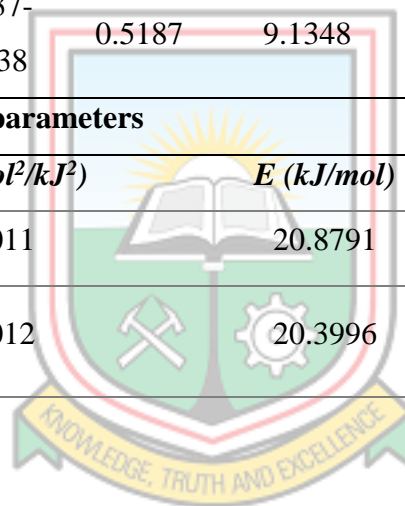


Figure 6.12 (a) Langmuir (b) Freundlich and (c) Dubinin-Radushkevich Isotherm for  $\text{Cd}^{2+}$  Adsorption by AgNP-PVA/NRL Nanofibre Composites (Osei *et al.*, 2023)

**Table 6.3 Parameters of Adsorption Isotherms for Cd<sup>2+</sup> Adsorption onto AgNP-PVA/NRL Nanofibre Composites**

Adsorbent	Langmuir parameters				Freundlich parameters				
	$q_{max}$ (mg/g)	$K_L$ (L/mg)	$R_L$	$R^2$	$MSE$ [(mg/g) <sup>2</sup> ]	$1/n$	$K_F$ [(mg/g)/(mg/L) <sup>1/n</sup> ]	$R^2$	$MSE$ [(mg/g) <sup>2</sup> ]
<b>0.01 M AgNP</b>	28.9897	3.0981	0.2440- 0.9700	0.4483	22.5407	0.2245	19.2994	0.7413	10.5678
<b>0.015 M AgNP</b>	16.1689	5.9596	0.1437- 0.9438	0.5187	9.1348	0.2315	13.6678	0.8066	3.6705
Adsorbent	D-R parameters				$R^2$	$MSE$ [(mg/g) <sup>2</sup> ]			
	$q_{DR}$ (mg/g)	$K_{DR}$ (mol <sup>2</sup> /kJ <sup>2</sup> )	$E$ (kJ/mol)						
<b>0.01 M AgNP</b>	47.7059	0.0011	20.8791		0.7238	11.2840			
<b>0.015 M AgNP</b>	35.4335	0.0012	20.3996		0.7904	3.9789			

(Osei *et al.*, 2023)



### 6.3.5 Adsorption Kinetic Study for Cd<sup>2+</sup>

Similar to the adsorption kinetic study of Hg, the experimental data for Cd<sup>2+</sup> adsorption by 0.01 M and 0.015 M AgNP were examined using the PFO, PSO, Elovich and intra-particle diffusion kinetic models. Plots for the four kinetic models are presented in Figure 6.13. In addition, the parameters of the kinetic models are also presented in Table 6.4.

For Cd<sup>2+</sup> adsorption by 0.01 M AgNP, the experimental data were a weak fit to PFO ( $R^2 = 0.5384$ ;  $MSE = 7.8203 \text{ (mg/g)}^2$ ), PSO ( $R^2 = 0.5349$ ;  $MSE = 7.8790 \text{ (mg/g)}^2$ ) and Elovich ( $R^2 = 0.5338$ ;  $MSE = 7.8978 \text{ (mg/g)}^2$ ) kinetic models. Although the experimental data were a weak fit to all the adsorption kinetic models used in this study, the data fit best to the PFO model. Also, the experimental data for 0.01 M AgNP was a poor fit to the intra-particle diffusion model ( $R^2 = 0.3333$ ;  $MSE = 11.2950 \text{ (mg/g)}^2$ ) (Table 6.4). Though the best fit for Cd<sup>2+</sup> adsorption by 0.01 M AgNP was the PFO kinetic model, which denotes physisorption, its isotherm data fitted best to the Freundlich's, which otherwise signifies chemisorption. It is worth noting that the disparity observed, whether the adsorption is physical or chemical, may be due to the weak  $R^2$  recorded in the PFO model. Weak fits do not accurately describe a system. Hence, it cannot be confirmed as physical or chemical adsorption. The weak and poor fit observed in all the kinetic models used in this study for Cd<sup>2+</sup> adsorption by 0.01 M AgNP may be due to the desorption recorded after 20 min and a sudden readsorption at 120 min. Another possibility may be due to the experiment nearing equilibrium or not reaching equilibrium in the study's time frame (Revellame *et al.*, 2020). In reviews on adsorption, Tran *et al.* (2017) and Revellame *et al.* (2020) mentioned that including experimental data long after reaching equilibrium or stopping the experiment extremely close to the equilibrium may lead to wrong inferences. Hence, extending the time frame beyond 120 min or reducing it to a few minutes after 20 min may be suitable for better results.

On the other hand, the experimental data for Cd<sup>2+</sup> adsorption by 0.015 M AgNP were a good fit to PFO ( $R^2 = 0.9214$ ;  $MSE = 6.2582 \text{ (mg/g)}^2$ ), PSO ( $R^2 = 0.9443$ ;  $MSE = 4.4371 \text{ (mg/g)}^2$ ), Elovich ( $R^2 = 0.9461$ ;  $MSE = 4.2957 \text{ (mg/g)}^2$ ) and the intra-particle diffusion ( $R^2 = 0.8006$ ;  $MSE = 15.8823 \text{ (mg/g)}^2$ ) kinetic models, with the best fit to the Elovich model (Table 6.4). Since Cd<sup>2+</sup> adsorption on 0.015 M AgNP fits best to the Freundlich isotherm and Elovich kinetic model, it can be assumed that the adsorption might have been chemisorption. The  $\alpha$  value for 0.015 M AgNP (12.8106 mg/(g × min)) was lower than 0.01 M AgNP (679.0428 mg/(g × min)), which means the initial adsorption of Cd<sup>2+</sup> by 0.015 M AgNP was slower

than that of 0.01 M AgNP. The  $\beta$  value, another important Elovich parameter, was also lower in 0.015 M AgNP (0.1793 g/mg) than in 0.01 M AgNP (1.0351 g/mg). The lower  $\beta$  value in 0.015 M AgNP signifies a relatively smaller amount of  $\text{Cd}^{2+}$  would desorb from 0.015 M AgNP within the experiment's time frame than the amount that will desorb from 0.01 M AgNP. Though the experimental data for  $\text{Cd}^{2+}$  adsorption by both nanofibre composites were poor fits to the intra-particle diffusion model, comparing their C values shows that 0.015 M AgNP (7.5959 mg/g) was higher than that of 0.01 M AgNP (4.5942 mg/g). The higher C value in 0.015 M AgNP shows that 0.015 M AgNP had a relatively bigger boundary layer; hence the better  $\text{Cd}^{2+}$  adsorption experienced.

Therefore, it may be possible that the presence of relatively more and smaller nanoparticles within the fibre resulted in the lower desorption constant and larger boundary layer in 0.015 M AgNP. Contrary to Hg adsorption, in  $\text{Cd}^{2+}$  adsorption, the AgNP adsorbed  $\text{Cd}^{2+}$  irrespective of its location in the fibre. This is discussed further in section 6.4.



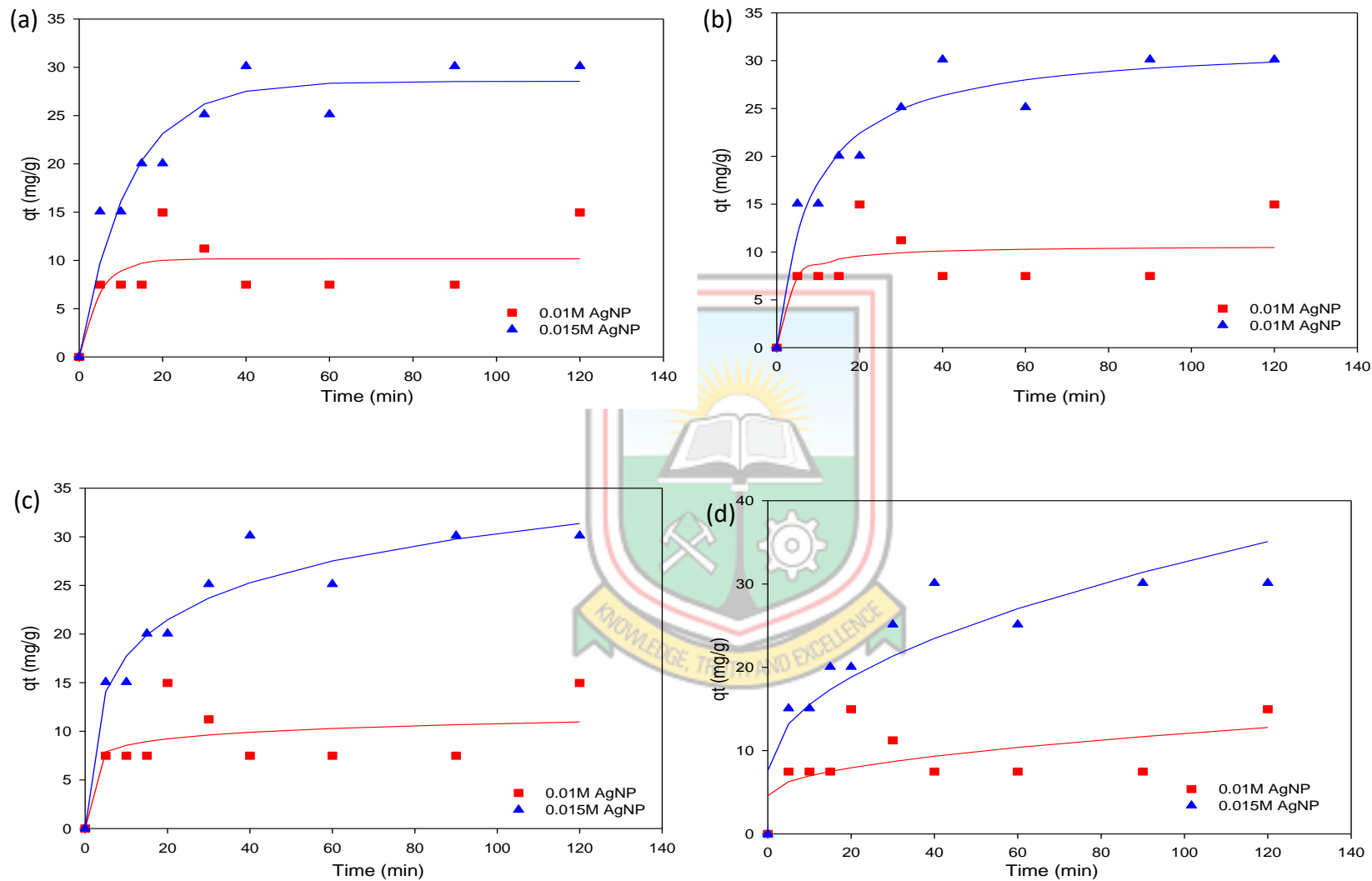


**Figure 6.13 (a) Pseudo-First Order (b) Pseudo-Second Order (c) Elovich and (d) Intra-Particle Diffusion Kinetic Models for Cd<sup>2+</sup> Adsorption by AgNP-PVA/NRL Nanofibre Composites (Osei *et al.*, 2023)**



**Table 6.4 Parameters of Adsorption Kinetics for Cd<sup>2+</sup> Adsorption onto AgNP-PVA/NRL Nanofibre Composites**

Model	Parameters	Adsorbent	
		0.01 M AgNP	0.015 M AgNP
PFO	q <sub>e</sub> (mg/g)	10.1604	28.5447
	k <sub>1</sub> (1/ min)	0.2074	0.0831
	<b>R<sup>2</sup></b>	0.5384	0.9214
	<b>MSE [(mg/g)<sup>2</sup>]</b>	7.8203	6.2582
PSO	q <sub>e</sub> (mg/g)	10.6641	31.9701
	k <sub>2</sub> [g/(mg × min)]	0.0416	0.0037
	<b>R<sup>2</sup></b>	0.5349	0.9443
	<b>MSE [(mg/g)<sup>2</sup>]</b>	7.8790	4.4371
Elovich	α [mg/(g × min)]	679.0428	12.8106
	β (g/mg)	1.0351	0.1793
	<b>R<sup>2</sup></b>	0.5338	0.9461
	<b>MSE [(mg/g)<sup>2</sup>]</b>	7.8978	4.2957
Intra-particle diffusion	k <sub>p</sub> [mg/(g × min <sup>1/2</sup> )]	0.7467	2.5093
	C (mg/g)	4.5942	7.5959
	<b>R<sup>2</sup></b>	0.3333	0.8006
	<b>MSE [(mg/g)<sup>2</sup>]</b>	11.2950	15.8823

(Osei *et al.*, 2023)

### 6.3.6 Morphology and Elemental Composition of AgNP-PVA/NRL Nanofibre Composites after Cd<sup>2+</sup> Adsorption

The morphology and elemental composition of the AgNP-PVA/NRL nanofibre composites after Cd<sup>2+</sup> adsorption are presented in Figure 6.14. The whitish spots (green arrows) in Figure 6.14a represent clusters of AgNP.

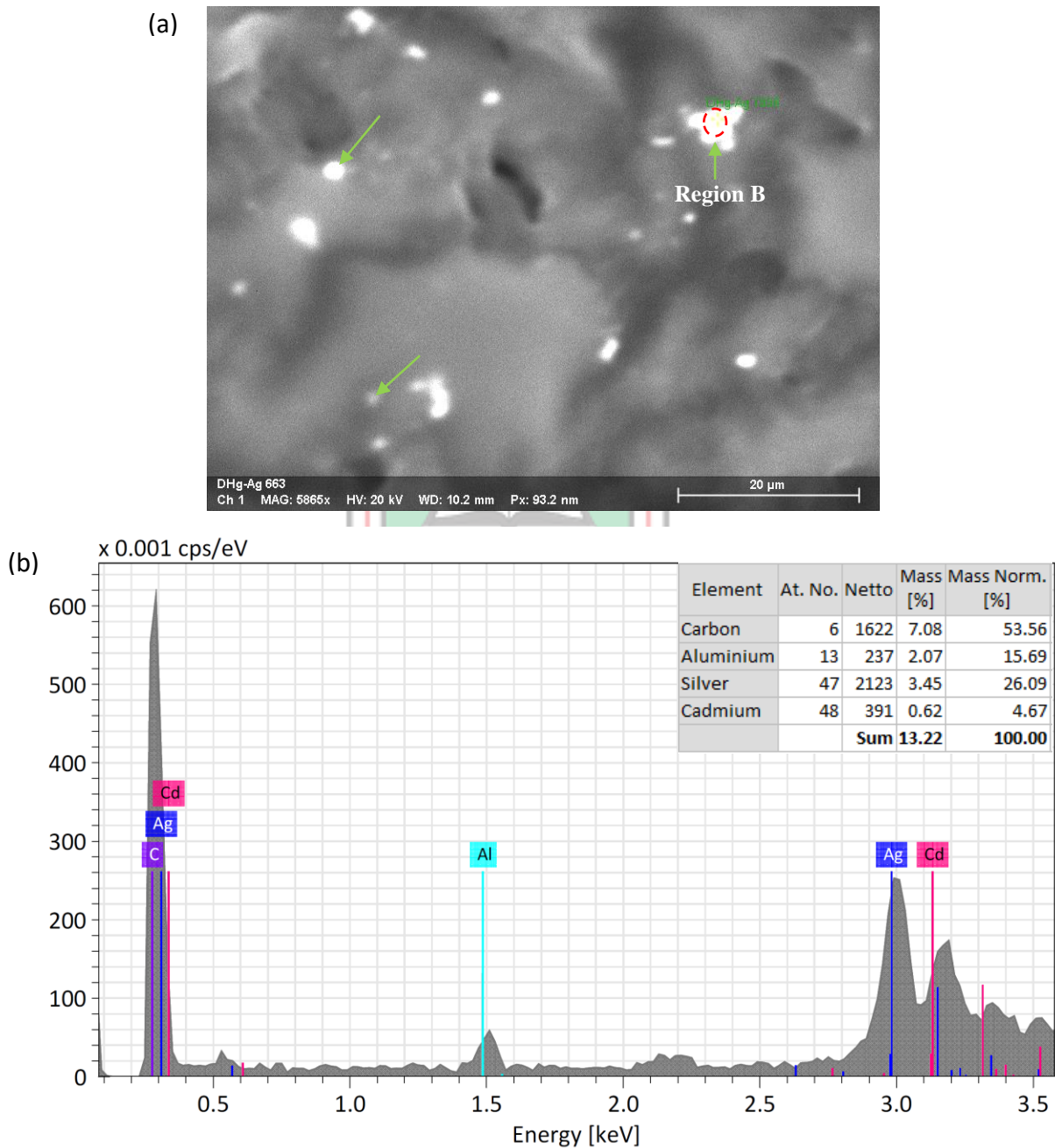


**Figure 6.14 (a) BSD-SEM Image with (b) EDX Analysis After Cd<sup>2+</sup> Adsorption by AgNP-PVA/NRL Nanofibre Composite (Osei *et al.*, 2023)**

Figure 6.14b shows the EDS analysis of Region B shown in Figure 6.14a, which is also a whitish spot. Figure 6.14b shows that Ag was detected as part of the spectrum, meaning the whitish spots (green arrows) were AgNP clusters. Also, from the EDS spectrum of Region B, it can be seen that  $\text{Cd}^{2+}$  was adsorbed from the aqueous solution onto the nanofiber composite. This shows that the nanofibre composite had indeed removed some  $\text{Cd}^{2+}$  from the solution. Aluminium appearing in the spectrum may originate from the aluminium foil used as a substrate to collect the electrospun fibres. Since matting was observed, it could be inferred that some aluminium might have clung to the AgNP-PVA/NRL nanofibre composite upon its removal for adsorption studies.

#### 6.4 Comparison of Hg Adsorption to Cd Adsorption by AgNP-PVA/NRL Nanofibre Composites

Both 0.01 M and 0.015 M AgNP could adsorb Hg better than adsorbing  $\text{Cd}^{2+}$  in solution. A higher  $q_{\text{max}}$ ,  $K_L$ ,  $K_F$ , and  $1/n$  values in Hg adsorption shows that the nanofibre composites could adsorb Hg more efficiently than  $\text{Cd}^{2+}$ . In contrast, the relatively higher mean adsorption energy ( $E$ ) in  $\text{Cd}^{2+}$  removal by both nanofibre composites probably signifies stronger bonds in  $\text{Cd}^{2+}$  adsorption than in Hg adsorption.

Although relatively more AgNP were present in the 0.015 M AgNP than 0.01 M AgNP, Hg adsorption was more efficient when most of the nanoparticles were on or near the surface of the fibre walls, as seen in 0.01 M AgNP. On the other hand, the location of AgNP seemed not to affect  $\text{Cd}^{2+}$  adsorption in the experiment's time frame. The nanofibre composite with relatively more AgNP, which is 0.015 M AgNP, adsorbed more  $\text{Cd}^{2+}$  from the solution.

Also, Hg adsorption was better in the nanofibre composite with larger nanoparticles (0.01 M AgNP), probably because most of the smaller-sized AgNP were within the fibre. Henglein (1998) pointed out (Equations (6.2) and (6.3)) that smaller Ag clusters cannot efficiently amalgamate with Hg but will instead reduce  $\text{Hg}^{2+}$  to  $\text{Hg}^0$ , which may then proceed in amalgamating with relatively larger Ag clusters. Moreover, since the AgNP were located within a solid matrix, Hg could not infiltrate it fast enough. This was contrary to literature where the adsorbent was in a liquid matrix (Katok *et al.*, 2012; Korobeinyk and Inglezakis, 2018). On the other hand, the nanofibre composite with a relatively smaller-sized AgNP, which is 0.015 M AgNP, adsorbed more  $\text{Cd}^{2+}$  from the solution. This shows

that the smaller atomic radius and density of  $\text{Cd}^{2+}$  relative to Hg might have positively affected  $\text{Cd}^{2+}$  adsorption by the nanofibre composites.

## 6.5 Summary

In separate experiments, the synthesised AgNP-PVA/NRL nanofibre composites can adsorb Hg and Cd from an aqueous solution. The percentages of Hg and  $\text{Cd}^{2+}$  removed depended on pH, contact time and initial concentration.

For both 0.01 M and 0.015 M AgNP, maximum uptake of Hg occurred at pH 7 and around 60 min. As the initial Hg concentration increased, the percentage of Hg removed decreased. Also, experimental data for Hg adsorption fit best to Langmuir isotherm for 0.01 M AgNP and D-R isotherm for 0.015 M AgNP. This shows that Hg adsorption by 0.01 M AgNP occurred in a monolayer fashion on the surface, whilst the porous nature of 0.015 M AgNP affected Hg adsorption. All these reflect that the location of the AgNP in these nanofibre composites is essential for Hg adsorption. The experimental data for Hg adsorption also fit best to the Elovich kinetic model for both 0.01 M and 0.015 M AgNP. This best fit assures that the Hg was chemisorbed. The nanofibre composite, 0.01 M AgNP, had a lower  $\beta$  (0.1217 g/mg) and larger C values (9.9354 mg/g) than 0.015 M AgNP ( $\beta = 0.3483$  g/mg;  $C = 6.6235$  mg/g), which confirms 0.01 M AgNP could adsorb Hg better than 0.015 M AgNP.

Maximum uptake of  $\text{Cd}^{2+}$  occurred at pH 7 and at a reaction time of 20 min for 0.01 M AgNP. That for 0.015 M AgNP occurred at pH 7 and at a reaction time of 40 min. Similar to Hg adsorption, as the initial  $\text{Cd}^{2+}$  concentration increased, the percentage of  $\text{Cd}^{2+}$  adsorbed decreased. For 0.01 M AgNP,  $\text{Cd}^{2+}$  adsorption data was a weak and fairly good fit to all three adsorption isotherm models used in this study. On the other hand, the  $\text{Cd}^{2+}$  adsorption data for 0.015 M AgNP was a fairly good fit for the Langmuir and D-R isotherms. The experimental data fit best to the Freundlich isotherm for both 0.01 M and 0.015 M AgNP, showing that the adsorption in both nanofibre composites occurred in a heterogeneous fashion. The  $\text{Cd}^{2+}$  adsorption data for 0.01 M AgNP was a weak and poor fit to all four adsorption kinetic models used in the study. Nevertheless, the data best fit the PFO kinetic model. The weak and poor fit for  $\text{Cd}^{2+}$  adsorption in 0.01 M AgNP suggests that the experiment's time frame be cut short after 20 min or extended beyond 120 min for better results. On the other hand,  $\text{Cd}^{2+}$  adsorption data for 0.015 M AgNP fit best to the Elovich kinetic model. In all, 0.015 M AgNP ( $\beta = 0.1793$  g/mg;  $C = 7.5959$  mg/g) adsorbed  $\text{Cd}^{2+}$

better than 0.01 M AgNP ( $\beta = 1.0351$  g/mg;  $C = 4.5942$  mg/g), and this also shows that the location of AgNP in the nanofibre did not affect  $Cd^{2+}$  adsorption within the experiment's time frame.



## CHAPTER 7

### COMPETITIVE ADSORPTION OF MERCURY AND CADMIUM FROM AQUEOUS SOLUTION USING AgNP-PVA/NRL NANOFIBRE COMPOSITES

This chapter outlines studies on the sorption of Hg and Cd<sup>2+</sup> in a binary system (Cd-Hg solution) by various AgNP-PVA/NRL nanofibre composites. The aim is to understand how efficiently the different AgNP-PVA/NRL nanofibre composites can remove Hg and Cd concurrently from an aqueous solution. The chapter also discusses the amount of Ag released into the solution after adsorption.

#### 7.1 Background

To determine the level of interference some metals pose in an adsorptive water treatment system, binary adsorption studies are of great significance (Goel *et al.*, 2004). Although pH, contact time and initial concentration for Hg and Cd adsorption by 0.01 M and 0.015 M AgNP have been optimised for maximum adsorption (Chapter 6), it is necessary to assess how efficiently the two metals will be adsorbed or the interference one will pose to the other in a binary system.

Increasing the adsorbent's surface area and the number of active interaction sites can positively influence adsorption (Ali, 2012). The number of active sites can be increased by increasing the adsorbent dose. According to Kipling (1965), an increment in the specific surface area of an adsorbent can be achieved by increasing its porosity, which sequentially will magnify selective adsorption. Conventionally electrospun nanofibres have limited porosity since fibres are tightly packed, forming thin sheets. The porosity of these fibres can be enhanced by forming stable 3D structures (Chen *et al.*, 2020). Sequential electrospinning, for instance, is one of the methods used to create stable 3D structures (Cortes *et al.*, 2017). In line with this, it is necessary to assess if increasing the adsorbent dose and surface area would positively affect the competitive adsorption of Hg and Cd in a typical binary system.

Although AgNP are beneficial in removing contaminants such as Hg and Cd from water, separating silver nanoparticles (AgNP) from the treated water will be expensive. This would defeat the purpose of using AgNP as an adsorbent in water treatment, as Ag in the nanofibre composite can dissolve and create a contamination problem (Roksana, 2016). In addition, excess Ag may cause argyria (Anon., 2011a; Anon., 2013). Therefore, it is necessary to

investigate the amount of Ag released into treated water by AgNP-PVA/NRL nanofibre composites after contaminant (Hg and Cd) removal from a typical binary system.

## 7.2 Efficiency of Various AgNP-PVA/NRL Nanofibre Composites to Adsorb Hg and Cd<sup>2+</sup> Simultaneously from A Binary System (Cd-Hg Solution)

To understand the behaviour of Hg and Cd<sup>2+</sup> adsorption by AgNP-PVA/NRL nanofibre composites in a binary system (Cd-Hg solution), the affinity of each adsorbate (Cd and Hg) by the nanofibre composites were studied. A 0.01 M AgNP, 0.015 M AgNP, and other AgNP-PVA/NRL nanofibre composites named Mix 1 (5 × 5 cm<sup>3</sup>), Mix 2 (5 × 5 cm<sup>3</sup>), and Mix 3 (5 × 10 cm<sup>3</sup>), were placed in an aqueous solution containing Cd and Hg. Mix 1 was a mixture of 0.01 M AgNP and 0.015 M AgNP electrospun concurrently. Mix 2 was also a mixture of 0.01 M AgNP and 0.015 M AgNP but electrospun sequentially; that is, 0.01 M AgNP was electrospun first and after 12 h of air drying, 0.015 M AgNP was electrospun onto the same collector. Mix 1 would form a 2D film, whilst Mix 2 was expected to form a porous scaffold to improve adsorption. Mix 1 and 2's synthesis have been described in Chapter 3. Mix 3 consisted of 5 × 5 cm<sup>3</sup> of 0.01 M AgNP and 5 × 5 cm<sup>3</sup> of 0.015 M AgNP.

In a batch experiment, 0.01 M AgNP, 0.015 M AgNP, Mix 1, Mix 2 and Mix 3 were placed in 50 mL of Cd-Hg solution. The solution's pH was kept at 7, with Cd<sup>2+</sup> and Hg concentrations at 0.10 and 0.05 mg/L, respectively. The solution's pH and initial concentrations were selected based on the maximum uptake of Cd<sup>2+</sup> and Hg in single-component adsorption studies (See Chapter 6). This was done to determine how Hg and Cd<sup>2+</sup> would compete for the adsorbent at the set parameters. Contact time was held at 60 min. Though the highest percentage of Cd<sup>2+</sup> removed by 0.01 M and 0.015 M AgNP occurred at 20 and 40 min, respectively, 60 min was selected. This was because a specific duration was needed to determine how the adsorption of one metal affected the other at a particular time. Also, the maximum amount of Hg was adsorbed at 60 min, which was the longest duration compared to Cd<sup>2+</sup> adsorption.

Figure 7.1 shows the removal efficiencies of 0.01 M AgNP, 0.015 M AgNP, Mix 1, Mix 2 and Mix 3 in adsorbing Cd<sup>2+</sup> and Hg from Cd-Hg solution. Table 7.1 shows the adsorption capacities of 0.01 M AgNP, 0.015 M AgNP, Mix 1, Mix 2 and Mix 3.

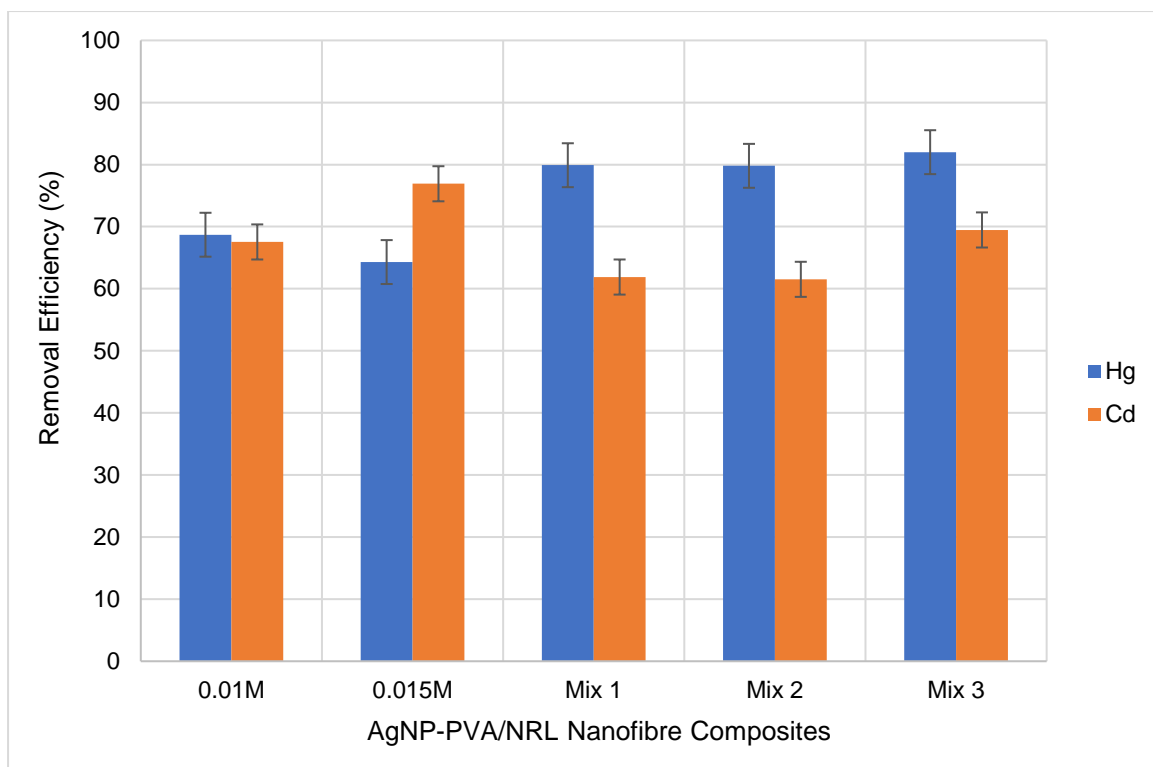


**Figure 7.1 Removal Efficiency of Hg and Cd<sup>2+</sup> from Cd-Hg Solution by AgNP-Nanofibre Composites**

**Table 7.1 Adsorption Capacity of Hg and Cd<sup>2+</sup> from Cd-Hg Solution by AgNP-PVA/NRL Nanofibre Composites**

Fibre Matrix (AgNP)	Adsorption Capacity [ $q_e$ (mg/g)]	
	Hg	Cd <sup>2+</sup>
0.01 M	4.3719	8.2398
0.015 M	2.7279	6.2779
Mix 1	2.0338	3.0118
Mix 2	2.0313	2.6548
Mix 3	2.0873	3.1243

The AgNP-PVA/NRL nanofibre composites' ability to remove Hg from the Cd-Hg solution was in the order: 0.015 M AgNP < 0.01 M AgNP < Mix 2 < Mix 1 < Mix 3, whilst that of Cd was in the order: 0.01 M AgNP < Mix 2 < Mix 1 < Mix 3 < 0.015 M AgNP. The nanofibre composite 0.01 M AgNP adsorbed 4.3719 mg/g (68.70%) of Hg and 8.2398 mg/g (67.54%) of Cd<sup>2+</sup>, whilst 0.015 M AgNP adsorbed 2.7279 mg/g (64.30%) of Hg and 6.2779 mg/g (76.91%) of Cd<sup>2+</sup> from solution. Mix 1, 2 and 3 adsorbed 2.0338 mg/g (79.90%),



2.0313 mg/g (79.80%) and 2.0873 mg/g (82.00%) of Hg, respectively, from the solution. Mix 1, 2 and 3 also adsorbed 3.0118 mg/g (61.88%), 2.6548 mg/g (61.52%) and 3.1243 mg/g (69.47%) of Cd<sup>2+</sup> from the same solution.

Figure 7.1 shows that 0.01 M AgNP adsorbed a higher percentage of Hg than Cd<sup>2+</sup>, whilst 0.015 M AgNP adsorbed a higher percentage of Cd<sup>2+</sup> than Hg. Mix 1, 2 and 3 adsorbed higher percentages of Hg than Cd<sup>2+</sup>. The trend for 0.01 M and 0.015 M AgNP was similar to that observed in Chapter 6 for Hg and Cd<sup>2+</sup> adsorption, which is, 0.01 M AgNP adsorbed Hg better, whilst 0.015 M AgNP adsorbed Cd<sup>2+</sup> better. On the other hand, the adsorption capacities of Cd<sup>2+</sup> were higher than that of Hg for all AgNP-PVA/NRL nanofibre composites (Table 7.1). This occurred because Cd<sup>2+</sup>'s initial concentration was higher than Hg, resulting in a higher uptake by calculation.

It is worth noting that the initial concentrations used in this experiment were chosen based on the highest fraction of Hg and Cd<sup>2+</sup> that were adsorbed in single-component adsorption studies. However, the removal efficiency of 0.01 M AgNP for Hg was reduced by about 20% (from 5.6637 mg/g to 4.3719 mg/g, representing about 89% to 69%) in the binary system. The decrease observed could be due to Hg and Cd<sup>2+</sup> competing for the same number of active sites for adsorption. Similar to Hg adsorption, Cd<sup>2+</sup> adsorption by 0.01 M AgNP reduced by ~26% (from 11.8747 mg/g to 8.2398 mg, representing ~ 93% to 68%). A difference of about 6% (about 26% (for Cd<sup>2+</sup>) less 20% (for Hg)) in deficiency indicates that 0.01 M AgNP performed better in adsorbing Hg than Cd<sup>2+</sup> in the binary system. The relatively higher removal efficiency of Hg by 0.01 M AgNP was likely due of the relatively larger AgNP located mainly on the surface of the nanofibre composite, as discussed in Chapter 6.

For 0.015 M AgNP, the removal efficiency for Hg reduced by approximately 25% (that is, 3.7758 mg/g to 2.7279 mg/g, representing ~ 89% to 64%) whilst that of Cd<sup>2+</sup> reduced by about 17% (that is, 7.9588 mg/g to 6.2779 mg/g, representing ~ 93% to 77%). It is evident that even in the binary system, 0.015 M AgNP could adsorb Cd<sup>2+</sup> better than Hg. This supports the hypothesis that in 0.015 M AgNP, most of the AgNP are located within the fibre wall, and their relatively smaller average size in 0.015 M AgNP (2.82 nm ± 0.04 nm), likely limited Hg's adsorption. The higher percentage of Cd<sup>2+</sup> removed than Hg shows that the smaller density (Cd = 8.65 g/cm<sup>3</sup>; Hg = 13.53 g/cm<sup>3</sup>) and atomic radius (calculated) (<sup>48</sup>Cd = 161 pm; <sup>80</sup>Hg = 171 pm) must have influenced Cd<sup>2+</sup>'s adsorption by enabling Cd<sup>2+</sup>

to infiltrate the fibre relatively easier (Anon., 2023e). As explained by Kipling (1965) on factors affecting competitive adsorption, the partial molecular sieve effect of porous adsorbents should not be overlooked if the adsorbates of the liquid mixture are of different sizes. This partial molecular sieve effect creates a degree of preferential adsorption, where larger components are excluded whilst smaller components are admitted into pores for adsorption (Kipling, 1965). Though relatively more AgNP exist within 0.015 M AgNP, the infiltration rate of metallic Hg into the fibres to bond with AgNP may be retarded because of its relatively higher density and calculated atomic radius.

Mix 1 and 2 had somewhat similar removal efficiencies for both Hg (Mix 1: 79.90%, 2.0338 mg/g; Mix 2: 79.80%, 2.0313 mg/g) and Cd<sup>2+</sup> (Mix 1: 61.88%, 3.0118 mg/g; Mix 2: 61.52%, 2.6548 mg/g). For both, a higher percentage of Hg was removed than Cd<sup>2+</sup>. It was anticipated that the percentages of Hg and Cd<sup>2+</sup> removed would increase since both 0.01 M and 0.015 M AgNP had been combined, which means the adsorbent dose had increased, and AgNP content would significantly increase. It is worth noting that there was a relatively small increase in the percentage of Hg removed in Mix 1 and 2 compared to 0.01 M and 0.015 M AgNP. On the other hand, there was a relatively small decrease in the percentage of Cd<sup>2+</sup> removed in Mix 1 and 2 compared to 0.01 M and 0.015 M AgNP.

This expectation did not materialise because doubling the amount of solution electrospun (16 mL) would increase the number of fibres and mattings per area. These fibres would mask others and possibly affect porosity. This would, in turn, reduce the surfaces available for adsorption. Hg adsorption fared relatively better in Mix 1 and 2 than in 0.01 M and 0.015 M AgNP because Hg is adsorbed better when the AgNP are near or on the fibre's surface. Therefore, the relatively larger and more nanoparticles on 0.01 M AgNP's surface and the few on 0.015 M AgNP's surface facilitated Hg adsorption by Mix 1 and 2. Conversely, percentage removal for Cd<sup>2+</sup> was reduced when Mix 1 and 2 were used compared to 0.01 M and 0.015 M AgNP. This is because Hg<sup>2+</sup> has a lower ionic potential (ionic potential is the ratio of the charge of a cation (Hg<sup>2+</sup>) to its radius, meaning Hg<sup>2+</sup> will readily lose its attached water molecules and form inner-sphere complexes (Eby, 2004). As already stated in Chapter 6, inner sphere complexes are firmly bound to adsorbent surfaces. Consequently, this may leave a few adsorption sites on the surface, but a lot within the fibre for Cd<sup>2+</sup> adsorption since Cd<sup>2+</sup> can infiltrate the fibres to bind with AgNP, as observed in Chapter 6. However, owing to the extra fibres of Mix 1 and 2 overlapping several others, it

will result in  $\text{Cd}^{2+}$  taking a longer period to infiltrate the fibres and bind with AgNP than in 0.01 M and 0.015 M AgNP. This explains the reduced removal efficiency of  $\text{Cd}^{2+}$  by Mix 1 and 2 with respect to 0.01 M and 0.015 M AgNP.

Secondly, it was also expected that the percentage removal of Hg and  $\text{Cd}^{2+}$  by Mix 1 and 2 and their adsorption capacity would differ significantly due to the mode of synthesis. It was anticipated that Mix 2 would adsorb more Hg and  $\text{Cd}^{2+}$  since sequential electrospinning produces stable 3D structures or scaffolds which are relatively more porous than the 2D thin layered structures (200 to 1000 nm in diameter) of non-sequential electrospinning (Wulkersdorfer *et al.*, 2010; Ahirwal *et al.*, 2013; Chen *et al.*, 2020). However, both expectations did not materialise.

The second expectation did not also materialise, probably due to the fact that sequential electrospinning method used in this study was ineffective in producing stable 3D scaffolds. For the first 8 h of electrospinning, 0.01 M  $\text{AgNO}_3$ -PVA/NRL produced a 2D thin layered structure due to repulsion of subsequent electrospun fibres caused by electrostatic charging of the scaffold after a few microns of the fibres had been deposited (Ahirwal *et al.*, 2013). Also, the 3D scaffold collapsed into a 2D thin layered structure because the fibres reached the collector moist and soft, and the solvent had not completely evaporated during flight (Sun *et al.*, 2012; Cortes *et al.*, 2017). Twelve (12) hours after electrospinning 0.01 M AgNP, a similar process was used to produce 0.015 M AgNP, which resulted in another 2D thin layered structure. This shows that in the end, only two stacks of 2D thin layered structure (a few hundred nanometres thick) had been produced. The compact 2D thin layered structure limited porosity and pore size, which in turn also limited both heavy metals' adsorption, especially  $\text{Cd}^{2+}$ . Therefore, leaving a 12 h gap for 0.01 M AgNP to solidify completely was insufficient to produce a stable 3D structure. Probably, if the sequence had been a few minutes of electrospinning 0.01 M AgNP, followed by another few minutes of electrospinning 0.015 M AgNP, and the cycle followed as such to form several layers, Mix 2 would have been more porous.

Alternatively, using the aforementioned method and electrospinning a simple leachable solution (like sucrose solution) between each layer, such as that conducted by Wulkersdorfer *et al.* (2010), would have increased the porosity of Mix 2. It is important to note that increasing the porosity of the adsorbent will improve adsorption since the surface area will

inevitably be enhanced (Kipling, 1965). This would have favoured both Hg and Cd<sup>2+</sup> adsorption.

Removal efficiencies of Hg and Cd<sup>2+</sup> were slightly higher in Mix 3 than in Mix 1 and 2. This was because two separate nanofibres were in the solution, meaning increased surface area for adsorption. Due to the perceived increase in surface area, it was anticipated that Hg and Cd<sup>2+</sup> adsorption by Mix 3 would increase by a relatively larger margin. The percentage of Hg removed by Mix 3 was relatively higher but fairly similar to its adsorption by Mix 1 and 2. The relatively small difference (~ 0.0549 mg/g, representing 2.62%) supports the idea that Hg adsorption is enhanced when nanoparticles are near or on the surface of the nanofibre. Removal efficiency of Cd<sup>2+</sup> by Mix 3 was also relatively higher than that of 0.01 M AgNP, Mix 1 and Mix 2. However, the percentage of Cd<sup>2+</sup> removed by Mix 3 was lower than that of 0.015 M AgNP. It was expected that having two separate nanofibres would increase Cd<sup>2+</sup> adsorption. However, the perceived increase in surface area for Mix 3 could not explain the relatively lower percentage of Cd<sup>2+</sup> recorded by Mix 3. The higher removal percentage of Hg than Cd<sup>2+</sup> in Mix 3 could also be attributed to Hg's lower ionic potential, hence forming stronger bonds attached to the adsorbent's surface.

### 7.3 Silver Released into Solution After Adsorption Experiment

This study's purpose was to synthesise AgNP to treat water without the nanoparticles forming part of the contamination problem; therefore, there was the need to investigate the amount of Ag remaining in the solution after adsorption studies. According to the World Health Organisation (WHO), in circumstances where Ag is used to preserve the bacteriological purity of drinking water, higher Ag concentrations of 0.10 mg/L or more cannot be tolerated without endangering health (Anon., 2011a). The amount of Ag remaining in the aqueous solution after adsorption studies for all AgNP-PVA/NRL nanofibre composites are presented in Table 7.2. Guidelines for Ag concentration in drinking water by the US Environmental Protection Agency (US EPA) and WHO are also presented in Table 7.3. From Table 7.2, the amount of Ag released into the aqueous solution were 0.0425 mg/L for 0.01 M AgNP to 0.2140 mg/L for Mix 2. This amount of Ag released was in the order: 0.01 M AgNP < Mix 1 < 0.015 M AgNP < Mix 3 < Mix 2. All AgNP-PVA/NRL nanofibre composites used in this study released Ag concentrations below the limit, except that of Mix 2.

**Table 7.2 Silver (Ag) Concentration in Aqueous Solutions After Hg and Cd Adsorption**

Fibre Matrix (AgNP)	Ag Concentration (mg/L)
0.01 M	0.0425
0.015 M	0.0510
Mix 1	0.0490
Mix 2	0.2140
Mix 3	0.0706

**Table 7.3 Guidelines for Ag Concentration in Drinking Water**

Guideline/Standard	Ag Concentration (mg/L)	Reference
US EPA SMCL*	0.1000	(Anon., 2013)
WHO-drinking water	0.1000	(Anon., 2011a)

\*Secondary Maximum Contaminant Level

The presence of Ag in the treated water were likely due to two reasons. Firstly, 50% PVA/NRL nanofibre, which was used as a matrix for AgNP synthesis, lost  $14.09 \pm 1.86\%$  in a weight loss test by dissolution (Chapter 4). Therefore, dissolution of the surfaces of the AgNP-PVA/NRL nanofibre composites containing AgNP must have resulted in the Ag concentrations in the solution. Secondly,  $\text{AgNO}_3$  on the fibres' surface, which might not have gone through reduction and stabilisation, must have dissolved and dissociated in the aqueous solution, therefore adding to Ag concentration.

Water treated with 0.015 M AgNP had a higher Ag concentration than 0.01 M AgNP. This resulted because the amount of Ag in 0.015 M AgNP ( $\sim 0.5893$  mg) was relatively higher than Ag in 0.01 M AgNP ( $\sim 0.3929$  mg). Although Ag concentration in water treated using 0.015 M AgNP was higher than that treated with 0.01 M AgNP, both were below the Secondary Maximum Contaminant Level (SMCL) of Ag (0.1000 mg/L) (Table 7.3). This result renders the treated water safe for consumption with respect to Ag concentration. Water treated with Mix 1, 2 and 3 was expected to have Ag concentrations higher than that of 0.01 M and 0.015 M AgNP since Ag content in these nanofibre composites was relatively higher. However, this was so for Mix 2 and 3 only.

The higher Ag concentration in water treated using Mix 3 than in that treated using 0.01 M AgNP, 0.015 M AgNP and Mix 1 was expected. However, the value of Ag concentration in water treated using Mix 3 being lower than that in water treated with Mix 2 was not expected. This is because, in the case of Mix 3, two separate nanofibres were used, whilst Mix 2 was a single fibre; therefore, Mix 3 would have a relatively higher surface area for a greater portion of the fibres to dissolve than in Mix 2. However, water treated with Mix 2 rather recorded the highest Ag concentration, and this needs further investigation.

#### 7.4 Summary

Competitive adsorption of Hg and Cd<sup>2+</sup> by AgNP-PVA/NRL nanofibre composites in a binary system (Cd-Hg solution) has been investigated. The removal efficiencies of Hg and Cd<sup>2+</sup> reduced in the binary system compared to that in the single-component adsorption studies since Hg and Cd<sup>2+</sup> competed for the same number of active sites. Similar to the trend for both metals' adsorption in single-component adsorption studies, 0.01 M AgNP adsorbed a relatively higher percentage of Hg than Cd<sup>2+</sup>, whilst 0.015 M AgNP adsorbed a relatively higher percentage of Cd<sup>2+</sup> than Hg. This was because there were relatively more larger nanoparticles on the surface of 0.01 M AgNP's fibres which facilitated Hg adsorption, whilst the relatively more nanoparticles within 0.015 M AgNP's fibres and relatively smaller density and atomic radius (calculated) facilitated Cd adsorption.

In Mix 1 and 2, Hg adsorption fared relatively better than Cd. The removal efficiencies of Hg by Mix 1 and 2 were also relatively better than by 0.01 M and 0.015 M AgNP. On the other hand, Cd's adsorption fared relatively poorer in Mix 1 and 2 than in 0.01 M and 0.015 M AgNP. Electrospinning 16 mL of 0.01 M/0.015 M AgNP solution for Mix 1 and 2 caused the extra fibres produced to overlap several others, therefore, limiting Cd's ability to infiltrate the fibres and bond with AgNP. Contrary to Cd's adsorption, Hg adsorption fared relatively better since its adsorption is mostly favoured when larger nanoparticles are on the fibres' surface. The overlapping of extra fibres did not negatively affect Hg adsorption. The relatively moderate difference between the removal efficiencies of both metals by Mix 1 and 2 and that of 0.01 M and 0.15M AgNP shows that the fibres had indeed overlapped, reducing porosity and adsorption. Also, the relatively small difference in Hg and Cd adsorption by Mix 1 and 2 shows that the sequential electrospinning method used for Mix 2 was ineffective. Both Hg and Cd adsorption by Mix 3 fared relatively better than all other AgNP-PVA/NRL nanofibre composites used in this study, except that of Cd, which fared

relatively poorer than that of 0.015 M AgNP. Also, the higher removal efficiency of Hg than Cd in Mix 1, 2 and 3 was because of the lower ionic potential of Hg than Cd, resulting in Hg forming inner-sphere complexes.

After Hg and Cd adsorption, the amount of Ag released into the treated water was also investigated. All five AgNP-PVA/NRL nanofibre composites released Ag into the aqueous solutions but were below the US EPA SMCL and WHO drinking water guidelines of 0.10 mg/L except Mix 2. The Ag concentrations recorded were because a portion of the matrix's surface (50% PVA/NRL used in AgNP synthesis) dissolved when in contact with an aqueous solution (Chapter 4). Also, AgNO<sub>3</sub> on the fibres' surface, which might not have gone through reduction and stabilisation, must have dissolved and dissociated in the aqueous solution, therefore adding to Ag concentration.



## CHAPTER 8

### CONCLUSIONS AND RECOMMENDATIONS

#### 8.1 Conclusions

This research sought to produce green silver nanoparticles (AgNP) incorporated in natural rubber latex (NRL)/polyvinyl alcohol (PVA) nanofibre (Ag-PVA/NRL) to remove contaminants such as Hg and Cd from wastewater. The conclusions made are presented in sections 8.1.1 – 8.1.3.

##### 8.1.1 Green Electrospinning of PVA/NRL Nanofibre

- Using water as the only solvent, NRL was successfully electrospun by adding PVA to improve its electrospinnability since latex could only be electrospayed at 15 – 26 kV. Adding PVA increased NRL's viscosity, thereby improving the PVA/NRL fibres' morphology.
- Scanning electron microscopy (SEM) analysis, fibre diameter and pore diameter analysis revealed that increasing PVA content caused the average diameters of the electrospun fibres to increase, with 60% and 70% PVA/NRL having the largest diameters. The trend was in the order: 40% PVA/NRL < 50% PVA/NRL < 100% PVA < 70% PVA/NRL < 60% PVA/NRL. Spindle-like structures formed along the fibres and caused 60% and 70% PVA/NRL to have the largest diameters. Fibres of 60% and 70% PVA/NRL were also relatively smoother.
- The average pore diameters were similar to the fibre diameter trend, with 60% and 70% PVA/NRL having the largest average pore diameters and 40% and 50% having the least average pore diameters. The smallest average fibre diameter and pore sizes made 40% and 50% PVA/NRL the most desirable for aqueous processes since such features are necessary for contaminant removal via adsorption. The general trend was that as PVA content increased, fibre diameter increased, pore diameter increased, and smoother fibres were produced with less matting.



- Fourier transform-infrared (FT-IR) analysis revealed that 60% and 70% PVA/NRL had a significant dissolvable fraction due to their relatively higher degree of hydrolysis (DH). This was confirmed by a weight loss test by dissolution.
- Weight loss by dissolution trend was in the order: 50% PVA/NRL < 40% PVA/NRL < 60% PVA/NRL < 70% PVA/NRL. With 50% PVA/NRL having the least dissolvable fraction and also being amongst the fibre films with the smallest fibre and pore diameter sizes. This fibre film was chosen as the best matrix or wall material for nanoparticle synthesis and loading and subsequently for application in aqueous processes such as contaminant removal.

#### 8.1.2 Green Synthesis of AgNP Incorporated in PVA/NRL Nanofibre Composite (Ag-PVA/NRL)

- Silver nanoparticles (AgNP) were successfully green synthesised in PVA/NRL nanofibre composites (0.01 M AgNP and 0.015 M AgNP) by adding AgNO<sub>3</sub> (0.01 M and 0.01 M AgNO<sub>3</sub>, respectively) as a precursor to the electrospinning solution (PVA/NRL solution) before AgNP growth occurred.
- SEM and energy dispersive x-ray spectroscopy (EDS) analysis revealed that AgNP formed were well dispersed in the nanocomposites. The AgNP in 0.01 M AgNP were primarily located near or on the fibre's surface, whilst that of 0.015 M AgNP were found within the fibre walls or relatively small for SEM to detect.
- A transmission electron microscopy (TEM) analysis revealed that the synthesised AgNP were somewhat spherical, with an average diameter of < 10 nm. The research also revealed that increasing AgNO<sub>3</sub> concentration resulted in relatively smaller-sized AgNP (0.015 M AgNP < 0.01 M AgNP).
- Crystallographic analysis by x-ray diffractometry (XRD) confirmed the formation of AgNP in the synthesised AgNP-PVA/NRL nanofibre composites. The amine group (of NRL) and hydroxyl group (of PVA) (FT-IR analysis) may have contributed to the reduction of Ag<sup>+</sup> to Ag<sup>0</sup>, whilst *cis*-isoprene (of NRL) might have been the principal stabilising agent for the AgNP.

### 8.1.3 Adsorption of Hg and Cd from Water by the Synthesised AgNP-PVA/NRL Nanofibre Composites

- In single-component adsorption experiments, the synthesised AgNP-PVA/NRL nanofibres successfully adsorbed Hg and Cd from aqueous solutions. The efficiency of the nanofibre composites to remove these heavy metals depended on pH, contact time and the initial concentration of the adsorbate solution.

#### *Adsorption of Hg from Water by AgNP-PVA/NRL Nanofibre Composites in Single-Component Adsorption Studies*

- Both synthesised AgNP-PVA/NRL nanofibre composites removed maximum amount of Hg at pH 7 and around 60 min. Removal efficiency of the nanofibre composites decreased with an increase in Hg's initial concentration. The Hg adsorption could be due to electrostatic adsorption and redox reaction, which lead to precipitation and amalgamation of Hg, but with amalgamation as the principal mechanism.
- The adsorption studies revealed that the AgNP-PVA/NRL nanofiber composites adsorbed Hg relatively better when the AgNPs were larger (0.01 M AgNP). Adsorption of Hg by 0.01 M AgNP occurred in a monolayer fashion following the Langmuir isotherm model. Adsorption of Hg in 0.015 M AgNP followed the Dubinin-Radushkevich (D-R) isotherm model. Experimental data for both 0.01 M and 0.015 M AgNP fitted best to Elovich kinetic model, which implies Hg was chemisorbed. The larger boundary layer ( $C = 9.9354$  mg/g) and lower desorption constant ( $\beta = 0.1217$  g/mg) of 0.01 M AgNP confirmed that 0.01 M AgNP was a better adsorber of Hg than 0.015 M AgNP ( $C = 6.6235$  mg/g;  $\beta = 0.3483$  g/mg).

#### *Adsorption of Cd<sup>2+</sup> from Water by AgNP-PVA/NRL Nanofibre Composites in Single-Component Adsorption Studies*

- Both synthesised AgNP-PVA/NRL nanofibre composites removed Cd<sup>2+</sup> from the aqueous solution at pH 7 but at different reaction times of 20 min for 0.01 M AgNP and 40 min for 0.015 M AgNP. The removal efficiency of the nanofibre composites decreased with an increase in Cd<sup>2+</sup>'s initial concentration. Cadmium possibly formed an alloy with Ag.

- The adsorption behaviour of both nanofiber composites followed Freundlich isotherm, meaning the adsorption occurred in a multilayered fashion. Experimental data for 0.01 M AgNP were a weak fit to all adsorption kinetic models tested in this study. Contrarily, Cd<sup>2+</sup> adsorption data for 0.015 M AgNP fitted best to the Elovich kinetic model, which implies that Cd<sup>2+</sup> was chemisorbed. The larger boundary layer (C = 7.5959 mg/g) and lower desorption constant ( $\beta = 0.1793$  g/mg) of 0.015 M AgNP confirmed that 0.015 M AgNP was a better adsorber of Cd<sup>2+</sup> than 0.01 M AgNP (C = 4.5942 mg/g;  $\beta = 1.0351$  g/mg).
- By comparison, the size of AgNP affected Hg adsorption, as larger AgNP (0.01 M AgNP) were preferred for better adsorption. Adsorption of Hg was relatively better when relatively more AgNP were located near or on the fibres' surface, whilst the location of AgNP did not affect Cd adsorption but rather its abundance.

*Adsorption of Hg and Cd<sup>2+</sup> from Water by AgNP-PVA/NRL Nanofibre Composites in Binary Adsorption Studies*

- In a binary adsorption system, the 0.01 M and 0.015 M AgNP successfully adsorbed Hg and Cd<sup>2+</sup> from aqueous solutions; however, at a deficit compared to removal efficiencies in single-component adsorption studies. Other nanofiber composites which were mixtures of 0.01 M and 0.015 M AgNP, namely: Mix 1, 2 and 3, also successfully adsorbed Hg and Cd.
- The trend for Hg adsorption from Cd-Hg solution was in the order: 0.015 M AgNP < 0.01 M AgNP < Mix 2 < Mix 1 < Mix 3. Adsorption of Cd<sup>2+</sup> by the nanocomposites was in the order: 0.01 M AgNP < Mix 2 < Mix 1 < Mix 3 < 0.015 M AgNP. The AgNP-PVA/NRL nanofibre composites adsorbed Hg relatively better than Cd<sup>2+</sup>, except in 0.015 M AgNP.

*Silver Concentration Released into Treated Water After Adsorption*

- The AgNP-PVA/NRL nanofibre composites released Ag concentrations into the solution after adsorption (0.0425 mg/L for 0.01 M AgNP to 0.2140 mg/L for Mix 2). However, the concentrations of Ag released were below US EPA SMCL and WHO

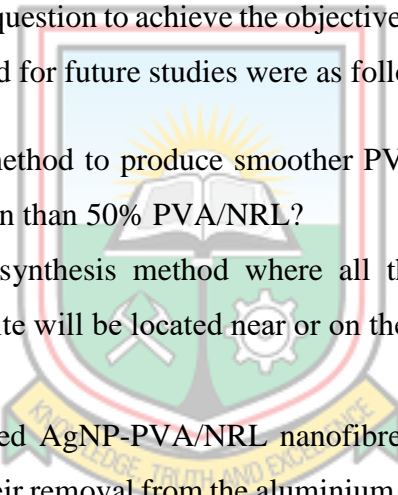
drinking water guidelines of 0.10 mg/L except for Mix 2. Hence the AgNP-PVA/NRL nanofibres were good enough for water treatment.

## 8.2 Significance and Contributions

This research provides meaningful contributions to literature as it addresses three major research gaps. Firstly, this research provides information on how PVA/NRL nanofibres can be electrospun without using harmful solvents. Secondly, it provides useful information on how AgNP can be synthesised in PVA/NRL nanofibres via electrospinning and without using harmful solvents. Lastly, this research provides information on the efficiency of AgNP-PVA/NRL nanofibre composites to remove Hg and Cd<sup>2+</sup> in water treatment.

## 8.3 Recommendations and Future Works

In answering the research question to achieve the objectives of this study, other queries were raised. The questions asked for future studies were as follows;

- 
- a) Is there a green method to produce smoother PVA/NRL fibre films with a lower dissolvable fraction than 50% PVA/NRL?
  - b) Is there a green synthesis method where all the AgNP formed in PVA/NRL nanofibre composite will be located near or on the fibres' surface and available for adsorption?
  - c) Can the synthesised AgNP-PVA/NRL nanofibre composites maintain their pore diameters upon their removal from the aluminium foil and during adsorption studies to achieve a higher surface-area to volume ratio?

Also, in line with the outcomes of this research, the following recommendations were made:

- a) Adsorption studies of Cd<sup>2+</sup> should be studied beyond 120 min in order to obtain more information about the adsorption behaviour and mechanism of 0.01 M AgNP. In addition, the adsorption data of Cd<sup>2+</sup> up to 20 min should also be analysed, and the two pieces of information (20 min adsorption data and beyond 120 min adsorption data) be compared for the most relevant data analysis and interpretation in terms of adsorption.
- b) Adsorption studies of Hg should also be studied beyond 120 min to determine if any relevant adsorption detail would be obtained.

- c) The competitive adsorption of Hg and Cd<sup>2+</sup> should be studied in a system with other contaminants.
- d) An x-ray photoelectron spectroscopy (XPS) analysis should be conducted on the AgNP-PVA/NRL nanofibre composites before and after adsorption studies to understand further the surface chemistry behaviour of the nanofibre composites in terms relevant to Cd<sup>2+</sup> and Hg adsorption.
- e) A green dissolvable solution should be sequentially electrospun along 0.01 M and 0.015 M AgNP in Mix 1 and 2 as this may produce stable more stable 3D structures and increase surface-area to volume ratio for adsorption studies (Wulkersdorfer *et al.*, 2010).
- f) Haematite and magnetite nanoparticles should also be incorporated into PVA/NRL nanofibre matrix, and their efficiency in removing heavy metals such as Pb and As, which also have adverse effects even at low concentrations, be studied.
- g) Stability of the spent nanofibre composite should be studied.



## REFERENCES

- Abu Bakar, N. H. H., Ismail, J. and Abu Bakar, M. (2007), "Synthesis and Characterization of Silver Nanoparticles in Natural Rubber", *Materials Chemistry and Physics*, Vol. 104, No. 2-3, pp. 276-283.
- Abu Bakar, N. H. H., Ismail, J. and Abu Bakar, M. (2010), "Silver Nanoparticles in Polyvinylpyrrolidone Grafted Natural Rubber", *Reactive and Functional Polymers*, Vol. 70, No. 3, pp. 168-174.
- Abunahel, B. M., Azman, N. Z. N. and Jamil, M. (2018), "Effect of Needle Diameter on the Morphological Structure of Electrospun N-Bi<sub>2</sub>O<sub>3</sub>/Epoxy-Pva Nanofiber Mats", *International Journal of Chemical and Materials Engineering*, Vol. 12, No. 6, pp. 296-299.
- Ahirwal, D., Hébraud, A., Kádár, R., Wilhelm, M. and Schlatter, G. (2013), "From Self-Assembly of Electrospun Nanofibers to 3d Cm Thick Hierarchical Foams", *Soft Matter*, Vol. 9, No. 11, pp. 3164-3172.
- Aik-Hwee, E., Kawahara, S. and Tanaka, Y. (1993), "Determination of Low Nitrogen Content of Purified Natural Rubber", *Journal of Natural Rubber Research*, Vol. 8, No. 2, pp. 109-113.
- Ajitha, B., Reddy, Y. A. K. and Reddy, P. S. (2015), "Biosynthesis of Silver Nanoparticles Using Momordica Charantia Leaf Broth: Evaluation of Their Innate Antimicrobial and Catalytic Activities", *Journal of Photochemistry and Photobiology B: Biology*, Vol. 146, pp. 1-9.
- Al-Qahtani, K. M. (2017), "Cadmium Removal from Aqueous Solution by Green Synthesis Zero Valent Silver Nanoparticles with *Benjamina* Leaves Extract", *Egyptian Journal of Aquatic Research*, Vol. 43, No. 4, pp. 269-274.
- Ali, I. (2012), "New Generation Absorbents for Water Treatment", *Chemical Reviews*, Vol. 112, No. 10, pp. 5073-5091.

- Angamma, C. J. and Jayaram, S. H. (2011), "Analysis of the Effects of Solution Conductivity on Electrospinning Process and Fiber Morphology", *IEEE Transactions on Industry Applications*, Vol. 47, pp. 1109-1117.
- Anon. (1996), *Analytical Methods for Atomic Absorption Spectroscopy*, The Perkin-Elmer Corporation,
- Anon. (2000a), "Mercury", In Chap. 6.9 of *Air Quality Guidelines for Europe*, World Health Organisation and Regional Office for Europe (eds.), 2nd edition, WHO Regional Office for Europe, Copenhagen, p. 15.
- Anon. (2000b), "Cadmium", *Air Quality Guidelines for Europe*, World Health Organisation and Regional Office for Europe (eds.), 2nd edition, WHO Regional Office for Europe, Copenhagen, p. 11.
- Anon. (2005), *Natural Rubber Latex Concentrate - Determination of Dry Rubber Content*, International Organisation for Standardisation, 4 pp.
- Anon. (2010), *Natural Rubber Latex Concentrate-Centrifuged or Creamed Ammonia-Preserved Types-Specification*, International Organisation for Standardisation, Switzerland, 8 pp.
- Anon. (2011a), *Guidelines for Drinking-Water Quality*, 4th edition, World Health Organisation, Malta, 541 pp.
- Anon. (2011b), *Latex, Rubber — Determination of Total Solids Content*, International Organisation for Standardisation, Switzerland, 7 pp.
- Anon. (2013), *Silver*, Water Quality Association, Illinois, 3 pp.
- Anon. (2015), *Instruction Manual: Evo Series Scanning Electron Microscope*, 4th edition, Carl Zeiss Microscopy Ltd., Jena,
- Anon. (2017), *Water Quality - Specification for Drinking Water*, Ghana Standards Authority, Accra, 34 pp.
- Anon. (2018), *Safety Data Sheet for Triton-X*: Cell Biolabs, Inc.  
<https://www.cellbiolabs.com/sites/default/files/SDS%20%28VPK-108->

- [H%29%20GHS.pdf#:~:text=Triton%20X-100%3A%20Toxicity%20to%20Daphnia%20and%20other%20aquatic,harmful%20to%20aquatic%20life%20with%20long%20lasting%20effects](#). Accessed: January 11, 2022.
- Anon. (2023a), *US EPA Archived Document: Consumer Fact Sheet On: Mercury*: United States Environmental Protection Agency. <https://archive.epa.gov/water/archive/web/pdf/archived-consumer-fact-sheet-on-mercury.pdf>. Accessed: July 28, 2023.
- Anon. (2023b), *National Primary Drinking Water Regulations*: United States Environmental Protection Agency. <https://www.epa.gov/ground-water-and-drinking-water/national-primary-drinking-water-regulations>. Accessed: July 28, 2023.
- Anon. (2023c), *Polyvinyl Alcohol*, Darmstadt: Merck KGaA. <https://www.sigmaaldrich.com/GH/en/substance/polyvinylalcohol123459002895>. Accessed: March 29, 2023.
- Anon. (2023d), *Transmission Electron Microscopy Vs Scanning Electron Microscopy*: ThermoFisher Scientific. Accessed: April 3, 2023.
- Anon. (2023e), *The Periodic Table of the Elements*. <https://www.webelements.com/>. Accessed: February 1, 2023.
- Aoshima, K. (2012), "Itai-Itai Disease: Cadmium-Induced Renal Tubular Osteomalacia", *Japanese Journal of Hygiene*, pp. 455-463.
- Aoshima, K. (2016), "Itai-Itai Disease: Renal Tubular Osteomalacia Induced by Environmental Exposure to Cadmium—Historical Review and Perspectives", *Soil Science and Plant Nutrition*, Vol. 62, No. 4, pp. 319-326.
- Arias, M. and van Dijk, P. J. (2019), "What Is Natural Rubber and Why Are We Searching for New Sources?", *Frontiers for Young Minds*, Vol. 7, No. 100, pp. 1-9.



- Ariffin, N., Abdullah, M. M. A. B., Mohd Arif Zainol, M. R. R., Murshed, M. F., Faris, M. A. and Bayuaji, R. (2017), "Review on Adsorption of Heavy Metal in Wastewater by Using Geopolymer", *MATEC Web of Conferences*, Vol. 97, pp. 1-8.
- Arsalani, S., Guidelli, E. J., Ferraz, J., Araujo, D. F. and Bruno, A. C. (2018), "Green Synthesis and Surface Modification of Iron Oxide Nanoparticles with Enhanced Magnetisation Using Natural Rubber Latex", *ASC Sustainable Chemistry and Engineering*, Vol. 6, No. 1, p. 19.
- Aslam, M., Kalyar, M. A. and Raza, Z. A. (2018), "Polyvinyl Alcohol: A Review of Research Status and Use of Polyvinyl Alcohol Based Nanocomposites", *Polymer Engineering & Science*, Vol. 58, No. 12, pp. 2119-2132.
- Awwad, A. M. and Salem, N. M. (2012), "A Green and Facile Approach for Synthesis of Magnetite Nanoparticles", *Nanoscience and Nanotechnology*, Vol. 2, No. 6, pp. 208-213.
- Azarian, M. H. and Boochathum, P. (2018), "Nanofiber Films of Chloroacetylated Natural Rubber/Poly(Vinyl Alcohol) by Electrospinning Technique: Silica Effects on Biodegradation", *Journal of Applied Polymer Science*, p. 46432.
- Azimi, A., Azari, A., Rezakazemi, M. and Ansarpour, M. (2017), "Removal of Heavy Metals from Industrial Wastewaters: A Review", *ChemBioEng Reviews*, Vol. 4, No. 1, pp. 37-59.
- Badi'ah, H. I., Seede, F., Supriyanto, G. and Zaidan, A. H. (2019), "Synthesis of Silver Nanoparticles and the Development in Analysis Method", *IOP Conference Series: Earth and Environmental Science*, Vol. 217. p. 012005.
- Balali-Mood, M., Naseri, K., Tahergorabi, Z., Khazdair, M. R. and Sadeghi, M. (2021), "Toxic Mechanisms of Five Heavy Metals: Mercury, Lead, Chromium, Cadmium, and Arsenic", *Front Pharmacol*, Vol. 12, p. 643972.
- Baraton, M.-I., Chen, X. and Gonsalves, K. E. (1996), "Application of Fourier Transform Infrared Spectroscopy to Nanostructured Materials Surface Characterization: Study of an Aluminum Nitride Powder Prepared Via Chemical Synthesis", In Chap. 22 of

- Nanotechnology: Molecularly Designed Materials*, Chow, G.-M. and Gonsalves, K. E. (eds.), ACS Publications, Washington, DC, pp. 312-333.
- Basheer, A. A. (2018), "New Generation Nano-Adsorbents for the Removal of Emerging Contaminants in Water", *Journal of Molecular Liquids*, Vol. 261, pp. 583-593.
- Bernhoft, R. A. (2012), "Mercury Toxicity and Treatment: A Review of the Literature", *J Environ Public Health*, Vol. 2012, p. 460508.
- Berthomieu, C. and Hienerwadel, R. (2009), "Fourier Transform Infrared (FTIR) Spectroscopy", *Photosynthesis Research*, Vol. 101, No. 2-3, pp. 157-170.
- Bhat, N. V., Nate, M. M., Kurup, M. B., Bambole, V. A. and Sabharwal, S. (2005), "Effect of  $\Gamma$ -Radiation on the Structure and Morphology of Polyvinyl Alcohol Films", *Nuclear Instruments and Methods in Physics Research Section B: Beam Interactions with Materials and Atoms*, Vol. 237, No. 3-4, pp. 585-592.
- Bhatia, S. (2016), *Natural Polymer Drug Delivery Systems: Nanoparticles, Plants and Algae*, Springer International Publishing, Switzerland, 225 pp.
- Blanchard, G., Maunaye, M. and Martin, G. (1984), "Removal of Heavy Metals from Waters by Means of Natural Zeolites", *Water Research*, Vol. 18, No. 12, pp. 1501-1507.
- Borges, F. A., Bolognesi, L. F. C., Trecco, A., Drago, B. d. C., de Arruda, L. B., Filho, P. N. L., Pierri, E. G., Graeff, C. F. d. O., dos Santos, A. G., Miranda, M. C. R. and Herculano, R. D. (2014), "Natural Rubber Latex: Study of Novel Carrier for *Casearia Sylvestris* Swartz Delivery", *IRSN Polymer Science*, Vol. 2014, p. 5.
- Cabrera, F. C., Mohan, H., dos Santos, R., Agostini, D. L. S., Aroca, R. F., Rodriguez-Perez, M. A. and Job, A. E. (2013), "Green Synthesis of Gold Nanoparticles with Self-Sustained Natural Rubber Membranes", *Journal of Nanomaterials*, Vol. 2013, p. 110.
- Camilli, L., Pisani, C., Gautron, E., Scarselli, M., Catrucci, P., D'Orazio, F., Passacantando, M., Moscone, D. and De Crescenzi, M. (2014), "A Three-Dimensional Carbon Nanotube Network for Water Treatment", *Nanotechnology*, Vol. 25, p. 7.

- Chen, K., He, J., Li, Y., Cai, X., Zhang, K., Liu, T., Hu, Y., Lin, D., Kong, L. and Liu, J. (2017a), "Removal of Cadmium and Lead Ions from Water by Sulfonated Magnetic Nanoparticle Adsorbents", *Journal of Colloid Interface Science*, Vol. 494, pp. 307-316.
- Chen, C., Tang, Y., Vlahovic, B. and Yan, F. (2017b), "Electrospun Polymer Nanofibers Decorated with Noble Metal Nanoparticles for Chemical Sensing", *Nanoscale Research Letters*, Vol. 12, No. 1, p. 451.
- Chen, Y., Shafiq, M., Liu, M., Morsi, Y. and Mo, X. (2020), "Advanced Fabrication for Electrospun Three-Dimensional Nanofiber Aerogels and Scaffolds", *Bioactive Materials*, Vol. 5, No. 4, pp. 963-979.
- Chinn, T. D. (2009), "Water Treatment", In Chap. 2 of *Environmental Engineering: Water, Wastewater, Soil and Groundwater Treatment and Remediation*, Nemerow, N. L., Agardy, F. J., Sullivan, P. and Salvato, J. A. (eds.), John Wiley and Sons, Inc, New Jersey, pp. 135-281.
- Chowdhury, I. H., Ghosh, S., Roy, M. and Naskar, M. K. (2014), "Green Synthesis of Water-Dispersible Silver Nanoparticles at Room Temperature Using Green Carambola (Star Fruit) Extract", *Journal of Sol-Gel Science and Technology*, Vol. 73, No. 1, pp. 199-207.
- Chung, I.-S., Lee, M.-Y., Shin, D.-H. and Jung, H.-R. (2010), "Three Systemic Argyria Cases after Ingestion of Colloidal Silver Solution", *International Journal of Dermatology*, Vol. 49, No. 10, pp. 1175-1177.
- Cinar, S., Gundul, G., Mavis, B. and Colak, U. (2011), "Synthesis of Silver Nanoparticles by Oleylamine-Oleic Acid Reduction and Its Use in Making Nanocable by Coaxial Electrospinning", *Journal of Nanoscience and Nanotechnology*, Vol. 11, No. 4, pp. 3669-3679.
- Colantonio, N. and Kim, Y. (2016), "Cadmium (II) Removal Mechanisms in Microbial Electrolysis Cells", *Journal of Hazardous Materials*, Vol. 311, pp. 134-141.
- Cornish, K., M. Bates, G., Slutzky, J. L., Meleshchuk, A., Xie, W., Sellers, K., Mathias, R., Boyd, M., Castaneda, R., Wright, M. and Borel, L. (2019), "Extractable Protein

- Levels in Latex Products and Their Associated Risks, Emphasizing American Dentistry", *Biology and Medicine*, Vol. 11, No. 2.
- Cortes, V., Polanco, S., Zhou, Y. and Tan, G. Z. (2017), "Fabrication of 3d Nanofiber Scaffold by Sequential Electrospinning", *Investigaciones de Los Alumnos*, pp. 1-9.
- Cosme, J. G. L., Silva, V. M., Nunes, R. R. C. and Picciani, P. H. S. (2016), "Development of Biobased Poly(Lactic Acid)/Epoxidized Natural Rubber Blends Processed by Electrospinning: Morphological, Structural and Thermal Properties", *Material Sciences and Applications*, Vol. 7, pp. 210-219.
- Costa, L. M. M., Mattoso, L. H. C. and Ferreira, M. (2013), "Electrospinning of PCL/Natural Rubber Blends", *Journal of Materials Science*, Vol. 48, No. 24, pp. 8501-8508.
- Danna, C. S., Cavalcante, D. G. S. M., Gomes, A. S., Kerche-Silva, L. E., Yoshihara, E., Osorio-Roman, I. O., Salmazo, L. O., Rodriguez-Perez, M. A., Aroca, R. F. and Job, A. E. (2016), "Silver Nanoparticles Embedded in Natural Rubber Films: Synthesis, Characterization and Evaluation of in Vitro Toxicity", *Journal of Nanomaterials*, Vol. 2016, p. 10.
- Das, B., Mondal, N. K., Bhaumik, R. and Roy, P. (2013), "Insight into Adsorption Equilibrium, Kinetics and Thermodynamics of Lead onto Alluvial Soil", *International Journal of Environmental Science and Technology*, Vol. 11, No. 4, pp. 1101-1114.
- Das, R. K. and Das, M. (2019), "Study of Silver Nanoparticle/Polyvinyl Alcohol Nanocomposite", *International Journal of Plastics Technology*, Vol. 23, No. 1, pp. 101-109.
- de Diego, A., Pecheyran, C., Tseng, C. M. and Donard, O. F. X. (1999), "Chapter 12 - Cryofocusing for on-Line Metal and Metalloid Speciation in the Environment", In Chap. 12 of *Flow Analysis with Atomic Spectrometric Detectors*, Sanz-Medel, A. (ed.), Elsevier, Amsterdam, pp. 375-406.

- Deitzel, J. M., Kleinmeyer, J., Harris, D. and Beck Tan, N. C. (2001), "The Effect of Processing Variables on the Morphology of Electrospun Nanofibers and Textiles", *Polymer*, Vol. 42, No. 1, pp. 261–272.
- Demir, M. M., Yiglor, I., Yiglor, E. and Erman, B. (2002), "Electrospinning of Polyurethane Fibers", *Polymer*, Vol. 43, pp. 3303-3309.
- Desai, R., Mankad, V., Gupta, S. and Jha, P. (2012), "Size Distribution of Silver Nanoparticles: UV-Visible Spectroscopic Assessment", *Nanoscience and Nanotechnology Letters*, Vol. 4, No. 1, pp. 30-34.
- Diringer, S. E., Feingold, B. J., Ortiz, E. J., Gallis, J. A., Araujo-Flores, J. M., Berky, A., Pan, W. K. and Hsu-Kim, H. (2015), "River Transport of Mercury from Artisanal and Small-Scale Gold Mining and Risks for Dietary Mercury Exposure in Madre De Dios, Peru", *Environmental Sciences: Processes and Impacts*, Vol. 17, No. 2, pp. 478-487.
- Doshi, J. and Reneker, D. H. (1995), "Electrospinning Process and Application of Electrospun Fibres", *Journal of Electrostics*, Vol. 35, pp. 151-160.
- Drever, J. I. (1997), "Adsorption", In Chap. 5 of *The Geochemistry of Natural Waters: Surface and Groundwater Environments*, 3rd edition, Prentice Hall, New Jersey, pp. 87-105.
- Duan, H., Wang, D. and Li, Y. (2015), "Green Chemistry for Nanoparticle Synthesis", *Chemical Society Reviews*, Vol. 44, No. 16, pp. 5778-5792.
- Duangthong, S., Rattanadaecha, K., Cheewasedtham, W., Wararattananurak, P. and Chooto, P. (2017), "Simple Digestion and Visible Spectrophotometry for Copper Determination in Natural Rubber Latex", *ScienceAsia*, Vol. 43, No. 6, pp. 369-376.
- Dubinin, M. M. and Radushkevich, L. V. (1947), "The Equation of the Characteristic Curve of Activated Charcoal", *Proceedings of the Academy of Sciences of the USSR: Physical Chemistry Section*, Vol. 55, pp. 331-337.

- Ealias, A. M. and Saravankumar, M. P. (2017), "A Review on the Classification, Characterisation, Synthesis of Nanoparticles and Their Application", *IOP Conference Series: Material Science and Engineering*, Vol. 263, No. 3, pp. 1-14.
- Eby, G. N. (2004), "The Continental Environment", In Chap. 9 of *Principles of Environmental Geochemistry*, Waveland Press, Inc., Illinois, pp. 313-386.
- El-Tawil, R. S., El-Wakeel, S. T., Abdel-Ghany, A. E., Abuzeid, H. A. M., Selim, K. A. and Hashem, A. M. (2019), "Silver/Quartz Nanocomposite as an Adsorbent for Removal of Mercury (Ii) Ions from Aqueous Solutions", *Heliyon*, Vol. 5, No. 9, p. e02415.
- Elkhatib, E., Mahdy, A., Sherif, F. and Elshemy, W. (2016), "Competitive Adsorption of Cadmium (II) from Aqueous Solutions onto Nanoparticles of Water Treatment Residual", *Journal of Nanomaterials*, Vol. 2016, pp. 1-10. p. 1.
- Erdem, E., Karapinar, N. and Donat, R. (2004), "The Removal of Heavy Metal Cations by Natural Zeolites", *Jornal of Colloid and Interface Science*, Vol. 280, No. 2, pp. 309-314.
- Esdaile, L. J. and Chalker, J. M. (2018), "The Mercury Problem in Artisanal and Small-Scale Gold Mining", *Chemistry*, Vol. 24, No. 27, pp. 6905-6916.
- Forrest, M. (2018), *Rubber Analysis: Characterisation, Failure Diagnosis and Reverse Engineering-Smithers Rapra Technology*, Smithers Rapra, UK, 434 pp.
- Freundlich, H. (1906), "Over the Adsorption in Solution", *Journal of Physical Chemistry*, Vol. 57, pp. 385-471.
- Ganzagh, M. A. A., Yousefpour, M. and Taherian, Z. (2016), "The Removal of Mercury (Ii) from Water by Ag Supported on Nanomesoporous Silica", *Journal of Chemical Biology*, Vol. 9, pp. 127-142.
- Gargiulo, V., Alfè, M., Lisi, L., Manfredi, C., Volino, S. and Di Natale, F. (2017), "Colloidal Carbon-Based Nanoparticles as Heavy Metal Adsorbent in Aqueous Solution: Cadmium Removal as a Case Study", *Water, Air, & Soil Pollution*, Vol. 228, No. 5, pp. 1-13.

- Gerwert, K. and Kötting, C. (2010), "Fourier Transform Infrared (FTIR) Spectroscopy", *Encyclopedia of Life Sciences*, pp. 1-8.
- Ghanipour, M. and Dorrnian, D. (2013), "Effect of Ag-Nanoparticles Doped in Polyvinyl Alcohol on the Structural and Optical Properties of Pva Films", *Journal of Nanomaterials*, Vol. 2013, pp. 1-10. p. 1.
- Goel, J., Kadirvelu, K. and Rajapogal, C. (2004), "Competitive Sorption of Cu(II), Pb(II) and Hg(II) Ions from Aqueous Solution Using Coconut Shell-Based Activated Carbon", *Adsorption Science and Technology*, Vol. 22, No. 3, pp. 257-273.
- Goher, M. E., Hassan, A. M., Abdel-Moniem, I. A., Fahmy, A. H., Abdo, M. H. and Elsayed, S. M. (2015), "Removal of Aluminum, Iron and Manganese Ions from Industrial Wastes Using Granular Activated Carbon and Amberlite Ir-120h", *The Egyptian Journal of Aquatic Research*, Vol. 41, No. 2, pp. 155-164.
- González, A. and de la Guardia, M. (2013), "Chapter 3 - Mineral Profile", In Chap. 2 of *Comprehensive Analytical Chemistry*, Elsevier, Amsterdam, pp. 51-76.
- Guidelli, E. J., Ramos, A. P., Zaniquelli, M. E. and Baffa, O. (2011), "Green Synthesis of Colloidal Silver Nanoparticles Using Natural Rubber Latex Extracted from *Hevea Brasiliensis*", *Spectrochimica Acta Part A: Molecular and Biomolecular Spectroscopy*, Vol. 82, No. 1, pp. 140-145.
- Gunatilake, S. K. (2015), "Methods of Removing Heavy Metals from Industrial Wastewater", *Journal of Multidisciplinary Engineering*, Vol. 1, No. 1, pp. 12-18.
- Gurusamy, V., Krishnamoorthy, R., Gopal, B., Veeraravagan, V. and P, N. (2016), "Systematic Investigation on Hydrazine Hydrate Assisted Reduction of Silver Nanoparticles and Its Antibacterial Properties", *Inorganic and Nano-Metal Chemistry*, Vol. 47, No. 5, pp. 761-767. p. 761.
- Gworek, B., Bemowska-Kalabun, O., Kijenska, M. and Wrzosek-Jakubowska, J. (2016), "Mercury in Marine and Oceanic Waters - a Review", *Water, Air, and Soil Pollution*, Vol. 227, No. 10, pp. 1-19.

- Hall, K. R., Eagleton, L. C., Acrivos, A. and Vermeulen, T. (1966), "Pore- and Solid-Diffusion Kinetics in Fixed-Bed Adsorption under Constant-Pattern Condition", *Industrial & Engineering Chemistry*, Vol. 5, No. 2, pp. 212-223.
- Hamza, Z. P., Dilfi, K. F. A., Muralidharan, M. N. and Kurian, T. (2008), "Microwave Oven for the Rapid Determination of Total Solids Content of Natural Rubber Latex", *International Journal of Polymeric Materials and Polymeric Biomaterials*, Vol. 57, No. 9, pp. 918-923.
- Han, T. Y., Chang, S. H., Lee, H. K. and Son, S.-J. (2011), "Successful Treatment of Argyria Using a Low-Fluence Q-Switched 1064-nm Nd:YAG Laser", *International Journal of Dermatology*, Vol. 50, No. 6, pp. 751-753.
- Haque, M. E., Akhtar, F., Dafader, N. C., Al-Siddique, F. R., Sen, A. R. and Ahmad, M. U. (1995), "Characterization of Natural Rubber Latex Concentrate from Bangladesh", *Journal of Macromolecular Science, Part A*, Vol. 32, No. sup4, pp. 435-445.
- Harpaz, D., Axelrod, T., Yitian, A. L., Eltzov, E., Marks, R. S. and Tok, A. I. Y. (2019), "Dissolvable Polyvinyl-Alcohol Film, a Time-Barrier to Modulate Sample Flow in a 3d-Printed Holder for Capillary Flow Paper Diagnostics", *Materials*, Vol. 12, No. 3, p. 343.
- Hasanuddin, N. H., Chien, T. Y., Abidin, A. Z., Bakar, N. H. H. A. and Leng, T. W. (2017), "Application of Low Cost Natural Rubber Films for Water Remediation", *Journal of Physical Science*, Vol. 28, No. 3, pp. 81-94.
- Henglein, A. (1998), "Colloidal Silver Nanoparticles: Photochemical Preparation and Interaction with O<sub>2</sub>, CCl<sub>4</sub>, and Some Metal Ions", *Chemistry of Materials*, Vol. 10, pp. 444-450.
- Henglein, A. and Brancewicz, C. (1997), "Absorption Spectra and Reactions of Colloidal Bimetallic Nanoparticles Containing Mercury", *Chemistry of Materials*, Vol. 9, pp. 2164-2167.
- Henglein, A. and Giersig, M. (1999), "Formation of Colloidal Silver Nanoparticles: Capping Action of Citrate", *Journal of Physical Chemistry B*, Vol. 103, No. 44, pp. 9533-9539.



- Ho, C. C. (2013), "The Production of Natural Rubber from Hevea Brasiliensis Latex: Colloidal Properties, Preservation, Purification and Processing", In Chap. 4 of *Natural Rubber Materials: Volume 1: Blends and IPNs*, Thomas, S., Chan, C. H., Pothen, L. A., R., R. K. and Maria, H. J. (eds.), The Royal Society of Chemistry, Cambridge, pp. 73-106.
- Ho, Y. S. and McKay, G. (1998), "A Comparison of Chemisorption Kinetic Models Applied to Pollutant Removal on Various Sorbents", *Trans IChemE*, Vol. 76, No. Part B, pp. 332-340.
- Hu, H. and Xu, K. (2020), "Physicochemical Technologies for HRP and Risk Control", In Chap. 8 of *High-Risk Pollutants in Wastewater*, Ren, H. and Zhang, X. (eds.), Elsevier, Amsterdam, pp. 169-207.
- Hu, J., Wang, X., Ding, B., Lin, J., Yu, J. and Sun, G. (2011), "One-Step Electro-Spinning/Netting Technique for Controllably Preparing Polyurethane Nano-Fiber/Net", *Macromol Rapid Commun*, Vol. 32, No. 21, pp. 1729-1734.
- Hu, Q., Wu, H., Zhang, L., Fong, H. and Tian, M. (2012), "Rubber Composite Fibers Containing Silver Nanoparticles Prepared by Electrospinning and in-Situ Chemical Crosslinking", *Express Polymer Letters*, Vol. 6, No. 4, pp. 258-265.
- Hu, Z. (2010), *Impact of Silver Nanoparticles on Wastewater Treatment*, Water Environment Research Foundation and IWA Publishing, London,
- Huang, Z.-M., Zhang, Y. Z., Kotaki, M. and Ramakrishna, S. (2003), "A Review on Polymer Nanofibers by Electrospinning and Their Applications in Nanocomposites", *Composites Science and Technology*, Vol. 63, No. 15, pp. 2223-2253.
- Husain, O., Lau, W., Edirisinghe, M. and Parhizkar, M. (2016), "Investigating the Particle to Fibre Transition Threshold During Electrohydrodynamic Atomization of a Polymer Solution", *Mater Sci Eng C Mater Biol Appl*, Vol. 65, pp. 240-250.
- Hwee, E. A. (2013), "Non-Rubbers and Abnormal Groups in Natural Rubber", In Chap. 3 of *Natural Rubber Materials, Volume 1: Blends and IPNs*, Thomas, S., Chan, C. H., Pothen, L. A., R., R. K. and Maria, H. J. (eds.), The Royal Society of Chemistry, United Kingdom, pp. 53-72.

- Idrees, N., Tabassum, B., Abd\_Allah, E. F., Hashem, A., Sarah, R. and Hashim, M. (2018), "Groundwater Contamination with Cadmium Concentrations in Some West U.P. Regions, India", *Saudi Journal of Biological Sciences*, Vol. 25, No. 7, pp. 1365-1368.
- Iravani, S. (2011), "Green Synthesis of Metal Nanoparticles Using Plants", *Green Chemistry*, Vol. 13, pp. 2638-2650.
- Jadhav, A., Wang, L. and Padhye, R. (2013), "Influence of Applied Voltage on Droplet Size Distribution in Electrospraying of Thermoplastic Polyurethane", *International Journal of Materials, Mechanics and Manufacturing*, pp. 287-289.
- Jadhav, A., Wang, L. J. and Padhye, R. (2012), "Effect of Applied Voltage on Polymer Aggregation in Electrospraying of Thermoplastic Polymer", *Advanced Materials Research*, Vol. 535-537, pp. 2522-2525.
- Jeevanandam, J., Barhoum, A., Chan, Y. S., Dufresne, A. and Danquah, M. K. (2018), "Review on Nanoparticles and Nanostructured Materials: History, Sources, Toxicity and Regulations", *Beilstein Journal of Nanotechnology*, Vol. 9, pp. 1050-1074. p. 1050.
- Jiang, K., Sun, T.-H., Sun, L.-N. and Li, H.-b. (2006), "Adsorption Characteristics of Copper, Lead, Zinc and Cadmium Ions by Tourmaline", *Journal of Environmental Sciences*, Vol. 18, No. 6, pp. 1221-1225.
- Katok, K. V., Whitby, R. L. D., Fukuda, T., Maekawa, T., Bezverkhyy, I., Mikhalovsky, S. V. and Cundy, A. B. (2012), "Hyperstoichiometric Interaction between Silver and Mercury at the Nanoscale", *Angewandte Chemie*, Vol. 124, No. 11, pp. 2686-2689.
- Khan, I., Saeed, K. and Khan, I. (2017), "Nanoparticles: Properties, Applications and Toxicities", *Arabian Journal of Chemistry*, Vol. 12, No. 7, pp. 908–931.
- Kim, S. J., Lee, C. K. and Kim, S. I. (2005), "Effect of Ionic Salts on the Processing of Poly(2-Acrylamido-2-Methyl-1-Propane Sulfonic Acid) Nanofibers", *Journal of Applied Polymer Science*, Vol. 96, No. 4, pp. 1388-1393. p. 1388.

- Kim, Y., Suh, H. S., Cha, H. J., Kim, S. H., Jeong, K. S. and Kim, D. H. (2009), "A Case of Generalized Argyria after Ingestion of Colloidal Silver Solution", *American Journal of Industrial Medicine*, Vol. 52, No. 3, pp. 246-250.
- Kipling, J. J. (1965), "Factors Influencing Competitive Adsorption at the Liquid–Solid Interface", In Chap. 10 of *Adsorption from Solutions of Non-Electrolytes*, pp. 164–190.
- Korobeinyk, A. V. and Inglezakis, V. J. (2018), "Silver Nanoparticles Synthesised within the Silica Matrix in Hyperstoichiometrical of Mercury from Aqueous Solutions", *IOP Conference Series: Earth and Environmental Science*, Vol. 182, p. 012013.
- Krishnappa, R. V. N., Desai, K. and Changmo, S. (2003), "Morphological Study of Electrospun Polycarbonates as a Function of the Solvent and Processing Voltage", *Journal of Materials Science*, Vol. 38, No. 11, pp. 2357-2365.
- Krstic, V. (2021), "Role of Zeolite Adsorbent in Water Treatment", In Chap. 14 of *Handbook of Nanomaterials for Wastewater Treatment: Fundamentals and Scale up Issues*, Bhanvase, B., Sonawane, S., Pawade, V. and Pandit, A. (eds.), Elsevier, Amsterdam, pp. 417-481.
- Kumar, S. V., Bafana, A. P., Pawar, P., Rahman, A., Dahoumane, S. A. and Jeffryes, C. S. (2018), "High Conversion Synthesis of <10 nm Starch-Stabilized Silver Nanoparticles Using Microwave Technology", *Scientific Reports*, Vol. 8, p. 5106.
- Kyrychenko, A., Pasko, D. A. and Kalugin, O. N. (2017), "Poly(Vinyl Alcohol) as a Water Protecting Agent for Silver Nanoparticles: The Role of Polymer Size and Structure", *Physical Chemistry Chemical Physics*, Vol. 19, No. 13, pp. 8742-8756.
- Lagergren, S. (1898), "About the Theory of So-Called Adsorption of Soluble Substances", *Kungliga Svenska Vetenskapsakademiens Handlingar*, Vol. 24, No. 4, pp. 1-39.
- Langmuir, I. (1918), "The Adsorption of Gases on Plane Surfaces of Glass, Mica and Platinum", *Journal of the American Chemical Society*, Vol. 40, No. 9, pp. 1361-1403.

- Li, K., Jia, X., Tang, A., Zhu, X., Meng, H. and Wang, Y. (2012), "Preparation of Spherical and Triangular Silver Nanoparticles by a Convenient Method", *Integrated Ferroelectrics*, Vol. 136, No. 1, pp. 9-14. p. 9.
- Lindblad, E. B. and Duroux, L. (2017), "Mineral Adjuvants", In Chap. 18 of *Immunopotentiators in Modern Vaccines*, Schijns, V. and O'Hagan, D. (eds.), Academic Press, pp. 347-375.
- Lu, H., Wang, J., Stoller, M., Wang, T., Bao, Y. and Hao, H. (2016), "An Overview of Nanomaterials for Water and Wastewater Treatment", *Advances in Materials Science and Engineering*, Vol. 2016, p. 10.
- Luo, W., Hickman, D., Keykhosravani, M., Wilson, J., Fink, J., Huang, L., Chen, D. and O'Donnell, S. (2020), "Identification and Characterization of a Triton X-100 Replacement for Virus Inactivation", *Biotechnol Prog*, Vol. 36, pp. 1-11.
- Mahmood, Q., Asif, M., Shaheen, S., Hayat, M. T. and Ali, S. (2019), "Cadmium Contamination in Water and Soil", In Chap. 6 of *Cadmium Toxicity and Tolerance in Plants*, Elsevier, pp. 141-161.
- Makarov, V. V., Love, A. J., Sinitsyna, O. V., Makarov, S. S., Yaminsky, I. V., Taliany, M. E. and Kalinina, N. O. (2014), "'Green' Nanotechnologies: Synthesis of Metal Nanoparticles Using Plants", *Acta Naturae*, Vol. 6, No. 1, pp. 35-43.
- Maneechakr, P. and Mongkollertlop, S. (2020), "Investigation on Adsorption Behaviors of Heavy Metal Ions ( $\text{Cd}^{2+}$ ,  $\text{Cr}^{3+}$ ,  $\text{Hg}^{2+}$  and  $\text{Pb}^{2+}$ ) through Low-Cost/Active Manganese Dioxide-Modified Magnetic Biochar Derived from Palm Kernel Cake Residue", *Journal of Environmental Chemical Engineering*, Vol. 8, No. 6, pp. 1-9.
- Mansur, H. S., Sadahira, C. M., Souza, A. N. and Mansur, A. A. P. (2008), "Ftir Spectroscopy Characterization of Poly (Vinyl Alcohol) Hydrogel with Different Hydrolysis Degree and Chemically Crosslinked with Glutaraldehyde", *Materials Science and Engineering: C*, Vol. 28, No. 4, pp. 539-548. p. 539.
- Mariella, M. (2019), "Atomic Absorption Spectrometry—Flame", In Chap. 2 of *Encyclopedia of Analytical Science*, Worsfold, P., Townshend, A., Poole, C. and Miro, M. (eds.), 3rd edition, Elsevier, pp. 129-136.

- Marimón-Bolívar, W., Tejeda-Benítez, L. and Herrera, A. P. (2018), "Removal of Mercury (II) from Water Using Magnetic Nanoparticles Coated with Amino Organic Ligands and Yam Peel Biomass", *Environmental Nanotechnology, Monitoring & Management*, Vol. 10, pp. 486-493. p. 486.
- Mavani, K. and Shah, M. (2013), "Synthesis of Silver Nanoparticles by Using Sodium Borohydride as a Reducing Agent", *International Journal of Engineering Research & Technology*, Vol. 2, No. 3, pp. 1-5.
- McLintock, I. (1967), "The Elovich Equation in Chemisorption Kinetics", *Nature*, Vol. 216.
- Mo, X. M., Xu, C. Y., Kotaki, M. and Ramakrishna, S. (2004), "Electrospun P(Lla-Cl) Nanofiber: A Biomimetic Extracellular Matrix for Smooth Muscle Cell and Endothelial Cell Proliferation", *Biomaterials*, Vol. 25, No. 10, pp. 1883-1890.
- Mohammadi, F., Yousefi, M. and Gharemanzadeh, R. (2019), "Green Synthesis, Characterization and Antimicrobial Activity of Silver Nanoparticles (AgNps) Using Leaves and Stems Extract of Some Plants", *Advanced Journal of Chemistry-Section A*, Vol. 2, No. 4, pp. 266-275. p. 266.
- Mohammed, A. and Abdullah, A. (2018), "Scanning Electron Microscopy (Sem): A Review", *Proceedings of 2018 International Conference on Hydraulics and Pneumatics - HERVEX*, pp. 1-9.
- Mohapatra, B., Kuriakose, S. and Mohapatra, S. (2015), "Rapid Green Synthesis of Silver Nanoparticles and Nanorods Using Piper Nigrum Extract", *Journal of Alloys and Compounds*, Vol. 637, pp. 119-126.
- Moldovan, B., David, L., Achim, M., Clichici, S. and Filip, G. A. (2016), "A Green Approach to Phytomediated Synthesis of Silver Nanoparticles Using Sambucus Nigra L. Fruits Extract and Their Antioxidant Activity", *Journal of Molecular Liquids*, Vol. 221, pp. 271-278.
- Mooibroek, H. and Cornish, K. (2000), "Alternative Sources of Natural Rubber", *Applied Microbiology Biotechnology*, Vol. 53, No. 4, pp. 355-365.

- Muppalaneni, S. (2013), "Polyvinyl Alcohol in Medicine and Pharmacy: A Perspective", *Journal of Developing Drugs*, Vol. 2, No. 3, pp. 1-5.
- Nakamura, T., Magara, H., Herbani, Y. and Sato, S. (2011), "Fabrication of Silver Nanoparticles by Highly Intense Laser Irradiation of Aqueous Solution", *Applied Physics A*, Vol. 104, No. 4, pp. 1021-1024.
- Nandiyanto, A. B. D., Oktiani, R. and Ragadhita, R. (2019), "How to Read and Interpret Ftir Spectroscopy of Organic Material", *Indonesian Journal of Science and Technology*, Vol. 4, No. 1. p. 97.
- Nasiruddin Khan, M. and Sarwar, A. (2012), "Determination of Points of Zero Charge of Natural and Treated Adsorbents", *Surface Review and Letters*, Vol. 14, No. 3, pp. 461-469. p. 461.
- Nielsen, J. B. (1992), "Toxicokinetics of Mercuric Chloride and Methylmercuric Chloride in Mice", *Journal of Toxicology and Environmental Health*, Vol. 37, No. 1, pp. 85-122.
- Nowicki, M., Zhao, Y., Boggess, S. L., Fluess, H., Paya-Milans, M., Staton, M. E., Houston, L. C., Hadziabdic, D. and Trigiano, R. N. (2019), "Taraxacum Kok-Saghyz (Rubber Dandelion) Genomic Microsatellite Loci Reveal Modest Genetic Diversity and Cross-Amplify Broadly to Related Species", *Sci Rep*, Vol. 9, No. 1, p. 1915.
- Omo-Ikerodah, E. E., Omokhafa, K. O., Akpobome, F. A. and Mokuwunye, M. U. (2009), "An Overview of the Potentials of Natural Rubber (*Hevea brasiliensis*) Engineering for the Production of Valuable Proteins", *African Journal of Biotechnology*, Vol. 8, No. 25, pp. 7303-7307.
- Orbecido, A., Yu, L. J., Chi, C. W. Y., Tangavaloo, V., Lim, K. W., A Tarawneh, M., Bungay, V., Beltran, A. and Aviso, K. (2019), "Protein Reduction of Natural Rubber Films through Leaching Solvent", *MATEC Web of Conferences*, Vol. 268, p. 5. p. 01011.
- Osei, L. B., Fosu, S. and Ndur, S. A. (2023), "Removal of Cadmium by Silver Nanoparticles Incorporated in Electrospun Natural Rubber Latex/Polyvinyl Alcohol Matrix", *Ghana Mining Journal*, Vol. 23, No. 1, pp. 11-21.

- Osei, L. B., Ndur, S. A. and Fosu, S. (2022), "Synthesis and Characterisation of Electrospun Natural Rubber Latex/Polyvinyl Alcohol for Application in Aqueous Processes", *Journal of Rubber Research*, Vol. 25, pp. 313-320.
- Padil, V. V. T., Waclawek, S. and Cernik, M. (2016), "Green Synthesis: Nanoparticles and Nanofibres Based on Tree Gums for Environmental Applications", *Ecological Chemistry Engineering S*, Vol. 23, No. 4, pp. 533-557.
- Palomba, V. and Frazzica, A. (2021), "15 - Modeling of Sorption Systems for Thermal Energy Storage", In Chap. 15 of *Advances in Thermal Energy Storage Systems (Second Edition)*, Cabeza, L. F. (ed.), Woodhead Publishing, pp. 453-475.
- Panichpakdee, J., Larпкиattaworn, S., Nuchchamong, S., Naruepai, B., Leekrajag, M. and Somwongsa, P. (2019), "Electrospinning of Natural Rubber Latex-Blended Polyvinyl Alcohol", *Materials Today: Proceedings*, Vol. 17, pp. 2020-2027.
- Park, J.-D. and Zheng, W. (2012), "Human Exposure and Health Effects of Inorganic and Elemental Mercury", *Journal of Preventive Medicine and Public Health*, Vol. 45, No. 6, pp. 344-352.
- Patterson, H. B. W. (2009), "Chapter 2 - Adsorption", In Chap. 2 of *Bleaching and Purifying Fats and Oils*, List, G. R. (ed.) 2nd edition, AOCS Press, pp. 53-67.
- Pietrojusti, A., Stockmann-Juvala, H., Lucaroni, F. and Savolainen, K. (2018), "Nanomaterial Exposure, Toxicity and Impact on Human Health", *Wiley Interdisciplinary Reviews: Nanomedicine and Nanobiotechnology*, Vol. 10, No. 5, pp. 1-21.
- Qu, X., Brame, J., Li, Q. and Alvarez, P. J. J. (2013), "Nanotechnology for a Safe and Sustainable Water Supply: Enabling Integrated Water Treatment and Reuse", *Accounts of Chemical Research*, Vol. 46, No. 3, pp. 834-843.
- Ramakrishna, S., Fujihara, K., Teo, W.-E., Lim, T.-C. and Ma, Z. (2005), *An Introduction to Electrospinning and Nanofibers*, World Scientific, Singapore, 382 pp.
- Ramsden (2005), "What Is Nanotechnology?", *Nanotechnology Perceptions*, Vol. 1, pp. 3-17.

- Ramsden, J. J. (2011), "What Is Nanotechnology?", In Chap. 1 of *Nanotechnology: An Introduction*, Ramsden, J. J. (ed.) 1st edition, William Andrew, pp. 1-14.
- Reneker, D. H. and Yarin, A. L. (2008), "Electrospinning Jets and Polymer Nanofibers", *Polymer*, Vol. 49, No. 10, pp. 2387-2425. p. 2387.
- Revellame, E. D., Fortela, D. L., Sharp, W., Hernandez, R. and Zappi, M. E. (2020), "Adsorption Kinetic Modeling Using Pseudo-First Order and Pseudo-Second Order Rate Laws: A Review", *Cleaner Engineering and Technology*, Vol. 1, pp. 1-13.
- Rippel, M. M. and Galembeck, F. (2009), "Nanostructures and Adhesion in Natural Rubber: New Era for a Classic", *Journal of the Brazilian Chemical Society*, Vol. 20, No. 6, pp. 1024-1030.
- Riyajan, S.-A. and Sukhlaaied, W. (2015), "Novel Modified Natural Rubber with Chitosan Nanofibers: Preparation and Properties", *Raw Materials and Applications*, Vol. 68, No. 11-12, pp. 39-45.
- Roginsky, S. and Zeldovich, Y. B. (1934), "The Catalytic Oxidation of Carbon Monoxide on Manganese Dioxide", *Acta Phys Chem USSR*, Vol. 1, p. 554.
- Roksana, M. (2016), "Eco-Friendly Alternative for Water Treatment from Nanotechnology", *Journal Nano Science and Technology*, Vol. 4, pp. 28-34.
- Rooshenass, P., Yahya, R. and Gan, S. N. (2018), "Preparation of Liquid Epoxidized Natural Rubber by Oxidative Degradation Using Periodic Acid, Potassium Permanganate and Uv-Radiation", *Journal of Polymers and the Environment*, Vol. 26, No. 4, pp. 1378-1392.
- Saengdee, L., Phinyocheep, P. and Daniel, P. (2020), "Chemical Modification of Natural Rubber in Latex Stage for Improved Thermal, Oil, Ozone and Mechanical Properties", *Journal of Polymer Research*, Vol. 27, No. 9, p. 13.
- Sagitha, P., Sarada, K. and Muraleedharan, K. (2016), "One-Pot Synthesis of Poly Vinyl Alcohol (Pva) Supported Silver Nanoparticles and Its Efficiency in Catalytic Reduction of Methylene Blue", *Transactions of Nonferrous Metals Society of China*, Vol. 26, No. 10, pp. 2693-2700. p. 2693.



- Sahu, S. C. and Hayes, W. (2017), "Toxicity of Nanomaterials Found in Human Environment: A Literature Review", *Toxicology Research and Application*, Vol. 1, pp. 1-13.
- Saif, S., Tahir, A. and Chen, Y. (2016), "Green Synthesis of Iron Nanoparticles and Their Environmental Applications and Implications", *Nanomaterials (Basel)*, Vol. 6, No. 11.
- Sakdapipanich, J. and Rojruthai, P. (2012), "Molecular Structure of Rubber and Its Characteristics Based on Recent Evidence", In Chap. 13 of *Biotechnology-Molecular Studies and Novel Applications for Improved Quality of Human Life*, Sammour, R. (ed.), InTech, Shanghai, China, pp. 213-238.
- Salehi, M., Li, X. and Whelton, A. J. (2017), "Metal Accumulation in Representative Plastic Drinking Water Plumbing Systems", *Journal - American Water Works Association*, Vol. 109, No. 11, pp. 479-493.
- Sarecka-Hujar, B., Balwierz, R., Ostrozka-Cieslik, A., Dyja, R., Lukowiec, D. and Jankowski, A. (Year), "Scanning Electron Microscopy and X-Ray Energy Dispersive Spectroscopy—Useful Tools in the Analysis of Pharmaceutical Products", *Journal of Physics: Conference Series*, ed.^eds., 2017, IOP Publishing, p.^pp. 012008.
- Sawyer, C. N., McCarty, P. L. and Parkin, G. F. (2003), *Chemistry for Environmental Engineering and Science*, 5th edition, McGraw Hill Education, New Dehli, 752 pp.
- Scimeca, M., Bischetti, S., Lamsira, H. K., Bonfiglio, R. and Bonanno, E. (2018), "Energy Dispersive X-Ray (Edx) Microanalysis: A Powerful Tool in Biomedical Research and Diagnosis", *European Journal of Histochemistry*, Vol. 62, No. 1, p. 2841.
- Scoullou, M. J., Vonkeman, G. H., Thornton, I. and Makuch, Z. (2001), *Mercury - Cadmium - Lead: Handbook for Sustainable Heavy Metals Policy*, Springer-Science+Business Media, Dordrecht,
- Sharma, R., Bisen, D. P., Shukla, U. and Sharma, B. G. (2012), "X-Ray Diffraction: A Powerful Method of Characterizing Nanomaterials", *Recent Research in Science and Technology*, Vol. 4, No. 8, pp. 77-79.

- Shi, X., Zhou, W., Ma, D., Ma, Q., Bridges, D., Ma, Y. and Hu, A. (2015), "Electrospinning of Nanofiber and Their Applications for Energy Devices", *Journal of Nanomaterials*, Vol. 16, No. 1, p. 122.
- Siddiqi, K. S., Husen, A. and Rao, R. A. K. (2018), "A Review on Biosynthesis of Silver Nanoparticles and Their Biocidal Properties", *Journal of Nanobiotechnology*, Vol. 16, No. 1, p. 14.
- Simons, H. L. 1966. *Us Patent 3280229*.
- Singh, A. K. (2016), "Nanoparticle Ecotoxicology", of *Engineered Nanoparticles*, pp. 343-450.
- Singh, N. B., Nagpal, G. and Agrawal, S. (2018), "Water Purification by Using Absorbents: A Review", *Environmental Technology & Innovation*, Vol. 11, pp. 187-240.
- Sirisomboon, P. and Lim, C. H. (2019), "Rapid Evaluation of Properties of Natural Rubber Latex and Its Products Using near-Infrared Spectroscopy", In Chap. 2 of *Organic Polymers*, Sand, A. and Zaki, E. (eds.), IntechOpen, p. 18.
- Stokes, D. (2008), *Principles and Practice of Variable Pressure/Environmental Scanning Electron Microscopy (VP-ESEM)*, Rainforth, M. (ed.), John Wiley & Sons, Cornwall, 214 pp.
- Stonebloom, S. H. and Scheller, H. V. (2019), "Transcriptome Analysis of Rubber Biosynthesis in Guayule (*Parthenium Argentatum* Gray)", *BMC Plant Biol*, Vol. 19, No. 1, p. 71.
- Stumm, W. (1992), *Chemistry of the Solid-Water Interface: Processes at the Mineral-Water and Particle-Water Interface in Natural Systems*, Wiley-Interscience, New York,
- Sumesh, E., Bootharaju, M. S., Anshup and Pradeep, T. (2011), "A Practical Silver Nanoparticle-Based Adsorbent for the Removal of Hg<sup>2+</sup> from Water", *Journal of Hazardous Materials*, Vol. 189, No. 1-2, pp. 450-457.
- Sun, B., Long, Y. Z., Yu, F., Li, M. M., Zhang, H. D., Li, W. J. and Xu, T. X. (2012), "Self-Assembly of a Three-Dimensional Fibrous Polymer Sponge by Electrospinning", *Nanoscale*, Vol. 4, No. 6, pp. 2134-2137.

- Takeo, N. (2005), *Atlas of Eh-Ph Diagrams: Intercomparison of Thermodynamic Database. Geological Survey of Japan Open File Report No.419*, National Institute of Advanced Industrial Science and Technology, Research Center for Deep Geological Environments, 285 pp.
- Tauanov, Z., Tsakiridis, P. E., Mikhalovsky, S. V. and Inglezakis, V. J. (2018), "Synthetic Coal Fly Ash-Derived Zeolites Doped with Silver Nanoparticles for Mercury (Ii) Removal from Water", *Journal of Environmental Management*, Vol. 224, pp. 164-171.
- Tauanov, Z., Tsakiridis, P. E., Shah, D. and Inglezakis, V. J. (2019), "Synthetic Sodalite Doped with Silver Nanoparticles: Characterization and Mercury (Ii) Removal from Aqueous Solutions", *Journal of Environmental Science and Health, Part A. Toxic/Hazardous Substances and Environmental Engineering*, Vol. 54, No. 9, pp. 951-959.
- Taweepreda, W. (2017), "Fabrication and Properties of Rubber Nanofiber from Electrospinning", In Chap. 6 of *Elastomers*, Cankaya, N. (ed.), IntechOpen, pp. 121-134.
- Tchounwou, P. B., Yedjou, C. G., Patlolla, A. K. and Sutton, D. J. (2012), "Heavy Metal Toxicity and the Environment", *Experientia. Supplementum*, Vol. 101, pp. 133-164.
- Thavasi, V., Singh, G. and Ramakrishna, S. (2008), "Electospun Nanofibres in Energy and Environmental Applications", *Energy and Environmental Science*, Vol. 1, No. 2, pp. 205-221.
- Tiwari, D. K., Behari, J. and Sen, P. (2008), "Application of Nanoparticle in Waste Water Treatment", *World Applied Sciences Journal*, Vol. 3, No. 3, pp. 417-423.
- Tran, H. N., You, S. J., Hosseini-Bandegharai, A. and Chao, H. P. (2017), "Mistakes and Inconsistencies Regarding Adsorption of Contaminants from Aqueous Solutions: A Critical Review", *Water Research*, Vol. 120, pp. 88-116.
- van Beilen, J. B. and Poirier, Y. (2007), "Guayule and Russian Dandelion as Alternative Sources of Natural Rubber", *Critical Reviews in Biotechnology*, Vol. 27, No. 4, pp. 217-231.

- Venkatachalam, P., Geetha, N., Sangeetha, P. and Thulaseedharan, A. (2013), "Natural Rubber Producing Plants: An Overview", *African Journal of Biotechnology*, Vol. 12, No. 12, pp. 1297-1310.
- Verma, R. and Dwivedi, P. (2013), "Heavy Metal Water Pollution - a Case Study", *Recent Research in Science and Technology*, Vol. 5, No. 5, pp. 98-99.
- Vida-Simiti, I., Jumate, N., Chicinas, I. and Batin, G. (2004), "Applications of Scanning Electron Microscopy (Sem) in Nanotechnology and Nanoscience", *Romanian Journal Physics*, Vol. 49, No. 9-10, pp. 955-965.
- von der Gathen, Y., Sander, I., Flagge, A., Bruning, T. and Raulf-Heimsoth, M. (2017), "Quantification of Protein and Latex Allergen Content of Various Natural Rubber Latex Products", *Allergologie Select*, Vol. 1, No. 2, pp. 109-119.
- Weber, W. J. and Morris, J. C. (1963), "Kinetics of Adsorption on Carbon from Solution", *Journal of the Sanitary Engineering Division*, Vol. 89, No. 2, pp. 31-60.
- Wulkersdorfer, B., Kao, K. K., Agopian, V. G., Ahn, A., Dunn, J. C., Wu, B. M. and Stelzner, M. (2010), "Bimodal Porous Scaffolds by Sequential Electrospinning of Poly(Glycolic Acid) with Sucrose Particles", *International Journal of Polymer Science*, Vol. 2010, pp. 1-9.
- Xue, J., Wu, T., Dai, Y. and Xia, Y. (2019), "Electrospinning and Electrospun Nanofibres: Methods, Materials and Applications", *Chemical Reviews*, Vol. 119, No. 8, pp. 5298-5418.
- Yamini, N. and Begum, S. K. A. (2020), "A Comprehensive Overview on Nanofiber Technology and Their Advancements in the Field of Pharmaceuticals", *International Journal of Research in Pharmaceutical Sciences and Technology*, Vol. 2, No. 2, pp. 51-58.
- Yew, Y. P., Shameli, K., Miyake, M., Kuwano, N., Khairudin, N. B. B. A., Mohamad, S. E. B. and Lee, K. X. (2016), "Green Synthesis of Magnetite (Fe<sub>3</sub>O<sub>4</sub>) Nanoparticles Using Seaweed (*Kappaphycus avlarezii*) Extract", *Nanoscale Research Letters*, Vol. 11, No. 11276.

Zhang, C. L. and Yu, S. H. (2014), "Nanoparticles Meet Electrospinning: Recent Advances and Future Prospects", *Chemical Society Reviews*, Vol. 43, No. 13, pp. 4423-4448.

Zhou, X. (2020), "Correction to the Calculation of Polanyi Potential from Dubinin-Rudushkevich Equation", *Journal of Hazardous Materials*, Vol. 384, p. 121101.

Zong, X., Kim, K., Fang, D., Rang, S., Hsiao, B. S. and Chu, B. (2002), "Structure and Process Relationship of Electrospun Bioabsorbable Nanofiber Membranes", *Polymer*, Vol. 43, pp. 4403-4412.

Zoroddu, M. A., Aaseth, J., Crisponi, G., Medici, S., Peana, M. and Nurchi, V. M. (2019), "The Essential Metals for Humans: A Brief Overview", *Journal of Inorganic Biochemistry*, Vol. 195, pp. 120-129.



## APPENDICES

### APPENDIX A: POINT OF ZERO CHARGE (PZC) ANALYSIS OF THE Ag-NP-PVA/NRL NANOFIBRE COMPOSITES

**Table A1: PZC Analysis for 0.01 M AgNP Nanofibre Composite**

0.01 M AgNP	
<i>Initial pH</i>	<i>Final pH</i>
2.96	3.02
3.89	4.01
4.95	4.98
5.97	5.66
6.92	6.24
7.99	6.52
9.18	6.85
9.93	7.67

**Table A2: PZC Analysis for 0.015 M AgNP Nanofibre Composite**

0.015 M AgNP	
<i>Initial pH</i>	<i>Final pH</i>
3.03	3.05
4.08	4.1
5.06	4.89
5.93	5.54
7.08	6.21
8.27	6.52
8.89	6.63
10.58	10.22

**APPENDIX B: MERCURY ADSORPTION FROM AQUEOUS SOLUTION BY  
AgNP-PVA/NRL NANOFIBRE COMPOSITES IN A SINGLE-COMPONENT  
ADSORPTION STUDY**

**Table B1: Effect of pH on Hg Adsorption by 0.01 M AgNP Nanofibre Composite**

<b>PVA/NRL</b>	
<b>pH</b>	<b><i>Hg Concentration (mg/L)</i></b>
	0.7534 (initial concentration)
<b>4.13</b>	0.7534
<b>4.88</b>	0.5906
<b>5.78</b>	0.6274
<b>6.50</b>	0.5906
<b>7.03</b>	0.3938
<b>8.12</b>	0.5545
<b>9.29</b>	0.5545

**Table B2: Effect of pH on Hg Adsorption by 0.015 M AgNP Nanofibre Composite**

<b>PVA/NRL</b>	
<b>pH</b>	<b><i>Hg Concentration (mg/L)</i></b>
	0.7534 (initial concentration)
<b>4.13</b>	0.7534
<b>4.88</b>	0.6825
<b>5.78</b>	0.5700
<b>6.50</b>	0.5749
<b>7.03</b>	0.5014
<b>8.12</b>	0.5381
<b>9.29</b>	0.4761

**Table B3: Effect of Contact Time on Hg Adsorption by PVA/NRL Nanofibre Composite**

<b>PVA/NRL</b>	
<b>Time (min)</b>	<b><i>Hg Concentration (mg/L)</i></b>
<b>0</b>	0.5000
<b>5</b>	0.4489
<b>10</b>	0.4095
<b>15</b>	0.4489
<b>20</b>	0.3990
<b>30</b>	0.3990
<b>40</b>	0.3465
<b>60</b>	0.3203
<b>90</b>	0.3203
<b>120</b>	0.2940

**Table B4: Effect of Contact Time on Hg Adsorption by 0.01 M AgNP Nanofibre Composite**

<b>0.01 M AgNP</b>	
<b>Time (min)</b>	<b><i>Hg Concentration (mg/L)</i></b>
<b>0</b>	0.5000
<b>5</b>	0.3334
<b>10</b>	0.3071
<b>15</b>	0.3071
<b>20</b>	0.2704
<b>30</b>	0.2310
<b>40</b>	0.2310
<b>60</b>	0.1785
<b>90</b>	0.1654
<b>120</b>	0.1549



**Table B5: Effect of Contact Time on Hg Adsorption by 0.015 M AgNP Nanofibre Composite**

<b>0.015 M AgNP</b>	
<b>Time (min)</b>	<b>Hg Concentration (mg/L)</b>
0	0.5000
5	0.3334
10	0.3203
15	0.3071
20	0.3203
30	0.3071
40	0.3071
60	0.2704
90	0.2441
120	0.2179

**Table B6: Effect of Initial Concentration on Hg Adsorption by 0.01 M AgNP Nanofibre Composite**

<b>0.01 M AgNP</b>	
<b>Initial Concentration (mg/L)</b>	<b>Hg Concentration (mg/L)</b>
0.01	0.0022
0.02	0.0028
0.05	0.0055
0.10	0.0276
0.20	0.0693
0.25	0.1050
0.40	0.1743
0.50	0.2188
0.60	0.2962
1.00	0.6100

**Table B7: Effect of Initial Concentration on Hg Adsorption by 0.015 M AgNP Nanofibre Composite**

<b>0.015 M AgNP</b>	
<b>Initial Concentration (mg/L)</b>	<b>Hg Concentration (mg/L)</b>
<b>0.01</b>	0.0011
<b>0.02</b>	0.0011
<b>0.05</b>	0.0055
<b>0.10</b>	0.0289
<b>0.20</b>	0.0635
<b>0.25</b>	0.0936
<b>0.40</b>	0.1978
<b>0.50</b>	0.2744
<b>0.60</b>	0.3720
<b>1.00</b>	0.6974



**APPENDIX C: CADMIUM ADSORPTION FROM AQUEOUS SOLUTION BY  
AgNP-PVA/NRL NANOFIBRE COMPOSITES IN A SINGLE-COMPONENT  
ADSORPTION STUDY**

**Table C1: Effect of pH on Cd Adsorption by 0.01 M AgNP Nanofibre Composite**

<b>0.01 M AgNP</b>	
<b>pH</b>	<b><i>Cd Concentration (mg/L)</i></b>
	1.0416 (initial concentration)
<b>4.13</b>	1.0070
<b>4.88</b>	1.0070
<b>5.78</b>	1.0070
<b>6.50</b>	0.8684
<b>7.03</b>	0.7287
<b>8.12</b>	0.9966
<b>9.29</b>	1.0416

**Table C2: Effect of pH on Cd Adsorption by 0.015 M AgNP Nanofibre Composite**

<b>0.015 M AgNP</b>	
<b>pH</b>	<b><i>Cd Concentration (mg/L)</i></b>
	1.0416 (initial concentration)
<b>4.13</b>	1.0070
<b>4.88</b>	1.0070
<b>5.78</b>	0.9723
<b>6.50</b>	0.8337
<b>7.03</b>	0.6941
<b>8.12</b>	0.9966
<b>9.29</b>	0.9966

**Table C3: Effect of Contact Time on Cd Adsorption by PVA/NRL Nanofibre Composite**

<b>PVA/NRL</b>	
<b>Time (min)</b>	<b><i>Cd Concentration (mg/L)</i></b>
<b>0</b>	1.0000
<b>5</b>	0.9587
<b>10</b>	0.9881
<b>15</b>	0.9293
<b>20</b>	0.9293
<b>30</b>	0.9293
<b>40</b>	0.9293
<b>60</b>	0.9293
<b>90</b>	0.8705
<b>120</b>	0.8705

**Table C4: Effect of Contact Time on Cd Adsorption by 0.01 M AgNP Nanofibre Composite**

<b>0.01 M AgNP</b>	
<b>Time (min)</b>	<b><i>Cd Concentration (mg/L)</i></b>
<b>0</b>	1.0000
<b>5</b>	0.9293
<b>10</b>	0.9293
<b>15</b>	0.9293
<b>20</b>	0.8705
<b>30</b>	0.8999
<b>40</b>	0.9293
<b>60</b>	0.9293
<b>90</b>	0.9293
<b>120</b>	0.8705

**Table C5: Effect of Contact Time on Cd Adsorption by 0.015 M AgNP Nanofibre Composite**

<b>0.015 M AgNP</b>	
<b>Time (min)</b>	<b><i>Cd Concentration (mg/L)</i></b>
0	1.0000
5	0.8106
10	0.8106
15	0.7518
20	0.7518
30	0.6920
40	0.6332
60	0.6920
90	0.6332
120	0.6332

**Table C6: Effect of Initial Concentration on Cd Adsorption by 0.01 M AgNP Nanofibre Composite**

<b>0.01 M AgNP</b>	
<b>Initial Concentration (mg/L)</b>	<b><i>Cd Concentration (mg/L)</i></b>
0.01	< 0.0020
0.02	< 0.0020
0.05	0.0033
0.10	0.0067
0.20	0.1460
0.25	0.1920
0.40	0.3112
0.50	0.4016
0.60	0.5000
1.00	0.8033

**Table C7: Effect of Initial Concentration on Cd Adsorption by 0.015 M AgNP Nanofibre Composite**

<b>0.015 M AgNP</b>	
<b>Initial Concentration (mg/L)</b>	<b><i>Cd Concentration (mg/L)</i></b>
<b>0.01</b>	< 0.0020
<b>0.02</b>	< 0.0020
<b>0.05</b>	0.0042
<b>0.10</b>	0.0062
<b>0.20</b>	0.1430
<b>0.25</b>	0.1900
<b>0.40</b>	0.3012
<b>0.50</b>	0.3838
<b>0.60</b>	0.4820
<b>1.00</b>	0.8033



**APPENDIX D: MERCURY AND CADMIUM ADSORPTION FROM AQUEOUS SOLUTION BY AgNP-PVA/NRL NANOFIBRE COMPOSITES IN A BINARY ADSORPTION STUDY**

**Table D1: Hg Adsorption by 0.01 M AgNP Nanofibre Composite from Cd-Hg Aqueous Solution**

<b>AgNP-PVA/NRL</b>	<b><i>Hg Concentration (mg/L)</i></b>
	0.0500 (initial concentration)
<b>0.01 M</b>	0.0157
<b>0.015 M</b>	0.0179
<b>Mix 1</b>	0.0101
<b>Mix 2</b>	0.0101
<b>Mix 3</b>	0.0090

**Table D2: Cd Adsorption by 0.01 M AgNP Nanofibre Composite from Cd-Hg Aqueous Solution**

<b>AgNP-PVA/NRL</b>	<b><i>Cd Concentration (mg/L)</i></b>
	0.1000 (initial concentration)
<b>0.01 M</b>	0.0310
<b>0.015 M</b>	0.0221
<b>Mix 1</b>	0.0364
<b>Mix 2</b>	0.0421
<b>Mix 3</b>	0.0334

## Index

### A

- AAS (Atomic Absorption Spectrophotometry), 33–34, 36, 40, 46, 50
- Abu Bakar, 16, 24, 52, 63, 69, 71, 75–78, 132
- adsorbate, 30–32, 46–50, 65, 82, 88, 90, 94, 99, 105, 117, 120
- adsorbate and adsorbent, 31
- adsorbate in solution, 32, 46
- adsorbate solution, 31, 45–46, 82, 99, 128
- adsorbed Hg, 88, 99, 119, 128–29
- adsorbed Hg and Cd, 128–29
- adsorbent, 1, 30–33, 45–48, 82–84, 90, 93, 96, 100, 105, 107, 111, 113, 116–17
- adsorbent dose, 116, 120
- adsorbent surfaces, 31, 84, 120
- adsorption, 1–3, 6–7, 15, 30, 32, 48, 51, 65, 83–84, 86–90, 99–105, 107–9, 111–17, 119–22, 124, 128–30, 145
- adsorption and water treatment, 51
- adsorption by AgNP-PVA/NRL nanofibre composites, 99, 102, 106, 110, 112, 117
- adsorption capacity, 46, 48, 90, 97, 117, 119, 121
- adsorption in water and wastewater treatment, 2
- Adsorption Isotherm, 32, 47, 81, 89, 93, 104, 107
- adsorption kinetic models, 32, 94, 108, 114, 129
- adsorption kinetics, 32, 49, 81, 96, 111
- adsorption mechanisms, 6, 32, 45, 48–49, 105
- adsorption process and initial concentration, 82, 99
- adsorption processes, 1, 30–32, 37, 49, 69, 82, 99
- Ag clusters, 75–76, 79, 85, 101
- Ag concentration in water, 123–24
- Ag concentrations, 122–23, 125, 129
- AgNO<sub>3</sub>, 16, 36, 43, 47, 123, 125, 127
- AgNO<sub>3</sub> concentration, 47, 70, 73, 75, 80
- AgNO<sub>3</sub>-PVA/NRL, 41–42, 121
- AgNO<sub>3</sub>-PVA/NRL solutions electrospun, 41, 47
- AgNP
- green, 4
  - producing, 11, 69
  - synthesise, 16–17, 68–69, 122
  - synthesised, 17–18, 127
  - synthesising, 3–4, 70, 73
- AgNP and PVA/NRL in AgNP-PVA/NRL nanofibre composites, 45
- AgNP-coated nanofibre, 42
- AgNP concentration in treated water, 18
- AgNP electrospun, 117
- AgNP fibre, 75
- AgNP growth, 17–19, 70, 75, 78, 127
- AgNP incorporated in PVA/NRL nanofibre composite, 4, 127
- AgNP Nanofibre, 47, 159, 163
- AgNP Nanofibre Composite, 71, 76–77, 80, 86, 100, 156, 158, 160–65
- AgNP-Nanofibre Composites, 118
- AgNP-NRL/PVA nanofibre composites, 44
- AgNP-PVA/NRL, 4, 6, 45, 69
- AgNP-PVA/NRL nanofiber composites, 87, 128
- AgNP-PVA/NRL Nanofibre, 4, 42, 45, 70, 79, 99, 113, 130
- synthesised, 4, 128
- AgNP-PVA/NRL Nanofibre Composite for Hg and Cd, 45
- AgNP-PVA/NRL Nanofibre Composites, 5–7, 44–46, 76–80, 82–84, 86, 89, 92–93, 95–96, 98–100, 104, 106–7, 110–12, 116–19, 122–25, 128–31
- AgNP-PVA/NRL Nanofibre Composites Adsorption Capacity, 118
- AgNP-PVA/NRL nanofibre composites and contact time, 103
- AgNP-PVA/NRL Nanofibre Composites in Hg Solution Agitated, 46
- AgNP-PVA/NRL Nanofibre Composites to Adsorb Hg and Cd, 117
- AgNP's fibres, 97–98, 124



AgNP synthesis, 5–6, 14–16, 36, 42, 65, 70, 123, 125  
AgNP synthesised in PVA/NRL nanofibre composite, 69  
amalgam, 8, 84–85  
amalgamation, 85–86, 128  
Aoshima, 10, 81, 134  
applied voltage, 20–22, 42, 55, 144  
aqueous solutions, 2, 4–7, 65–66, 79, 81, 97, 99–100, 102–3, 113–14, 116–17, 122–23, 125, 128–29, 140–41, 153  
    separate, 5–6, 81  
Atomic Absorption Spectrophotometry. *See* AAS

## B

basic terms used in adsorption processes, 30  
binary system, 7, 116–17, 119, 124  
biopolymer, 2–3, 22, 25, 52  
brasiliensis, 23, 36

## C

cation adsorption, 83, 100  
cations, 83–84, 100–101, 120  
Cd Adsorption, 116, 124–25, 129, 161–65  
Cd Adsorption by AgNP-PVA/NRL Nanofibre, 113  
Cd Adsorption Fibre Matrix, 123  
Cd Concentration, 11, 40, 161–65  
Cd-Hg Solution by AgNP-PVA/NRL Nanofibre Composites, 118  
Cd's adsorption, 124  
Characterisation of AgNP-PVA/NRL Nanofibre Composite, 76–77  
Characterisation of AgNP-PVA/NRL Nanofibre Composite by X-Ray Diffractometry, 76  
Characterisation of Electrospun PVA/NRL Nanofibre, 6  
Characterisation of Nanoparticles and Nanofibres, 25  
characteristics, physical, 27  
chemical adsorption, 30–31, 108  
chemisorption, 30–31, 90, 105, 108  
Comparison of Hg Adsorption to Cd Adsorption, 113

Competitive Adsorption of Mercury and Cadmium, 6  
composites  
    nanofibre-nanoparticle, 28  
    synthesised nanofibre, 69  
Concentration in Aqueous Solutions, 123  
concentrations, 4–5, 23, 35, 37, 48, 52–53, 103–4, 114, 165  
    lower, 88–89  
contact time, 4–6, 46, 49, 86–88, 97, 99, 102–3, 114, 116–17, 158–59, 162–63  
contaminant removal in water treatment by adsorption, 3  
Crystallography of AgNP-PVA/NRL Nanofibre Composites, 44

## D

dissolution, 25, 42, 51, 65, 67–68, 123, 127  
distance, 20, 22, 40, 43–44  
distilled water, 37–38, 40, 42, 50, 65, 67  
DRC (Dry Rubber Content), 23, 35, 37–39, 52–53, 133  
Drever, 31, 83–84, 100, 139  
drinking water, 3, 9, 11, 122, 133  
drying, 38, 43, 52–53, 66, 70–71, 79  
Dry Rubber Content. *See* DRC  
Dubinin-Radushkevich Isotherm for Hg Adsorption by AgNP-PVA/NRL Nanofibre Composites, 92

## E

effect of contact time, 49, 86–87, 103  
Effect of Contact Time on Hg Adsorption, 86, 158–59  
effect of initial concentration, 89, 103–4  
effect of initial concentration on Cd, 103  
Effect of Initial Concentration on Hg Adsorption, 88, 159–60  
electrospinning, 3–5, 19–21, 40, 42, 51–52, 54–55, 57, 59, 65, 67–70, 121, 124, 149, 152–53  
Electrospinning NRL, 5, 35, 40, 42  
electrospinning of nanofibres, 57  
electrospinning PVA/NRL, 41  
electrospinning PVA/NRL solutions, 6, 42, 57

Electrosprayed NRL, 6, 51, 55–56, 59  
 electrospaying, 19–21, 55, 58, 144  
 electrospaying PVA/NRL, 58  
 electrospun, 3–5, 20, 22, 40–43, 47, 51, 55,  
 58–61, 67, 71, 117, 126, 130–31  
 Electrospun AgNP-PVA/NRL, 70  
 electrospun fibres, 20–22, 42–44, 62–63,  
 113, 121, 126, 139  
 Electrospun Nanofibre Composites, 44  
 electrospun nanofibre fabrication, 52  
 electrospun nanofibres, 35, 45, 51, 116, 154  
 green, 52  
 producing green, 51  
 electrospun NRL, 44, 70  
 electrospun PVA/NRL fibre, 65  
 electrospun PVA/NRL nanofibre  
 composites, 5  
 electrospun PVA/NRL nanofibres, 6, 45  
 electrostatic adsorption, 30–31, 86, 128  
 elemental composition, 5–6, 25, 27–29, 44,  
 69–70, 72, 98, 112  
 Elovich, 95–96, 108, 110–11  
 Elovich kinetic model, 94, 108, 114, 128–29  
 Elovich model, 49, 94, 108  
 Equation, 16, 29, 38–39, 43, 46–49, 78, 83,  
 85, 101–2, 105, 113  
 experiment's time frame, 91, 97, 105, 109,  
 113–15

**F**

fibre diameter, 19, 21–22, 59, 62, 126  
 average, 59, 61  
 fibre diameter distribution, 44, 59, 61  
 fibre diameter distribution of PVA and  
 PVA/NRL nanofibres, 44  
 fibre films, 55, 62, 65, 127  
 electrospun PVA/NRL, 51  
 smoother PVA/NRL, 130  
 fibre matrix, 3, 69, 80, 118  
 fibre molecules, 65  
 fibres, 3–4, 19–21, 41–44, 58, 61–63, 65–  
 67, 71–72, 87–89, 91, 98–99, 109, 116,  
 120–21, 123–26, 129–30  
 continuous, 21, 59, 61  
 electrospun NRL, 3, 70  
 extra, 120, 124

smooth, 59, 61, 67  
 thinner, 22, 41, 57  
 weight of, 43  
 fibre's surface, 70–71, 97, 120, 127  
 films, fabricated PVA/NRL nanofibre, 51  
 fit  
 best, 108, 114  
 poor, 108, 114  
 flow rate, 20, 22, 40, 42  
 FT-IR spectra of PVA/NRL and AgNP  
 nanofibre composites, 77  
 FT-IR Spectra of PVA/NRL Nanofibre and  
 AgNP-PVA/NRL Nanofibre  
 Composites, 78

## G

green AgNP in PVA/NRL, 4  
 green arrows, 98–99, 112–13  
 Green Synthesis and Characterisation of  
 Electrospun PVA/NRL Nanofibre, 6  
 Green Synthesis of AgNP Incorporated in  
 PVA/NRL Nanofibre Composite, 127  
 Guidelines for Ag concentration in drinking  
 water, 122–23

**H**

heavy metals, 1–2, 4, 8, 81, 121, 128, 135–  
 36  
 Henglein, 16, 75–76, 84–85, 101, 113, 142  
 Hg Adsorption, 82, 86–88, 90, 93, 96–99,  
 103, 113–14, 119–20, 122, 124, 128–  
 29, 131, 157–60  
 affected, 114, 129  
 facilitated, 120, 124  
 Hg adsorption by AgNP-PVA/NRL  
 nanofibre composites, 82, 86, 92, 95, 98  
 Hg adsorption fit, 114  
 Hg and Cd adsorption, 116, 125  
 Hg and Cd adsorption by Mix, 124  
 Hg and Cd Adsorption Fibre Matrix, 123  
 Hg by AgNP-PVA/NRL nanofibre  
 composites, 82–83, 86, 89  
 Hg removal, 84, 88–89, 121, 152  
 high temperatures, 11, 13–14, 16, 33, 37

## I

initial concentration, 5–6, 46, 82, 84, 88–89, 99, 102–4, 114, 116–17, 119, 128, 157, 159–61, 163–65

Intra-Particle Diffusion Kinetic Models for Hg Adsorption by AgNP-PVA/NRL Nanofibre Composites, 95

ions, 30–31, 78, 83–84, 101–2, 140–41

isoprene, 17, 23–24, 77–80, 127

isotherms, 32, 47–48, 89–90, 104–5, 114

## J

Jadhav, 55, 144

## K

kinetic models, 94, 108

Kyrychenko, 17, 25, 145

## L

Langmuir isotherm, 32, 90, 105, 114

larger area for nanoparticle attachment and adsorption, 62

larger nanoparticles, 75–76, 113, 124

latex, 23, 37, 52, 54, 126, 133

## M

magnifications, 44, 75

Mansur, 25, 63–64, 77, 146

materials, 2, 5, 8, 11, 18–19, 28, 30, 35, 136, 142, 144, 149, 154

matings, 60–62, 65, 113, 120, 126

mercury, 2, 6, 8–9, 33, 36–37, 81, 133–35, 139–41, 144–45, 147, 151, 153

metallic Hg, 8, 84, 87–88, 90, 97–98, 120

mixtures of AgNP-PVA/NRL nanofibre composites, 7

Morphology and Elemental Composition of AgNP-PVA/NRL Nanofibre, 70

Morphology and Elemental Composition of AgNP-PVA/NRL Nanofibre Composites, 98, 112

morphology of electrosprayed NRL and electrospun PVA/NRL fibre films, 51

morphology of nanofibres and nanoparticles on nanofibre surfaces, 27

## N

nanofibre composites, 6–7, 44–46, 48, 50, 69–71, 73, 76, 78–79, 81, 83, 88–90, 99–102, 105, 113–14, 128

nanofibre composites in aqueous solution, 81

nanofibre composites in solution, 45

nanofibre fabrication, 4, 19

nanofibre matrix, 75

nanofibres

electrospun PVA/NRL, 4, 57

separate, 122, 124

nanofibres and nanoparticles, 25, 27

nanomaterials, 2–3, 11, 13, 18, 25, 32, 136, 138, 140–41, 145–46, 151–52

nanoparticle loading, 51–52, 61, 65

nanoparticle loading and adsorption, 65

Nanoparticle Loading and Application in Aqueous Solutions, 6

nanoparticle-nanofibre, 5

nanoparticles, 2–3, 5, 7, 11–15, 17–18, 24–25, 27–29, 42, 44, 51–52, 69–73, 75, 122, 144, 153–54

produced, 75

nanoparticles and nanofibre strands, 27

Nanoparticles in Water Treatment, 17–18

nanotechnology, 2, 11, 25, 135–37, 144, 149–50, 154

nanowastewater residue, 11, 13

natural rubber, 2–3, 17–18, 22–24, 37, 67, 132, 134, 143, 147–48, 150, 153

natural rubber latex. *See* NRL

NRL (natural rubber latex), 2–6, 16–17, 22–24, 35–41, 45, 51–55, 57–58, 63–64, 67–70, 75–78, 80, 126–27, 135–36, 139, 142

NRL and PVA in electrospun PVA/NRL nanofibres, 45

NRL nanofibre matrix, 24, 37

## O

optimum ratio of NRL to PVA for electrospun nanofibre fabrication, 52

orbital shaker, 42, 45–46

Osei, 25, 59–62, 64, 66–67, 100, 103–4, 106–7, 110–12, 148–49

## P

Parameters of Adsorption Isotherms for Hg Adsorption, 93  
Parameters of Adsorption Kinetics for Hg Adsorption, 96  
PFO (pseudo-first order), 32, 49, 81, 94–97, 108, 110–11, 150  
PFO equation, 49, 94  
physical adsorption, 30–31  
physical characteristics of nanofibres and nanoparticles, 27  
Point of Zero Charge. *See* PZC  
Point of Zero Charge Analyses of AgNP-PVA/NRL Nanofibre Composites, 45  
polymers, 3, 20, 22, 25, 29, 44, 51–52, 139, 150, 155  
Polyvinyl Alcohol. *See* PVA  
pore diameters, 27, 62, 67, 126, 130  
Pore Diameters of PVA/NRL Fibre Films, 62  
porosity, 18, 116, 120–21  
proteins, 16–17, 23–24, 52–53, 154  
pseudo-first order. *See* PFO  
pseudo-second order. *See* PSO  
PSO (pseudo-second order), 32, 49, 81, 94–97, 108, 110–11, 150  
PVA (Polyvinyl Alcohol), 3–5, 17, 22, 24–25, 35, 42, 44–45, 51–52, 58–61, 63–65, 67–69, 77–78, 126–27, 135–36, 148–50  
PVA and AgNP-NRL/PVA nanofibre composites, 44  
PVA and PVA/NRL fibre films, 63  
PVA and PVA/NRL solutions, 5, 40  
PVA content, 61, 63–65, 126  
PVA/NRL, 4, 35, 40, 42, 45, 54, 59–68, 76–78, 87, 102–3, 125–27, 130  
PVA/NRL and AgNO<sub>3</sub>-PVA/NRL Solutions, 41  
PVA/NRL and NRL Fibre Films, 64  
PVA/NRL fibre diameter distribution trend, 62  
PVA/NRL fibre films, 62–63, 65–67  
PVA/NRL fibre matrix, 80  
PVA/NRL fibres, 65, 126

PVA/NRL Nanofibre and AgNP-PVA/NRL Nanofibre Composites, 78  
PVA/NRL nanofibre composites, 6, 70, 127  
PVA/NRL Nanofibre Matrix, 79, 131  
PVA/NRL nanofibres, 4–5, 35, 42–44, 51, 69, 77, 87, 103, 123, 126, 130  
PVA/NRL Nanofibres PVA/NRL Ratio, 66  
PVA/NRL solution, 5, 40, 42–43, 54, 59, 61, 127  
PVA/NRL Solutions Shear, 54  
PVA/NRL spectra, 63  
PZC (Point of Zero Charge), 5–6, 36, 45, 69, 79–80, 83–84, 86, 100, 156

## R

Ramakrishna, 19–22, 51, 54, 58, 61, 143, 147, 149, 153  
Ramsden, 11, 149–50  
Rayleigh's Jet, 19, 55–57  
recommendations, 7, 126, 130  
removal efficiencies, 7, 13–15, 46, 81–82, 117–20, 124, 128–29  
removal of Cd, 99–100, 102–3  
rubber, 22–23, 133, 151

## S

Sagitha, 25, 70, 78, 150  
Sawyer, 30–32, 47–48, 105, 151  
scaffolds, 121, 137  
sediments, 8–10  
Sharma, 29, 151  
size of nanoparticles and nanofibre diameters, 27  
Smaller average fibre diameters, 61  
solution, 20–21, 32–33, 35–36, 40–43, 45–47, 50, 54, 65–66, 69–70, 82–84, 87–91, 98–100, 113, 116–19, 122–23  
polymer, 22, 143  
standard, 36  
Solutions for Electrospinning, 40  
Sorption of Hg by AgNP-PVA/NRL Nanofibre Composites, 82  
specimen, 26–29  
spectrum, 28, 77, 99, 113  
spinneret, 19–22, 41–42, 58  
spinneret sizes, 40, 55, 58

stabilising agent, 16, 69, 75–76, 78–79, 127  
Stokes, 26–27, 152  
surface, 18, 21, 27–28, 30–32, 56–57, 69–  
72, 76, 83–84, 86–89, 91, 97, 113–14,  
119–20, 122–25, 129–30  
surface area, 18, 31, 116, 121–22  
surface area-to-volume ratio, 3, 62  
higher, 3, 69  
surface charge, 45, 79, 81, 83  
surface charge of AgNP-PVA/NRL  
nanofibre composites, 79  
surface functionalisation, 5–6, 25, 28  
surface tension, 19–21  
synthesised AgNP-PVA/NRL nanofibre  
composites, 5–7, 81, 114, 127–28, 130  
system, adsorptive water treatment, 116

## T

Takeo, 84–85, 101, 153  
Tauanov, 14, 16, 18, 69, 84–86, 153  
Taylor Cone, 19, 21–22, 56–57  
Tchounwou, 9–10, 153  
Texture, 56–57  
thickness, 38, 50, 55–57, 73, 97  
thinner, 55, 57  
time, 22, 49, 58, 87, 95, 103, 110, 117, 158–  
59, 162–63  
Total solid content. *See* TSC  
Toxicological Effects of Nanoparticles in  
Water Treatment, 18  
Tran, 30, 32, 45, 47, 49, 90, 94, 108, 153  
treated water, 2, 12–15, 18, 25, 42, 51, 69–  
70, 116–17, 123, 125, 129  
treated water by AgNP-PVA/NRL nanofibre  
composites, 117  
trend for Hg adsorption, 129  
trend in Hg adsorption, 103  
TSC (Total solid content), 23, 37–38, 52–53

## U

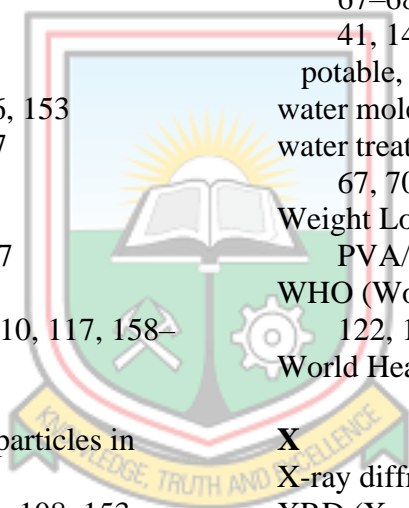
ultrafiltration, 12–15, 18  
uptake, sharpest, 100, 102

## V

Viscosities of NRL and PVA/NRL  
solutions, 54  
viscosity, 20–21, 42, 54, 58, 61  
voltages, 21, 40, 55, 57–58  
high, 19–21, 27

## W

wastewater, 1, 3–4, 11, 37, 81, 126, 135,  
137, 143  
wastewater in competitive adsorption, 4  
Wastewater Nanoparticle/ Nanocomposite,  
13  
wastewater treatment, 1–2, 13–14, 18, 30,  
143, 145–46  
water, 1–4, 8, 10–11, 17–18, 25, 51–52, 64,  
67–68, 122–24, 126, 128, 136–37, 140–  
41, 146–47, 152–53  
potable, 8  
water molecules, 64–65  
water treatment, 1, 3–5, 7, 11, 17–19, 25, 51,  
67, 70, 130, 132, 136–37, 145  
Weight Loss Test by Dissolution on  
PVA/NRL Nanofibres, 42  
WHO (World Health Organisation), 9, 11,  
122, 129, 133  
World Health Organisation. *See* WHO  
**X**  
X-ray diffractometry. *See* XRD  
XRD (X-ray diffractometry), 29, 44, 69, 76,  
80, 127



# LINDA BENTUMA OSEI-- Thesis

## ORIGINALITY REPORT

13%

SIMILARITY INDEX

10%

INTERNET SOURCES

10%

PUBLICATIONS

3%

STUDENT PAPERS

## PRIMARY SOURCES

1	<a href="https://link.springer.com">link.springer.com</a> Internet Source	3%
2	Linda Bentuma Osei, Samuel Agyarko Ndur, Shadrack Fosu. "Synthesis and characterisation of electrospun natural rubber latex/polyvinyl alcohol for application in aqueous processes", Journal of Rubber Research, 2022 Publication	1%
3	<a href="https://www.mdpi.com">www.mdpi.com</a> Internet Source	1%
4	<a href="https://www.science.gov">www.science.gov</a> Internet Source	<1%
5	<a href="https://mdpi-res.com">mdpi-res.com</a> Internet Source	<1%
6	Hai Nguyen Tran, Sheng-Jie You, Ahmad Hosseini-Bandegharai, Huan-Ping Chao. "Mistakes and inconsistencies regarding adsorption of contaminants from aqueous	<1%



# Synthesis and characterisation of electrospun natural rubber latex/polyvinyl alcohol for application in aqueous processes

Linda Bentuma Osei<sup>1</sup> · Samuel Agyarko Ndur<sup>1</sup> · Shadrack Fosu<sup>1</sup>

Received: 8 April 2022 / Accepted: 19 September 2022  
© The Author(s), under exclusive licence to Malaysian Rubber Board 2022

## Abstract

Advances in nanofibre application, such as water treatment, have increased the need to identify renewable resources and green methods for nanofibre production. In this study, natural rubber latex (NRL) mixed with polyvinyl alcohol (PVA) was electrospun to form nanofibre films, and the best PVA/NRL ratio suitable for aqueous applications was determined. The films were characterised by scanning electron microscopy (SEM), Fourier-transform infrared (FT-IR) spectroscopy and a weight loss test by dissolution. SEM images revealed relatively thicker and smoother fibres, with larger average pore diameters in fibre films with higher PVA content (60% PVA/NRL and 70% PVA/NRL). Fibre films with lower PVA content (40% PVA/NRL and 50% PVA/NRL) had relatively thinner fibres and smaller average pore diameters, which are desirable characteristics for contaminant adsorption. The FT-IR spectroscopy indicated that 60% PVA/NRL and 70% PVA/NRL would be more soluble in water than 40% PVA/NRL and 50% PVA/NRL due to the intense peaks of C=O stretching of acetate groups ( $1738\text{ cm}^{-1}$ ) observed in fibre films with higher PVA content. This was confirmed in a weight loss test, which revealed that though increasing PVA content (60 and 70%) improved NRL's electrospinnability, the increased PVA content caused a loss of fibre film mass in water. Therefore, 50% PVA/NRL will be a better option for application in aqueous processes.

**Keywords** Electrospinning · Nanofibres · Natural rubber latex · Polyvinyl alcohol

## Introduction

Nanofibers are materials with fibre diameters less than 500 nm [1, 2]. In recent years, nanofibres have been used in several fields such as filtration, water treatment, drug delivery, tissue engineering, wound dressing and as a template for nanoparticle loading [3–6]. Nanofibres can be fabricated in a non-woven form through self-assembly, electrospinning, drawing, phase separation and template synthesis. However, electrospinning has proven the most convenient method [5].

In electrospinning, a charged fluid is ejected from a spinneret, causing the fluid to stretch, dry and form fine fibres, usually in the micro or nano range [2]. This forms a fibrous film with high porosity, small fibre-to-fibre distance and a high surface area-to-volume ratio; hence, sought-after in filtration, water treatment and as a template for nanoparticle loading processes. Currently, several non-renewable

resources, some of which are hazardous (organic solvents such as acetone, dimethylformamide (DMF) and methylene chloride), have been exploited in producing electrospun fibres [3]. This has necessitated researchers to seek renewable resources for electrospinning to help build environmentally sustainable nanofiber alternatives which are non-hazardous or less toxic. Electrospinning of alternative materials, such as natural rubber latex (NRL) and polyvinyl alcohol (PVA), with water as a solvent, could be utilised as potential nanofiber.

Natural rubber (NR) is an elastomer used in the automotive, agricultural, clothing and medical industries, among others. It has unique properties such as exceptional elasticity, resistance to abrasion, pliability at low temperatures and insulating properties, making it irreplaceable compared to its synthetic counterpart in some applications [7, 8]. Natural rubber latex (NRL) is biocompatible for biomedical applications and nanoparticle synthesis. From over 2500 plant species, NRL from *Hevea brasiliensis* is the sole source with commercial relevance. The *Hevea* tree is extensively grown in South-East Asia, Central Africa and West Africa, including Ghana [9, 10]. Latex from *H. brasiliensis* contains

✉ Linda Bentuma Osei  
lbosei@umat.edu.gh

<sup>1</sup> Department of Environmental and Safety Engineering,  
University of Mines and Technology, Tarkwa, Ghana

# Removal of Cadmium by Silver Nanoparticles Incorporated in Electrospun Natural Rubber Latex/Polyvinyl Alcohol Matrix\*

<sup>1</sup>L. B. Osei\*, <sup>1</sup>S. Fosu, and <sup>1</sup>S. A. Ndur

<sup>1</sup>University of Mines and Technology, Box 237, Tarkwa, Ghana

Osei, L. B., Fosu, S., Ndur, S. A. (2023), "Removal of Cadmium by Silver Nanoparticles Incorporated in Electrospun Natural Rubber Latex/Polyvinyl Alcohol Matrix", *Ghana Mining Journal*, Vol. 23, No. 1, pp. 11-21.

## Abstract

In this study, the efficiency of silver nanoparticles (AgNP) incorporated into electrospun natural rubber latex/polyvinyl alcohol (NRL/PVA) nanofibre matrix to remove Cd<sup>2+</sup> from aqueous solution was examined. Electrospun AgNP-NRL/PVA nanofibre composites were produced using silver nitrate (AgNO<sub>3</sub>) concentrations of 0.01 M and 0.015 M. Maximum Cd<sup>2+</sup> was adsorbed at pH 7 for both nanofibre composites but at different reaction times of 20 min for 0.01 M AgNP and 40 min for 0.015 M AgNP. The maximum adsorption for 0.01 M AgNP was 14.9674 mg/g and 30.1129 mg/g for 0.015 M AgNP. Adsorption data were tested with Langmuir, Freundlich and Dubinin-Radushkevich (D-R) isotherms as well as pseudo-first order (PFO), pseudo-second order (PSO), Elovich and intra-particle diffusion kinetic models. Cadmium adsorption by both nanofibre composites fitted best to Freundlich isotherm. Adsorption data for 0.01 M AgNP fitted best to PFO kinetic model, whilst that of 0.015 M AgNP fitted best to Elovich kinetic model, with 0.015 M AgNP having a lower desorption constant and larger boundary layer ( $\beta = 0.1793$  g/mg;  $C = 7.5959$  mg/g) than 0.01 M AgNP ( $\beta = 1.0351$  g/mg;  $C = 4.5942$  mg/g). The nanofibre, 0.015 M AgNP, fitting best to Freundlich isotherm and Elovich kinetic model, showed that Cd<sup>2+</sup> was chemisorbed. In general, 0.015 M AgNP was more efficient in adsorbing Cd<sup>2+</sup> than 0.01 M AgNP. After the adsorption process, silver (Ag) concentration in the treated water (0.01 M AgNP = 0.0425 mg/L, 0.015 M AgNP = 0.0510 mg/L) was below US EPA and WHO guidelines of 0.10 mg/L for both nanofibre composites, rendering the treated water good enough for human use. Therefore, this work has shown the potential of AgNP incorporated in an electrospun NRL/PVA nanofibre matrix to remove contaminants (Cd<sup>2+</sup>) from contaminated water.

**Keywords:** Silver Nanoparticles, Cadmium Adsorption, Natural Rubber Latex, Polyvinyl Alcohol, Electrospun Nanofibre

## 1 Introduction

Cadmium (Cd<sup>2+</sup>) is a heavy metal with no known biological function to the human body but has detrimental health effects when cadmium-contaminated water is consumed (Mahmood *et al.*, 2019). Due to Cd<sup>2+</sup>'s bioaccumulative nature, chronic exposure to low concentrations is considered harmful. Ingesting acute doses of Cd<sup>2+</sup> can cause gastrointestinal tract erosion, hepatic dysfunction and kidney damage (Tchounwou *et al.*, 2012). Long-term exposure may lead to Itai-Itai disease, which is characterised by softening of the bones and severe bone pain (Aoshima, 2016).

Cadmium is released into water bodies through corrosion of galvanised water supply pipes, desorption from some plastic water supply pipes, municipal landfill leachates, runoff from the application of Cd-laden fertilisers and pesticides, and effluents from mining and smelting sites (Elkhatib *et al.*, 2016; Salehi *et al.*, 2017; Mahmood *et al.*, 2019). Although humans are mostly exposed to Cd<sup>2+</sup> through food consumption (Anon., 2011), Cd<sup>2+</sup> in runoff and irrigation waters and aquatic bodies settle in soils and sediments (Aoshima, 2016; Elkhatib *et al.*, 2016; Balali-Mood *et al.*, 2021). Cadmium is assimilated by plants such as leafy vegetables, seeds, grains and potatoes, which is subsequently consumed by humans (Aoshima, 2012; Tchounwou *et al.*, 2012; Aoshima, 2016).

This shows that Cd<sup>2+</sup> ingested by humans can be limited mainly by reducing Cd-laden effluent release and Cd<sup>2+</sup> concentration in irrigation water.

Treating contaminated water containing low concentrations of Cd<sup>2+</sup> is challenging, particularly in countries with lax regulations on Cd<sup>2+</sup> discharge. Cadmium can be removed from wastewater using techniques such as ion exchange and tight membrane filtration. However, these methods require large quantities of chemicals for resin regeneration, and since the membranes are prone to fouling, it leads to high operational costs (Colantonio and Kim, 2016). It is, therefore, not cost-effective to use these advanced methods to treat Cd<sup>2+</sup> at low concentrations (Colantonio and Kim, 2016).

In recent years, nanoparticles have proven superior to their bulk counterparts in removing heavy metals from water (Shao-Feng *et al.*, 2005; Kango and Kumar, 2016; Tavker *et al.*, 2021). For instance, silver nanoparticles (AgNP) have the potential to adsorb Cd<sup>2+</sup> efficiently from water (Al-Qahtani, 2017). However, a pressing challenge is that nanoparticles mostly remain in treated water after the removal of contaminants. Due to the toxicological nature of nanoparticles, having these nanoparticles in treated water is not advisable (Sahu and Hayes, 2017; Pietrousti *et al.*, 2018). Furthermore, removing AgNP from the treated

\*Manuscript received February 23, 2023

Revised version accepted June 18, 2023

<https://doi.org/10.4314/gm.v22i1.1>